The PI3K/AKT pathway regulates cell fate identities during early mouse development

Anna Maria Geiselmann

Sorbonne Université

Ecole doctorale Complexité du Vivant (ED515)

Epigénomique, Prolifération et Identité Cellulaire – Institut Pasteur

The PI3K/AKT pathway regulates cell fate identities during early mouse development

Par Anna Maria GEISELMANN

Thèse de doctorat de Biologie

Dirigée par Michel COHEN-TANNOUDJI

Présentée et soutenue publiquement le 31 Mai 2022

Devant un jury composé de :

Président : Thierry JAFFREDO, Directeur de recherche

Rapporteur : Jérôme COLLIGNON, Directeur de recherche

Rapportrice : Alice JOUNEAU, Chargée de recherche

Examinatrice : Claire CHAZAUD, Directrice de recherche

Examinateur : Jérôme ARTUS, Maitre de conférence

Directeur de thèse : Michel COHEN-TANNOUDJI, Directeur de recherche

We are all broken, that's how the light gets in. - Ernest Hemingway

Abstract

The early mouse embryo is a unique paradigm for regulative development which requires a fine-tuned balance between plasticity and commitment. In just a few days, the fertilized egg forms a multicellular embryo which is able to attach to and develop intricate connections with the mother's uterine tissue. Initially equivalent, early embryonic cells become restricted in their developmental potential and commit to a specific cell identity while keeping short windows of responsiveness to react to external cues or developmental perturbations. Shortly before implantation, the inner cell mass (ICM) of early blastocysts differentiates into the epiblast (Epi), that will give rise to the fetus, and the primitive endoderm (PrE), at the origin of extraembryonic tissues. Previous studies have established a regulatory network, involving the transcription factors (TFs) NANOG and GATA6 and the FGF/ERK signaling, which controls many aspects of this differentiation process. However, several questions remain about the underlying mechanisms controlling the generation of the first embryonic lineages. The objective of this thesis was to study the role of PI3K/AKT signaling during blastocyst development when first Epi, then PrE cells arise from the uncommitted pool of ICM cells. My work demonstrates that PI3K/AKT is constitutively active during preimplantation development and that variations of signaling activities occur during mid to late blastocyst stages. By modulating pathway activity, I could demonstrate that PI3K/AKT activity is a premise for Epi formation as the Epi-specific TFs NANOG and SOX2 are dramatically reduced and endodermal SOX17 is activated in the absence of PI3K/AKT. I further provide evidence that the regulation of TF patterning in the ICM is, at least in part, mediated by the PI3K/AKT downstream target GSK3. Single cell RNA sequencing (scRNAseq) revealed that PI3K/AKT inhibition induced marginal alterations in the inner cell transcriptome, indicating that PI3K/AKT regulates TFs levels through post-transcriptional mechanisms. Surprisingly, I observed upregulation of SOX17 when PI3K/AKT is inhibited in *Gata6* mutant embryos which suggests that initiation of PrE fate requires the release of PI3K/AKT inhibition.

In conclusion, this PhD project illustrates that PI3K/AKT, a pathway often associated with controlling survival, proliferation and metabolism, acts also as a mediator of cell fate during a specific and limited period of early mouse development. We propose that PI3K/AKT guards the pluripotency of forming Epi progenitors by maintaining the expression of key Epi markers while simultaneously preventing differentiation towards PrE fate. Thus, my work gives novel and important insights into the regulation of the Epi master TF NANOG in early embryos and

identifies signals other than FGF/ERK signaling that participate in lineage decisions independently of the latter.

Résumé

L'embryon précoce de la souris est un modèle unique de développement régulatif nécessitant un équilibre délicat entre plasticité et différentiation irréversible. En quelques jours seulement, l'œuf fécondé forme un embryon multicellulaire capable de s'attacher au tissu utérin de la mère et de développer des connexions complexes avec celui-ci. Initialement équivalentes, les cellules de l'embryon précoce voient leur potentiel de différentiation se restreindre et s'engagent vers une destinée cellulaire spécifique tout en conservant la capacité de répondre, dans des fenêtres de temps bien définies, aux signaux externes et aux perturbations du développement. Peu avant l'implantation, la masse cellulaire interne (MCI) des blastocystes précoces se différencie en épiblaste (Epi), qui donnera naissance au fœtus, et en endoderme primitif (PrE), à l'origine de tissus extra-embryonnaires. Des études antérieures ont établi qu'un réseau de régulation, impliquant les facteurs de transcription (FTs) NANOG et GATA6 et la signalisation FGF/ERK, contrôle de nombreux aspects de ce processus de différenciation. Cependant, plusieurs questions demeurent quant aux processus biologiques sous-jacents contrôlant la génération des premiers lignages embryonnaires. L'objectif de cette thèse était d'étudier le rôle de la signalisation PI3K/AKT dans le blastocyste, lorsque les cellules Epi, puis PrE, se forment à partir du pool de cellules indifférenciées de la MCI. Mon travail montre que PI3K/AKT est constitutivement actif pendant le développement préimplantatoire et que des variations d'activité entre cellules apparaissent aux stades blastocystes intermédiaires et tardifs. En modulant l'activité de la voie, j'ai pu montrer que l'activité de PI3K/AKT est une condition préalable à la formation de l'Epi, car les FTs spécifiques de l'Epi NANOG et SOX2 sont considérablement diminués et SOX17, un FT du PrE, est activé en absence d'activité PI3K/AKT. J'apporte en outre la preuve que la régulation des niveaux d'expression des FT dans la MCI est, au moins en partie, médiée par GSK3, une cible directe de PI3K/AKT. Le séquençage ARN en cellule unique (scRNAseq) a révélé que l'inhibition de PI3K/AKT induit des changements minimes dans le transcriptome des cellules internes, indiquant que la voie PI3K/AKT régule les niveaux des FTs par des mécanismes post-transcriptionnels. De manière surprenante, j'ai observé une régulation à la hausse de SOX17 lorsque PI3K/AKT est inhibé dans les embryons mutants *Gata6*, ce qui suggère que l'initiation de la différenciation en PrE nécessite la levée de l'inhibition de PI3K/AKT.

En conclusion, ce projet de thèse illustre que PI3K/AKT, une voie souvent associée au contrôle de la survie, de la prolifération et du métabolisme, agit également comme médiateur du destin

cellulaire pendant une période spécifique et limitée du développement précoce de la souris. Nous proposons que PI3K/AKT préserve la pluripotence des progéniteurs Epi en formation en maintenant l'expression de marqueurs clés du lignage tout en empêchant la différenciation vers le PrE. Ainsi, mon travail donne un aperçu nouveau et important de la régulation du FT de pluripotence clé NANOG dans les embryons précoces et identifie des signaux autres que la signalisation FGF/ERK qui participent aux décisions de lignage indépendamment de cette dernière.

Acknowledgements

First, I would like to thank all the members of the jury for their time and consideration. Equally, many thanks to the members of my thesis committee, Claire Chazaud, Jean-Léon Maitre and Catherine Jessus for following my progress over the years. Your scientific advice but also your open ear for discussions about my professional future was highly valued.

Next and most importantly, I would like to express my deep gratitude towards Michel Cohen-Tannoudji, my thesis director, who supervised me during two Master internships and my PhD. Michel, thank you for your guidance, your patience and your trust. You showed me the importance of objectively evaluating my own data which is crucial in a scientific community where the pressure to publish continuously increases. I know that a few grey hair on your head are my fault, with my tendency to say 'no' to new suggestions and my questionable stress management at times. You heard from me 'il y'a un problème' more than anything else but your support always continued. I found a real mentor in you and I hope the next student has the chance to grow as a scientist under your supervision just as I did.

Also, I want to acknowledge all the current and past lab members that I had the honor to work with at Pasteur. Thank you for sharing both successful and frustrating moments during the years, for letting me benefit from your experience and for being good company in and outside of the lab. I want to mention Sylvain here, who supervised me when I joined Pasteur and who introduced me to the beauty of the blastocyst. Also, I also want to thank Pablo who gave me the opportunity to finish my PhD in his unit.

Special thanks to Sandrine who has accompanied my scientific journey in Paris since day one. Sandrine, my PhD wouldn't have been possible without you – I owe you a lot and your value to this lab is exceptional. Thank you for teaching me, for always taking the time when I needed help and for ignoring my mood swings.

Thanks to my friends in Paris, Munich and Freiburg - you all helped me to survive this rollercoaster ride. You made me feel at home when I was lost, you offered a distraction whenever I felt overwhelmed and you reminded me that there's a world outside of this science bubble. I love you all.

Finally, a big thanks to my family and especially my parents. Your unconditional support keeps me going every day and is the source of my motivation and strength. You always trusted my choices and assured me that it is okay to fail - you would be proud of me regardless. I love you with all my heart and I will be forever grateful that you made all this possible.

Table of contents

List of Figures and Tables

Introduction

Introduction

Mammalian preimplantation development is a unique period of embryology which has fascinated scientists since decades. The fact that the early mouse embryo can be relatively easily recovered before implantation and cultured for days under defined conditions makes it a compelling model organism for a variety of biological questions. Despite its simplicity in terms of cell number and developmental pace, an important number of biologically pivotal events and mechanisms are present and at work including genome activation, tissue compaction, lumen formation, polarization, lineage patterning, cell sorting and programmed cell death.

The general concept of how a single zygote develops into a mature blastocyst comprising three distinct lineages has long been described (Figure 1). Still, we are far from fully understanding how distinct cell identities are established through the combination of transcription factor networks and cell signaling. One critical event represents the segregation of the pluripotent epiblast (Epi), deriving the embryo proper, from the extra-embryonic primitive endoderm (PrE), later contributing to the yolk sac, out of a common uncommitted progenitor pool on the third day of pre-implantation development. Although central signals of PrE specification have been identified, our understanding of the mechanisms which are directing Epi fate remains limited.

The following introduction aims to give a brief overview about existing knowledge of mechanisms of Epi and PrE specification and introduce remaining open questions. It will become apparent which critical aspects of Epi formation are still far from being understood and how my PhD project was conceptualized to increase the understanding of this process.

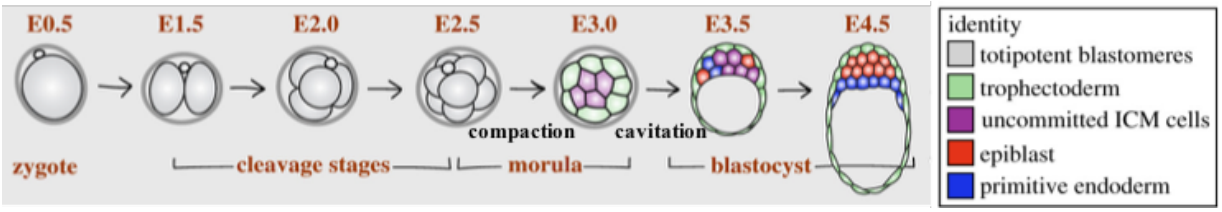

<u>Figure 1:</u> Developmental progression of the early mouse embryo from fertilization to implantation (adapted from Saiz & Hadjantonakis, 2020).

I. Lineage formation in the early embryo

A. From fertilization to the morula stage

1. The first lineage decision

The following subchapter briefly summarizes developmental events preceding the period of Epi/PrE specification which is the scientific focus of this work. Pre-implantation development, which comprises the embryo's journey from the oviduct to the uterus, begins with the fertilization of the mouse oocyte resulting in the formation of the zygote.

At the end of the 1-cell stage, the zygote experiences the first wave of active transcription, also referred to as zygotic genome activation (ZGA). Surrounded by a protective proteinaceous shell, the zona pellucida (ZP), the zygote subsequently undergoes three asynchronous cell divisions to generate eight morphologically identical blastomeres. Next, the blastomeres of the 8-cell stage embryo will flatten to increase their intercellular contacts in a process called compaction. This morphogenetic event transforms the embryo into a more spherical shape and is driven by the actomyosin cortex (Maître et al., 2016). By increasing the surface tension at the apical domain of each blastomere through contraction pulses, a driving force is generated towards the basal side leading to compaction at cell-cell contacts.

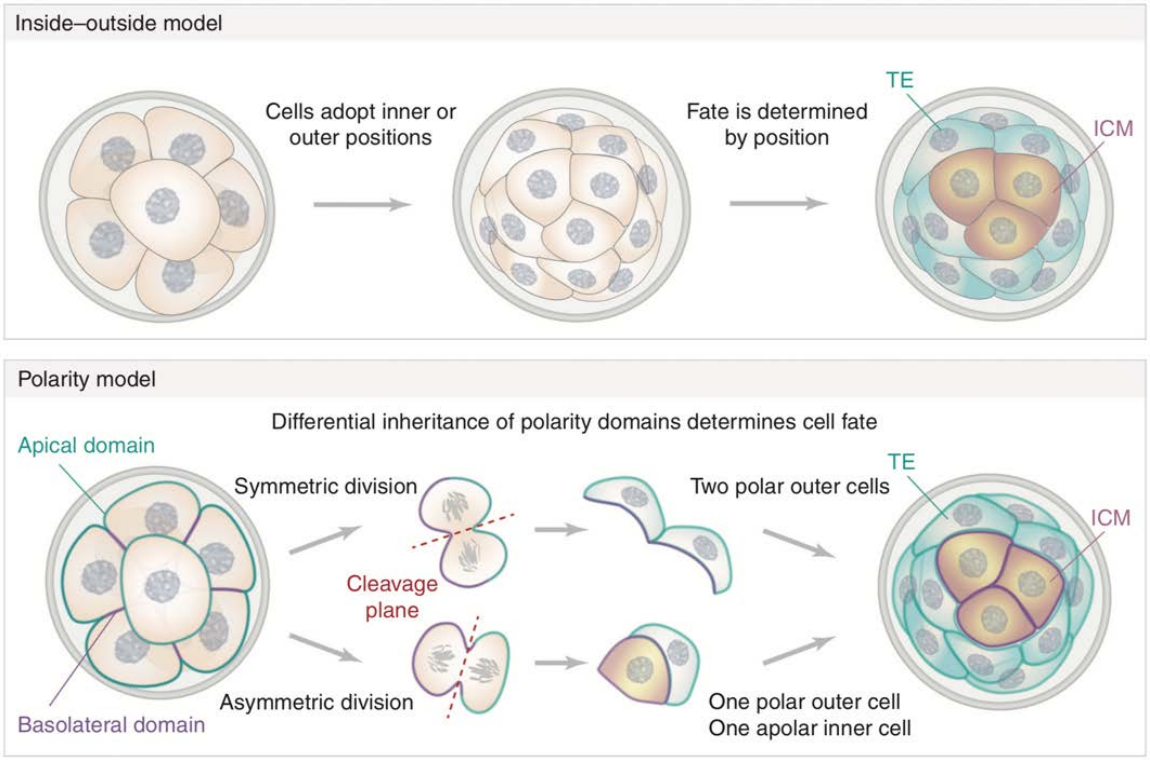

Figure 2: The inside–outside and polarity models of the first lineage decision (White & Plachta, 2020).

With the transition from 8- to 16-cell stage the symmetry of the embryo is broken by the formation of two different cell populations, namely the inner and outer cells. The spatial segregation of these cells is accompanied by the acquisition of distinct cellular identities. While blastomeres positioned inside the embryo at the 16-cell stage will acquire inner cell mass (ICM) fate, cells facing outward will specify towards trophectoderm (TE). Over the years, two models aiming to explain the generation of asymmetry temporally coinciding with the first lineage decision have been proposed (Figure 2). The inside-outside model (Tarkowski & Wróblewska, 1967) hypothesizes that cells sense their position by the extent of their cell-cell contacts and that their fate is determined accordingly at the 16-cell stage. Aggregation experiments revealed that the majority of blastomeres originating from 16-ell stage embryos adjust their fate to the new position, while cells from 32-cell stage embryos tend to relocate to their initial position in aggregates (Suwinska et al., 2008).

In contrast, the cell polarity model (Johnson & Ziomek, 1981a) is based on the discovery of blastomere polarization, thus the presence of polar (outer cell) and apolar (inner cell) cells at the 16-cell stage. The existence of polarity was detected by the accumulation of subcellular components like microvilli, cytoskeletal elements, endosomes, and microtubules on the apical pole (Johnson & Ziomek, 1981b; Johnson & McConnell, 2004). It was proposed that depending on the angle of cell division, cells inherited a distinct amount of polarity determinants during asymmetric cell divisions which in turn defined their position within the embryo. In recent years, the combination of modelled and experimental data revealed that the unequal distribution of the apical domain of blastomeres during asymmetric cell division causes distinct tensions and contractility in daughter cells (Maître et al., 2016). Hence, apolar cells holding higher levels of cortical actomyosin and therefore higher contractility become internalized and contribute to the ICM. This indicates that the apical domain drives symmetry breaking and TE/ICM patterning in the early embryo, thereby revealing a robust self-organizing capacity (Korotkevich et al., 2017; Maître et al., 2016) (Figure 3). It is currently unclear which mechanisms are regulating the formation of the apical domain, however new data suggests the involvement of two actin remodeling factors, Transcription Factor AP-2 Gamma (TFAP2c) and transcriptional activator of TEA Domain family member 4 (TEAD4) (Zhu et al., 2020). Deletion of *Tfap2c* and *Tead4* eliminated expression of essential actin regulators like ezrin and reduced the size of actin clusters which ultimately form the apical domain (Zhu et al., 2020). Still, how exactly ezrin recruitment is facilitated remains to be investigated.

In addition to actomyosin, the cytoskeleton of early embryos is composed of a variety of intermediate filaments, including keratins. Recent analysis showed that keratins are already

heterogeneously expressed at the 8-cell stage and localize in outer blastomeres (Lim et al., 2020). The authors conclude that keratins establish cell polarity before the inner-outer segregation takes place and bias cell fate before the apical domain of cells is unequally distributed during asymmetric cell divisions. However, preimplantation development proceeds normally in the absence of keratins and only results in embryonic lethality around E9.5 due to fragility of trophoblast giant cells (Hesse et al., 2000).

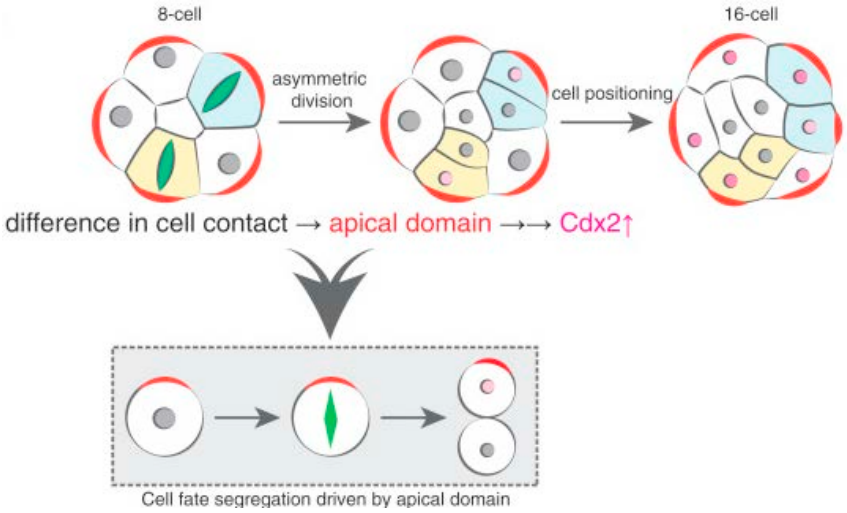

<u>Figure 3:</u> Model of symmetry breaking in mouse development.
The presence of contact-free cell surface in outside cells directs formation of the apical domain that, in turn, induces asymmetric division and TE-fate specification (adopted from Korotkevich et al., 2017).

It appears that in the case of the first cell fate decision morphogenetic movements are upstream of specification. Thus, the position of cells, defined by apicobasal cues, regulates signaling pathways and TF expression which control ICM/TE lineage commitment. The activity of the HIPPO pathway, which is considered to be the key driver of ICM/TE specification, seems to depend on cellular properties. Specifically, cell shape and contractility are linked to the subcellular localization of Yes-Associated Protein 1 (YAP), TEAD4 and member of the HIPPO cascade. While YAP localizes to the nucleus to activate the transcription of key TE markers like Caudal type homeobox 2 (CDX2) and GATA binding protein 3 (GATA3) (Nishioka et al., 2009; Ralston et al., 2010) in polar/outer cells, the phosphorylation by Large Tumor Suppressor (LATS) kinases leads to nuclear extrusion of YAP in apolar ICM cells (Figure 4). Notably, evidence demonstrating a direct response of YAP to mechanical signaling is lacking, thus it remains to be determined if mechanosensing is an important factor in this first event of lineage allocation.

Interestingly, CDX2 expression is not completely abolished in *Tead*$^{-/-}$ embryos, suggesting that its activation does not solely depend on YAP/TEAD (Yagi et al., 2007). Furthermore, the fact that embryos lacking TEAD are incapable of forming TE, raises the question if CDX2 alone governs TE specification. In 2005, Strumpf and colleagues demonstrated that CDX2 is necessary for proper preimplantation development as *Cdx2* mutant

embryos fail to implant. This is probably due to the failure of *Cdx2*$^{-/-}$ embryos to repress NANOG and OCT4 in outer cells which ultimately leads to the death of these cells (Strumpf et al., 2005).

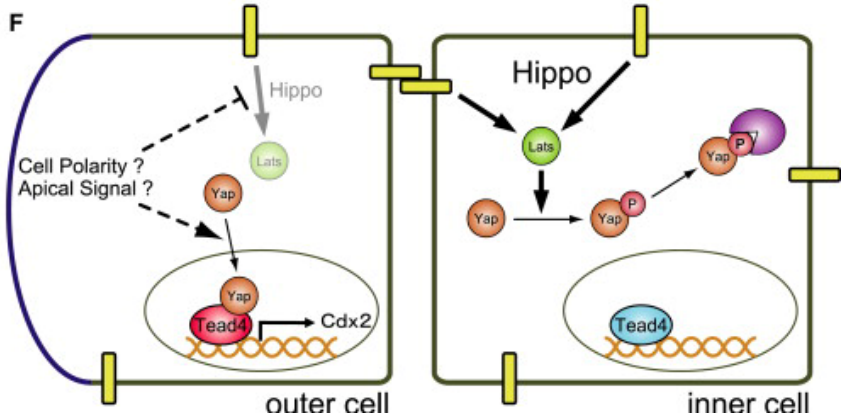

Figure 4: Cell Position Controls Nuclear Localization of Yap (Nishioka et al., 2009).
In inner cells (right), Yap is phosphorylated by Lats and is excluded from the nuclei. Consequently, Tead4 remains inactive and cells adopt an ICM fate. In outer cells (left), lower levels of Yap phosphorylation allow for its nuclear accumulation, which leads to activation of Tead4 and the transcription of TE-specific genes like Cdx2.

Data from *in vitro* cultured TE-like stem cells (see subchapter C) proposed that GATA3 can temporally compensate for loss of CDX2 and is sufficient for TE initiation but not maintenance (Ralston et al., 2010).

In parallel to promoting the expression of TE genes, YAP/TEAD represses SOX2 in TE cells which is one of the major pluripotency TFs (Wicklow et al., 2014). SOX2 represents the first ICM-specific marker by becoming restricted to inner cells as early as the 16-cell stage (see chapter II). Intriguingly, ICM/TE specification normally proceeds in embryos lacking SOX2 suggesting a genetic redundancy with other regulators of ICM fate (Wicklow et al., 2014). To this day, little is known about the mechanisms of ICM specification. Consequently, most of our current knowledge regarding the first lineage decision focuses on the mechanisms of TE specification.

2. The controversy of predetermination versus regulative development

In contrast to other model organisms of developmental biology like *Drosophila melanogaster*, *Caenorhabditis elegans* and *Xenopus laevis*, the mouse embryo does not experience apparent symmetry breaking until the 8-cell stage. Yet, there is an ongoing debate in the field about whether inequality in the totipotency of blastomeres arises during earlier stages of development. With the emergence of single-cell RNA-sequencing, an initial bias in transcriptional signatures between blastomeres could already be detected after the first cleavage at the 2-cell stage and an increase in heterogeneity could be observed until the 16-cell stage (Shi et al., 2015). However, in the opinion of the authors small biases inevitably arise through partitioning error during the first cell division and the increase in transcriptional activity after the ZGA contributes to a continuing cell-to-cell asymmetry until the morula stage. This is consistent with the notion that the ultimate cell fate of a blastomere depends on cell position, cell-cell contacts and cell polarity rather than pre-patterning (Lorthongpanich et al., 2012), although heterogeneities may emerge during the first three cell divisions. Therefore, inequalities on a transcriptional level between blastomeres until the 16-cell stage are likely the consequence of the randomness and stochastic nature of early embryo development.

Rather than transcriptomics, studies supporting the idea of prepatterning are mostly focused on cell history or based on observations on epigenetic levels. In 2005, Piotrowska-Nitsche et al. proposed that cells of a 4-cell stage embryo have distinct developmental potentials based on their spatial origin, thus their ability to form viable chimaeras differs (Piotrowska-Nitsche et al., 2005). However, the spatial origin of the blastomeres was defined based on the position of the second polar body (2PB) which is technically debatable as the ancestral location of the 2PB was never thoroughly examined. Data coming from the same lab illustrated molecular differences between 4-cell stage blastomeres at the levels of H3R26 methylation (Torres-Padilla et al., 2007). They concluded that increased H3R26 methylation levels predispose cells to contribute to the ICM; however, the used techniques prevented further embryo development and thereby lineage tracing.

Furthermore, it was proposed that differences in TF kinetics at the 4-cell stage could induce lineage bias. In one study, the authors injected and photoactivated an OCT4-GFP fusion protein in 4-cell stage blastomeres and measured the nuclear fluorescent intensity over time. They reasoned that in cells showing high intensity fluctuations, OCT4 has a high nuclear import and export rate due to decreased access to DNA binding sites (Plachta et al., 2011). By analyzing cell division patterns, they observed that over 80% of the cells with high OCT4

kinetics undergo symmetric division and become outer cells. Another study demonstrated that the duration of SOX2-DNA interaction varies between blastomeres starting at the 4-cell stage (White et al., 2016). According to their results, SOX2-injected cells that showed long-lived DNA binding have a higher probability to contribute to the pluripotent ICM at the 16-cell stage. However, in both studies the mechanisms which lead to differences in TF-DNA binding dynamics are unclear and it remains to be investigated if duration of binding itself affects fate choice.

Despite reports about early prepatterning, outer cells retain their plasticity until the 32-cell stage (Posfai et al., 2017). In Cdx2-eGFP fusion knock-in embryos the level of eGFP serves as a faithful readout for HIPPO activity and high eGFP correlates with nuclear accumulation of YAP (Posfai et al., 2017). The authors demonstrated that starting from the 16-cell stage eGFP expression gradually increases in outer cells and that Cdx2-eGFP high cells could contribute to the ICM of chimeras until the 32-cell stage (Figure 5). Thus, although inequality between blastomeres on a post-transcriptional level might arise as early as the 4-cell stage, the inner and outer cells of the embryo display a high level of regulative capacity until the 32-cell stage.

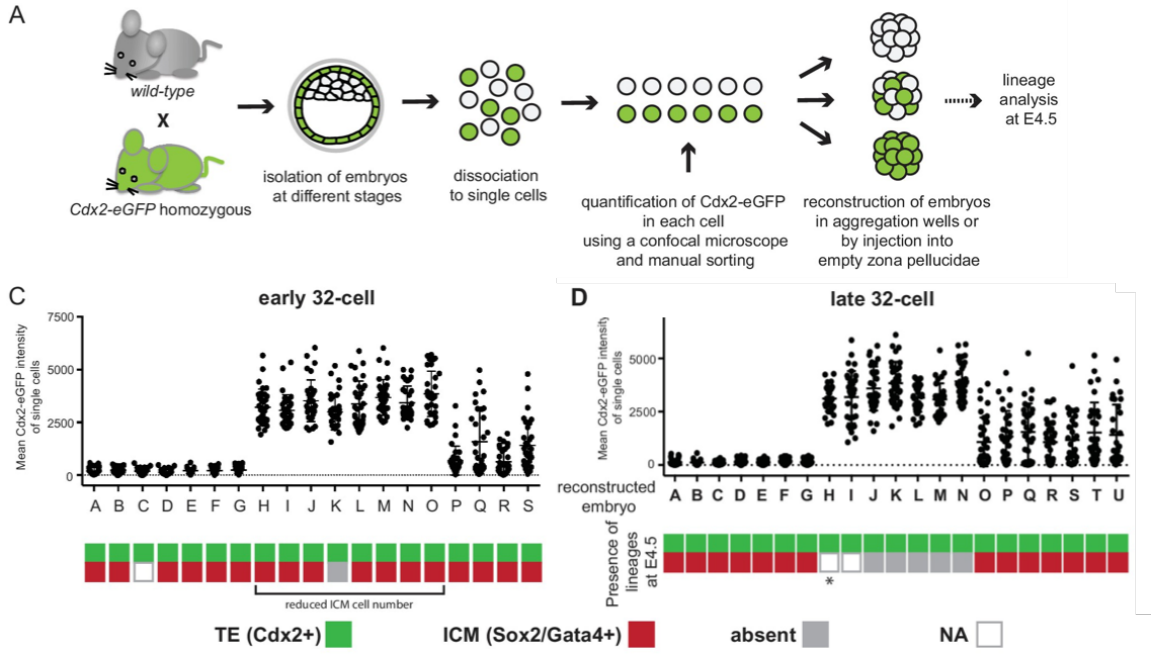

Figure 5: Embryos reconstructed entirely from Cdx2-eGFP high cells lose their potential to recapitulate ICM and TE lineages between early and late 32-cell stage.

(A) Experimental outline to reconstruct embryos entirely of Cdx2-eGFP low, high or random cells. (C-D) Plots showing embryo reconstructions from single cells isolated from (C) early 32 cell and (D) late 32 cell stages. Each embryo (X axis, labeled with letters) was reconstructed from Cdx2-eGFP-quantified (Y axis) single cells. Color-coding below indicates the presence of Cdx2 positive TE (green) and Sox2 or Gata4 positive ICM (red) cells in reconstructed embryos at E4.5. Grey indicates the absence of a lineage; white (N/A) indicates the embryo was lost. (Posfai et al., 2017).

B. The specification of Epi and PrE

1. The central genetic players of Epi/PrE specification

This subchapter describes the central genetic drivers of Epi/PrE specification and introduces the different models about how specification is initiated. In my definition, specification is a process when cells transition from a precursor to a progenitor state and does not necessarily include the commitment to the respective fate.

After the ICM/TE lineage formation and starting at the 32-cell stage, the sherical symmetry of the embryo is broken by the formation of a liquid-filled cavity, called the blastocoel, at the interface between TE and ICM cells. Directional pumping of fluid continuously increases the volume of the cavity and segregates the ICM towards one side of the embryo. A recent study demonstrated that blastocoel formation is initiated by the appearance of microlumen at cell-cell-contacts which fracture once the force generated by the osmotic gradient increases (Dumortier et al., 2019). They also showed that the reason why lumen preferably form at the interface of TE and ICM are differences in cell contractility between the two cell populations.

Coinciding with cavity formation, the embryo undergoes the second cell fate decision during which ICM cells specify towards either Epi or PrE between E3.0 and E3.75 (~32- to 64-cell stage). Before the discovery of Epi/PrE lineage markers, the mechanisms of this 24h long specification process were quite obscure. Only after specification, when Epi and PrE cells undergo a process of cell sorting to form two spatially distinct compartments within the embryo, morphological differences between the lineages do become apparent. Following the inside-outside hypothesis of ICM/TE formation, cell position was thought to be the main driver of the second cell fate decision as well (Rossant, 1975). However, with the development of lineage-specific markers it became clear that ICM cells do not form a layer of PrE at the roof of the cavity.

The earliest markers of Epi and PrE to be present in the embryo are the transcription factors NANOG and GATA binding protein 6 (GATA6), respectively, which start to be expressed at the 8-cell stage (Chazaud et al., 2006; Kurimoto et al., 2006). After initially being co-expressed in all blastomeres, they gradually become restricted to either Epi or PrE progenitors during the course of specification (Guo et al., 2010; Plusa et al., 2008). This unique distribution of mutually exclusive NANOG and GATA6 in the ICM of the blastocyst is often referred to as the ‘salt and pepper’ expression pattern (Chazaud et al., 2006). Epi/PrE

specification proceeds asynchronously, with Epi progenitors being established first (Bessonnard et al., 2014; Bessonnard et al., 2017; Gerbe et al., 2008; Plusa et al., 2008; Saiz et al., 2016). ICM cells show a high variability in the protein levels of either NANOG or GATA6, suggesting that the loss of one marker rather than the increase of another is determining cell fate (Bessonnard et al., 2014; Guo et al., 2010). In this thesis, Epi cells are defined as NANOG+/GATA6-, PrE cells as NANOG-/GATA6+ and co-expressing cells when expression of both markers is visible.

The characterization of *Nanog* and *Gata6* mutants revealed that both genes function as master regulators of the Epi and PrE lineage, respectively. While in *Nanog* mutants all cells exclusively express GATA6 (Frankenberg et al., 2011), the ICM of *Gata6* mutants becomes entirely NANOG-positive (Bessonnard et al., 2014; Schrode et al., 2014). Interestingly, Epi is established earlier in *Gata6* heterozygous embryos, while PrE progenitors are formed delayed and in reduced number. This dose-sensitive phenotype might be the consequence of an underlying NANOG/GATA6 antagonism; however, the deletion of one *Nanog* allele does not change Epi/PrE ratios in early embryos (Miyanari & Torres-Padilla, 2012).

In addition to NANOG and GATA6, the morphogen FGF4 has a central role in the establishment of the salt and pepper pattern. *Fgf4* is the first ICM marker to become heterogeneously expressed at E3.25 by specifically becoming upregulated in prospective Epi precursors (Guo et al., 2010; Kurimoto et al., 2006; Ohnishi et al., 2014) and is absent in *Nanog* mutant embryo (Frankenberg et al., 2011). Blocking FGF signaling by pharmacological inhibitors or knocking out different cascade nodes like *Grb2, Fgf4 or Fgf1/2* induces Epi fate in all ICM cells (Chazaud et al., 2006; Kang et al., 2013; Krawchuk et al., 2013; Nichols et al., 2009; Yamanaka et al., 2010), while the activation of FGF signaling by adding recombinant FGF4 to the embryonic culture leads to an ICM solely composed of PrE-like cells (Yamanaka et al., 2010). The analysis of *Fgf4* mutant embryos revealed that GATA6 persists until the early blastocyst stage and that NANOG levels are slightly increased (Kang et al., 2013; Krawchuk et al., 2013). Additional experiments demonstrated that excess of FGF4 inhibits NANOG independently of GATA6 (Bessonnard et al., 2014) and GATA6 inhibition in the absence of FGF signaling does not require NANOG (Frankenberg et al., 2011).

Mathematical modelling has provided insights in how the formation of Epi and PrE progenitors could be achieved by a gene regulatory network (GRN) composed of NANOG, GATA6 and FGF4 (Bessonnard et al., 2014; Tosenberger et al., 2017) (Figure 6). As defined parameters the mutual inhibition of NANOG and GATA6 as well as the promotion of GATA6 and inhibition of NANOG expression by FGF signaling were set. The model predicted that

molecular noise initiates Epi specification, which is represented by the promotion of NANOG in a few ICM cells and the consecutive upregulation of *Fgf4*. Consequently, locally increased FGF4 concentrations lead to the induction of PrE fate in Epi-surrounding cells which can account for the asynchronous progression of Epi/PrE lineage formation. Despite the fact that the model accurately replicated *in vivo* observations, it remains unclear if in fact noise causes the differences in ICM cells which ultimately trigger the conversion of a precursor cell into an Epi progenitor. The hypotheses regarding the mechanisms of Epi initiation are discussed below.

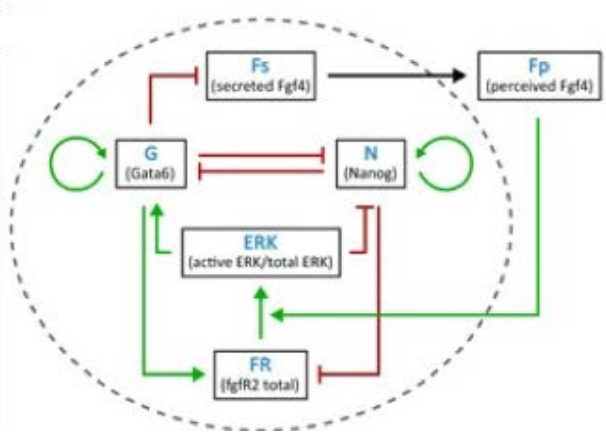

Figure 6: Gene regulatory networks orchestrating Epi/PrE specification in the ICM.
Schematic representation of the GRN describing the interactions between the TFs Nanog and Gata6 , together with the interplay between these factors, secreted Fgf4 and Fgfr2 (adopted from (Tosenberger et al., 2017)).

2. The origin and plasticity of Epi/PrE cells

As for the first cell fate decision, the field is in debate if ICM cells which are generated during two successive and asymmetric cell divisions between the 8- to 32-cell stage underlie prepatterning. Based on cell tracking experiments between morula and late blastocyst stage, it was proposed that cells which are internalized during the first wave of cell division carry a bias towards Epi, while inner cells resulting from the second one have an increased probability to become PrE (Morris et al., 2010). This idea was challenged by a study from Yamanaka et al., which followed the contribution of first and second wave cells to Epi and PrE until post-implantation stages (Yamanaka et al., 2010). Their observations state that both rounds of cell divisions give rise to progenitors of Epi and PrE in an unbiased and stochastic manner. Accordingly, the analysis of single-cell qPCR data does not reveal any clustering within the ICM making lineage precursors undistinguishable before late blastocyst stage (Ohnishi et al., 2014). This coincides with the finding that although the majority of ICM cells is specified at E3.75, a proportion of blastomeres retains the plasticity to change their identity (Grabarek et al., 2012; Yamanaka et al., 2010). Transplantation experiments revealed that inner cell plasticity is maintained until ~E4.0, with Epi progenitors being restricted earlier than PrE cells (Grabarek et al., 2012). In conclusion, even though a lineage bias could theoretically be

present in the ICM immediately after the first lineage decision, additional mechanisms are required for full lineage commitment.

3. Potential mechanisms of Epi initiation

In contrast to the first cell fate decision, cell position or polarity is unlikely to be the major driver of Epi/PrE specification. The early onset of lineage transcription factors expression and subsequent acquisition of cell fate in a salt and pepper fashion (Chazaud et al., 2006) strongly suggests that cell-to-cell heterogeneities promoting Epi/PrE lineage segregation depend on other factors than solely positional constraints. Ultimate evidence is lacking but three models aiming to explain the mechanism of Epi induction have been proposed. The first one hypothesizes that the reduction of ERK activity in a few ICM cells is sufficient to enable the specification towards Epi fate (Bessonnard et al., 2014). Indeed, when embryos are cultured in the presence of a MEK inhibitor during a prolonged duration which includes the period of Epi/PrE specification (E2.5 to E3.75 or E4.5), all ICM cells adopt an Epi-like fate (Bessonnard et al., 2014; Saiz et al., 2016). However, when the treatment is limited to the early phase of specification (E2.75 to E3.25), the ICM of these embryos is composed of both Epi-like and coexpressing cells (Bessonnard et al., 2017; Saiz et al., 2016) (Figure 7). Therefore, despite the absence of ERK signaling, the conversion of the whole ICM towards an Epi-like state is incomplete and cells harboring bipotential remain. This suggests that other factors in addition to the decrease of ERK activity are required to trigger Epi lineage formation.

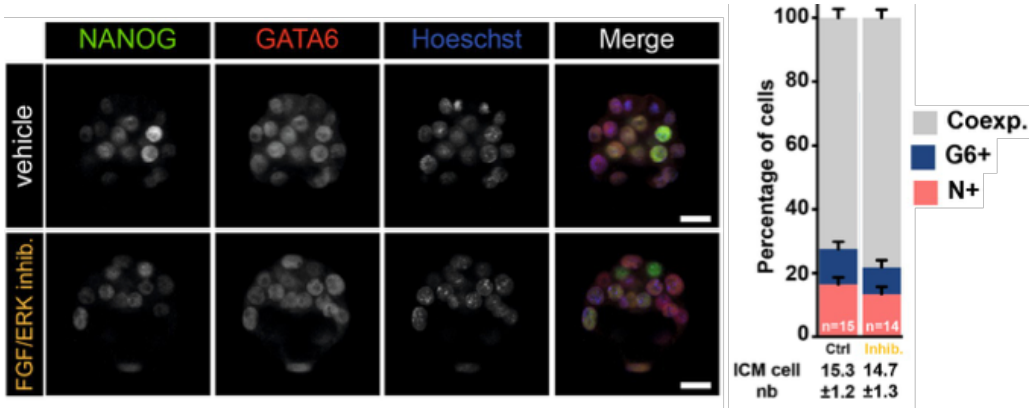

Figure 7: Modulation of FGF/ERK signaling during early specification (Bessonnard et al., 2017).
Immunodetection of NANOG (green) and GATA6 (red) in embryos cultured from E2.75 to E3.25 with or withour FGF/ERK inhibitor and distribution of ICM cells expressing NANOG (N+, red), GATA6 (G6+, blue) or both markers (Coexp., grey). Pictures correspond to a projection of 5 confocal optical slices. Scale bar: 20 µm. Error bars indicate SEM. n, number of embryos analyzed.

The second theory proposes that the establishment of Epi progenitors is a stochastic process facilitated by transcriptional noise in a few ICM cells that ultimately skews NANOG/GATA6 ratios (Ohnishi et al., 2014). However, the simulation of random transcriptional noise in a mathematical model could not replicate events of specification as they are observed *in vivo* indicating that the initiation of Epi rather underlies tightly regulated mechanisms (De Mot et al., 2016). Interestingly, NANOG starts to be heterogeneously expressed as early as the 16-cell stage (Dietrich & Hiiragi, 2007) and correlates with a set of TFs at the 32-cell stage that could collectively induce *Fgf4* (Allègre et al., 2019). Still, if this Epi-fate driving cluster of genes is a result of stochasticity is not clear.

The third model states that the acquisition of either Epi or PrE cell identity is potentially connected to cell history (Chisholm & Houliston, 1987; Krupa et al., 2014; Mihajlovic et al., 2015; Morris et al., 2013). Analysis of the distribution of cytokeratin filaments, which are characteristic for extraembryonic lineages, showed that inner cells generated during the first cell division (8- to 16-cell stage) lose these filaments while cells arising from the second cell division (16- to 32-cell stage) maintain their expression (Chisholm & Houliston, 1987). The authors hypothesized that the acquisition of Epi fate, which implies the reduction of cytokeratins, depends on the duration spent on an inner position and that consequently cells which are produced later during the second round of cleavage specify towards PrE. Going in the same direction, two following studies postulated that Epi and PrE precursors inherit distinct cellular competences during the two consecutive cell divisions between the 8- and 32-cell stage. They stated that ICM cells generated during the first cell division (8- to 16-cell stage) express lower levels of *Fgfr2* and slightly elevated *Fgf4* in comparison to cells which arise during the transition from 16- to 32-cell stage and this could impact their responsiveness to developmental signals (Morris et al., 2013; Krupa et al., 2014). However, *Fgfr2* mutant embryos show a relatively mild phenotype during Epi/PrE specification, making FGFR2 a rather unlikely candidate to induce cell fate bias (Kang et al., 2017; Molotkov et al., 2017). It also contradicts another study demonstrating that cell identity could not be correlated to cell origin in tracing experiments following the fate of cells generated through the first and second wave of inner cell formation (Yamanaka et al., 2010). Hence, although the timing when inner cells are produced may be a contributing factor in cell fate allocation, other mechanisms appear to be required.

Rather than being an active process, Epi specification could imply the prevention of differentiation and maintenance of a pluripotent state. Potential mechanisms in order to protect Epi identity while promoting PrE fate by FGF4 section will be discussed below. Even if Epi is

considered as a default state, the source of heterogeneities allowing Epi/PrE segregation remains an open question.

4. Cell sorting and survival

Following Epi/PrE specification, the cells of the ICM sort into two spatially distinct populations within the embryo leading to a separation of the Epi from the cavity by a layer of PrE cells. Simultaneously, potentially defective cells are removed from the embryo by selective apoptosis. It has recently been shown that the elimination of specified Epi cells is mediated in a TEAD-YAP dependent manner (Hashimoto & Sasaki, 2019). Strikingly, YAP has been shown to accumulate in the nuclei of ICM cells starting at the mid blastocyst stage and finally restrict to SOX2-positive Epi cells after specification, suggesting that TEAD activity gradually increased during the formation of Epi (Hashimoto & Sasaki, 2019). By creating wildtype *Yap1*$^{-/-}$ mosaic embryos which have reduced TEAD activity, the authors provided evidence that Epi cells with lower TEAD activity are eliminated by caspase-dependent apoptosis (Hashimoto & Sasaki, 2019). Thus, differences in TEAD activity between Epi cells induces cell competition to exclusively maintain cells with high levels of TEAD. Furthermore, several signals that are important for PrE propagation have also been shown to be essential for lineage survival. In 2010, Artus et al. demonstrated that loss of *Platelet Derived Growth Factor Receptor alpha (Pdgfra)*, which is an early marker of PrE progenitors, led to a reduced number of PrE cells in implanting embryos while sorting remained unaffected (Artus et al., 2010). It could later be shown that PDGF regulates PrE survival through its downstream targets PI3K/mTOR and that an increase in PI3K/mTOR inhibitors also causes Epi cells to undergo apoptosis (Bessonnard et al., 2019) (Figure 8). Similarly, maternal/zygotic inactivation of *Stat3* in early embryos caused cell death in ICM but not TE cells after Epi/PrE specification, indicating the temporal requirement of JAK/STAT signaling for cell survival (Do et al., 2013). However, treatment of embryos with a JAK inhibitor during the period of cell sorting could not replicate these results (Bessonnard et al., 2019).

Although the mechanisms underlying the rearrangement of Epi and PrE are not fully understood, the migration of PrE has been shown to be actin-dependent (Meilhac et al., 2009) and to be terminated once PrE cells reach the surface between ICM and cavity (Plusa et al., 2008). The contact with the cavity leads to PrE polarization induced by the accumulation of LRP2 and DAB2 at the apical surface of PrE cells (Gerbe et al., 2008). Conversely, PrE cells which remain deeper in the ICM ultimately lose *Pdgfra* expression or undergo apoptosis (Plusa

et al., 2008). Several studies have proposed that the distinct adhesion properties of Epi and PrE could be the driving forces behind this cell sorting process (Chazaud et al., 2006; Plusa et al., 2008; Gerbe et al., 2008), but further evidence is required to substantiate this theory.

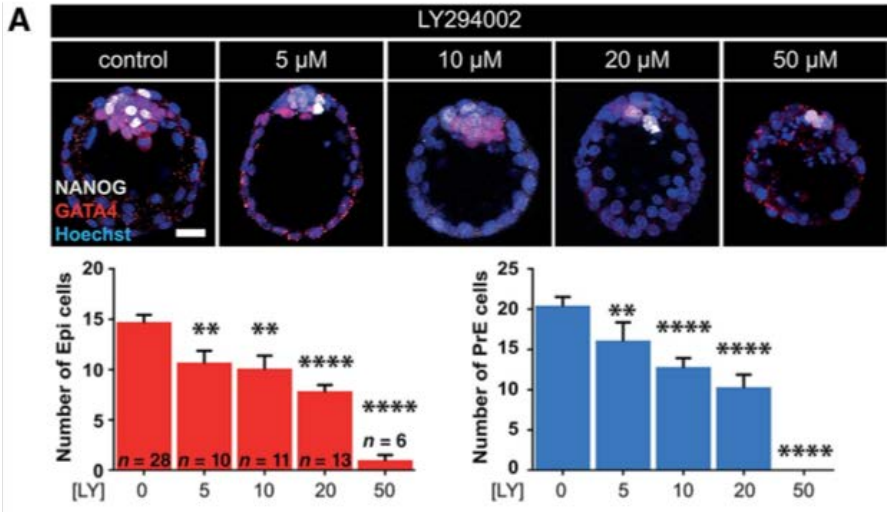

Figure 8: PI3K mediates inner cell mass cell survival (Bessonnard et al., 2019).
(A) Wild-type CD1 embryos were cultured from E3.75 to E4.5 in presence or absence of LY29402. Number of NANOG-positive (gray) and GATA4-positive or GATA6-positive (red) cells were quantified. Pictures correspond to a projection of five confocal optical slices. Scale bar: 20 µm. Error bars indicate SEM. *n*, number of embryos analyzed. Statistical Mann–Whitney tests are indicated when significant (**, $p < .01$; ***, ****, $p < .0001$).

C. *In vitro* approaches to study embryonic lineages

Depending on the scientific question the use of early mouse embryos as a research model can represent various challenges. The scarcity of material as well as the limitations of embryonic culture often require the application of alternative systems like *in vitro* stem cell models. In contrast to embryos, stem cells can be amplified, indefinitely cultured and the establishment of genetically modified lineages is less time consuming. Due to these technical advantages as well as ethical considerations, the derivation and utilization of different stem cell types can be favorable in many contexts, including in studies addressing mechanisms of cell fate specification. However, stem cells remain a cellular proxy - they can mimic many developmental states and processes but can currently not completely substitute the embryo as model organism. I will briefly introduce the stem cell lines that are derived from the early mouse embryo as they are commonly referred to in the consulted literature.

1. TS cells as a proxy for the TE lineage

In the embryo, the TE constitutes a one-cell epithelial layer encapsulating the ICM and the blastocoel which will mediate the implantation into the uterine tissue. Polar TE which is in contact with the ICM differentiates into extraembryonic ectoderm (ExE), the ectoplacental cone (EPC), and secondary giant cells, while the mural TE surrounding the cavity gives rise to non-proliferating primary trophoblast giant cells (TGCs). Trophoblast stem (TS) cells represent the TE lineage of the embryo and are derived from postimplantation stage E6.5-E8.5 (Tanaka et al., 1998). Like the embryonic TE, they exhibit an epithelial-like morphology and have a similar transcriptomic profile. When injected into blastocysts, TS cells contribute to the TE and its derivatives. However, the contribution to the different types of TE derivatives varies, indicating certain limits of developmental potential (Tanaka et al., 1998). Similarly, when differentiation of TS cells is induced *in vitro* by the absence of growth factors, they primarily differentiate into TGGs. To maintain TS cells, FGF4 which is secreted by Epi *in vivo* is added to the medium and they are co-cultured with fibroblasts. The signals needed to promote self-renewal and prevent differentiation of TS cells are transforming growth factor β (TGFβ), as well as Activin and Nodal (Erlebacher et al., 2004; Guzman-Ayala et al., 2004; Ma et al., 2001). Key transcriptional regulators of embryonic TE like *Gata3*, *Eomes* and *Tcfap2c* are equally important for TS cell maintenance *in vitro* and are sufficient to reprogram fibroblast into induced TS cells (Benchetrit et al., 2015).

2. Embryonic stem (ES) cells representing the Epi lineage

The Epi is characterized by the ability to give rise to the embryo proper, including the three germ layers but also some extra-embryonic lineages like the yolk sac mesoderm. The derivation of ES cells from different developmental stages allows to mimic distinct stages of Epi maturation and pluripotency states.

2.1 Naive ES cells

Naive mouse (mES) ES cells representing the preimplantation Epi of E4.5 stage embryos (Boroviak et al., 2015) were successfully derived from preimplantation embryos by seeding ICMs on embryonic feeder cells in the presence of serum (Evans & Kaufman, 1981; Martin, 1981). They displayed unlimited self-renewal capacity, preferably contributed to the host Epi when injected into blastocyst and grew into teratocarcinomas when grafted in adult mice. Changing the composition of the medium highly benefited the culture efficiency and allowed the derivation of a variety of genetic backgrounds. In the absence of feeders, naive ES cells can be maintained under serum/Leukemia Inhibitory Factor (LIF) conditions. LIF has been shown to promote pluripotency by activating the canonical JAK/STAT pathway (A. G. Smith et al., 1988). Conversely, the inactivation of STAT3, a member of the JAK/STAT cascade, or c-Myc, a target gene of STAT3, leads to loss of pluripotency and differentiation. Interestingly, LIF signaling is not required for maintaining Epi *in vivo* or embryo development in general, but leads to infertility (Stewart et al., 1992).

Alternatively, naive ES cells can be cultured in the combination of LIF and a two inhibitor (2i) cocktail. 2i blocks the MAPK/ERK pathway, a known driver of differentiation, by inhibiting MEK activity and indirectly stimulates WNT activity, known for maintaining self-renewal, by inhibiting its antagonist GSK-3 (Buehr et al., 2008; Ying et al., 2008).

Although many genes expressed in the preimplantation Epi are also expressed in naive ES cells, their role in maintaining pluripotent identity can differ in these systems. *Oct4* and *Sox2* mutant embryos fail to maintain Epi after Epi/PrE specification (Frum et al., 2013; Nichols et al., 1998; Wicklow et al., 2014) and naive ES cells differentiate in absence of *Oct4* or *Sox2* (Mitsui et al., 2003; Niwa et al., 2009). However, while embryos deficient for *Nanog* fail to maintain an ICM and die around E5.5 (Mitsui et al., 2003), deletion of *Nanog* in ES cells does not affect self-renewal but rather biases the cells towards differentiation (Chambers et al., 2007). Conversely, while *Tbx3* and *Esrrb* are essential to maintain pluripotency *in vitro*, they are not required for Epi development during preimplantation (Davenport et al., 2003; Luo et

al., 1997). Thus, despite the similarities in TF patterns and signaling cues between naive ES cells and preimplantation Epi, the regulating mechanisms show significant differences. Interestingly, the efficiency to derive naive ES cell colonies from single cells of preimplantation embryos before E4.5 is significantly lower (Boroviak et al., 2014). In fact, while approximately 50% of the Epi cells isolated from E4.5 could give rise to ES cell lines, single cells from E3.25-E3.5 embryos rarely formed colonies in 2i/LIF conditions on gelatin (Boroviak et al., 2014). The fact that the capacity to generate ES cell lines was restored when withdrawing the MEK/ERK inhibitor or by providing an extracellular matrix, suggests that early ICM cells need to acquire Epi identity before efficiently forming colonies. The authors hypothesize that laminin and downstream signaling PI3K could drive the transition from unspecified ICM to Epi. Remarkably, embryos deficient for laminin show defects in Epi/PrE segregation and die at E5.5 (Smyth et al., 1999). Thus, to this day there is no *in vitro* model resembling an ICM-like state.

2.2 Primed ES cells

Epiblast stem cells (EpiSCs) derived from the Epi of E5.5 to E8.0 stage embryos are considered to be in a primed pluripotent state and serve as a proxy for post-implantation Epi (Brons et al., 2007; Tesar et al., 2007). EpiSCs maintenance requires FGF2 and ACTIVIN A which has similar signaling properties as NODAL. Both in EpiSCs and in post-implantation Epi, *Activin A/Nodal* prevent neural differentiation and maintain NANOG (Camus et al., 2006; Mesnard et al., 2006; Vallier et al., 2009). Similar to the post-implantation Epi, EpiSCs do not express markers of naive pluripotency like *Rex1, Klf4* and *Fgf4* but express genes linked to primed identity like *Pou3f1/Oct6, Fgf5* and *Otx2* (Brons et al., 2007). In contrast to the post-implantation Epi, EpiSCs maintain *Nanog*, although NANOG levels are reduced in comparison to naive ES cells (Guo et al., 2009).

The comparison of EpiSCs isolated at different timepoints between E5.5 to E8.0 revealed that transcriptionally and functionally they all resemble late-gastrulation stage embryos (Kojima et al., 2014) and have therefore limited potential to study germ layer specification. It has previously been shown that the transition from naive to primed pluripotency can be achieved *in vitro* by culturing naive ES cells in EpiSC medium (Guo et al., 2009).
Notably, human embryo-derived ES (hES) cells closely resemble EpiSCs in morphology and equally require FGF2 and ACTIVIN A/NODAL to remain in an undifferentiated state. Like EpiSCs, hES cells are in a primed pluripotent state.

3. Extraembryonic endoderm (ExEn) stem cells representing the PrE lineage

3.1 Embryo-derived XEN cells

The first PrE-derived stem cells were named eXtraembryonic ENdoderm (XEN) cells and since serve as a model for the PrE and its derivatives, the visceral endoderm (VE) and parietal endoderm (PE) (Kunath et al., 2005). Initially, the derivation of XEN was performed using similar culture conditions as for TS or ES cells. ICMs or whole blastocyst were plated on a layer of fibroblasts and cultured in a medium containing FGF4 and LIF. Once XEN outgrowths are formed in a FGF4-ERK-dependent manner, they can be maintained in a simple serum-containing medium without feeders or growth factors. XEN cells represent the post-implantation PrE and despite expressing markers of both VE and PE, XEN cells preferentially contribute to PE when injected into blastocyst (Kunath et al., 2005). Very recently, Ohinata and colleagues reported the derivation of primitive endoderm stem cells (PrESCs) which display properties of the preimplantation E4.5 PrE (Ohinata et al., 2022). By culturing PrE-derived cells from blastocysts under serum free conditions with a high dosage of CHIR and addition of FGF4 and PDGFRa, they established PrE derivates of an earlier stage than XEN cells.

3.2 Induced XEN (iXEN) cells

A straightforward approach to obtain XEN-like cells is to convert ES cells by inducing ectopic expression of *Gata4* or *Gata6* (Fujikura et al., 2002; Shimosato et al., 2007). Overexpression of one of these GATA factors is sufficient to achieve similar molecular and functional characteristics like embryo-derived XEN cells, including the ability to contribute to PrE lineages in chimeras (Shimosato et al., 2007). Interestingly, ectopic expression of GATA factors leads to an upregulation of endogenous *Gata4* or *Gata6* and consequently endogenous GATA6 activates the PrE genes Sox17 and Sox7 (Niakan et al., 2010; Shimosato et al., 2007). Similarly, the transient expression of *Sox17* transforms ES cells into a XEN-like state by binding and activating other PrE-genes like *Gata4* and *Gata6* (Niakan et al., 2010). SOX17 also binds to *Nanog*, *Sox2* and *Oct4* to repress pluripotency.

3.3 Growth factor induced XEN-like cells

Another way to establish XEN-like cells is to add the growth factors retinoic acid (RA) and ACTIVIN A to mES culture inducing stable XEN (cXEN) cells (Cho et al., 2012). cXEN cells highly resemble iXEN on a morphological and transcriptional level and like embryo-derived XEN cells differentiate towards VE in response to BMP4 (Artus et al., 2012; Cho et al., 2012). The adaption of the mES conversion protocol by growth factors allowed the derivation of naive endoderm (nEnd) cells which resembles the preimplantation state of PrE (Anderson et al., 2017). By using ACTIVIN A and WNT3, nEnd cells express PrE markers like *Gata6, Pdgfra* and *Sox7* on a similar level like embryo-derived XEN cells but retain low levels of pluripotency genes like *Oct4* and *Esrrb* (Anderson et al., 2017).

3.4 Using XEN-like cells to model Epi/PrE specification

In order to model Epi/PrE specification which implicates the transition from a NANOG/GATA6 coexpressing towards a mutually exclusive expression state *in vitro*, Schroeter and colleagues used doxycycline-inducible system to transiently express GATA6-FLAG in mES cells (Raina et al., 2021; Schröter et al., 2015). A 6h pulse of doxycycline resulted in the coexpression of inducible GATA6-FLAG and NANOG in individual cells and while exogenous GATA6-FLAG was downregulated after 24h, some cells were shown to activate GATA4 while downregulating NANOG (Figure 9). By using doxycycline-inducible GATA4 the number of GATA4+/NANOG- cells could be increased and the induction of GATA4 above a certain threshold stabilized this mutually exclusive cell state in an irreversible manner. The PrE-like differentiation of mES cells by GATA4 pulses proceeded in a FGF/ERK-dependent manner. Interestingly, the inhibition of ERK signaling prior to doxycycline treatment increased the efficiency of GATA4 induction, suggesting distinct requirements of ERK signaling before and after PrE-like differentiation.

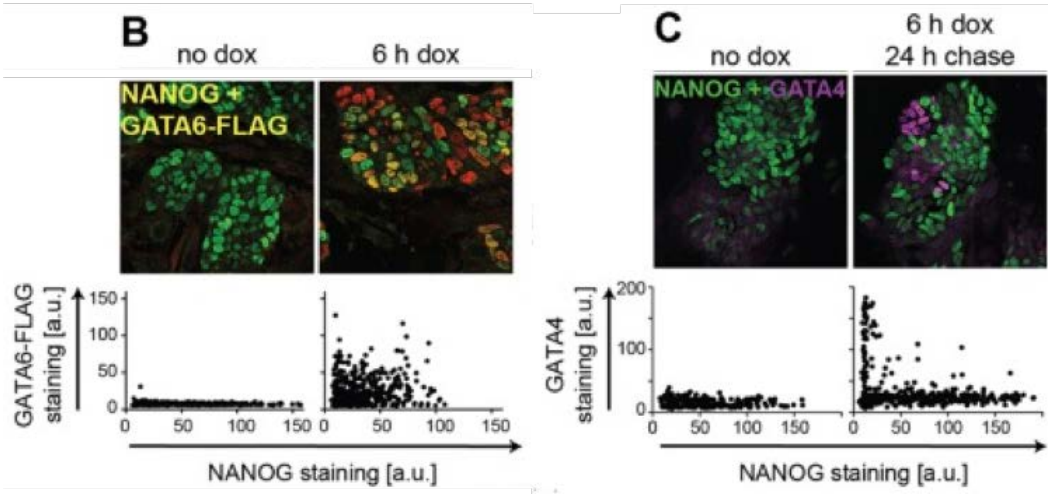

<u>Figure 9:</u> Induced transgene expression creates TF patterning similar to the situation in ICM (Schröter et al., 2015).

(B) Immunostaining (upper panel) and quantification (lower panel) of untreated (left) or doxycycline-treated (right) inducible ESCs indicates co-expression of NANOG and GATA6-FLAG in individual cells after 6 h of doxycycline treatment. Co-expression is limited because of heterogeneous NANOG and GATA6-FLAG expression in the presence of serum and feeders. (C) Immunostaining (upper panels) and quantification (lower panels) of NANOG and GATA4 expression 24h after the end of a 6h doxycycline pulse. GATA4 expression depends on doxycycline treatment, and is mutually exclusive with NANOG expression.

II. Regulation of lineage-specific TFs involved in Epi/PrE specification

A. Mechanisms controlling Epi-associated TFs

In this subchapter I am briefly introducing the three naive pluripotency TF NANOG, OCT4 and SOX2. The focus lies on them, as the deletion of these genes leads to early embryonic lethality and disrupts Epi/PrE specification.

1. NANOG

Our knowledge about NANOG regulation during preimplantation development is currently limited and mechanisms of NANOG initiation around the 8-cell stage remain obscure. The following paragraph therefore mostly focuses on data acquired in mES cells *in vitro.*

The discovery of divergent homeobox domain protein NANOG goes back to a study from Chambers and colleagues when they showed that *Nanog* has the ability to maintain pluripotency in ES cells in the absence of LIF (Chambers et al., 2003). Inactivation of *Nanog* causes loss of pluripotency and differentiation of ES cells, whereas embryos deficient for *Nanog* fail to maintain ICM cells and are dying during per-implantation around E5.5 (Mitsui et al., 2003).

Despite causing an early and lethal phenotype in embryos, the persistent expression of pluripotency genes including *Oct4* in *Nanog* null ES cells (Mitsui et al., 2003) suggested that *Nanog* is not essential for the maintenance of pluripotency *in vitro*. Indeed, conditional knockout of *Nanog* predisposes ES cells to differentiate but does not affect their ability to self-renew (Chambers et al., 2007). Also, *Nanog* null ES cells successfully contribute to all germ layers of chimeras, however the maturation of primordial germ cells is defective. Interestingly, the depletion of only one *Nanog* allele leads to the differentiation of ES cells into derivatives of the three germ layers (Hatano et al., 2005). These results suggest that *Nanog* is a gatekeeper of naive pluripotency by preventing multilineage differentiation *in vitro* and promoting ICM formation as well as germline development *in vivo*. In fact, at the time of implantation when Epi cells transition from a naive state to primed pluripotency, NANOG starts to be downregulated (Ohnishi et al., 2014).

Nanog has been shown to be regulated by multiple TFs and signaling pathways in ES cells. For instance, TCF3 and p53 have been shown to repress NANOG by binding to promoter regions (Lin et al., 2005; Pereira et al., 2006), while binding of OCT4-SOX2 promotes NANOG expression (Rodda et al., 2005). Although *Nanog* overexpression can circumvent the requirement of LIF/STAT3 for self-renewal in ES cells (Chambers et al., 2003), LIF signaling

can act upstream of NANOG in order to activate expression by upregulating *Tbx3* via the PI3K/AKT pathway (Niwa et al., 2009). Blocking PI3K signaling, either by using the PI3K inhibitor LY294002 or by expressing a dominant negative form of the p85 regulatory subunit of class I PI3K (Δp85), significantly reduces NANOG in ES cells (Storm et al., 2007) (Figure 10A-B). The authors postulate that NANOG regulation by the PI3K pathway is likely mediated by glycogen synthase kinase 3 (GSK3), which is a negatively regulated substrate of the PI3K/AKT axis. Indeed, expression of constitutively active GSK-3β S9A which can no longer be inhibited by PI3K/AKT-mediated phosphorylation phenocopies the reduction of NANOG seen by PI3K inhibition (Storm et al., 2007) (Figure 10C). Notably, the inhibitory cocktail 2i used for ES cell culture contains GSK3 inhibitor CHIR99021 which prevents blocking canonical WNT signaling activity through stabilization of β-catenin (Ying et al., 2008).

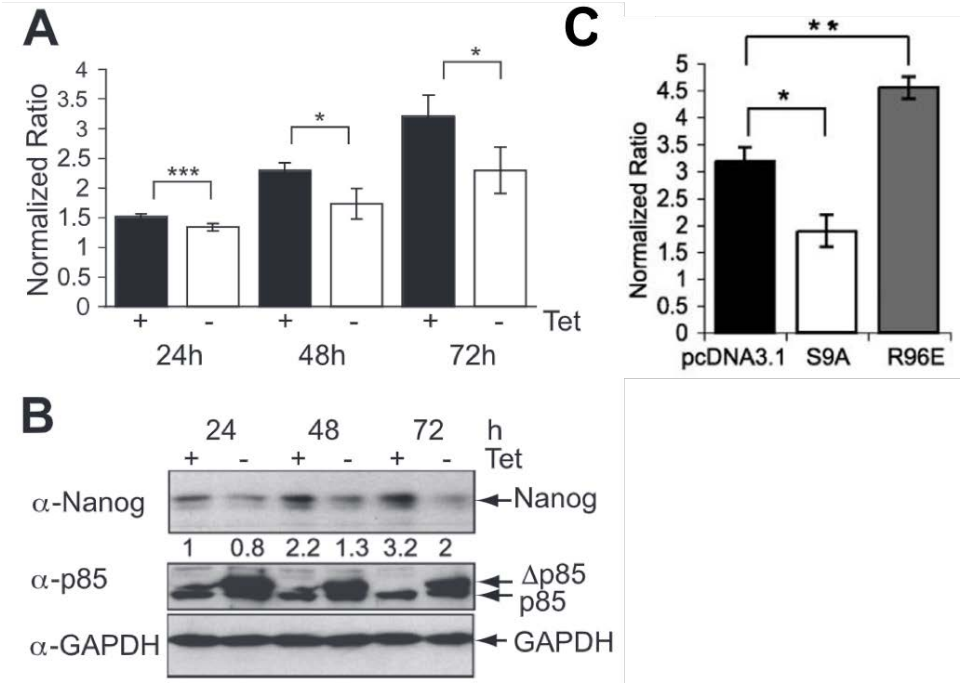

<u>Figure 10:</u> GSK3 plays a functional role in regulation of *Nanog* expression and self-renewal via PI3K (Storm et al., 2007).

(A) E14Δp85 transfectants were induced to express p85Δ by removal of Tet(-Tet) or maintained in 500 ng/ml Tet as a control (+Tet). RNA (A) or protein (B) were extracted at the times indicated. (A) qRT-PCR was performed and *Nanog* RNA expression normalized relative to b-actin levels. The data are the average and S.D. of quadruplicate samples. *,p<0.05; **, p<0.01; ***,p<0.005. (B) 20g of protein/sample were immunoblotted with the antibodies indicated. (C) ES cells were transiently transfected with either control expression plasmid (pcDNA3.1) or versions of pcDNA3.1 encoding the S9A GSK-3mutant or the R96E GSK-3mutant. The average and S.E. of quadruplicate samples are shown from two independent experiments. The values below the anti-*Nanog* blots represent the ratio of *Nanog* expression normalized to GAPDH expression.

Previously, it was demonstrated that while suppression of ERK promotes self-renewal of ES cells, ERK activation induces differentiation (Burdon et al., 1999). In fact, ERK1 can bind and phosphorylate NANOG *in vitro* and decrease NANOG levels by enhancing its ubiquitination (Kim et al., 2014).

Furthermore, *Nanog* is indirectly regulated by components of the bone morphogenetic protein (BMP)/SMAD pathway which is part of the TGF-β superfamily. BMP/SMAD activity has been shown to block neural differentiation (Ying et al., 2003) and BMP4, which is produced by feeder cells used in ES cell culture, has been proven to activate the negative regulator of the ERK pathway *Dusp9* (Li et al., 2012). Thus, NANOG is indirectly maintained by BMP/SMAD-mediated inhibition of ERK.

Hence, while many signals affecting NANOG have been identified *in vitro*, little is known about the direct regulators of NANOG initiation and maintenance in early embryos.

2. OCT4 and SOX2

Together with NANOG, the transcription factors Octamer binding protein 4 (OCT4) and SRY-Box transcription factor 2 (SOX2) form a network of core regulators of pluripotency, important for the maintenance of stemness *in vitro* and preimplantation development *in vivo*. In ES cells, OCT4 and SOX2 often form a heterodimer and regulate in synergy many pluripotency-associated factors, including their own expression (Okumura-Nakanishi et al., 2005; Tomioka et al., 2002). The following paragraph discusses the role of OCT4 and SOX2 during Epi/PrE specification which is mostly based on the analysis of mutant embryos.

Zygotic OCT4 expression starts between the 4- and 8-cell stage and like NANOG, gradually restricts to Epi progenitors. However, the Epi-specific expression pattern of OCT4 occurs later than NANOG and low protein levels remain detectable in PrE cells after specification (Guo et al., 2010). *Oct4* depletion leads to embryonic lethality around implantation and while ICM formation proceeds normally, the TE marker CDX2 is expressed in a few ICM cells (Nichols et al., 1998). This indicates the importance of OCT4 for maintenance of ICM identity. Interestingly, *Oct4* is not required for the activation of *Nanog* and correct salt and pepper pattern formation and in the absence of *Oct4* NANOG levels become significantly upregulated in the ICM (Frum et al., 2013). However, OCT4 is critical for maintenance of GATA6 and the activation of late PrE markers in established PrE progenitors as *Fgf4* levels are reduced in the absence of *Oct4* (Frum et al., 2013). Thus, while OCT4 is

indispensable for the *in vitro* establishment and maintenance of ICM-derived ES cells, it shows a cell autonomous role in promoting PrE after specification in the early embryo.

In contrast to NANOG and OCT4, SOX2 is not expressed in every blastomere of the 8-cell stage embryo but specifically appears in cells that internalize between the 8- and 32 cell stage (Guo et al., 2010). Like for OCT4, the restriction of SOX2 to the Epi lineage happens later in comparison to NANOG and progressively continues until E4.25. Deletion of *Sox2* is embryonically lethal shortly after implantation; however, developmental defects do not occur until after specification at E3.75 (Wicklow et al., 2014). *Sox2* mutants fail to maintain the expression of Epi-specific genes like NANOG and OCT4 in Epi progenitors and the induction of PrE-associated genes is delayed (Figure 11). As for OCT4, the failure to promote PrE fate in the absence of *Sox2* is likely connected with low levels of FGF4 in these embryos.

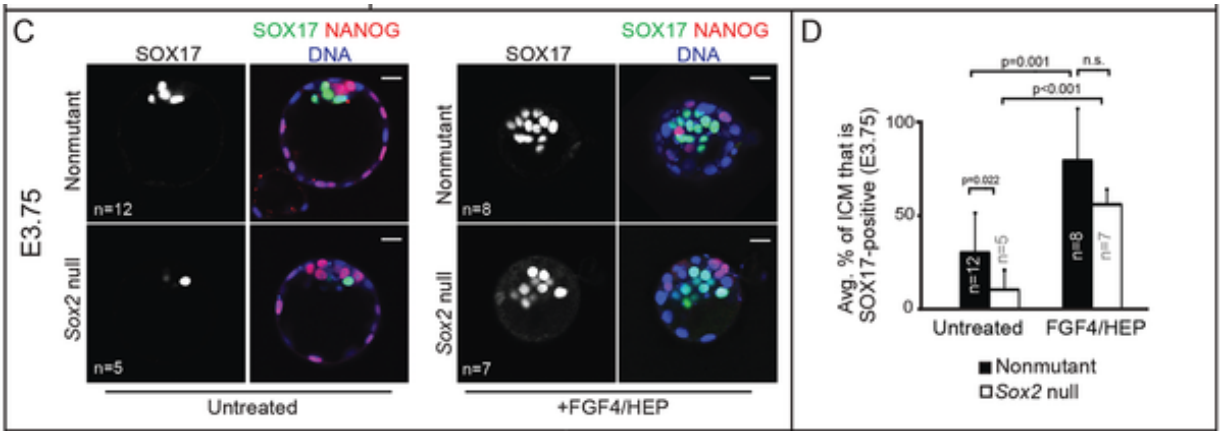

Figure 11: Sox2 promotes PrE development non cell-autonomously via FGF4 (Wicklow et al., 2014).
(C) At E3.75 NANOG is detected in untreated Sox2 null embryos but SOX17 is detected significantly reduced (left). SOX17 can be rescued by FGF/HEP treatment in treated Sox2 null embryos (right). (D) Quantification of the experiment shown in panel C. Bar=20µm, p-value calculated by ANOVA.

To conclude, the expression of OCT4 and SOX2 is dispensable for the initiation of *Nanog* and the course of Epi/PrE specification. Nevertheless, they become essential after imitation of Epi/PrE specification for the maintenance of the Epi lineage (SOX2) and the propagation of PrE identity (OCT4 and SOX2).

B. Mechanisms controlling PrE-associated TFs

This subchapter discusses literature regarding the regulation of the early PrE marker GATA6 as well as SOX17, GATA4 and SOX7 which are activated in a consecutive manner during PrE formation.

1. GATA6

The zinc finger TF GATA6 is the earliest known marker of the PrE lineage but similarly to NANOG, little is known about the mechanisms of expression initiation around the 8-cell stage. In contrast to NANOG, GATA6 is maintained during implantation and homozygous *Gata*6 mutant embryos die before gastrulation around E6.5 due to defects in endoderm formation and cell death in the ectoderm (Morrisey et al., 1998). In fact, *Gata6*$^{-/-}$ embryos are completely deficient of PrE as essential lineage factors like PDGFRa, SOX17, GATA4 and DAB2 are absent and fail to be restored by FGF4 administration (Bessonnard et al., 2014; Schrode et al., 2014). This indicates that GATA6 can be placed at the top of the hierarchy in regulating PrE specification. Interestingly, PrE cells are specified in heterozygous *Gata6* embryos, however they are less in number and their formation is delayed (Schrode et al., 2014).

In ES cells, ectopic expression of *Gata6* is sufficient to induce extra-embryonic endoderm differentiation (Fujikura et al., 2002, Shimosato et al., 2007), while *Gata6* mutant ES cells fail to initiate cXEN cell conversion (Cho et al., 2012). Overexpression of *Gata6* in ES cells triggers the activation of PrE genes like *Gata4* and *Sox17* independently of *Fgf4* (Wamaitha et al., 2015). While *Gata6* is initiated in the absence of FGF signaling in early embryos, *Gata4* and *Sox17* expression is compromised (Frankenberg et al. 2011; Frum et al. 2013; Schrode et al. 2014). Unlike for the differentiation of embryo-derived ES cells to XEN cells, GATA6 simultaneously acts as transcriptional activator and repressor in *Gata6* during iXEN conversion by binding target genes including *Gata4, Sox17, Pdgfra* and *Sox7* but also in the promoter region of *Nanog* (Wamaitha et al., 2015). However, it is currently unclear if GATA6 also directly inhibits *Nanog* in early embryos *in vivo.*

The fact that the induction of the GATA6 downstream targets *Gata4* and *Sox17* fails in the absence of FGF signaling suggests that GATA6 requires a certain threshold. Recently, GATA6 was shown to auto-activate expression by binding its own promoter *in vivo* and *in vitro,* thereby creating a positive feedback regulatory loop (Meng et al., 2018). Strikingly, GATA6 can be phosphorylated at a consensus phosphorylation site (PYS^{264}P) by ERK, thereby promoting GATA6 autoactivation in differentiating ES cells (Meng et al., 2018). However,

cells with mutated phosphorylation sites maintain low levels of GATA6 expression, suggesting that phosphorylation by ERK enhances the potency of GATA6 to promote its own transcription. Interestingly, GATA6 can also be phosphorylated by AKT2 at Ser^{290} upon mTORC1 inhibition in human vascular smooth muscle cells (VSMCs) (Xie et al., 2015). After vascular injury, VSMCs were treated with the mTORC1 inhibitor rapamycin to promote differentiation which is mediated by GATA6 (Xie et al., 2015.). The authors report that AKT2-mediated phosphorylation stabilizes GATA6 in the nucleus and increases its binding to DNA which in turn promotes the transcription of target genes and represses proliferation (Xie et al., 2015). It would be interesting to see if these results are translatable and GATA6 is also regulated by phosphorylation in early embryos. For instance, the activation of ERK by Epi-secreted FGF4 and consequently the increased autoactivation of GATA6 could be an important aspect of PrE fate acquisition and maintenance.

Currently, little is known about the transcriptional regulation of *Gata6* in early embryos and in PrE-like cells. Although during the conversion of ES cells to cXEN or nEnd cells with ACTIVIN A and retinoic acid or WNT3, Gata6 mRNA gradually increases and stabilizes at day 7 after induction (Cho et al., 2012; Anderson et al., 2017), the regulatory mechanisms remain obscure.

2. SOX17, GATA4 and SOX7

Different from the Epi lineage, GATA6 is the only early expressed PrE marker. Once PrE progenitors (NANOG-/GATA6+) are established the key PrE-specific transcription factors SRY-Box transcription factor 17 (SOX17), GATA binding protein 4 (GATA4) and SRY-Box transcription factor 7 (SOX7) are activated in a sequential manner (Artus et al., 2011).
Like GATA6, SOX17, GATA4 and SOX7 are present in PrE derivatives; however in contrast to *Gata6* mutant embryos, Epi/PrE specification correctly proceeds in embryos deficient for Sox17, Gata4 or Sox7 (Artus et al., 2011; Molkentin et al., 1997; Wat et al., 2012).

The activation of SOX17 requires GATA6 and FGF/ERK activity (Bessonnard et al., 2014; Schrode et al., 2014) and coincides with the restriction of SOX2 to Epi progenitors (Artus et al., 2011). When expressed in ES cells, SOX17 forms a complex with OCT4 to activate endoderm-specific genes like *Pdgfra* by binding to enhancer regions (Aksoy et al., 2013). Like GATA6, SOX17 binds the *Nanog* promoter during iXEN conversion but not in embryo-derived XEN differentation and *Sox17* null ES cells are unable to convert towards a XEN-like state (Niakan et al., 2010). In contrast to GATA6 and SOX17, GATA4 becomes exclusively

activated in definitive PrE cells (NANOG-/SOX2-) and is therefore considered as the first marker of PrE commitment (Artus et al., 2011; Plusa et al., 2008; Chazaud et al., 2006). Similar to SOX17, GATA6, ERK signaling and OCT4 are a premise for GATA4 activation (Schrode et al., 2014; Frum et al., 2013). SOX7 is the last PrE-specific factor to become expressed in the late blastocyst. Interestingly, SOX7 only appears in PrE cells that have already undergone cell sorting and face the cavity roof (Artus et al., 2011). Unlike GATA6 and GATA4, overexpression of *Sox7* fails to induce XEN-like cell fate in ES cells and *Sox7*-null ES cells can undergo XEN conversion (Kinoshita et al., 2015).

Finally, the absence of a preimplantation phenotype upon *Sox17*, *Gata4* or *Sox7* deletion suggests that they may have redundant and/or dispensable roles in PrE before implantation and their regulation is not fully understood.

III. The roles of ERK and PI3K signaling in regulating cell identity

This subchapter discusses the implication of the two conserved signaling pathways ERK and PI3K in cell fate choice. While the function of ERK in Epi/PrE specification has been studied quite extensively, the role of PI3K in lineage formation is poorly defined and mostly based on observations conducted *in vitro*.

A. FGF4/ERK signaling

In mammals, Fibroblast Growth Factor (FGF) signaling is mediated by a ligand-receptor interaction that results in the autophosphorylation of tyrosine residues in the intracellular region of a FGF receptor (FGFR) (Lin et al., 1997). The activated phospho-tyrosine receptor residues mediate the recruitment of the adaptor protein Growth Factor Receptor bound protein 2 (GRB2) which in turn localizes to the cell membrane to activate Resistance to Audiogenic Seizures (RAS) (Kouhara et al., 1997) (Figure 12). Active RAS recruits its effector protein RAF which proceeds to phosphorylate the first kinases of the Mitogen- Activated Protein Kinase (MAPK) cascade, MEKs. Finally, after being activated by MEK-mediated phosphorylation (B. E. Xu et al., 1999), Extracellular signal-regulated Kinase (ERK) induced downstream responses like expression of target genes and cytoskeletal rearrangements.

1. The regulation of Epi/PrE specification by different members of the FGF4/ERK pathway

During pre-implantation mouse development, out of 22 FGF ligands and five FGFRs, FGF4, FGFR1 and FGFR2 are predominantly implicated in Epi/PrE specification (Ohnishi et al., 2014). The observation that *Fgfr2* is predominantly expressed in PrE cells (Guo et al., 2010; Kurimoto et al., 2006; Ohnishi et al., 2014) initially indicated that FGF4 was transduced by FGFR2 in emerging PrE progenitors. Yet, the analysis of *Fgfr1* and *Fgfr2* mutants revealed that FGFR1 which is expressed in all ICM cells is critical for the establishment of PrE identity (Kang et al., 2017; Molotkov et al., 2017). While *Fgfr1* mutant embryos display defective PrE specification and fail to maintain GATA6, *Fgfr2* deficiency causes a mild phenotype with a slight increase in co-expressing cells (Kang et al., 2017). Loss of *Fgfr2* can be compensated by *Fgfr1* but not vice versa, demonstrating the lack of functional redundancy. Interestingly, starting from E3.25 *Fgfr1* is ubiquitously expressed in all ICM and TE cells, suggesting that the entity of embryonic cells has a similar capacity to receive FGF signaling (Guo et al., 2010;

Kang et al., 2017; Ohnishi et al., 2014). However, *Fgfr1* mutant embryos correctly specify TE cells, although in reduced numbers, suggesting the involvement of FGF signaling in the expansion of the TE (Kang et al., 2017).

Concerning Epi/PrE specification, it was proposed that, although FGFR1 is equally present in both Epi and PrE precursor cells, the two cell types have distinct feedback mechanisms to regulate the output of downstream signaling (Kang et al., 2017). While the FGF signaling targets *Etv4-5* and *Spry4* are present in all ICM cells, *Dusp4* is preferentially expressed in PrE cells (Kang et al., 2017). The authors hypothesized that the lineage-specific distribution of FGF targets allows the precise regulation of ERK signaling activity in a context dependent manner to preserve Epi versus PrE identity. While in Epi cells *Etv4-5* and *Spry4* could block MEK/ERK through a negative feedback loop, *Dusp4* could fine-tune ERK activity to preserve temporal plasticity in PrE. This can only partially be true, as single cell RNA sequencing data revealed that *Spry4* but not *Etv4* is expressed at the beginning of specification at the 16-cell stage (Posfai et al., 2017), thus making *Etv4* a rather unlikely candidate for ERK inhibition.

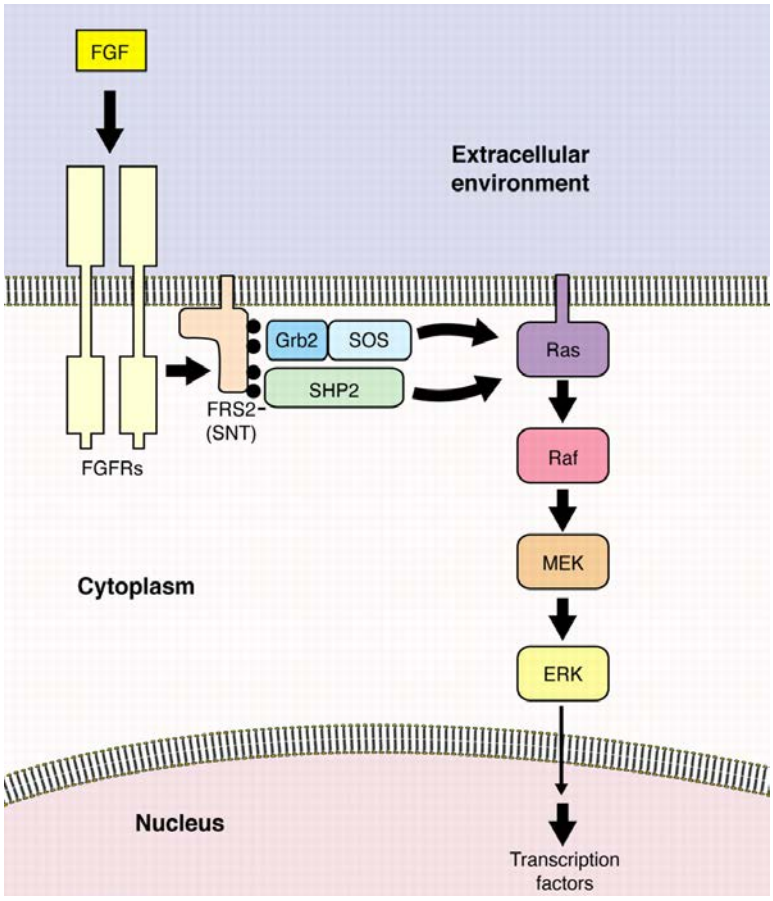

Figure 12: Scheme of FGF/ERK signaling cascade.

FGFR activation induces tyrosine phosphorylation (black circles) of GRB2 and promotes the sustained activation of RAS and ERK cascade (adopted from (Goldfarb, 2001)).

Recently, a study could confirm the PrE-specific expression of *Dusp4* and could show that the accumulation of *Dusp4* directly follows ERK activity (Azami et al., 2019). DUSP4 was barely

detectable in *Nanog* mutants which correlates with the absence of FGF4 in these embryos. Also, Azami and colleagues observed an enrichment of ETV5 in Epi progenitors and proposed that *Etv5* is not positively regulated by FGF/ERK signaling but rather depends on NANOG. In ES cells, it has been shown that *Etv5* is a transcriptional target of NANOG (Loh et al., 2006). Consequently, NANOG activates both *Fgf4* and *Etv5* in Epi which will lead to (1) the induction of PrE fate in surrounding cells and (2) the preservation of Epi identity by inhibiting ERK activity.

The dosage and timing of FGF signaling is critical to acquire a salt and pepper distribution of distinct lineage progenitors and the distribution and response to the morphogen FGF4 needs to be precisely regulated to achieve the desired Epi/PrE ratio. It became apparent that the understanding of the mechanism of FGF4 signal transmission is incomplete when rescue experiments with recombinant FGF4 in *Fgf4* mutants failed to restore the salt and pepper pattern of Epi and PrE cells. Kang et al. reported that the addition of different doses of FGF4 failed to establish a balanced number of Epi and PrE cells (Kang et al., 2013). Depending on the dosage, the attempted rescue resulted in two phenotypes: embryos with an ICM entirely composed of NANOG- or GATA6-positive cells. This might suggest that FGF4 needs to be heterogeneously distributed and the treatment with FGF4 of the entire embryo cannot recapitulate the differences in local FGF4 concentration. Interestingly, a conversion of all ICM cells towards PrE fate can only be achieved with high FGF4 concentrations that largely exceed endogenous levels and are probably saturating in wild type embryos (Yamanaka et al., 2010). These results point to the existence of an underlying fine-tuned signaling transduction mechanism which could require cell-cell contact. Surprisingly, a following study from the same lab observed a progressive increase of PrE proportions in a FGF4 dose-dependent manner when conducting rescue experiments in *Fgf4* mutants (Krawchuk et al., 2013). The reason for the discrepancy between these studies is currently unknown.

2. The analysis and visualization of FGF4/ERK signaling dynamics

To better understand ERK dynamics during preimplantation development, Azami et al. performed pERK immunostainings on fixed embryos of different stages (Azami et al., 2019) (Figure 13). Beginning at around E3.0, a few NANOG/GATA6 coexpressing cells start to show a signal for pERK. With the progression of Epi/PrE specification, the number of pERK-positive cells increases and is mainly detectable in PrE progenitors ($NANOG^-/GATA6^+$). Interestingly, not all PrE cells showed pERK expression and after specification at around E4.5 pERK could

also be localized in few Epi cells. Likely, FGF signaling is required for Epi maturation and downregulation of NANOG, as *Fgfr1* mutant embryos maintain NANOG levels at E4.5 (Kang et al., 2017; Molotkov et al., 2017).

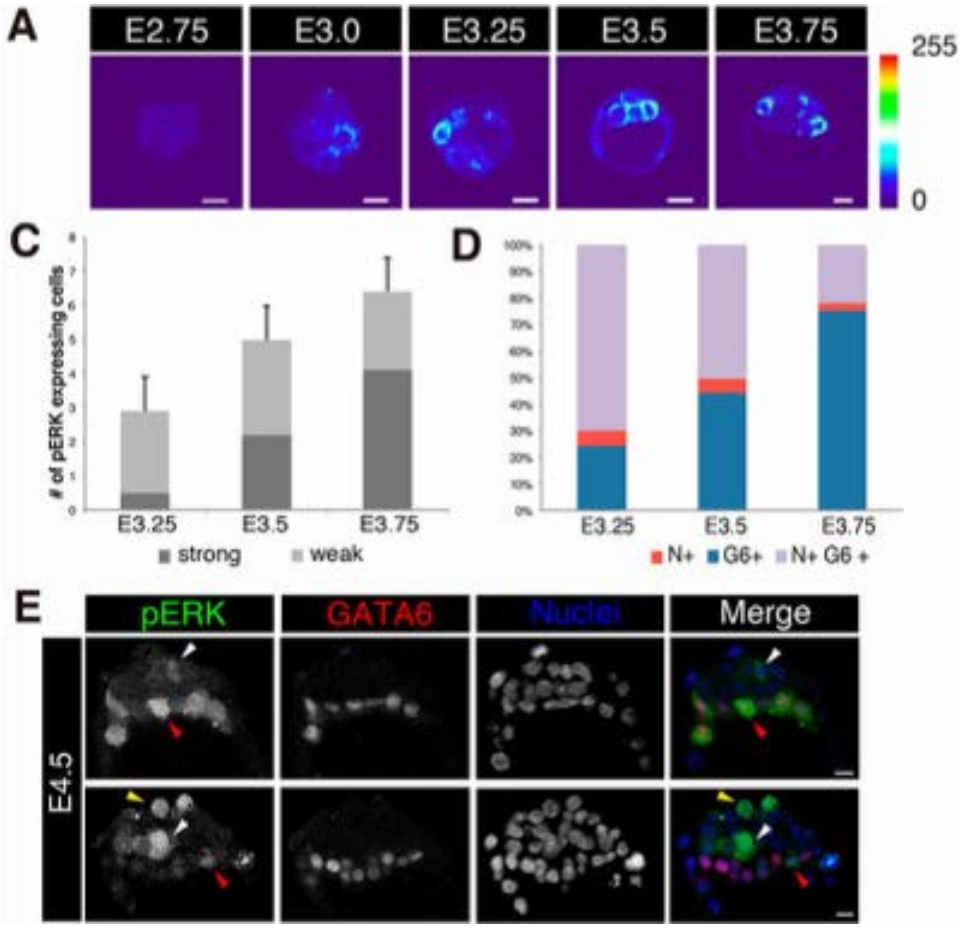

Figure 13: ERK phosphorylation during Epi/PrE specification (Azami et al., 2019).
(A) Immunolocalisation of pERK from E2.75 to E3.75. Colour scale indicates signal intensity. (C) Number of pERK-labelled cells in the ICM at E3.25, E3.5 and E3.75. Data are represented as mean±s.e.m. (D) Distribution of the ICM pERK-labelled cells between NANOG+/GATA6− (N+), NANOG−/GATA6+ (G6+) and NANOG+/GATA6+ (N+ G6+) populations at E3.25, E3.5 and E3.75. (E) Expression in two representative E4.5 embryos showing ERK phosphorylation in some PrE cells labelled by GATA6 (red arrows), in some Epi cells (white arrows) and in some TE cells (yellow arrows). Scale bars: 10 μm.

In 2020, Simon and colleagues took the analysis of ERK dynamics a step further by using a new generation of kinase activity reporter called kinase translocation reporter (KTR) which allows a quantitative assessment of ERK activity in individual cells *in vivo.* This type of genetically encoded biosensor translates phosphorylation into a nucleo-cytoplasmic shuttling event which can be visualized by fluorescent microscopy (De la Cova et al., 2017) (Figure 14A). The mouse line was generated by integrating an ERK-KTR-mClover construct under the control of a CAG promoter into the *Hprt* locus on the X-Chromosome (Simon et al., 2020). In

accordance with previous pERK staining (Azami et al., 2019), live imaging of embryos expressing the ERK-KTR showed sustained and strong ERK activity in the majority of PrE cells. However, baseline levels of ERK activity with infrequent pulses that could not be captured by immunofluorescence, were detected in Epi cells (Figure 14B). It remains obscure if the observed differences in ERK level and duration are ultimately linked to cell fate choice, as the authors did not perform lineage tracing in parallel.

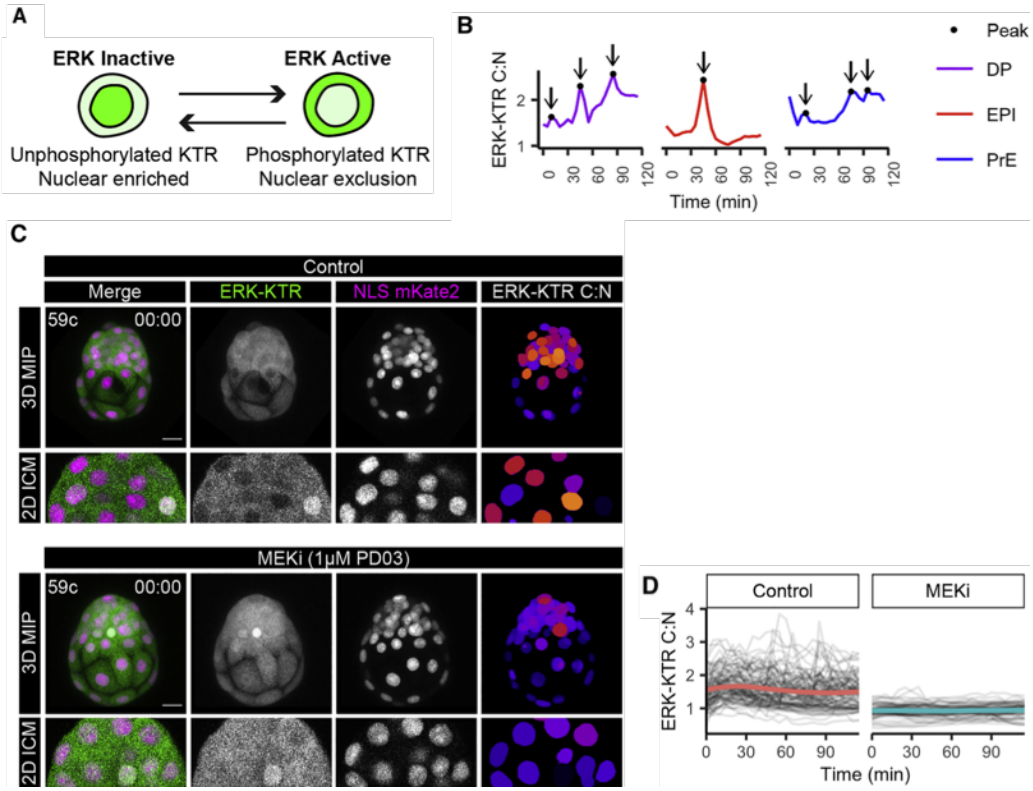

Figure 14: An ERK-KTR mouse line for live visualization of ERK activity *in vivo* (Simon et al., 2020).

(A) Schematic of ERK-KTR. (B) Single-cell traces of ERK-KTR C:N over 2-h time-lapse. Color coding indicate lineage as shown. Arrows indicate peaks. (C) First frame of time-lapse confocal images of ERK-KTR and NLS-mKate2 (nuclear reporter) expressing embryos in control and MEKi. Max intensity projections (MIPs) and magnification of a single z slice at midpoint through the ICM are shown. (D) Traces of ICM cell ERK-KTR C:N values over the course of the 2-h time-lapse imaging in littermate control versus MEKi conditions.

3. The role of FGF4/ERK signaling during specification in other mammals

While the expression of key lineage-specific TFs including NANOG, SOX2, GATA6 and SOX17 is conserved in human, bovine, rabbit and pig embryos, the role of FGF/ERK during Epi/PrE specification differs between species.

Similar to mice, the whole ICM of bovine embryos converts to PrE-like fate in the presence of FGF4 and the inhibition of MEK increases the ratio of Epi versus PrE progenitors (Kuijk et al., 2012). However, the absence of MEK/ERK signaling does not completely prevent the formation of PrE cells, suggesting the involvement of additional factors in PrE specification. Like in murine and bovine species, FGF4 treatment induces a PrE-like phenotype in all ICM cells in rabbit embryos and leads to the migration of SOX17-positive cells on the surface between TE and the cavity (Piliszek et al., 2017). Interestingly, blocking ERK signaling with the MEK inhibitor does not affect NANOG/GATA6 patterning but prevents SOX17 activation and causes a caspase-dependent reduction of ICM cell number of approximately 50% (Piliszek et al., 2017). Similarly, inhibition of MEK does not prevent the segregation of NANOG- and GATA4-positive cells but affects the number of ICM cells in pig embryos (Rodríguez et al., 2012). Finally, the blocking of FGF/ERK activity both up- and downstream of MEK is not affecting Epi/PrE specification in human embryos (Roode et al., 2012). These results suggest that the requirement of MEK/ERK signaling is divergent for lineage development across different mammalian species and seems pronounced in early mouse embryos.

B. The PI3K/AKT pathway

1. Description of the pathway

Phosphoinositide 3-kinase (PI3K) and its canonical downstream target protein kinase B (AKT) are highly conserved regulators of metabolism, growth, survival and proliferation (Figure 15). In mammals three classes of PI3K and three AKT isoforms are expressed.

The most studied class I PI3K, forming heterodimers including one of seven regulatory (p85) and one of three catalytic (p110) subunits encoded by either *Pik3ca, Pik3cb* or *Pik3cd*, stimulates the conversion of lipid PtdIns-3,4-P_2 ($PI3,4P_2$) into PtdIns-3,4,5-P_3 (PIP_3) (Carpenter et al., 1990) which in turn act as second messengers to recruit proteins containing a pleckstrin homology (PH) domain like AKT proteins to the plasma membrane (Alessi et al., 1996). The PI3K/AKT cascade can be activated by an abundance of input signals which bind to receptor tyrosine kinases (RTK) and G-protein coupled receptor (GPCR) families. Input signals include growth factors like insulin and insulin growth factor 1 (IGF-1). Conversely, PI3K activity is antagonized by the tumor suppressor phosphatase and tensin homolog (PTEN) which acts as a PIP_3 phosphatase (Maehama & Dixon, 1998).

The recruitment of AKT to the membrane induces conformational changes and facilitates the phosphorylation of amino acid residues T308 by phosphoinositide-dependent

protein kinase 1 (PDK1) and S473 by mechanistic Target of Rapamycin Complex 2 (mTORC2) which are required for full activation (Alessi et al., 1996). AKT activates a large variety of targets including kinases, TFs, regulators of small G proteins and vesicle trafficking, metabolic enzymes, E3 ubiquitin ligases and cell cycle regulators by phosphorylating their serine and threonine residues.

One of the first substrates to be identified was glycogen synthase kinase 3 (GSK3) (Cross et al., 1995) which is mostly known for its action in the WNT-β-catenin pathway. Phosphorylation of GSK3 by AKT creates a pseudosubstrate that prevents the binding of GSK3 targets and thereby inhibits GSK3 activity. By inhibiting or marking proteins for degradation that primarily drive proliferation and survival, GSK3 antagonizes these processes in the absence of AKT activity. Another prominent substrate of AKT are Forkhead Box O (FoxO) transcription factors that are excluded from the nucleus and blocked from inducing transcription of downstream factors by AKT-mediated phosphorylation (Brunet et al., 1999). Depending on the context, the relocation of FOXO to the cytoplasm upon AKT activation can prevent apoptosis, cell cycle arrest and inhibition of growth.

Essential for the regulation of cellular processes like growth and metabolism that are associated with PI3K/AKT activity is mTOR Complex 1 (mTORC1) which was initially mechanistically characterized nearly 30 years ago (Brown et al., 1994). mTORC1 promotes protein synthesis mostly through phosphorylation of its key effector p70S6 Kinase 1 (S6K1) which stimulates mRNA translation initiation and enhances translation efficiency (Holz et al., 2005). Importantly, mTORC1-mediated activation of S6K1 can transform glucose metabolism from oxidative phosphorylation to glycolysis and thereby support de novo lipid biosynthesis (Düvel et al., 2010). Equally regulated by S6K1 phosphorylation is ribosomal protein 6 (RPS6) (Gressner & Wool, 1974) which was the first posttranslational modification identified in the ribosome. Although the functional consequences of RPS6 phosphorylation are not fully understood, pRPS6 represents a reliable readout for PI3K/AKT/mTORC1 activity.

Another way of mTORC1 to promote cell growth is the regulation of cell turnover by suppressing mechanisms like autophagy. Indeed, mTORC1 has been shown to prevent the activation of autophagy-initiating kinase ULK1 by AMP activated protein kinase AMPK (J. Kim et al., 2011). Also, mTORC1 can limit the degradation rate of proteins by blocking the ubiquitination of long-lived proteins and thereby potentially increase their stability (Zhao et al., 2015).

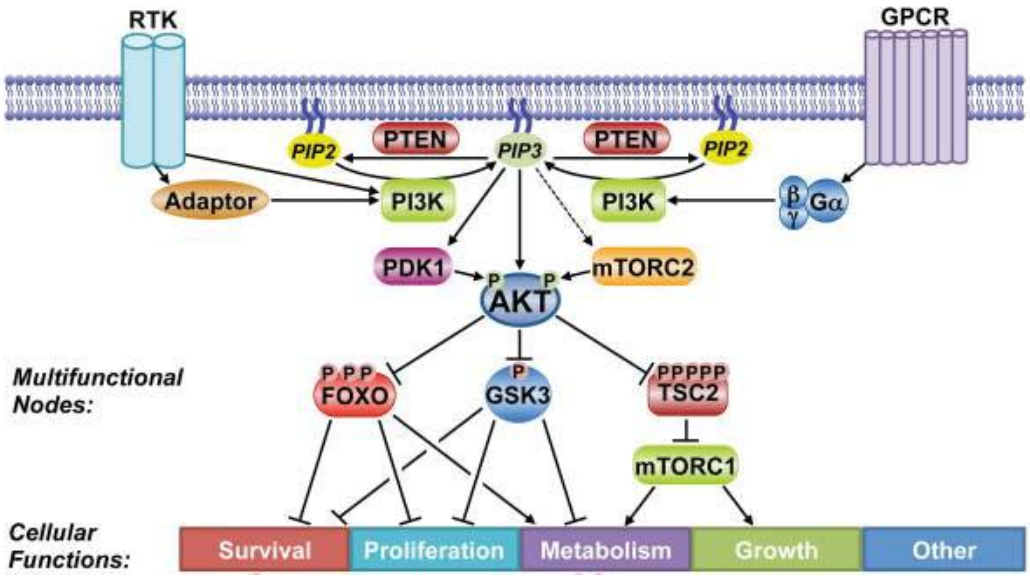

Figure 15: Substrates and functions of the PI3K/AKT signaling network (Manning & Toker, 2017).

2. PI3K as a requirement of pluripotency preservation *in vitro*

PI3K/AKT plays a crucial role in the homeostasis of various cellular functions. Core members of the pathway are frequently deregulated in human malignancies like cancer and therefore have received a lot of interest and attention from the scientific community (Thorpe et al., 2015). In contrast, the importance of PI3K/AKT signaling for development has been overlooked, although the deficiency of many pathway nodes results in embryonic lethality of mice (Table 1). Transcripts of PI3K pathway members including *Pik3ca, Pik3cb, Pik3cd, Akt1/2, mTOR, Pten, Foxo1/3* and *Gsk3a/b* are detectable in early embryos starting from the zygote stage (Boroviak et al., 2015, 2018). Importantly, the inactivation of the p110alpha subunit of PI3K leads to developmental arrest between E9.5 and E10.5 (Bi et al., 1999) and deletion of the p110beta subunit causes lethality during peri-implantation (Bi et al., 2002). Furthermore, the knockout of both *Akt1* and *Akt2* causes severe growth defects and death shortly after birth (Peng et al., 2003) and in the absence of *mTOR* ICM and TE cells fail to proliferate and embryos die shortly after implantation (Murakami et al., 2004).

While embryonic lethality highlights the significance of PI3K/AKT for embryonic development, it also constrains the investigation of signaling disruption in the embryo. Alternatively, PI3K/AKT functions are often addressed *in vitro* by using embryo-derived stem cells. Interestingly, by using these model systems it became apparent that PI3K/AKT is essential to maintain key stem cell characteristics like self-renewal in mouse (Paling et al.,

2004) and human (Zhou et al., 2009) ES cells. In the absence of PI3K signaling, pluripotency genes like *Nanog* are downregulated and cells differentiate towards mesodermal or endodermal fate by upregulating genes like *Gata6* and *Gata4* (Paling et al., 2004; Zhou et al., 2009). Intriguingly, blocking PI3K activity with 5µM of the PI3K inhibitor LY294002 (LY), a dose close to the reported IC_{50} value for inhibition of class I_A PI3Ks, only mildly affects mES cell survival or proliferation properties (Paling et al., 2004) and loss of pluripotency in hES cells is not a consequence of growth inhibition (Zhou et al., 2009). Only LY concentrations of 25µM and higher have been shown to negatively impact mES proliferation (Jirmanova et al., 2002). This strongly suggests that the sphere of PI3K activity is wider than assumed and, in some contexts, PI3K may act as a regulator of the pluripotent state and identity of cells.

Table 1: Summary of knockout mice with germline deletion of key PI3K/AKT/mTOR signaling genes (Yu and Cui 2016).

Genetic manipulation	Reported phenotype	References
PI3K		
Class I		
p110α$^{-/-}$	Embryonic lethality around E9.5-10.5	(Bi et al., 1999)
p110α$^{D933A/D933A}$	Growth retardation at E9 and death at E10-11	(Foukas et al., 2006)
p110β$^{-/-}$	Embryonic lethality at ~E3.5	(Bi et al., 2002)
p110β$^{K805R/K805R}$	Develop normally but small with metabolic defect; male infertility	(Ciraolo et al., 2008)
p110δ$^{-/-}$	Develop normally but with defects in lymphocyte development	(Ciraolo et al., 2008)
p110γ$^{-/-}$	Develop normally but with impaired thymocyte development and T-cell activation	(Sasaki et al., 2000)
p85a-p55a-p50a$^{-/-}$*	Perinatal lethality; extensive hepatocyte necrosis	(Fruman et al., 2000)
p85a$^{-/-}$	Hypoglycaemia; increased insulin sensitivity	(Terauchi et al., 1999)
p85b$^{-/-}$	Hypoinsulinemia; hypoglycemia; improved insulin sensitivity	(Ueki et al., 2002)
Class II		
Pi3kc2a (*Pik3c2a*)$^{-/-}$	Growth retardation from E8.5 onwards; death at E10.5-11.5	(Yoshioka et al., 2012)
Pi3kc2a truncation	Viable but smaller with less fat; late-onset kidney failure	(Harris et al., 2011)
Pi3kc2b$^{-/-}$	Develop normally with no obvious phenotype	(Harada et al., 2005)
Class III		
Vps34-del	Embryonic lethality at E7.5-8.5, with normal epiblast but abnormal visceral endoderm cells	(Zhou et al., 2011)
PTEN		
Pten$^{-/-}$	Embryonic lethality at ~E8	(Di Cristofano et al., 1998)
AKT		
Akt1$^{-/-}$	Mild growth retardation; accelerated apoptosis in thymus and testes	(Chen et al., 2001)
Akt2$^{-/-}$	Insulin resistance phenotype	(Cho et al., 2001)
Akt3$^{-/-}$	Smaller brain size	(Tschopp et al., 2005)
Akt1$^{-/-}$ and *Akt2*$^{-/-}$	50% smaller; immediate post-natal death	(Peng et al., 2003)
Akt1$^{-/-}$ and *Akt3*$^{-/-}$	Embryonic lethality at E10.5-11.5, possibly due to placenta vasculature defects	(Yang et al., 2005)
Akt2$^{-/-}$ and *Akt3*$^{-/-}$	Combined phenotype of *Akt2*$^{-/-}$ and *Akt3*$^{-/-}$	(Dummler et al., 2006)
TSC/RHEB		
Tsc1$^{-/-}$	Embryonic lethality at E10.5-11.5 with failed closure of neural tube	(Kobayashi et al., 2001)
Tsc2$^{-/-}$	Embryonic lethality at E9.5-12.5 with defective neural tube or liver development	(Rennebeck et al., 1998)
Rheb$^{-/-}$	Embryonic lethality at E10.5-12.5 with defective cardiovascular development	(Goorden et al., 2011)
mTORC		
Mtor$^{-/-}$	Embryonic lethality at E5.5-6.5; proliferation defect of ICM and trophoblast giant cells	(Murakami et al., 2004)
Rptor$^{-/-}$	Embryonic lethality at E5.5-6.5; implanted blastocysts fail to expand	(Guertin et al., 2006)
Mlst8$^{-/-}$	Embryonic lethality at E10.5; severe vasculature defects	(Guertin et al., 2006)
Rictor$^{-/-}$	Embryonic lethal at E10.5-11.5; severe vasculature defects	(Guertin et al., 2006; Shiota et al., 2006)
Sin1$^{-/-}$	Embryonic lethality at E10.5-11.5	(Jacinto et al., 2006)

**Pi3kr1* gene.

The upregulation of PI3K in both mES cells and hES cells provided further evidence that PI3K acts as a guardian of stemness. Knockdown of *Pten* increases the potential of self-renewal, leads to an upregulation of NANOG and OCT4 and impairs the ability to undergo multilineage differentiation in mES cells (Lindgren et al., 2011) and hES cells (Alva et al., 2011). Injection of *Pten*$^{-/-}$ mES cells in mice causes the formation of large, undifferentiated tumors that do not include cells of the three germ layers (Lindgren et al., 2011) and hES cells deficient for *Pten*

do not convert into PrE-like states (Alva et al., 2011). Similarly, enhanced stemness and impaired differentiation was observed when *Akt* is constitutively activated in mES cells (Watanabe et al., 2006), when *PIK3CA,* a gene encoding the p110α catalytic subunit of PI3K, is overexpressed in human iPS cells (Madsen et al., 2019). Equal results are obtained when mES cells are homozygously mutated for GSK3α/β (Doble et al., 2007), however the involvement of PI3K signaling was not assessed in this study.

3. PI3K upstream candidates in the maintenance of pluripotency

Although pluripotency of mES and hES requires PI3K signaling, it is currently unclear what signals induce PI3K activity. As mentioned earlier, LIF signaling can act upstream of the PI3K/AKT pathway and activate NANOG by upregulating *Tbx3* (Niwa et al., 2009). Interestingly, *Akt1* can maintain the self-renewing properties of mES cells in the absence of LIF (Pritsker et al., 2006), further supporting that PI3K/AKT can operate downstream of LIF. AKT1-dependent regulation of pluripotency in mES cells could be mediated by AKT1 cofactor TCL1, which has been identified as an essential gene for self-renewal in a microarray functional screen during retinoic-acid-induced differentiation (Ivanova et al., 2006).

It remains a challenge to decipher if PI3K induction is mediated by canonical growth factor stimulation or activation of other pathways like ERK. PI3K and ERK have been shown to respond to the same upstream ligands including INSULIN, insulin growth factors (IGFs) and FGF which are essential for hES culture (Sacco et al., 2009; Singh et al., 2012). However, FGF can be replaced by IGF1 and HEREGULIN to maintain hES cells, suggesting that FGF is acting through PI3K and not ERK (Bendall et al., 2007). In fact, under defined culture conditions INSULIN but not FGF activates PI3K signaling to safeguard the pluripotency of hES cells (Ho et al., 2015). Interestingly, hES cells synthesize the endogenous peptide ELABELA (ELA) which like INSULIN and IGFs activates PI3K signaling by binding to a currently unknown receptor (Ho et al., 2015). ELA alone is sufficient to preserve stemness of hES cells by activating PI3K and in the absence of ELA, hES are unable to proliferate, undergo apoptosis and eventually differentiate (Ho et al., 2015). In mES cells, a RAS-like protein called ERAS has been shown to activate PI3K by binding at the p110 subunit (Takahashi et al., 2003). However, *Eras* deficiency does not have any effect on the self-renewing capacity and is not interacting with RAF in mES cells suggesting PI3K-mediated regulation of pluripotency is independent of ERAS (Takahashi et al., 2003). Apart from growth factors and interactions with other pathways, PI3K/AKT signaling has been shown to be activated by mechanotransduction

in a malignant context. Two studies have demonstrated that stiffening of the extracellular matrix (ECM) enhances focal adhesion in a PI3K-dependent manner and promotes tumor progression and invasion in breast cancer mouse models (Levental et al., 2009; Rubashkin et al., 2014). Mechanical cues like an increase in tension or force can stimulate integrin signaling or trigger the assembly of mechanotransducer complexes like vinculin and thereby facilitate the activation of PI3K by PIP3 phosphorylation (Levental et al., 2009; Rubashkin et al., 2014). However, if PI3K mechanosignaling also plays a role in the maintenance of pluripotency in mES and hES cells is currently unclear.

4. PI3K downstream candidates in the maintenance of pluripotency

Despite the increasing amount of data establishing PI3K as a central player in pluripotency control in mammalian stem cells, little is known about the downstream mechanisms. One possibility could be that the AKT-mediated inhibition of GSK3 prevents the degradation of Yamanaka factor and pluripotency factor MYC (Bechard & Dalton, 2009). Stability of MYC is crucial for self-renewal, as *Myc* deficiency results in differentiation of mES (Cartwright et al., 2005). However, active GSK3b is required for the maintenance of pluripotency and NANOG expression in hES cells, as the depletion of GSK3b leads to the relocalisation of WNT effector β-catenin to the nucleus and the induction of the mesoendoderm program (Singh et al., 2012). This discrepancy may exist because the effect of GSK3b inhibitor BIO highly depends on the used concentration. While low doses of BIO indeed cause MYC stabilization, high doses facilitate differentiation by activation of β-catenin/WNT signaling (Singh et al., 2012). The authors further hypothesize that PI3K indirectly promotes GSK3b activity by blocking ERK which can phosphorylate GSK3b at the same serine residue as AKT (Singh et al., 2012). Another study established FOXO1 in hES cells and FOXO1/3 in mES cells as an essential component of the circuitry of pluripotency (Zhang et al., 2011). Reduction of *Foxo1* mRNA levels by short hairpin RNAs (shRNAs) in hES cells resulted in rapid downregulation of OCT4, NANOG and SOX2 and spontaneous differentiation as shown by the induction of mesodermal genes like *Gata2* and *brachyury* as well as endodermal markers like *Sox17* and *Gata4* (Zhang et al., 2011). On the contrary, lentiviral-mediated ectopic FOXO1 expression caused a significant upregulation of OCT4, NANOG, SOX2 and KLF4 and endogenous FOXO1 was shown to specifically bind to sequences within regulatory regions of *Oct4* and *Sox2* by chromatin immunoprecipitation (ChiP) (Zhang et al., 2011). Although FOXO1 and FOXO3 are both targets of PI3K/AKT, FOXO1 is mostly nuclear while FOXO3

accumulates in the cytoplasm in hES cells (Zhang et al., 2011). FGF-mediated activation of PI3K/AKT induces FOXO1 phosphorylation which is reversible by LY-induced PI3K inhibition (Zhang et al., 2011). This indicates that other signals apart from PI3K/AKT regulate FOXO1 and prevent nuclear export upon AKT-dependent phosphorylation. While targeting FOXO3 did not affect the expression of pluripotency genes in hES cells, in mES cells the expression of both FOXO1 and FOXO3 is crucial to maintain pluripotency (Zhang et al., 2011). The shRNA-mediated knockdown of *Foxo1* or *Foxo3* led to a decrease of *Nanog*, *Sox2*, *Oct4*, and *Klf4* levels and induced differentiation (Zhang et al., 2011). Unlike in hES cells, reduction of *Foxo1* or *Foxo3* does not activate an endodermal program but leads to a significant increase in TE marker *Cdx2* (Zhang et al., 2011). Considering their important role in the maintenance of mES pluripotency, it is surprising that FOXO1 and FOXO3 are dispensable for early mouse development. *Foxo1* null embryos die at E10.5 due to defects in vascular development, while Foxo3 mutant mice are viable and show age-dependent infertility (Hosaka et al., 2004). If this is solely a result of FOXO1/3 redundancy, remains to be ascertained.

In addition to canonical PI3K/AKT signaling, AKT1 has been shown to promote pluripotency by directly stabilizing OCT4 and SOX2 in a phosphorylation-dependent manner (Fang et al., 2014; Y. Lin et al., 2012). In embryonal carcinoma cells (ECCs) which are the stem cells of teratocarcinomas and the malignant counterpart of ES cells, AKT1-mediated phosphorylation of OCT4 at threonine 235 prevents proteolysis and increases the binding to the *cis*-regulatory elements of different pluripotency genes like *Nanog*, *Sox2* and *Oct4* as well as cell survival genes including Akt1 (Lin et al., 2012). In mES cells, phosphorylation of SOX2 threonine 118 by AKT1 stabilizes SOX2 by preventing the methylation of SOX2 at K119 residue by SET7 (Fang et al., 2014). *Akt1* knockdown stimulates SOX2 ubiquitination and subsequent degradation via proteasome pathway, induces differentiation and loss of self-renewal capacity in mES cells (Fang et al., 2014).

Since the regulation of pluripotency by PI3K appears to be independent from proliferation and survival *in vitro*, it could be mediated by epigenetic changes depending on cellular metabolism. In cancer cells, oncogenic AKT activity increases histone acetylation levels by controlling the production of metabolite acetyl coenzyme A (acetyl-CoA) which in turn is suspected to facilitate tumor growth (Lee et al., 2014). In hES cells, MYC has been shown to regulate the transcription of metabolic genes that are required for the maintenance of elevated glycolysis (Cliff et al., 2017). When hES cells undergo differentiation towards definitive endoderm and mesoderm, downregulation of MYC causes a metabolic switch (Cliff

et al., 2017). However, if the role of MYC in stemness versus lineage formation is directly coupled to the regulation of metabolic activity is unclear.

5. The role of PI3K during preimplantation mouse development

The dynamics of PI3K activity as well as the significance of PI3K signaling for preimplantation mouse development are poorly defined. Except for the knockout of p110beta subunit which causes embryonic lethality during peri-implantation (Bi et al., 2002), the deficiency of most PI3K/AKT pathway members do not show preimplantation phenotypes and may be a reason why the importance of this pathway has been largely overlooked.

In 2005, Riley et al. reported that the p85 and p110 subunits of PI3K as well as AKT are detectable by western blot and immunofluorescence during all stages of early embryo development starting at the 1-cell stage (Riley et al., 2005). However, they do not provide any data to confirm the specificity of the antibodies in their immunofluorescence stainings. In turn, Halet and colleagues used a PIP_3-specific GFP-tagged PH domain as a readout of PI3/AKT activity and found it to be constitutively produced during all preimplantation stages (Halet et al., 2008). Expression of the GFP-tagged PH domain was detected at all cell-cell contacts from the 2-cell to blastocyst stage and reduced upon treatment with 10µM of LY294002 (Halet et al., 2008). As previously mentioned, on a transcriptional level PI3K pathway members including *Pik3ca, Pik3cb, Pik3cd, Akt1/2, mTOR, Pten, Foxo1/3* and *Gsk3a/b* are detectable in early embryos starting from the zygote stage (Boroviak et al., 2015, 2018). Thus, although members of canonical PI3K/AKT signaling are present in early embryos, more research is needed to further describe the dynamics of PI3K/AKT activity.

Several studies have demonstrated that the addition of INSULIN or IGF-1 to both mouse and human embryo culture increases the number of ICM cells, reduces cell death, results in a higher number of embryos reaching the blastocyst stage and induces earlier hatching (Campbell et al., 2012; Harvey & Kaye, 1992; T.-C. Lin et al., 2003; Spanos et al., 2000). In both mouse and human embryos, IGF-1 treatment specifically increases Epi cell number and this is mediated by PI3K/AKT activation (Campbell et al., 2012; Wamaitha et al., 2020). Conversely, the inhibition of PI3K/AKT by LY294002 has been shown to disturb early mouse development during different stages of preimplantation. While 1-cell stage embryos which are continuously exposed to PI3K inhibitor LY294002 fail to develop beyond the 2-cell stage, the development from 2-cell to 16-cell stage is not impaired by LY294002 (Halet et al., 2008). Treatment with the PI3K inhibitor for 20h starting at the 16-cell stage results in dramatic cell

death and developmental arrest (Halet et al., 2008). This is consistent with observations from Bessonnard et al. who showed that inhibition of PI3K/mTOR signaling leads to a dose-dependent decrease in ICM cell number in blastocyst after Epi/PrE specification (Bessonnard et al., 2019). Although most of the discussed evidence suggests that PI3K/AKT is mainly implicated in the regulation of proliferation and survival during preimplantation mouse development, it should be noted that most of these results are based on prolonged exposure of embryos to pharmacological agents. Also, keeping embryos under either low- or high-density conditions can have an impact on the developmental delay caused by ex vivo The usage of molecules is a simple and straightforward way to explore the regulation of different signaling pathways in the early embryo, however extended periods of treatment can bias conclusions. The duration of treatment should be carefully chosen regarding to the developmental process of interest.

6. Potential role of PI3K in differentiation after pluripotency exit

Another aspect that is far from understood is the involvement of PI3K in lineage specification once cells lose their pluripotent identity. Mutating TSC Complex Subunit 2 (TSC2) which is a negative regulator of mTORC1, induces embryonic lethality in rats and leads to dramatic overgrowth in the forebrain (Rennebeck et al., 1998). Although overgrowth can be seen as an expected consequence of mTORC1 deregulation, the variety of cell types present in the tumor and the overall loss of tissue architecture indicates further implications of mTORC1 in neural fate determination. Interestingly, PI3K inhibition biases hES cells to differentiate towards endoderm and mesoderm but not neuroectoderm (Zhou et al., 2009). It remains to be investigated if PI3K has an active role in directing neural differentiation or if it rather inhibits the commitment towards other lineages.

In conclusion, although research of the last three decades has revealed a lot about the up- and downstream components of the PI3K pathway, central questions about the underlying mechanisms remain. PI3K is involved in controlling most cellular processes but its output appears highly context-dependent and complex. Finally, studies that explored the role of PI3K in the regulation of pluripotency were predominantly conducted with mammalian stem cells and it is currently unclear to what degree these findings are transferable to early embryonic development.

C. Interaction of ERK and PI3K signaling

One of the reasons why regulatory mechanisms of PI3K are difficult to interpret is that PI3K frequently interacts with other signaling pathways which adds an extra level of complexity. The PI3K cascade has a particular close relationship with the RAS/ERK pathway and depending on the context, they inhibit, activate or compensate for each other. Here, I am quickly summarizing on which level PI3K/ERK interactions have been reported in the literature and more precisely in the regulation of pluripotency in mES and hES cells.

1. PI3K/ERK interactions on different levels

Regarding cross-inhibition, the protein kinase c-RAF upstream of ERK was one of the first substrates shown to interact with AKT (Rommel et al., 1999). AKT phosphorylates c-RAF and thereby prevents activation of ERK in differentiated muscle cells (Rommel et al., 1999). Conversely, ERK can prevent PI3K signal transduction by binding GRB2 Associated Binding Protein 1 (GAB1) which usually recruits PI3K to activated receptors (C. F. Yu et al., 2002). GAB1 function is blocked by ERK-mediated phosphorylation (Lehr et al., 2004) and an increased association of GAB1 with PI3K resulting in higher pAKT levels is observed upon ERK inhibition in human embryonic kidney (HEK) cells (Yu et al., 2002).

Concerning cross-activation, RAS has been shown to directly bind PI3K which allosterically activates PI3K, seen by an increase of PIP_3 (Rodriguez-Viciana et al., 1994). After strong stimulation, ERK induces PI3K signaling activity in an AKT-independent manner by phosphorylating RAPTOR which is part of mTORC1 (Foster et al., 2010). ERK can also indirectly activate mTORC1 by phosphorylating a mTORC1 antagonist, Tuberous sclerosis complex 2 (TSC2), which promotes the tumorigenic potential of HEK cells (Ma et al., 2005). However, there are also indications that strong ERK activation by calcium rather inhibits mTORC1 function by interaction with MAPK scaffolding proteins (Dougherty et al., 2009).
Pathway convergence, thus the targeting of the same substrate, could be observed in a breast cancer mouse model where ERK acts on PI3K downstream factor FOXO3A (J. Y. Yang et al., 2008). ERK-mediated phosphorylation targeted FOXO3A for degradation and promoted tumor growth in the absence of FOXO3A-dependent apoptosis (Yang et al., 2008). Furthermore, ERK has been shown to inhibit PI3K cascade member GSK3b leading to the stabilization of oncogenic β-catenin in human-derived carcinoma cells (Ding et al., 2005).

In conclusion, interactions of the PI3K and ERK pathway have been observed on multiple levels leading to distinct and highly context-dependent signaling outputs. This

emphasizes that neither PI3K nor ERK should be studied in isolation and their ability to act on the same substrates should always be considered.

2. PI3K/AKT interaction in the regulation of pluripotency *in vitro*

In mES cells, PI3K/AKT has an important role in the maintenance of pluripotency and this may in part be facilitated by the inhibition of differentiating signals of the ERK axis. Upon inhibition of PI3K activity either by LY294002 or by the expression of Δp85, Paling and colleagues observed an increase in LIF-induced activation of ERK1 and 2 (Paling et al., 2004). The incubation with the MEK inhibitors, PD98059 and U0126, both reversed the upregulation of ERK1/2 and led to a recovery in self-renewal in cultures expressing Δp85 (Paling et al., 2004). Similarly, mES cells deficient for the p85α regulatory subunit of class I_A PI3Ks showed an increase in ERK activity upon IGF-1 stimulation (Hallmann et al., 2003). This indicates that PI3K inhibits ERK to preserve an undifferentiated state in mES, however the exact mechanism of this interaction remains elusive.

Likewise, treatment with LY294002 in hES cells increases ERK1/2 phosphorylation but also results in elevated levels of phosphorylated GSK3b which represents inhibition of GSK3b activity (Singh et al., 2012). While GSK3a/b activation is suppressed by AKT-mediated phosphorylation in mES cells (Paling et al., 2004; Niwa et al., 2009), GSK3b inhibition is prevented in hES cells by AKT-dependent blocking of ERK activity (Singh et al., 2012). Immunoprecipitation assays showed interaction of AKT1 and cRAF in hES cells, while in the absence of PI3K/AKT signaling cRAF bound ERK1/2 and GSK3b (Singh et al., 2012).

Thus, although the PI3K/AKT downstream signaling appears to be different across species, the inhibition of ERK signaling by PI3K/AKT to maintain pluripotency *in vitro* is conserved. While the FGF/ERK signaling is also promoting differentiation in the early embryo, it is currently unclear if PI3K signaling plays a role in maintaining the pluripotency of the Epi and if this is mediated by interaction with the ERK pathway.

Paper in preparation « PI3K/AKT signaling regulates lineage-specific TF levels in the ICM progenitors of early mouse embryos »

Paper in preparation « PI3K/AKT signaling regulates lineage-specific TF levels in the ICM progenitors of early mouse embryos »

My introduction discussed important aspects of Epi/PrE specification but also heavily focused on PI3K/AKT signaling. I wish to briefly explain how our interest in this pathway arose and which initial results motivated us to study it in early embryos.

The laboratory of Michel Cohen-Tannoudji uses the preimplantation mouse embryo and mES cells to understand how early lineages are formed through combination of TF networks and cell signaling processes. Before coming to Paris, I conducted an internship in the laboratory of Daria Onichtchouk at the University of Freiburg, studying epigenetic mechanisms during ZGA in zebrafish. I wished to continue investigating processes during early embryogenesis in mammals and therefore joined Michel's team in January 2017 for my Master 1 (M1) internship. Under the supervision of Sylvain Bessonnard, a post-doc in the lab at the time, I conducted a phenotypic characterization of *Argonaute 2 (Ago2)* deficient embryos during mid and late blastocyst stages which contributed to a study published with collaborators from Switzerland (Ngondo et al., 2018). Meanwhile, Sylvain Bessonnard discovered that PI3K/AKT/mTOR signaling is regulating Epi/PrE survival after specification when Epi and PrE undergo sorting (Bessonnard et al., 2019). After his departure, I stayed with Michel for my M2 internship and started investigating the role of PI3K/AKT during earlier stages of preimplantation mouse development, specifically during the 24h time window of Epi/PrE specification. To our surprise, we observed a dramatic reduction of NANOG in embryos which I treated with the commonly used PI3K/AKT inhibitor LY294002 (LY). We hypothesized that PI3K/AKT might have a previously undiscovered role in the regulation of ICM specification and we decided to conceptualize a PhD project based on this initial finding. I presented this project at the concours of the doctoral school Complexité du Vivant from the Sorbonne University and received a three-year fellowship starting in October of 2018. For my fourth year of PhD, I received funding from the fondation ARC pour la recherche sur le cancer.

My PhD had three major objectives: (1) to decipher in-depth how the modulation of PI3K/AKT activity affects ICM identities, (2) to investigate if PI3K/AKT and FGF/ERK signaling act in synergy to drive ICM specification and (3) to develop a tool which allows us to visualize the dynamics of PI3K/AKT signaling in the developing embryo in real-time.

The results are divided in two parts, first presenting the paper we wrote based on the main results of my PhD and second the complementary results which includes additional data I produced. Our data provides evidence that PI3K/AKT signaling is indeed an important

regulator of Epi/PrE specification and that PI3K/AKT governs a dual role during lineage formation by controlling both Epi- and PrE-specific TF levels. We will upload the paper to the preprint server bioRxiv and submit to a journal in the following weeks.

PI3K/AKT signaling regulates lineage-specific transcription factors levels in the Inner Cell Mass progenitors of early mouse embryos

Anna Geiselmann[1, 2, 3, 4], Sandrine Vandormael-Pournin[1, 3, 4], Vincent Laville[4], Sébastien Mella[5], Pablo Navarro[1, 4] and Michel Cohen-Tannoudji[1, 3, 4 #]

[1] Institut Pasteur, Université Paris Cité, CNRS UMR3738, Epigenomics, Proliferation, and the Identity of Cells, Department of Developmental and Stem Cell Biology, F-75015 Paris, France.
[2] Sorbonne Université, Complexité du Vivant, F-75005, Paris, France.
[3] Early Mammalian Development and Stem Cell Biology, Institut Pasteur, CNRS UMR 3738, F-75015, Paris, France.
[4] Department of Developmental and Stem Cell Biology, Institut Pasteur, CNRS UMR 3738, F-75015, Paris, France.
[5] Institut Pasteur, Bioinformatics and Biostatistics Hub (C3BI), F-75015, Paris, France.
[#] Corresponding author and lead contact: Michel Cohen-Tannoudji, Early Mammalian Development and Stem Cell Biology, Institut Pasteur, CNRS UMR 3738, 25 rue du Dr. Roux, F-75015, Paris, France; E-mail: m-cohen@pasteur.fr; Phone: 33 1 45 68 84 86; Fax: 33 1 45 68 86 34; website: https://research.pasteur.fr/en/team/group-michel-cohen-tannoudji/.

Running title: PI3K regulates key TFs expression in ICM progenitors

Keywords: Mouse preimplantation embryo, Epiblast, Primitive endoderm, Inner cell mass, Lineage specification, NANOG

Abstract

The inner cell mass (ICM) of early mouse embryos is specified into Epiblast (Epi) and primitive endoderm (PrE) lineages to form a blastocyst competent for implantation. The antagonistic transcription factors (TFs) NANOG and GATA6 in combination with FGF/ERK signaling are central actors in ICM fate choice. However how the bipotent ICM progenitor state is maintained despite coexpression of antagonistic factors and what initiates their specification are not fully understood yet. Here, we show that PI3K/AKT is constitutively active during preimplantation development. Importantly, using pharmacological inhibition during the period of ICM progenitor generation, we found that PI3K/AKT is required in ICM progenitors to maintain the pluripotency TFs NANOG, ESRRb and SOX2 and to downregulate SOX17, the expression of which normally signs entry in PrE differentiation program. We also showed that PI3K/AKT control NANOG levels independently of ERK signaling. We further provide evidence that PI3K/AKT regulates TF levels through post-transcriptional mechanisms possibly involving GSK3. Finally, the analysis of mutant embryos revealed that *Sox17* activation is not solely dependent on *Gata6.* We propose that through its dual action, PI3K/AKT signaling contributes to the bipotent ICM state and that its modulation may help drive progression towards Epi or PrE fate.

Introduction

During mouse preimplantation development, transcription factors (TFs)-controlled networks and coordinated cell signalings orchestrate the formation of the first three embryonic lineages composing the implanting blastocyst: the pluripotent epiblast (Epi) that will give rise to the fetus and the extraembryonic mesoderm and the trophectoderm (TE) and primitive endoderm (PrE) that will contribute to the placenta and the endoderm layers of the yolk sacs, respectively. Initially, TE and inner cell mass (ICM) fates are established during the 4th and 5th division. Shortly after, during blastocyst formation, individual ICM cells acquire PrE or Epi fate in an asynchronous manner and without predefined spatial patterns leading to mutually exclusive expression of lineage specific markers in a 'salt-and-pepper' distribution (Chazaud et al., 2006; Plusa et al., 2008). ICM bipotential progenitors coexpress Epi-specific NANOG and SOX2 and PrE-specific GATA6 TFs. Differentiation towards Epi progenitors is associated with the disappearance of GATA6 while PrE progenitors no longer express NANOG first and other pluripotency factors such as SOX2 and OCT4 subsequently, and sequentially activate PrE-specific TFs including SOX17, GATA4 and SOX7 (Artus et al., 2011). NANOG and GATA6 act as major regulators of their respective lineage (Bessonnard et al., 2014; Frankenberg et al., 2011; Schrode et al., 2014) and the Fibroblast Growth Factor (FGF)/Extracellular signal-Regulated Kinase (ERK) signaling pathway plays a major role in driving PrE fate acquisition. Indeed, inactivation of genes of the pathway or treatment with inhibitors prevents PrE formation (Chazaud et al., 2006; Kang et al., 2013; Kang et al., 2017; Molotkov et al., 2017; Nichols et al., 2009; Yamanaka et al., 2010), whereas overactivation of the pathway can bias the entire ICM towards the PrE lineage (Saiz et al., 2016; Yamanaka et al., 2010). In fact, Epi progenitors are established first (Bessonnard et al., 2014; Bessonnard et al., 2017; Saiz et al., 2016) and the upregulation of *Fgf4* expression triggers PrE fate in surrounding uncommitted ICM cells by inducing ERK signaling (Azami et al., 2019; Frankenberg et al., 2011; Kang et al., 2017). Although the Epi marker NANOG is expressed in all ICM cells of *Gata6* mutant embryos, no PrE progenitors are formed and the expression of PrE markers SOX17 and GATA4 fails to be rescued by exogenous FGF4 (Bessonnard et al., 2014; Schrode et al., 2014). Thus, GATA6 and FGF/ERK signaling are acting in synergy to promote PrE identity.

Relatively simple Gene Regulatory Networks, centered around direct mutual inhibition between NANOG and GATA6 and integrating positive and negative feedback from the FGF/ERK pathway, allow to model many aspects of Epi and PrE cell fate decision (Mot et al., 2016; Saiz et al., 2019; Tosenberger et al., 2017). However, how the initial separation between

Epi and PrE fate is controlled is not fully understood yet. Our previous results showed that ICM progenitors are heterogeneous independently from NANOG, GATA6 and FGF/ERK activities and that NANOG is required to initiate Epi cell differentiation (Allègre et al., 2019). Regulation of NANOG levels in ICM progenitors is therefore central to drive the initial bias towards Epi or PrE fate. Noteworthy, most of our current knowledge on NANOG regulation comes from work on pluripotent stem cells and much less is known about transcriptional and post-transcriptional regulation of *Nanog in vivo* in Epi cells and even less in ICM progenitors which express both GATA6 and NANOG-and are endowed with different properties and potentialities.

The Phosphoinositide 3-kinase (PI3K)/ protein kinase B (AKT) signaling pathway plays critical roles in metabolism, proliferation and survival of most cell types. Besides these essential cellular functions, PI3K/AKT is key for maintenance of pluripotency in mouse and human pluripotent stem cells (Yu and Cui, 2016). Acting downstream of LIF and IGF1, PI3K/AKT activity is required to sustain expression of pluripotency factors including TBX3 and NANOG (Hishida et al., 2015; Niwa et al., 2009; Storm et al., 2007; Storm et al., 2009; Wamaitha et al., 2020). There are evidences that the pathway is active in preimplantation embryos (Halet et al., 2008; Riley et al., 2005) where it is likely to mediate the actions of trophic factors present in maternal fluids or produced by the embryos themselves. Indeed, treatments with IGF-1/Insulin or pharmacological inhibitors point to an implication of the pathway in growth and survival of preimplantation embryos in various mammals including humans (Campbell et al., 2012; Lin et al., 2003; Lu et al., 2004; Ramos-Ibeas et al., 2019; Wamaitha et al., 2020). Recently, we further showed that, in the mouse embryo, PI3K/AKT/mTOR is critically required for the survival of both Epi and PrE after their specification (Bessonnard et al., 2019). How PI3K/AKT activity is regulated in the embryo and whether it is linked to pluripotency during Epi establishment remains largely unknown.

In this study, we addressed the role of PI3K/AKT signaling during differentiation of bipotent ICM progenitors into Epi and PrE in the mouse embryo. Using phosphorylated ribosomal protein S6 (pRPS6) as a readout of the pathway, we demonstrated that PI3K is active during all preimplantation development and increases in mid/late blastocysts. By modulating its activity, we showed that PI3K regulates NANOG and other TFs levels during the early phase of ICM specification and that such regulation occurs primarily at the posttranscriptional level.

Results

PI3K/AKT pathway is active during preimplantation embryos

To monitor PI3K/AKT activity during preimplantation development, we analyzed the levels of phosphorylated ribosome protein S6 (pRPS6), a well-established downstream target and widely used readout of PI3K/AKT pathway activation (Meyuhas, 2015). We first analyzed the levels of total and phosphorylated RPS6 in two-cell-stage to late blastocyst stage (embryonic day (E) 4.0) embryos (Figure 1A). As expected for an integral component of the small ribosomal subunit, RPS6 was detected in the cytoplasm of all blastomeres and at all stages. During preimplantation development, total RPS6 levels increased and peaked at early blastocyst (E3.25) stage (Figure 1A and S1A). Similar to total RPS6, pRPS6 was detected in all cells and at all stages and up to E3.25 followed the same trend than total RPS6 expression (Figure 1A and S1A). Accordingly, the ratio of pRPS6 over total RPS6 cytoplasmic levels was quite homogeneous between blastomeres and stable over this developmental period (Figure 1B). In contrast, heterogeneous pRPS6 levels were observed at later stages in both inner and outer cells (Figure 1A-B). To address whether variation in pRPS6 levels in inner cells was correlated with Epi and PrE differentiation occurring at that time, we quantified pRPS6, NANOG and GATA6 levels in inner cells of E3.25, E3.75 and E4.0 embryos. We found no correlations between RPS6 phosphorylation and NANOG or GATA6 levels (Figure S1B-D) suggesting that increased levels of pRPS6 are not linked to Epi or PrE fate acquisition. It may rather reflect other cellular processes such as PI3K/AKT-mediated survival of Epi and PrE progenitors once specified (Bessonnard et al., 2019).

RPS6 phosphorylation is mainly catalyzed by S6 kinase (S6K) upon mammalian target of rapamycin complex 1 (mTORC1) activation but can also occur through other pathways including 90-kDa rpS6 Kinase (RSK) upon MEK/ERK activation. To determine which pathways are responsible for RPS6 phosphorylation during preimplantation development, we cultured E2.75 embryos for 24h with various inhibitors: the PI3K inhibitor LY294002 (LY), the mTOR inhibitors Rapamycin and INK128, or the Mitogen-activated protein kinase (MEK) inhibitor PD0325901 (PD03). We observed a complete disappearance of pRPS6 staining upon PI3K or mTOR inhibition (Figure 1C-D, S1E). In contrast, pRPS6 staining seemed unaffected by PD03 treatment (Figure 1E). Collectively, our data show that PI3K/AKT/mTOR is constitutively active throughout preimplantation development and uncover disparate and more intense activities once the first three embryonic lineages are established.

PI3K/AKT maintains NANOG in ICM progenitors

Next, we monitored the consequences of PI3K inhibition on NANOG expression by treating embryos with LY during various time windows. NANOG expression is first detected at the 8-cell stage (Plusa et al., 2008). To test a possible role of PI3K/AKT in the onset of NANOG expression, we treated 2-cell stage embryos for 24h until they reached the 8-cell stage. Treated embryos developed normally and showed NANOG staining (Figure S2A) indicating that PI3K/AKT activity is not required for the initiation of *Nanog* expression. We then treated E2.75 morulae for 24h, a period during which ICM progenitors are produced and initiate their specification into Epi and PrE. Strikingly, we observed that although both LY and vehicle treated embryos progressed similarly to mid-blastocyst stage (~53-57 cells), a dramatic reduction in the number of NANOG-positive but not GATA6-positive cells was observed upon PI3K inhibition (Figure 2A). Quantification of NANOG and GATA6 levels in inner cells showed a strong reduction of NANOG levels upon PI3K inhibition while GATA6 levels were hardly affected (Figure 2B). Treatment of E2.75 embryos for a shorter period of time (16 hours), until they reached early-blastocyst (30-38 cells) stage, or of E3.0 (27-32 cells) early blastocysts for 8 hours gave similar results (Figure S2B-E). In contrast, E3.25 (~47-55 cells) embryos treated for 8 hours showed no strong alteration of NANOG levels (Figure 2C-D). Together, these observations suggest that PI3K/AKT inhibition impact NANOG levels during the birth of ICM progenitors and the initial phase of Epi/PrE specification, but not at a later phase.

Since PI3K/AKT pathway plays major roles in cell survival and proliferation, the diminution of NANOG-positive cells in LY-treated embryos could result from selective elimination or reduced proliferation of NANOG-positive inner cells. To address this possibility, we first compared the number of mitosis and fragmented nuclei in LY-treated compared to control (vehicle-treated) embryos. As shown in Figure S2F, no differences were observed between the two types of embryos whatever the time window used for treatment. We then performed live imaging of E2.75 H2B-GFP-expressing embryos treated or not with LY for 24 hours. H2B-GFP allowed tracking of mitosis and assessing nuclear fragmentation as a mark of cell death over the course of the movies. Control and LY- treated embryos were indistinguishable in terms of proliferation and cell death (Figure S2G-H). We thus conclude from these observations that LY treatment has no impact on cell survival or cell division at morulae and early/mid-blastocyst stages.

Finally, we investigated whether ICM progenitors with no or low NANOG levels following PI3K inhibition were irreversibly restricted to PrE fate. To that end, we first incubated E2.75 embryos with LY for 24 hours, fixed some embryos to verify the efficacy of the treatment

and released the remaining embryos from the inhibitor for 16 hours (Figure 2E). Surprisingly, we found no differences between embryos initially treated with the inhibitor or the vehicle, both showing a cluster of NANOG-only Epi progenitors segregating from a layer of GATA6-only PrE progenitors (Figure 2F). We were unable to assessed whether prolonged incubation with the inhibitor would lead to irreversible extinction of *Nanog* expression since, as previously reported, LY treatment of late blastocysts compromised inner cell survival (Figure S3A-B and data not shown).

We thus report that PI3K is maintaining NANOG by a proliferation and survival-independent mechanism during the early phase of specification when Epi progenitors are formed.

PI3K regulates Epi and PrE TFs levels independently of ERK activity

Having established that LY treatment strongly impacts NANOG levels during blastocyst formation, we undertook the analysis of PI3K inhibition on the expression of additional lineage-specific TFs. SRY-Box Transcription Factor 2 (SOX2) and Estrogen related receptor beta (ESRRb) are present in ICM progenitors and become progressively restricted to Epi lineage (Okamura et al., 2019; Wicklow et al., 2014). Similar to NANOG, SOX2 levels in inner cells were significantly reduced after 24 hours of PI3K inhibition (Figure 3A-B). However, and unlike NANOG, SOX2 levels were less affected after shorter duration of inhibition (Figure S3C-D). Similar results were obtained for ESSRB (Figure S3E). In contrast, expression levels of POU Class 5 Homeobox 1 (POU5F1/OCT4) and Kruppel Like Factor 4 (KLF4) pluripotency TFs, that become restricted to Epi subsequently (Guo et al., 2010; Morgani and Brickman, 2015), were significantly increased upon PI3K inhibition (Figure S3F-I).

In absence of NANOG or SOX2, PrE differentiation is compromised as a result of decreased *Fgf4* expression (Frankenberg et al., 2011; Wicklow et al., 2014). Hence, *Nanog*- and *Sox2*-deficient E3.75 blastocysts failed to activate SRY-Box transcription factor 17 (SOX17) and GATA4 binding protein 4 (GATA4) which are normally expressed in a sequential and ERK-dependent manner in PrE progenitors (Artus et al., 2011). Since both NANOG and SOX2 levels are significantly reduced upon PI3K inhibition, we expected a delayed or defective PrE differentiation in LY treated embryos. Contrary to our expectations, high levels of SOX17 were detected in all inner cells of E2.75 treated with LY for 24h (Figure 3C-D). GATA4 expression was not detected in control or LY-treated E2.75 + 24h (Figure S3J). We thus cultured E3.0 for 12h and obtained robust GATA4 expression in the control condition (Figure

S3A). Conversely, addition of LY, together with the pan-caspase inhibitor Z-VAD to limit LY-induced inner cell death at mid/late blastocyst stage, resulted in the lack of GATA4 expression (Figure S3A-B). Our data therefore show that PI3K negatively regulates SOX17 expression in the embryo and when inhibited, ICM cells progress to a GATA6- and SOX17-positive state but are unable to activate downstream PrE markers such as *Gata4*.

Similar to PI3K inhibition, the addition of high concentration of FGF2/4 and heparin during the period of Epi/PrE specification is sufficient to repress NANOG and SOX2 and upregulate SOX17 (Wicklow et al., 2014; Yamanaka et al., 2010). Together with the previously identified crosstalks between PI3K/AKT and RAF/MEK/ERK pathways (Mendoza et al., 2011; Zimmermann and Moelling, 1999), this raised the possibility that the effect of LY on lineage specific TFs is mediated, at least in part, through MEK/ERK. To address this possibility, we first compared embryos cultured with LY and with FGF2 and heparin and found that, contrary to PI3K inhibition, activation of MEK/ERK by exogenous FGF, during the same time window, promoted GATA4 expression (Figure S3J-K). Next, we asked whether the impact of PI3K inhibition was modified by simultaneous inhibition of MEK. Consistent with previous reports (Bessonnard et al., 2017; Saiz et al., 2016; Yamanaka et al., 2010), E2.75 embryos treated for 24h with the MEK inhibitor PD03 exhibited NANOG expression in all ICM cells and lacked SOX17 expression (Figure 3E-F). Strikingly, the simultaneous inhibition of PI3K and MEK or PI3K inhibition alone led to the same phenotype, characterized by reduced NANOG and SOX17 upregulation. Thus, our data demonstrate that PI3K inhibition affects TFs levels in ICM progenitors independently of MEK/ERK activity.

Noticeably, SOX17, which is specifically expressed in emergent PrE under normal conditions, was upregulated upon PI3K inhibition not only in ICM but also in TE cells (Figure 3C, E). Despite this, the key transcriptional TE drivers, Caudal type homeobox 2 (CDX2) and GATA binding protein 3 (GATA3), were hardly affected by LY treatment (Figure S3K).

Collectively, our data show that PI3K controls, through a mechanism not relying on MEK/ERK, the protein levels of key members of the pluripotency network of TFs as well as SOX17, the first TFs activated during PrE differentiation.

PI3K inhibition induces modest alterations of inner cells transcriptome

To investigate whether PI3K inhibition was affecting inner cell identity beyond TFs levels, single-cell RNA sequencing (scRNAseq) was performed. ICMs were immunosurgically isolated from E2.75 embryos treated for 16 and 24 hours with vehicle or LY and manually dissociated into single cells. As a reference, single inner cells were also collected from non-

cultured E3.25 (~47-55 cells), E3.75 (~63-69 cells) and E4.0 (~96-108 cells) blastocysts. Single cells from each stage and condition were obtained from two to three independent experiments, each including multiple litters, and processed with the low-input RNA-seq method initially developped by Tang and collaborators (Tang et al., 2009). A total of 170 out of 194 single cells (20x E3.25, 22x E3.75, 14x E4.0, 31x E2.75+16h ctl, 31x E2.75+16h LY, 28x E2.75+24h ctl, 24x E2.75+24h LY) passed the quality control. First, we integrated our dataset with published scRNA-seq datasets from 16-, 32- and 64-cell stage embryos (262 cells) (Posfai et al., 2017), and from E3.5 and E4.5 embryos (1083 cells) (Mohammed et al., 2017; Nowotschin et al., 2019) using Scanorama which facilitates the integration of different dataset sizes and sources by identifying and merging shared cell types (Hie et al., 2019). We projected the combined data using uniform manifold approximation and projection (UMAP) (Figure 4A) which reflected developmental lineage progression in accordance with lineage-specific markers (Figure 4B and S4A). To assign cell populations by lineage identities, we applied clustering on a nearest neighbor graph (Butler et al., 2018) and identified 9 clusters which distinguished inner cells and ICM progenitors (clusters 1 and 6), Epi (clusters 0 and 7), PrE (clusters 3, 4 and 2) and outer cells and TE (clusters 5 and 8) differentiation (Figure 4C and S4B). Our reference cells were distributed accordingly to their developmental stage, with E3.25 cells being clustered with ICM progenitors, early Epi and early PrE cells and the majority of E4.0 cells being clustered with Epi and PrE cells (Figure S4C). Consistent with our immunostaining analyses, most vehicle-treated cells mapped to early ICM progenitor cluster 1 at 16h while more than two thirds of the cells were found in clusters 6, 0, 3 and 4 at 24h (Figure 4D). In contrast, all LY-treated cells but four were found in ICM progenitors cluster 1, regardless of culture duration, suggesting that PI3K inhibition prevented ICM progenitor differentiation. UMAP plot of control and LY-treated cells showed segregation of cells according to time in culture but extensive mixing according to treatment (Figure 4E). Accordingly, a very limited number of genes (8 upregulated and 2 downregulated in vehicle compared to LY treated ICM cells, FDR<10%, Table S5) were found differentially expressed between control and LY-treated cells. Genes that were depleted in LY-treated cells tend to be upregulated in Epi and PrE (Figure 4F), consistent with the notion that LY treatment prevented ICM progenitor differentiation.

Next, we looked, in our dataset, at expression of a set of relevant genes, in particular those coding for the TFs we analyzed by immunostaining. In contrast to proteins levels, *Nanog*, *Esrrb* and *Sox2* mRNA levels were hardly affected by LY treatment (Figure 4G and S4D). Similarly, no upregulation of *Sox17* was observed in LY-treated cells. Interestingly, *Fgf4* mRNA levels were low in LY-treated cells (Figure 4G). This is consistent with the reduced NANOG and

SOX2 levels triggered by LY treatment since previous studies have reported reduced *Fgf4* mRNA levels in *Nanog* and *Sox2* mutant embryos (Frankenberg et al., 2011; Wicklow et al., 2014). Altogether, this analysis indicates that the regulation of lineage-specific TFs in ICM progenitors is not acting primarily at the transcriptional level and rather acts at a post-transcriptional level.

GSK3, a downstream effector of PI3K/AKT, regulates NANOG levels in ICM progenitors

Next, we searched for the effectors acting downstream of PI3K and potentially involved in the regulation of Epi and PrE TFs. First, we addressed the role of mTOR using mTORC1 (Rapamycin) and dual (INK128) inhibitors. Inhibition of mTORC1 and mTORC2 signaling did not alter NANOG expression (Figure 5A-B and S5A-B) indicating that mTOR is not acting downstream of PI3K/AKT to maintain NANOG levels. FOXO TFs are downstream direct targets of PI3K/AKT being translocated to the cytosol upon AKT-mediated phosphorylation (Brunet et al., 1999). Importantly, FOXO1 and FOXO3 proteins have been shown to regulate pluripotency in human and mouse ES respectively, possibly through direct transcriptional regulation of *Sox2 and Pou5f1/Oct4* pluripotency genes (Zhang et al., 2011). Both nuclear and cytoplasmic FOXO3 staining were observed in control blastocysts with some cells showing nuclear accumulation and others nuclear exclusion (Figure 5C). Such heterogeneous nucleocytoplasmic distribution may reflect the heterogenous PI3K/AKT activity we uncovered at this stage. Accordingly, we observed a clear FOXO3 nuclear accumulation in most cells of LY-treated embryos (Figure 5C). Assuming that the positive transcriptional regulation of FOXO proteins on pluripotent Epi TFs is not only operational in ES cells but also *in vivo* in the embryo, this suggests that FOXO3 is not the main effector acting downstream of PI3K/AKT in ICM progenitors to positively regulate SOX2 and NANOG levels. Another well-known target of AKT is the glycogen synthase kinase 3 (GSK3) α/β, the activity of which is inhibited upon AKT phosphorylation (Cross et al., 1995). In ES cells, inhibition of GSK3α/β activity by PI3K/AKT has been proposed to participate to NANOG upregulation and maintenance of pluripotency (Niwa et al., 2009; Paling et al., 2004; Singh et al., 2012). We treated E2.75 morulae for 24h with the GSK3 inhibitor CHIR99021 (CHIR) and observed a significant upregulation of NANOG levels (Figure 5D-E). This shows that NANOG levels in ICM progenitors are regulated by GSK3α/β activity. Therefore, PI3K/AKT is likely to act through GSK3 kinase to regulate TFs levels in ICM progenitors.

PI3K regulates SOX17 expression in ICM progenitors independently of GATA6

We next investigated whether NANOG and GATA6, which are critically required for the formation of Epi and PrE respectively, could mediate some or all of the action of PI3K/AKT during ICM cell specification. In *Nanog* mutant blastocysts, all ICM cells express GATA6 but are unable to initiate *Sox17* and *Gata4* expression unless being treated with exogenous FGF and heparin (Frankenberg et al., 2011). *Nanog*-deficient embryos treated for 24h with LY were undistinguishable from their wild-type or heterozygous littermates (Figure 6A-B). Notably, SOX17 upregulation was not affected by the absence of NANOG demonstrating that NANOG is not required for PI3K/AKT-mediated repression of SOX17.

In *Gata6* mutant blastocysts, NANOG is expressed in all ICM cells (Bessonnard et al., 2014; Schrode et al., 2014). Interestingly and contrary to their wild-type and heterozygous littermates, zygotic (Figure S6C) as well as maternal and zygotic (Figure 6C) *Gata6* homozygous mutants displayed robust NANOG nuclear staining in most inner cells following LY treatment. Quantification, performed after pooling experiments with limited variation in intensity levels across them (Figure S6A-B), confirmed that NANOG levels were significantly higher in *Gata6* mutant embryos (Figure 6D, S6D). GATA6 is therefore required for efficient downregulation of NANOG upon PI3K inhibition. Whether PI3K acts through GATA6 to modulate NANOG levels or whether this is due to higher NANOG levels in ICM progenitors of *Gata6-/-* embryos irrespective of PI3K activity (Bessonnard et al., 2014) remains to be determined. GATA6 is critically required for *Sox17* activation and exogenous FGF4 is unable to rescue SOX17 expression in *Gata6-/-* embryos (Bessonnard et al., 2014; Schrode et al., 2014). Contrary to expectations, SOX17 was detected in LY-treated *Gata6* deficient embryos, although at lower levels than in their heterozygous littermates (Figure 6C-D). Thus, contrary to the prevailing view of PrE fate emergence, SOX17 can be activated independently from GATA6 when PI3K/AKT signaling is inhibited. This raises the possibility that both a positive input from GATA6 and a release from a negative PI3K/AKT input are required for ICM progression towards PrE fate.

DISCUSSION

In this study, we investigated whether the regulation of NANOG by PI3K, that has been largely described in mouse ES cells, was also operating during the establishment of the pluripotent Epi in the mouse embryo. We showed that PI3K/AKT is active during preimplantation development and positively controls NANOG levels in ICM progenitors during the early phase of Epi/PrE specification. PI3K signaling sustains the expression of other Epi TFs such as SOX2 and ESSRb but not of OCT4 and KLF4, and represses that of SOX17, the detection of which normally represents the first sign of progression towards PrE fate. We further showed that PI3K is not acting through MEK/ERK to modulate the levels of these TFs. Our results therefore establish PI3K signaling as a new important player in the regulation of key Epi and PrE TFs in the mouse blastocyst. At the early step of ICM differentiation, when FGF/ERK signaling is less prominent, variations in PI3K activity in ICM progenitors might destabilize the gene regulatory network defining the bipotent ICM progenitor state thereby helping driving cell towards Epi or PrE fate.

Epi/PrE specification is a rapid process that occurs in a few hours and implies the downregulation of either NANOG or GATA6 followed by the reinforcement of the pluripotency program in Epi progenitors and the sequential activation of lineage-specific TFs and genes in PrE progenitors. Initial downregulation of NANOG and GATA6 could result from multiple mechanisms acting both at the transcriptional and post-transcriptional levels. Our transcriptomic analysis suggests that PI3K-mediated regulation is not acting primarily at the transcriptional level in ICM progenitors. This is reminiscent of observations made in LY-treated ES cells showing a clear decrease in NANOG protein levels after 8 hours while *Nanog* mRNA levels started to be affected after 24 to 48 hours (Hishida et al., 2015; Storm et al., 2007). NANOG has a short half-live (1-3 hours compared to 6h or more for OCT4 in ES cells (Sanchez-Ripoll et al., 2013), therefore variations in mRNA levels or translation efficiency rapidly impact NANOG levels. Importantly, PI3K acts upstream of mTORC signaling that, when inhibited in both mouse blastocyst and ES cells, induces a paused state characterized by major downregulations in general transcription and translation (Bulut-Karslioglu et al., 2016; Xu et al., 2021). In this study, we showed that inhibition of mTORC signaling during the early phase of ICM specification did not alter NANOG levels indicating that NANOG downregulation following PI3K inhibition was not simply a consequence of global inhibition of mRNA and protein synthesis. PI3K can also modulate protein levels through AKT-mediated phosphorylation. Of note, AKT has been shown to directly phosphorylate SOX2, OCT4 and

KLF4 and modulate their stability (Chen et al., 2013; Fang et al., 2014; Lin et al., 2012). If such mechanism were controlling NANOG levels, NANOG being not a known direct target of AKT, this would imply an indirect action through an intermediate factor controlling NANOG stability. Interestingly, we previously showed that NANOG is markedly downregulated when the proteasome is inhibited revealing the existence of a short-lived negative regulator of NANOG expression or stability in ICM and Epi progenitors (Bessonnard et al., 2017). The identity of this regulator and whether it is a target of AKT is currently unknown.

PI3K has been shown to regulate pluripotency in ES cells through additional mechanisms including FOXO TFs. However, both subcellular localization of FOXO3 and lack of transcriptional response in LY-treated embryos argue against such mechanism having a prominent role in the embryo in ICM progenitors. In contrast, our data suggest that GSK3 acts downstream of, or in parallel to, PI3K/AKT to regulate NANOG. In ES cells, GSK3 activity has been shown to negatively regulate *Nanog* through either stabilization of TCF7L1, which together with β-catenin represses the transcription of Nanog (Wray et al., 2011; Yi et al., 2011) or through destabilization of c-MYC, which promotes pluripotency and represses PrE program (Bechard and Dalton, 2009; Cartwright et al., 2005; Singh et al., 2012; Smith et al., 2010). Through AKT-mediated inhibitory phosphorylation, continuous PI3K signaling could help to keep in check GSK3 activity and thereby to maintain NANOG levels in ICM progenitors. GSK inhibition has also been shown to enhance *Nanog* mRNA translation in ES cells (Sanchez-Ripoll et al., 2013). In the future, it will be important to determine which of these mechanisms are at play to regulate NANOG levels in ICM progenitors.

Both *Gata6* and FGF/ERK signaling negatively regulate *Nanog* expression in embryo and ES cells. We found that NANOG downregulation following PI3K inhibition was less efficient in *Gata6* mutant embryos suggesting that PI3K regulates NANOG at least in part through GATA6. In contrast, we showed that PI3K is not acting through ERK and, contrary to other cells including ES cells (Mendoza et al., 2011; Paling et al., 2004), PI3K/AKT and RAS/ERK pathways do not seem to be interconnected in ICM progenitors. Independence from ERK signaling was further confirmed by the fact that NANOG downregulation occurs in absence of ICM progenitor maturation and *Fgf4* upregulation, as evidenced by our scRNAseq analysis of LY-treated ICM cells. Interestingly, no impact on NANOG levels was observed when PI3K was inhibited at later stage (E3.25, ~50 cells). At that time, coordinated expression of pluripotency markers has been set up (Allègre et al., 2019) which may render ICM cells able to cope more easily with downregulation of a few TFs. When applied at E2.75, before the establishment of coordinated expression, PI3K inhibition may delay the establishment of such

coordinated expression and consequently delay ICM maturation. An alternative but non-exclusive explanation is that the control of TFs levels by PI3K is temporally regulated.

We also discovered that, besides positive regulation of pluripotency TFs levels, PI3K is involved in SOX17 downregulation in ICM progenitors, probably through post-transcriptional mechanisms. *Sox17* is transcribed before ICM cells engage into PrE fate but SOX17 protein accumulation becomes evident in PrE progenitors with low NANOG levels (Morris et al., 2010; Niakan et al., 2010). Post-transcriptional downregulation of SOX17 would endow ICM progenitors with the ability to respond rapidly to changes in intrinsic and extrinsic cues and adopt a PrE fate. Indeed, SOX17 is bound together with GATA6 at PrE regulatory elements (Thompson et al., 2021; Wamaitha et al., 2015) and contributes to the establishment of the PrE transcriptional network following ectopic expression of GATA6 or growth factors induced conversion of ES cells (Cho et al., 2012; Niakan et al., 2010). Rapid upregulation of SOX17 might also be important to quickly redistribute OCT4 from pluripotency to PrE enhancers through competition with SOX2 for OCT4 binding (Aksoy et al., 2013). In the embryo, *Sox17* expression is triggered by *Gata6* together with FGF signaling. Here we showed that SOX17 expression occurs when PI3K is inhibited and *Fgf4* expression is low as well as in absence of GATA6. This novel finding demonstrates that, in the embryo, *Sox17* is not a strict downstream target of *Gata6* and that other factors participate to its initial transcriptional activation before the takeover by *Gata6* and FGF signaling.

While we focused our analysis on ICM progenitors, we noticed that PI3K inhibition impinges on NANOG and SOX17 levels in TE as well (see Figure 3 for example) but not on GATA3 and CDX2 levels (Figure S3K). *Nanog* and *Gata6* start to be expressed together with *Cdx2* at the 8-cell stage. While CDX2 is known to repress expression of ICM genes in the TE (Strumpf et al., 2005), NANOG and GATA6 proteins are detected in TE up to mid blastocyst stage (Plusa et al., 2008). Our observations indicate that PI3K activity in outer and TE cells may contribute to the persistence of NANOG after its transcription is turned off. They also suggest that initial expression of *Sox17* is not restricted to inner cells and ICM progenitors.

In conclusion, our study unravels a dual role of PI3K/AKT signaling in the maintenance of the pluripotent TFs NANOG, ESRRb and SOX2 and in the downregulation of SOX17 levels before or at the onset of Epi and PrE specification. Although PI3K/AKT and GSK3 are known to be critical determinants of pluripotency in mouse ES cells for a long time, evidences for PI3K/AKT regulating early embryonic fate were lacking so far. There are many reasons for this, in particular the fact that the role of PI3K seems to be critical only before the establishment of a robust pluripotency network and the rise of the FGF/ERK signaling pathway. The fact that

specification events occur very rapidly in the mouse preimplantation embryo and the PI3K/AKT pathway regulates proliferation and survival once lineages are established has also delayed the discovery of the initial role of PI3K in regulating ICM progenitor identity. Our findings will be instrumental to reevaluate the role of PI3K/AKT signaling during cell fate decisions in other mammalian embryos. Recent observations in pig (Ramos-Ibeas et al., 2019) and human (Wamaitha et al., 2020) preimplantation embryos suggest that regulation of *Nanog* and *Sox17* by PI3K may be conserved across species.

AKNOWLEDGMENTS

We are grateful to the staff of the animal facility of Institut Pasteur for animal care and their help during this work. We thank Jean-Yves Tinevez from the Image Analysis Hub of Institut Pasteur for his help with the Icy software. Many thanks to Maud Borensztein and Raquel Pérez-Palacios for their advice on single cell cDNA and library preparation. This work was supported by the Institut Pasteur, the Centre National de la Recherche Scientifique and the Agence Nationale de la Recherche (ANR-10-LABX-73-01 REVIVE). A.G. was supported by Sorbonne Université and received fellowship from the French Ministère de l'Enseignement Supérieur et de la recherche, the Fondation ARC pour la Recherche sur le Cancer and the REVIVE Labex.

Competing interests: The authors declare no competing interest.

AUTHORS CONTRIBUTIONS

A.G., Conception and design, Acquisition of data, Analysis and interpretation of data, Drafting or revising the article; S.V.-P., Acquisition of data; V.L., S.M. Analysis and interpretation of data; P.N., Analysis and interpretation of data, Drafting or revising the article; M.C.-T., Conception and design, Analysis and interpretation of data, Drafting or revising the article.

MATERIALS AND METHODS

Embryo collection and culture

All experiments were performed according to the French and European regulations on care and protection of laboratory animals (EC Directive 86/609, French Law 2001-486 issued on June 6, 2001) and were approved by the Institut Pasteur ethics committee. All mice were kept in a 14h light cycle from 7am to 9pm, except mice used to obtain E3.0 embryos which were kept in a 14h light cycle from 2pm to 1am. WT preimplantation embryos were obtained from natural mating of CD1 mice (Charles River Laboratories, France). Embryos were staged according to the date of the vaginal plug (E0.5) at noon and collected by flushing oviducts or uteri with FHM medium (Millipore). Embryos were cultured at low density in KSOM+AA medium (Millipore) using 4-well plates (Nunc) at 37°C, 8% CO2. The pharmacological molecules which were added to the culture are listed in Table 1. The solvent which was used to resuspend the molecules was added to the culture containing the control embryos.

Table 1: **List of used molecules.**

Molecule	Final concentration	Manufacturer
LY294002	10µM	Cell Signaling Technology, 9901S
PD0325901	1µM	Axon Medchem, 1408
INK128	100nM	Selleckchem, S2811
CHIR9910	3µM	Axon Medchem, 1386
FGF2	1µM	Gibco, PHG0367
Heparin	1µg/ml	Sigma, H3149-10KU
Z-VAD-FMK	20µM	Focusbiomolecules, 10-2614
Rapamycin	10µM	Sigma, R8781

Mutant mice and genotyping

Zygotic *Gata6*$^{+/-}$ mice were the result of mating *Gata6*$^{tm2.2Sad}$ males (Sodhi et al., 2006) with Tg(Pgk1-cre)1Lni females (Lallemand et al., 1998). By crossing *Gata6*$^{+/-}$ mice, 25% of the obtained embryos were *Gata6*$^{-/-}$. To achieve maternal-zygotic deletion of *Gata6*, we first crossed female *Zp3Cre*$^{Tg/Tg}$ mice (Vries et al., 2000) with *Gata6*$^{flox/flox}$ males (Sodhi et al., 2006) to produce *Zp3Cre*$^{Tg/0}$*;GATA6*$^{flox/+}$ females. Crossing these females with CD1 males, led to Cre-recombination of *Gata6* in 100% of the offspring and we used the resulting *Zp3Cre*$^{Tg/0}$*;GATA6*$^{+/-}$ males for the final mating. To produce the females for the final mating, we crossed female *Zp3Cre*$^{Tg/Tg}$ mice with *Zp3Cre*$^{Tg/0}$*;GATA6*$^{flox/+}$ males to produce *GATA6*$^{flox/+}$ males which are homozygous for *Zp3Cre.* When crossing the resulting *Zp3Cre*$^{Tg/Tg}$*;GATA6*$^{flox/+}$ females again with homozygous for *Zp3Cre; GATA6*$^{flox/+}$ males, the females for the final crossing with the genotype *Zp3Cre*$^{Tg/Tg}$*;GATA6*$^{flox/-}$ were obtained. Finally, mating of *Zp3Cre*$^{Tg/Tg}$*;GATA6*$^{flox/-}$ females with

Zp3Cre$^{Tg/0}$;GATA6$^{+/-}$ males resulted in the maternal-zygotic deletion of *Gata6* in 50% of the embryos. *Nanog$^{-/-}$* embryos were obtained by mating mice carrying *Nanog^{tm1Yam}* mutation (Mitsui et al., 2003). For live imaging experiments, heterozygous *CAG::H2B-EGFP* males(Hadjantonakis and Papaioannou, 2004) were crossed with female CD1 to obtain H2B-EGFP expressing embryos with a frequency of 50%. Embryo genotyping was performed after confocal imaging by incubating single embryos in lysis buffer (10mM TrisHCl ph8; 50mM KCl; 0.01% gelatine; 300µg/ml Proteinase K (Thermo Fisher)) at 56°C for 1h. Proteinase K was inactivated at 95°C for 10 minutes. The used primers and PCR program are listed in Table 2.

Table2: **List of genotyping primers.**

Gene	primer sequences	PCR program	expected size
Gata6	G6-del-F : 5'-AGTCTCCCTGTCATTCTTCCTGCTC-3' G6-del-R : 5'-TGATCAAACCTGGGTCTACACTCCTA-3' G6-WT-F : 5'-GTGGTTGTAAGGCGGTTTGT-3' G6-WT-R : 5'-ACGCGAGCTCCAGAAAAAGT-3'	30sec 98°C 25x (10 sec 98°C 15 sec 61°C 60 sec 72°C) 3 min 95°C	del : 568kb flox : 250kb WT : 159kb
Nanog	N-KO-F: 5'- CAGAATGCAGACAGGTCTACAGCCCG-3' N-WT-R : 5'-AATGGGCTGACCGCTTCCTCGTGCTT-3' N-KO-R : 5'-GGCCCAGCTGTGTGCACTCAA-3'	5 min 95°C 21x (10 sec 95°C 10 sec 62°C 60 sec 72°C) 7 min 95°C	del: 600bp WT: 889bp

Whole-mount immunostaining

For immunofluorescence stainings, embryos were fixed with 4% paraformaldehyde (PFA) in PBS for 15 minutes at room temperature (RT) and washed three times with 0.1% PBS Tween. Embryos were permeabilized with PBS 0.1% Triton-X100 (PBX) for 30 minutes at RT and incubated in blocking solution (10% donkey serum in PBX) for 1h. Embryos were treated with primary antibodies (Table 3) diluted in blocking solution at 4°C overnight. After three washes with PBX, embryos were incubated with secondary antibodies (Table 4) diluted 1/300 in PBX for at least 1h. Nuclear staining was achieved by Hoechst 33342 (Thermo Fisher).

Table 3: **List of primary antibodies.**

Protein	Host	Dilution	Manufacturer
NANOG	rat	1/200	eBioscience, MLC-51
GATA6	rabbit	1/100	Cell Signaling Technology, 5851
GATA6	goat	1/100	R&D, AF1700

CDX2	mouse	1/100	BioGenex, MU392A-UC
SOX17	goat	1/100	R&D, AF1924
SOX2	rat	1/200	eBioscience, 14-9811-80
OCT4	goat	1/100	Santa Cruz, sc-8628
GATA4	goat	1/100	Santa Cruz, sc-1237
GATA3	goat	1/100	R&D, AF2605
pRPS6	rabbit	1/100	Cell Signaling Technology, 2211S
RPS6	mouse	1/100	Cell Signaling Technology, 5G10
FOXO3	rabbit	1/100	Cell Signaling Technology, 2280P

Table 4 : **List of secondary antibodies.**

Fluorochrome	Host	Dilution	Manufacturer
Alexa 488	rat, rabbit, goat, mouse	1/300	Thermo Fisher, A11055
Alexa 546	rat, rabbit, goat, mouse	1/300	Thermo Fisher, A11056
Alexa 647	rat, rabbit, goat, mouse	1/300	Thermo Fisher, A31571

Confocal microscopy

All images were acquired by using a Zeiss LSM800 confocal microscope. Embryos were placed in an in-house developed and produced eggbox imaging device (Vandormael-Pournin et al., 2021) to facilitate a multi-positioning setup and scanned using a plan-apochromat 20x objective without immersion. Images were acquired using bi-directional scanning, 2-line averaging, 2x zoom and 1 airy unit pinhole. Stacks were created with a 2µm step, generating 16-bit (512x512px) images. For live imaging, embryos were imaged in a 10 min time interval for a total of 24h and maintained in a humified incubation chamber at 37°C in 5% CO_2.

Image analysis

ImageJ (NIH) was used to manually perform cell counting, obtain projections of optical slices and add scale bars. Quantification of nuclear fluorescence intensities was achieved using the Spots creation wizard of the IMARIS (Bitplane) software. To correct the z-associated attenuation of fluorescence, nuclear signals were normalized by dividing their values by the corresponding value of Hoechst. Calculation of the background level was performed by dividing the average of the mean fluorescence intensities of randomly chosen cytoplasmic spots with the average of Hoechst fluorescence.

The Icy software (Institut Pasteur) was used to measure mean fluorescence intensities of cytoplasmic proteins. For each cell a 2D region of interest (ROI) was manually drawn in the nucleus and cytoplasm. In order to compare protein levels between different developmental stages, the values of Hoechst were corrected according to the nuclear volume of the

corresponding stage before they were used to normalize the measured nuclear and cytoplasmic signals. The correction factors for each stage were obtained from (Aguirre-Lavin et al., 2012).

Statistical analysis

The Graphpad software was used to perform statistical tests. The non-parametric Wilcoxon-Mann-Whitney test was applied to assess statistical significance of cell counts and the Kolmogorov-Smirnov test was used to calculate significance of normalized fluorescence intensities. Significant correlation was determined by fitting data to linear regression model.

Single cell isolation, library preparation and sequencing

The ZP of embryos was removed using acidic Tyrode's solution (Sigma) and single ICM were isolated by immunosurgery. First, embryos were cultured for 30 minutes at 37°C in anti-mouse red blood cell serum from rabbit (Rockland) and transferred to guinea pig complement serum (Sigma) for 20 minutes at 37°C. The lysed TE cells were carefully removed by mouth pipetting in PBS containing acetylated bovine serum albumin (ac-BSA). To obtain single cells, isolated ICM were briefly exposed to TripLE (Gibco) and then manually dissociated by repeated mouth pipetting with 40µm glass pipettes in PBS/ac-BSA. Single cells were individually picked into 1.5ml Eppendorf tubes, directly transferred to -80°C or immediately processed. Following the protocol of (Tang et al., 2010) and adapted by (Borensztein et al., 2018), mRNAs from every single cell were extracted, reverse-transcribed from 3'UTR and amplified. As a quality check, the amplification yield of the housekeeping genes Gapdh (F-5'-CCCCAACACTGAGCATCTCC-3', R-5'-ATTATGGGGGTCTGGGATGG-3') and Hprt (F-5'-CCTGTGGCCATCTGCCTAGT, R-5'-GGGACGCAGCAACTGACATT-3') was assessed by RT-qPCR using SyBR Green solution on a LightCycler480 (Roche). The cDNAs of every single cell were purified using the DNA Clean & Concentrator Kit (Zymo) and loaded and run on 2% agarose gels. cDNAs larger than approximately 500kb were excised from the gel and purified using the Zymoclean Gel DNA Recovery Kit (Zymo). The concentration of the purified cDNAs was quantified using the Qubit dsDNA HS Assay Kit (Thermo Fisher). The Nextera XT DNA Library Prep Kit (Illumina) was performed according to manufacturer's instructions to prepare the single cell libraries. First, during the process of tagmentation the cDNAs are fragmented and tagged with adapter sequences by a transposase. Then, the tagmented cDNAs were amplified using a unique combination of i5 and i7 indexes and purified using AMPure XP beads (Beckman Coulter). To control for the appropriate size distribution of 250-1000bp of the libraries a high sensitivity bioanalyzer (Agilent Technologies) was used and the concentration again determined via Qubit. The libraries were pooled at a concentration of

1nM, denatured with 0.2 N NaOH and diluted to 20pM. The sequencing was run on a NextSeq 550 (Illumina).

scRNAseq analysis

Sequencing quality control, mapping and expression quantification

Sequences were demultiplexed using bcl2fastq v2.20.0 and trimmed to remove adapters and low quality end bases using cutadapt v2.9. After trimming, reads shorter than 20 bases were discarded. Reads were then aligned to the *mm10* mouse reference genome using STAR (v2.7.9a) with default options (Dobin et al., 2013). Mapped reads with a quality score >20 were then quantitated using the RSEM pipeline (v1.3.3) with the *--single-cell-prior* option (2).

Data filtering

Quality control and data filtering were performed separately for the two sequencing runs. In both runs, cells with more than 10 million reads or 20% of reads mapping to mitonchondrial genes or more than 1% of spike-ins reads were filtered out. Cells expressing fewer than 4800 genes or the March run and fewer than 4,000 genes in the May run were excluded from the downstream analyses. 170 cells out of the 185 sequenced cells were kept for downstream analyses.

Data integration and downstream analyses

Sequenced cells were integrated with data from previously published datasets (Mohammed et al., 2017; Nowotschin et al., 2019; Posfai et al., 2017). Before integration, a check for quality control and a data filtering step was performed on each individual run from Nowotschin et al. (Nowotschin et al., 2019). The different thresholds used for each of these runs are detailed in Table S1. The datasets were normalized as counts per million, log-transformed and then integrated using Scanorama version 1.7.1 (Hie et al., 2019). Variable genes in each individual datasets were identified by computing the standardized variance for each gene and the 324 genes tagged as variable in at least 4 different sequencing runs were used for data integration. Cells were then clustered using the standard workflow from Seurat version 4.1.0 (Butler et al., 2018). Differentially expressed genes were identified using the MAST pipeline accounting for the data origin as implemented in Seurat.

REFERENCES

Aguirre-Lavin, T., Adenot, P., Bonnet-Garnier, A., Lehmann, G., Fleurot, R., Boulesteix, C., Debey, P. and Beaujean, N. (2012). 3D-FISH analysis of embryonic nuclei in mouse highlights several abrupt changes of nuclear organization during preimplantation development. *Bmc Dev Biol* 12, 30–30.

Aksoy, I., Jauch, R., Chen, J., Dyla, M., Divakar, U., Bogu, G. K., Teo, R., Ng, C. K. L., Herath, W., Lili, S., et al. (2013). Oct4 switches partnering from Sox2 to Sox17 to reinterpret the enhancer code and specify endoderm. *The EMBO Journal* 32, 938–953.

Allègre, N., Chauveau, S., Dennis, C., Renaud, Y., Estrella, L. V., Pouchin, P., Cohen-Tannoudji, M. and Chazaud, C. (2019). A Nanog-dependent gene cluster initiates the specification of the pluripotent epiblast. *Biorxiv* 141, 707679.

Artus, J., Piliszek, A. and Hadjantonakis, A.-K. K. (2011). The primitive endoderm lineage of the mouse blastocyst: sequential transcription factor activation and regulation of differentiation by Sox17. *Developmental Biology* 350, 393–404.

Azami, T., Bassalert, C., Allègre, N., Estrella, L. V., Pouchin, P., Ema, M. and Chazaud, C. (2019). Regulation of the ERK signalling pathway in the developing mouse blastocyst. *Development* 146, dev177139.

Bechard, M. and Dalton, S. (2009). Subcellular localization of glycogen synthase kinase 3beta controls embryonic stem cell self-renewal. *Mol Cell Biol* 29, 2092–104.

Bessonnard, S., Mot, L. D., Gonze, D., Barriol, M., Dennis, C., Goldbeter, A., Dupont, G. and Chazaud, C. (2014). Gata6, Nanog and Erk signaling control cell fate in the inner cell mass through a tristable regulatory network. *Development* 141, 3637–3648.

Bessonnard, S., Coqueran, S., Vandormael-Pournin, S., Dufour, A., Artus, J. and Cohen-Tannoudji, M. (2017). ICM conversion to epiblast by FGF/ERK inhibition is limited in time and requires transcription and protein degradation. *Sci. Rep.* 7, 12285.

Bessonnard, S., Vandormael-Pournin, S., Coqueran, S., Cohen-Tannoudji, M. and Artus, J. (2019). PDGF Signaling in Primitive Endoderm Cell Survival Is Mediated by PI3K-mTOR Through p53-Independent Mechanism. *Stem Cells* 37, 888–898.

Borensztein, M., Syx, L., Servant, N. and Heard, E. (2018). Transcriptome Profiling of Single Mouse Oocytes. *Methods Mol. Biol.* 1818, 51–65.

Boroviak, T., Loos, R., Lombard, P., Okahara, J., Behr, R., Sasaki, E., Nichols, J., Smith, A. G. and Bertone, P. (2015). Lineage-Specific Profiling Delineates the Emergence and Progression of Naive Pluripotency in Mammalian Embryogenesis. *Dev. Cell* 35, 366–382.

Brunet, A., Bonni, A., Zigmond, M. J., Lin, M. Z., Juo, P., Hu, L. S., Anderson, M. J., Arden, K. C., Blenis, J. and Greenberg, M. E. (1999). Akt Promotes Cell Survival by Phosphorylating and Inhibiting a Forkhead Transcription Factor. *Cell* 96, 857–868.

Bulut-Karslioglu, A., Biechele, S., Jin, H., Macrae, T. A., Hejna, M., Gertsenstein, M., Song, J. S. and Ramalho-Santos, M. (2016). Inhibition of mTOR induces a paused pluripotent state. *Nature* 540, 119–123.

Butler, A., Hoffman, P., Smibert, P., Papalexi, E. and Satija, R. (2018). Integrating single-cell transcriptomic data across different conditions, technologies, and species. *Nat Biotechnol* 36, 411–420.

Campbell, J. M., Nottle, M. B., Vassiliev, I., Mitchell, M. and Lane, M. (2012). Insulin increases epiblast cell number of in vitro cultured mouse embryos via the PI3K/GSK3/p53 pathway. *Stem Cells and Development* 21, 2430–2441.

Cartwright, P., McLean, C., Sheppard, A., Rivett, D., Jones, K. and Dalton, S. (2005). LIF/STAT3 controls ES cell self-renewal and pluripotency by a Myc-dependent mechanism. *Development* 132, 885–896.

Chazaud, C., Yamanaka, Y., Pawson, T. and Rossant, J. (2006). Early lineage segregation between epiblast and primitive endoderm in mouse blastocysts through the Grb2-MAPK pathway. *Dev. Cell* 10, 615–624.

Chen, B., Xue, Z., Yang, G., Shi, B., Yang, B., Yan, Y., Wang, X., Han, D., Huang, Y. and Dong, W. (2013). Akt-Signal Integration Is Involved in the Differentiation of Embryonal Carcinoma Cells. *Plos One* 8, e64877.

Cho, L. T. Y., Wamaitha, S. E., Tsai, I. J., Artus, J., Sherwood, R. I., Pedersen, R. A., Hadjantonakis, A.-K. and Niakan, K. K. (2012). Conversion from mouse embryonic to extra-embryonic endoderm stem cells reveals distinct differentiation capacities of pluripotent stem cell states. *Development* 139, 2866–2877.

Cross, D. A. E., Alessi, D. R., Cohen, P., Andjelkovich, M. and Hemmings, B. A. (1995). Inhibition of glycogen synthase kinase-3 by insulin mediated by protein kinase B. *Nature* 378, 785–789.

Dobin, A., Davis, C. A., Schlesinger, F., Drenkow, J., Zaleski, C., Jha, S., Batut, P., Chaisson, M. and Gingeras, T. R. (2013). STAR: ultrafast universal RNA-seq aligner. *Bioinformatics* 29, 15–21.

Fang, L., Zhang, L., Wei, W., Jin, X., Wang, P., Tong, Y., Li, J., Du, J. X. and Wong, J. (2014). A methylation-phosphorylation switch determines Sox2 stability and function in ESC maintenance or differentiation. *Molecular Cell* 55, 537–551.

Frankenberg, S., Gerbe, F., Bessonnard, S., Belville, C., Pouchin, P., Bardot, O. and Chazaud, C. (2011). Primitive endoderm differentiates via a three-step mechanism involving Nanog and RTK signaling. *Dev. Cell* 21, 1005–1013.

Guo, G., Huss, M., Tong, G. Q., Wang, C., Sun, L. L., Clarke, N. D. and Robson, P. (2010). Resolution of Cell Fate Decisions Revealed by Single-Cell Gene Expression Analysis from Zygote to Blastocyst. *Dev Cell* 18, 675–685.

Hadjantonakis, A.-K. and Papaioannou, V. E. (2004). Dynamic in vivo imaging and cell tracking using a histone fluorescent protein fusion in mice. *Bmc Biotechnol* 4, 33.

Halet, G., Viard, P. and Carroll, J. (2008). Constitutive PtdIns(3,4,5)P3 synthesis promotes the development and survival of early mammalian embryos. *Development* 135, 425–429.

Hie, B., Bryson, B. and Berger, B. (2019). Efficient integration of heterogeneous single-cell transcriptomes using Scanorama. *Nat Biotechnol* 37, 685–691.

Hishida, T., Nakachi, Y., Mizuno, Y., Katano, M., Okazaki, Y., Ema, M., Takahashi, S., Hirasaki, M., Suzuki, A., Ueda, A., et al. (2015). Functional Compensation Between Myc and PI3K Signaling Supports Self-Renewal of Embryonic Stem Cells. *Stem Cells* 33, 713–725.

Kang, M., Piliszek, A., Artus, J. and Hadjantonakis, A.-K. K. (2013). FGF4 is required for lineage restriction and salt-and-pepper distribution of primitive endoderm factors but not their initial expression in the mouse. *Development* 140, 267–279.

Kang, M., Garg, V. and Hadjantonakis, A.-K. K. (2017). Lineage Establishment and Progression within the Inner Cell Mass of the Mouse Blastocyst Requires FGFR1 and FGFR2. *Dev. Cell* 41, 496-510.e5.

Lallemand, Y., Luria, V., Haffner-Krausz, R. and Lonai, P. (1998). Maternally expressed PGK-Cre transgene as a tool for early and uniform activation of the Cre site-specific recombinase. *Transgenic Res* 7, 105–112.

Lin, T.-C., Yen, J.-M., Gong, K.-B., Hsu, T.-T. and Chen, L.-R. (2003). IGF-1/IGFBP-1 increases blastocyst formation and total blastocyst cell number in mouse embryo culture and facilitates the establishment of a stem-cell line. *BMC Cell Biol.* 4, 14.

Lin, Y., Yang, Y., Li, W., Chen, Q., Li, J., Pan, X., Zhou, L., Liu, C., Chen, C., He, J., et al. (2012). Reciprocal regulation of Akt and Oct4 promotes the self-renewal and survival of embryonal carcinoma cells. *Molecular Cell* 48, 627–640.

Lu, D. P., Chandrakanthan, V., Cahana, A., Ishii, S. and O'Neill, C. (2004). Trophic signals acting via phosphatidylinositol-3 kinase are required for normal pre-implantation mouse embryo development. *J Cell Sci* 117, 1567–1576.

Mendoza, M. C., Er, E. E. and Blenis, J. (2011). The Ras-ERK and PI3K-mTOR pathways: cross-talk and compensation. *Trends in Biochemical Sciences* 36, 320–328.

Meyuhas, O. (2015). Chapter Two Ribosomal Protein S6 Phosphorylation Four Decades of Research.pp. 41–73. International Review of Cell and Molecular Biology.

Mohammed, H., Hernando-Herraez, I., Savino, A., Scialdone, A., Macaulay, I., Mulas, C., Chandra, T., Voet, T., Dean, W., Nichols, J., et al. (2017). Single-Cell Landscape of Transcriptional Heterogeneity and Cell Fate Decisions during Mouse Early Gastrulation. *Cell Rep* 20, 1215–1228.

Molotkov, A., Mazot, P., Brewer, J. R., Cinalli, R. M. and Soriano, P. (2017). Distinct Requirements for FGFR1 and FGFR2 in Primitive Endoderm Development and Exit from Pluripotency. *Dev. Cell* 41, 511-526.e4.

Morgani, S. M. and Brickman, J. M. (2015). LIF supports primitive endoderm expansion during pre-implantation development. *Development* 142, 3488–3499.

Morris, S. A., Teo, R. T. Y., Li, H., Robson, P., Glover, D. M. and Zernicka-Goetz, M. (2010). Origin and formation of the first two distinct cell types of the inner cell mass in the mouse embryo. *Proc. Natl. Acad. Sci. U.S.A.* 107, 6364–6369.

Mot, L. D., Gonze, D., Bessonnard, S., Chazaud, C., Goldbeter, A. and Dupont, G. (2016). Cell Fate Specification Based on Tristability in the Inner Cell Mass of Mouse Blastocysts. *Biophysical Journal* 110, 710–722.

Niakan, K. K., Ji, H., Maehr, R., Vokes, S. A., Rodolfa, K. T., Sherwood, R. I., Yamaki, M., Dimos, J. T., Chen, A. E., Melton, D. A., et al. (2010). Sox17 promotes differentiation in mouse embryonic stem cells by directly regulating extraembryonic gene expression and indirectly antagonizing self-renewal. *Genes & Development* 24, 312–326.

Nichols, J., Silva, J. C. R., Roode, M. and Smith, A. G. (2009). Suppression of Erk signalling promotes ground state pluripotency in the mouse embryo. *Development* 136, 3215–3222.

Niwa, H., Ogawa, K., Shimosato, D. and Adachi, K. (2009). A parallel circuit of LIF signalling pathways maintains pluripotency of mouse ES cells. *Nature* 460, 118–122.

Nowotschin, S., Setty, M., Kuo, Y.-Y., Liu, V., Garg, V., Sharma, R., Simon, C. S., Saiz, N., Gardner, R., Boutet, S. C., et al. (2019). The emergent landscape of the mouse gut endoderm at single-cell resolution. *Nature* 569, 361–367.

Okamura, E., Tam, O. H., Posfai, E., Li, L., Cockburn, K., Lee, C. Q. E., Garner, J. and Rossant, J. (2019). Esrrb function is required for proper primordial germ cell development in presomite stage mouse embryos. *Dev Biol* 455, 382–392.

Paling, N. R. D., Wheadon, H., Bone, H. K. and Welham, M. J. (2004). Regulation of embryonic stem cell self-renewal by phosphoinositide 3-kinase-dependent signaling. *J. Biol. Chem.* 279, 48063–48070.

Plusa, B., Piliszek, A., Frankenberg, S., Artus, J. and Hadjantonakis, A.-K. K. (2008). Distinct sequential cell behaviours direct primitive endoderm formation in the mouse blastocyst. *Development* 135, 3081–3091.

Posfai, E., Petropoulos, S., Barros, F. R. O. de, Schell, J. P., Jurisica, I., Sandberg, R., Lanner, F. and Rossant, J. (2017). Position- and Hippo signaling-dependent plasticity during lineage segregation in the early mouse embryo. *Elife* 6, e22906.

Ramos-Ibeas, P., Sang, F., Zhu, Q., Tang, W. W. C., Withey, S., Klisch, D., Wood, L., Loose, M., Surani, M. A. and Alberio, R. (2019). Pluripotency and X chromosome dynamics revealed in pig pre-gastrulating embryos by single cell analysis. *Nature Communications* 10, 500.

Riley, J. K., Carayannopoulos, M. O., Wyman, A. H., Chi, M., Ratajczak, C. K. and Moley, K. H. (2005). The PI3K/Akt pathway is present and functional in the preimplantation mouse embryo. *Developmental Biology* 284, 377–386.

Saiz, N., Williams, K. M., Seshan, V. E. and Hadjantonakis, A.-K. K. (2016). Asynchronous fate decisions by single cells collectively ensure consistent lineage composition in the mouse blastocyst. *Nature Communications* 7, 13463.

Saiz, N., Mora-Bitria, L., Rahman, S., George, H., Herder, J. P., Garcia-Ojalvo, J. and Hadjantonakis, A.-K. (2019). Growth-factor-mediated coupling between lineage size and cell fate choice underlies robustness of mammalian development. *Elife* 9, e56079.

Sanchez-Ripoll, Y., Bone, H. K., Owen, T., Guedes, A. M. V., Abranches, E., Kumpfmueller, B., Spriggs, R. V., Henrique, D. and Welham, M. J. (2013). Glycogen Synthase Kinase-3 Inhibition Enhances Translation of Pluripotency-Associated Transcription Factors to Contribute to Maintenance of Mouse Embryonic Stem Cell Self-Renewal. *Plos One* 8, e60148.

Schrode, N., Saiz, N., Talia, S. D. and Hadjantonakis, A.-K. K. (2014). GATA6 levels modulate primitive endoderm cell fate choice and timing in the mouse blastocyst. *Dev. Cell* 29, 454–467.

Singh, A. M., Bechard, M., Smith, K. and Dalton, S. (2012). Reconciling the different roles of Gsk3β in "naïve" and "primed" pluripotent stem cells. *Cell Cycle* 11, 2991–2996.

Smith, K. N., Singh, A. M. and Dalton, S. (2010). Myc Represses Primitive Endoderm Differentiation in Pluripotent Stem Cells. *Cell Stem Cell* 7, 343–354.

Sodhi, C. P., Li, J. and Duncan, S. A. (2006). Generation of mice harbouring a conditional loss-of-function allele of Gata6. *Bmc Dev Biol* 6, 19–19.

Storm, M. P., Bone, H. K., Beck, C. G., Bourillot, P.-Y., Schreiber, V., Damiano, T., Nelson, A., Savatier, P. and Welham, M. J. (2007). Regulation of Nanog expression by phosphoinositide 3-kinase-dependent signaling in murine embryonic stem cells. *J. Biol. Chem.* 282, 6265–6273.

Storm, M. P., Kumpfmueller, B., Thompson, B., Kolde, R., Vilo, J., Hummel, O., Schulz, H. and Welham, M. J. (2009). Characterization of the Phosphoinositide 3-Kinase-Dependent Transcriptome in Murine Embryonic Stem Cells: Identification of Novel Regulators of Pluripotency. *Stem Cells* 27, 764–775.

Strumpf, D., Mao, C.-A., Yamanaka, Y., Ralston, A., Chawengsaksophak, K., Beck, F. and Rossant, J. (2005). Cdx2 is required for correct cell fate specification and differentiation of trophectoderm in the mouse blastocyst. *Development* 132, 2093–2102.

Tang, F., Barbacioru, C., Wang, Y., Nordman, E., Lee, C., Xu, N., Wang, X., Bodeau, J., Tuch, B. B., Siddiqui, A., et al. (2009). mRNA-Seq whole-transcriptome analysis of a single cell. *Nat Methods* 6, 377–382.

Tang, F., Barbacioru, C., Nordman, E., Li, B., Xu, N., Bashkirov, V. I., Lao, K. and Surani, M. A. (2010). RNA-Seq analysis to capture the transcriptome landscape of a single cell. *Nature Protocols* 5, 516–535.

Thompson, J. J., Lee, D. J., Mitra, A., Frail, S., Dale, R. and Rocha, P. P. (2021). Rapid redistribution and extensive binding of NANOG and GATA6 at shared regulatory elements underlie specification of divergent cell fates. *Biorxiv* 2021.07.28.454132.

Tosenberger, A., Gonze, D., Bessonnard, S., Cohen-Tannoudji, M., Chazaud, C. and Dupont, G. (2017). A multiscale model of early cell lineage specification including cell division. *Npj Syst Biology Appl* 3, 16.

Vandormael-Pournin, S., Frachon, E., Gobaa, S. and Cohen-Tannoudji, M. (2021). Microfabricated Device for High-Resolution Imaging of Preimplantation Embryos. *Methods Mol. Biol.* 2214, 11–30.

Vries, W. N. de, Binns, L. T., Fancher, K. S., Dean, J., Moore, R., Kemler, R. and Knowles, B. B. (2000). Expression of Cre recombinase in mouse oocytes: a means to study maternal effect genes. *Genesis* 26, 110–112.

Wamaitha, S. E., Valle, I. D., Cho, L. T. Y., Wei, Y., Fogarty, N. M. E., Blakeley, P., Sherwood, R. I., Ji, H. and Niakan, K. K. (2015). Gata6 potently initiates reprograming of pluripotent and differentiated cells to extraembryonic endoderm stem cells. *Genes & Development* 29, 1239–1255.

Wamaitha, S. E., Grybel, K. J., Alanis-Lobato, G., Gerri, C., Ogushi, S., McCarthy, A., Mahadevaiah, S. K., Healy, L., Lea, R. A., Molina-Arcas, M., et al. (2020). IGF1-mediated human embryonic stem cell self-renewal recapitulates the embryonic niche. *Nat Commun* 11, 764.

Wicklow, E., Blij, S., Frum, T., Hirate, Y., Lang, R. A., Sasaki, H. and Ralston, A. (2014). HIPPO Pathway Members Restrict SOX2 to the Inner Cell Mass Where It Promotes ICM Fates in the Mouse Blastocyst. *Plos Genet* 10, e1004618.

Wray, J., Kalkan, T., Gomez-Lopez, S., Eckardt, D., Cook, A., Kemler, R. and Smith, A. (2011). Inhibition of glycogen synthase kinase-3 alleviates Tcf3 repression of the pluripotency network and increases embryonic stem cell resistance to differentiation. *Nat Cell Biol* 13, 838–845.

Xu, X., Ahmed, T., Wang, L., Cao, X., Zhang, Z., Wang, M., Lv, Y., Kanwal, S., Tariq, M., Lin, R., et al. (2021). The mTORC1-eIF4F axis controls paused pluripotency. *EMBO reports* e53081.

Yamanaka, Y., Lanner, F. and Rossant, J. (2010). FGF signal-dependent segregation of primitive endoderm and epiblast in the mouse blastocyst. *Development* 137, 715–724.

Yi, F., Pereira, L., Hoffman, J. A., Shy, B. R., Yuen, C. M., Liu, D. R. and Merrill, B. J. (2011). Opposing effects of Tcf3 and Tcf1 control Wnt stimulation of embryonic stem cell self-renewal. *Nature Cell Biology* 13, 762–770.

Yu, J. S. L. and Cui, W. (2016). Proliferation, survival and metabolism: the role of PI3K/AKT/mTOR signalling in pluripotency and cell fate determination. *Development* 143, 3050–3060.

Zhang, X., Yalcin, S., Lee, D.-F., Yeh, T.-Y. J., Lee, S.-M., Su, J., Mungamuri, S. K., Rimmelé, P., Kennedy, M., Sellers, R., et al. (2011). FOXO1 is an essential regulator of pluripotency in human embryonic stem cells. *Nature Cell Biology* 13, 1092–1099.

Zimmermann, S. and Moelling, K. (1999). Phosphorylation and regulation of Raf by Akt (protein kinase B). *Science* 286, 1741–1744.

FIGURES

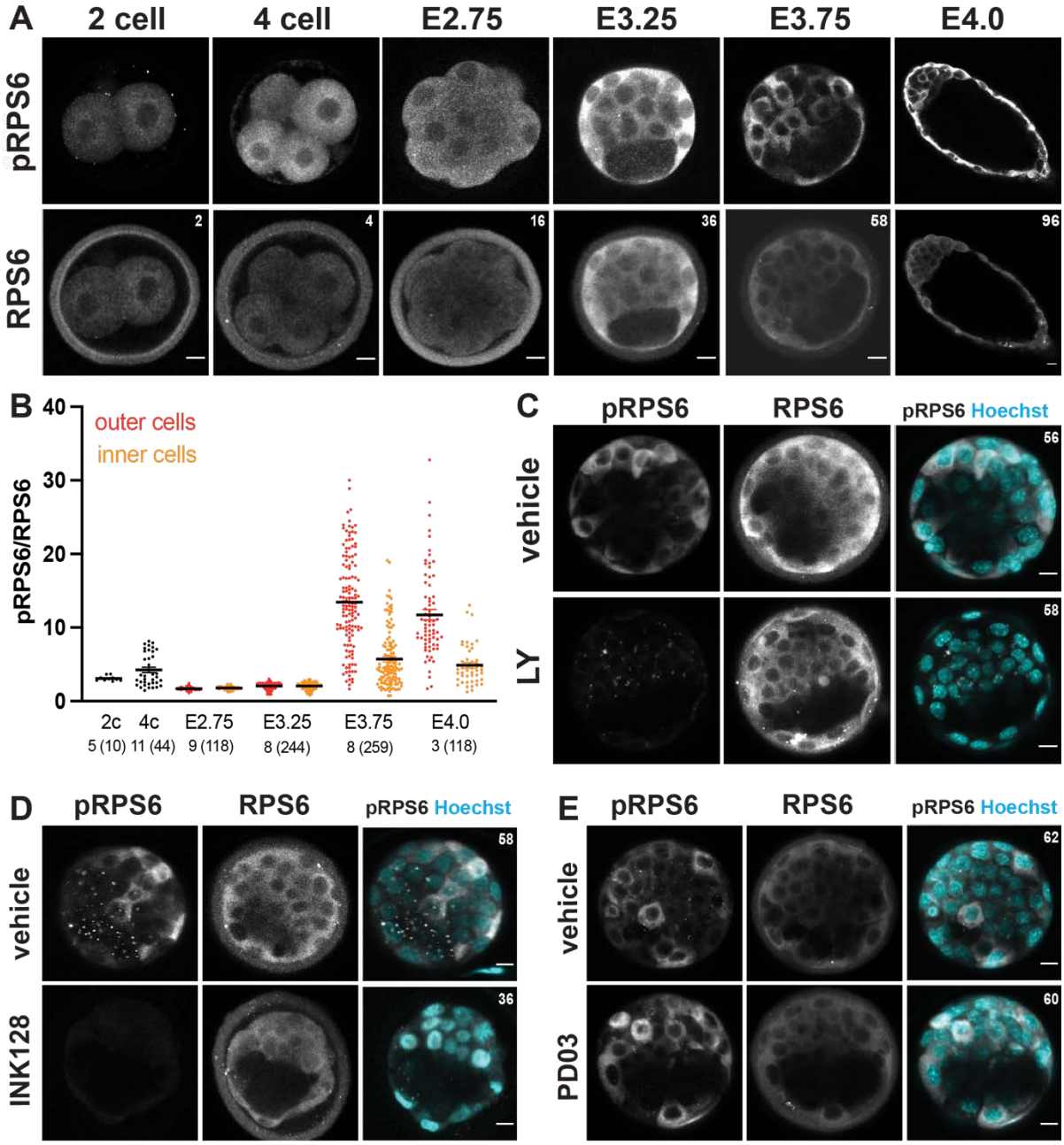

Figure 1 : pRPS6 staining reveals two phases of PI3K/AKT activity during preimplantation development

(A) Immunostaining of pRPS6 and RPS6 (grey) from 2 cell stage to E4.0. Distinct pRPS6 levels are visible in E3.75 and E4.0. (B) Ratio of pRPS6/RPS6 quantification levels in inner and outer cells from 2 cell stage to E4.0. Number of embryos and analyzed cells per stage are indicated at the bottom. (C-E) Immunodetection of pRPS6, RPS6 (grey) and Hoechst (cyan) in embryos cultured from E2.75 for 24h in (C) the PI3K inhibitor, (D) the mTORC1 and mTORC2 dual inhibitor INK128 or (E) the ERK inhibitor PD03. Data are from one experiment, representative of two (A-B, D-E) and four (C) independent experiments. Pictures do correspond to a single (A) or the projection of 5 (D-E) optical slices. Number of cells per embryo are indicated on the top right of images. Scale bar = 20µM.

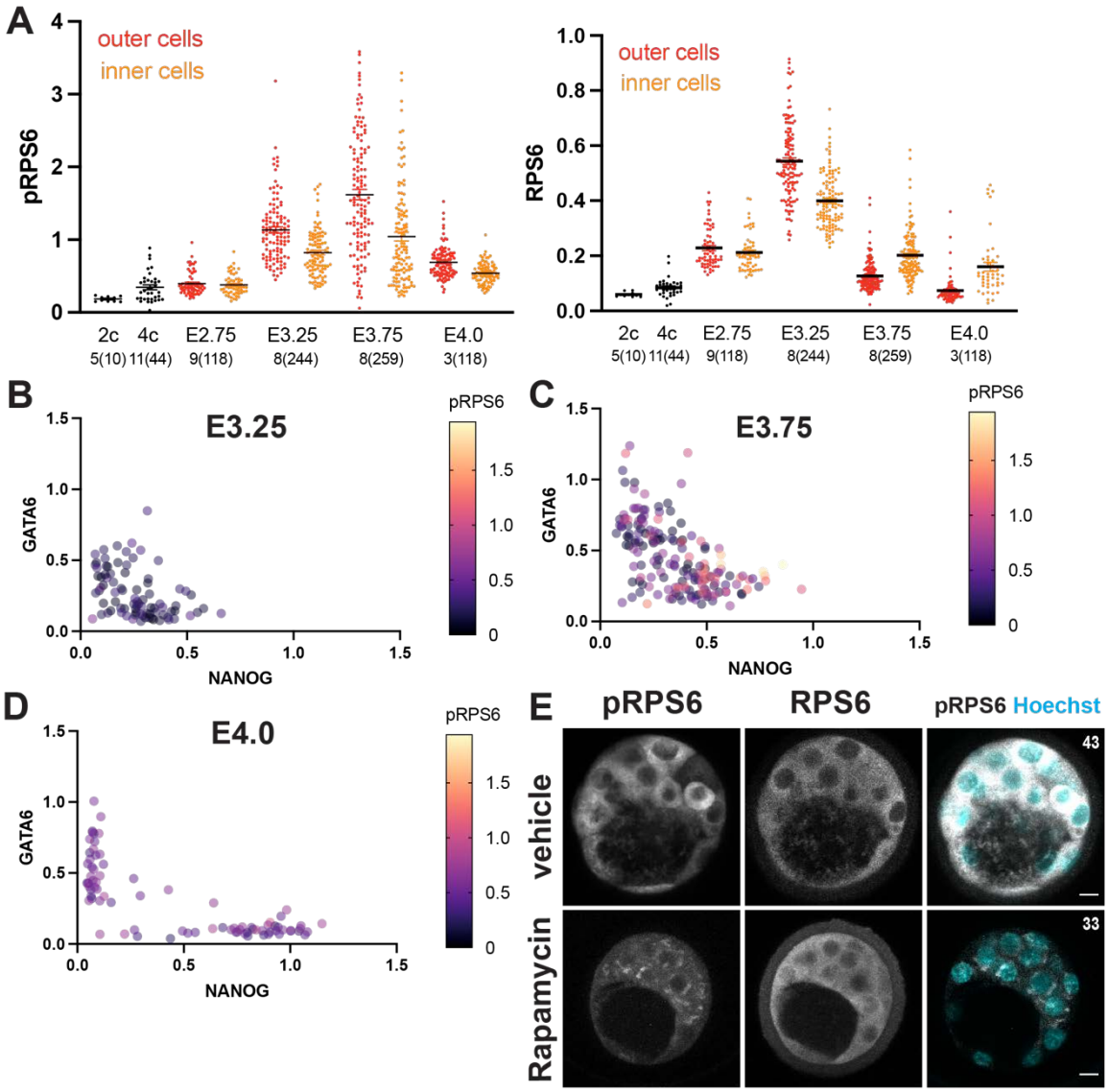

Figure S1: pRPS6 levels show no correlation with NANOG and GATA6 during blastocyst stages.

(A) Quantification of pRPS6 (left) and RPS6 (right) levels in inner and outer cells from 2 cell stage to E4.0. Number of embryos and analyzed cells per stage indicated at the bottom. Level of nuclear GATA6/NANOG and cytoplasmic pRPS6 in inner cells of (B) E3.25, (C) E3.75 and (D) E4.0 embryos. (E) Immunodetection of pRPS6, RPS6 (grey) and Hoechst (cyan) in embryos cultured from E2.75 for 24h in mTORC1 inhibitor Rapamycin. Data are from one experiment, representative of two independent experiments. Pictures do correspond to the projection of 5 optical slices. Number of cells per embryo indicated on the top right of images. Scale bar = 20µM.

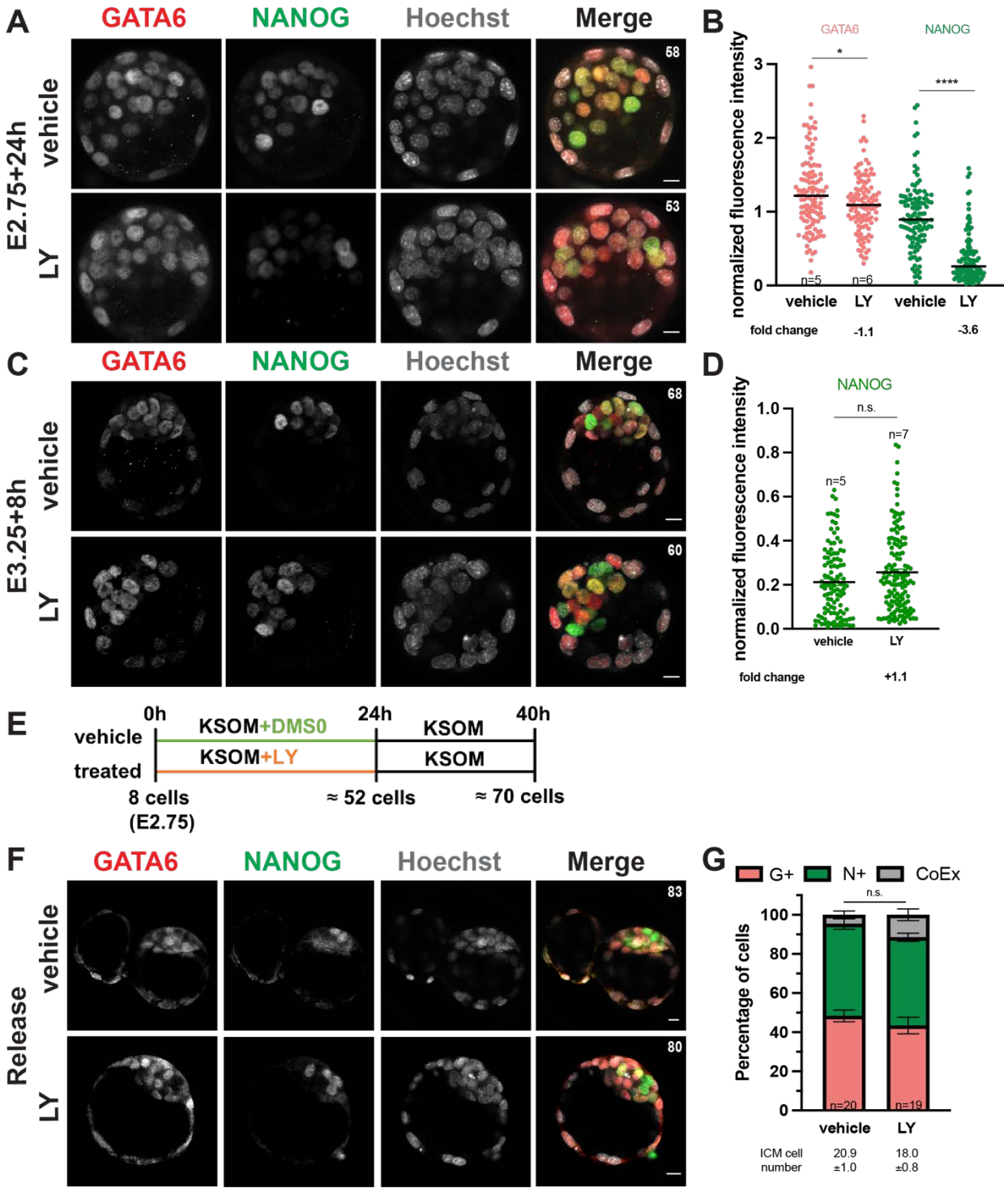

Figure 2: PI3K/AKT maintains NANOG during Epi/PrE specification.
(A) Immunodetection of GATA6 (red), NANOG (green) and Hoechst (grey) and (B) quantification of GATA6 (red) and NANOG (green) in embryos cultured for 24h from E2.75. (C) Immunodetection of GATA6 (red), NANOG (green) and Hoechst (grey) and (D) quantification of NANOG (green) in embryos cultured for 8h from E3.25. (E) Schematic representation of the performed release experiment. Embryos were cultured 24h starting from E2.75 in KSOM containing either DMSO (vehicle) or LY (treated). Subsequently embryos of both conditions were transferred to KSOM alone for 16h before fixation. (F) Immunodetection of GATA6 (red), NANOG (green) and Hoechst (grey) and (G) distribution of GATA6 (G+, red), NANOG (N+, green) or both markers (CoEx, grey) in embryos at the end of the release

experiment. Graph shows results of two independent experiments. Pictures correspond to the projection of 5 optical slices. Data are from one experiment, representative of >10 (A-B) and 3 (C-D, F) independent experiments. Number of cells per embryo are indicated on the top right of images. Scale bar = 20µM. Statistical significance (*$p < 0.05$, ****$p < 0.0001$) and insignificance (n.s.) indicated. Error bars show SEM. n, number of embryos.

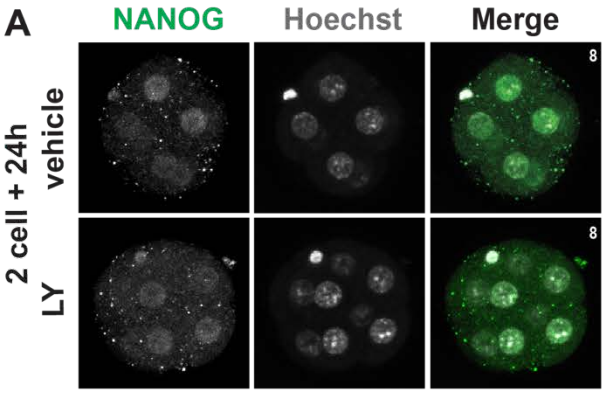

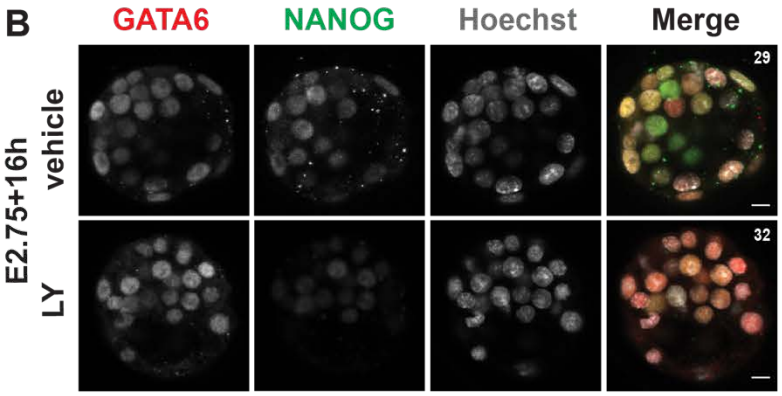

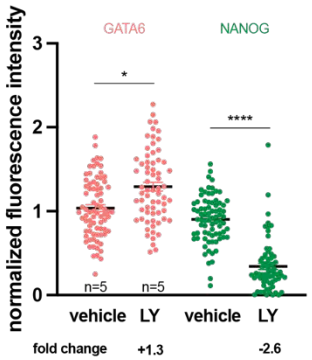

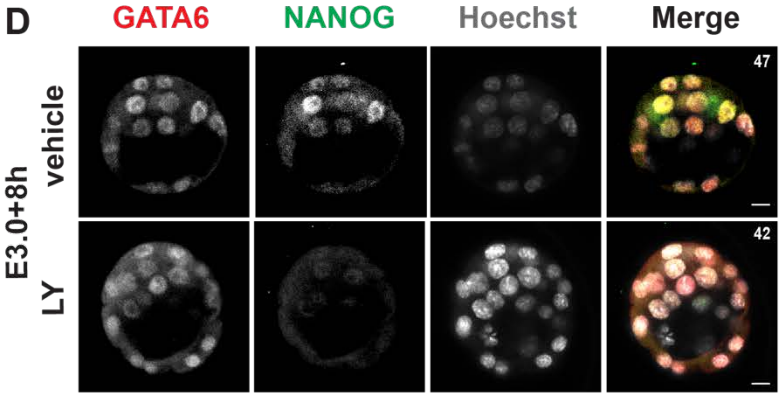

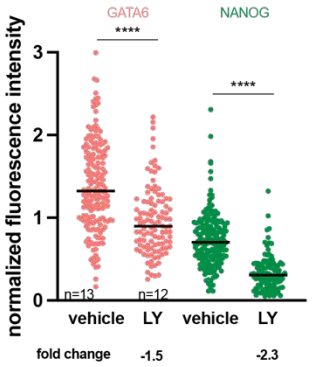

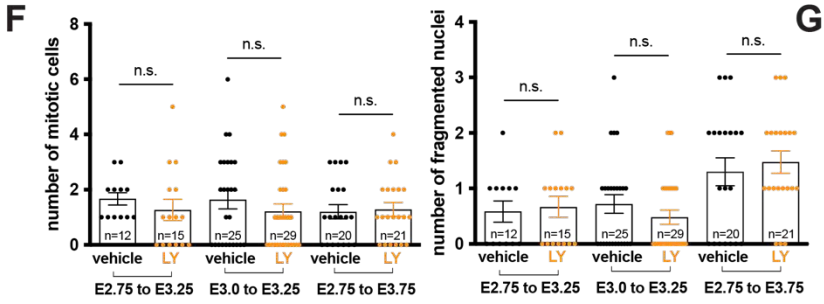

G

	DMSO n=9	LY n=9
n (t=0)	11.0 ± 0.5	11.6 ± 0.78
n (t=24h)	56.6 ± 1.34	55.3 ± 1.18
n (mitosis)	45.6 ± 1.40	43.8 ± 1.36
n (cell death)	0.44 ± 0.24	0.67 ± 0.24

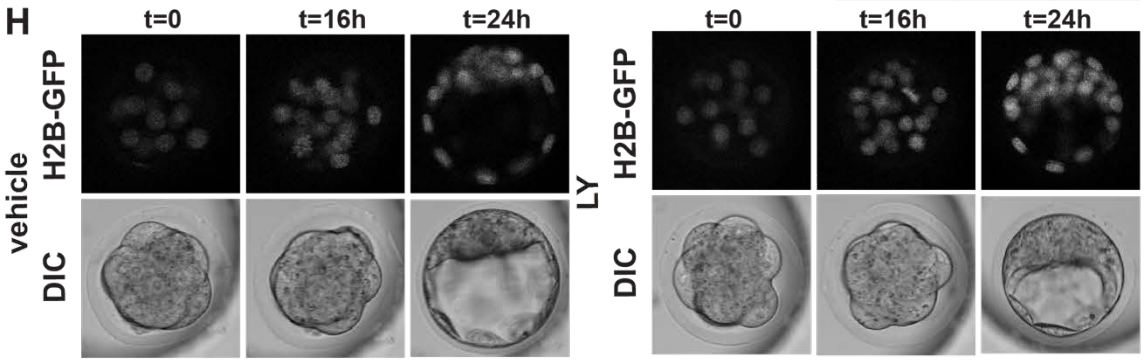

Figure S2: PI3K/AKT regulates NANOG through survival and proliferation independent mechanisms.
(A) Immunodetection of NANOG (green) and Hoechst (grey) in embryos cultured for 24h from the 2-cell stage. (B) Immunodetection and (C) quantification of GATA6 (red), NANOG (green) and Hoechst (grey) in embryos cultured for 16h from E2.75. (D) Immunodetection and (E) quantification of GATA6 (red), NANOG (green) and Hoechst (grey) in embryos cultured for 8h from E3.0. (F) Number of mitotic cells (left) and cells undergoing cell death (right) in fixed embryos cultured for different durations in absence or presence of LY. Graphs show the results of three independent experiments. (G) Total cell number at the start and the end of live imaging, cumulative number of mitotic cells and of cells undergoing cell death and (H) images of vehicle and LY treated embryos expressing H2B-GFP at the start of live imaging (t=0), after 16h (t=16h) and after 24h (t=24h). Data are from one experiment, representative of at least two (A, H) and more than 4 (B-E) independent experiments. Pictures do correspond to the projection of 10 (A) or 5 (B, D, H) optical slices. Number of cells per embryo indicated on the top right of images. Scale bar = 20µM. Statistical significance ($*p < 0.05$, $****p < 0.0001$) and insignificance (n.s.) indicated. Error bars show SEM. n, number of embryos.

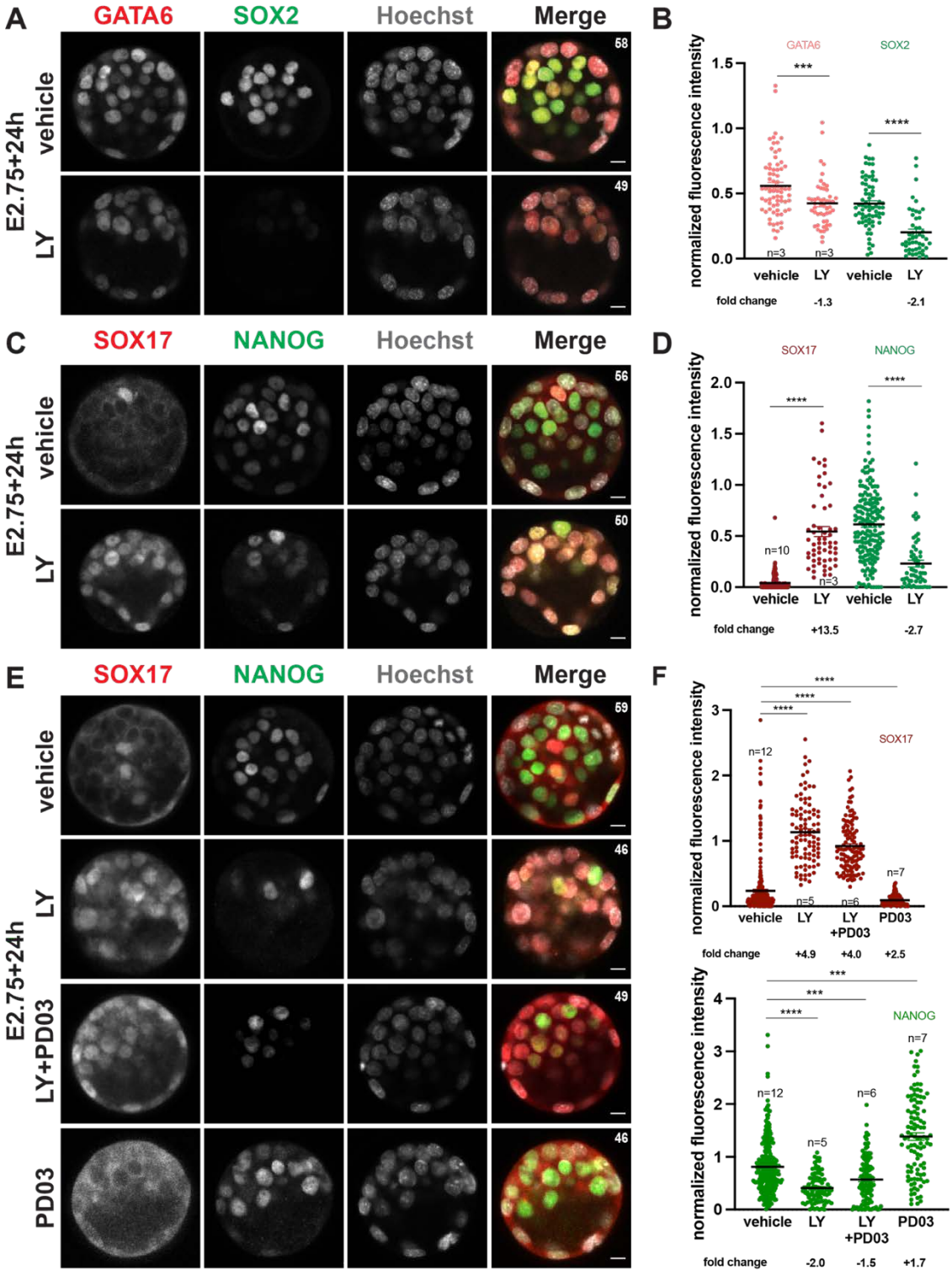

Figure 3: PI3K regulates TF patterning of Epi and PrE lineages independently of ERK activity.

(A) Immunodetection and (B) quantification of GATA6 (red), SOX2 (green) and Hoechst (grey) in embryos cultured for 24h from E2.75. (C,E)Immunodetection and (D,F) quantification of SOX17 (red), NANOG (green) and Hoechst (grey) in embryos cultured for 24h from E2.75. Data are from one experiment, representative of more than 4 (A-D) and three (E-F) independent experiments. Pictures do correspond to the projection 5 optical slices. Number of cells per embryo indicated on the top right of images. Scale bar = 20µM. Statistical significance (***$p < 0.001$, ****$p < 0.0001$) and insignificance (n.s.) are indicated. Error bars show SEM. n, number of embryos.

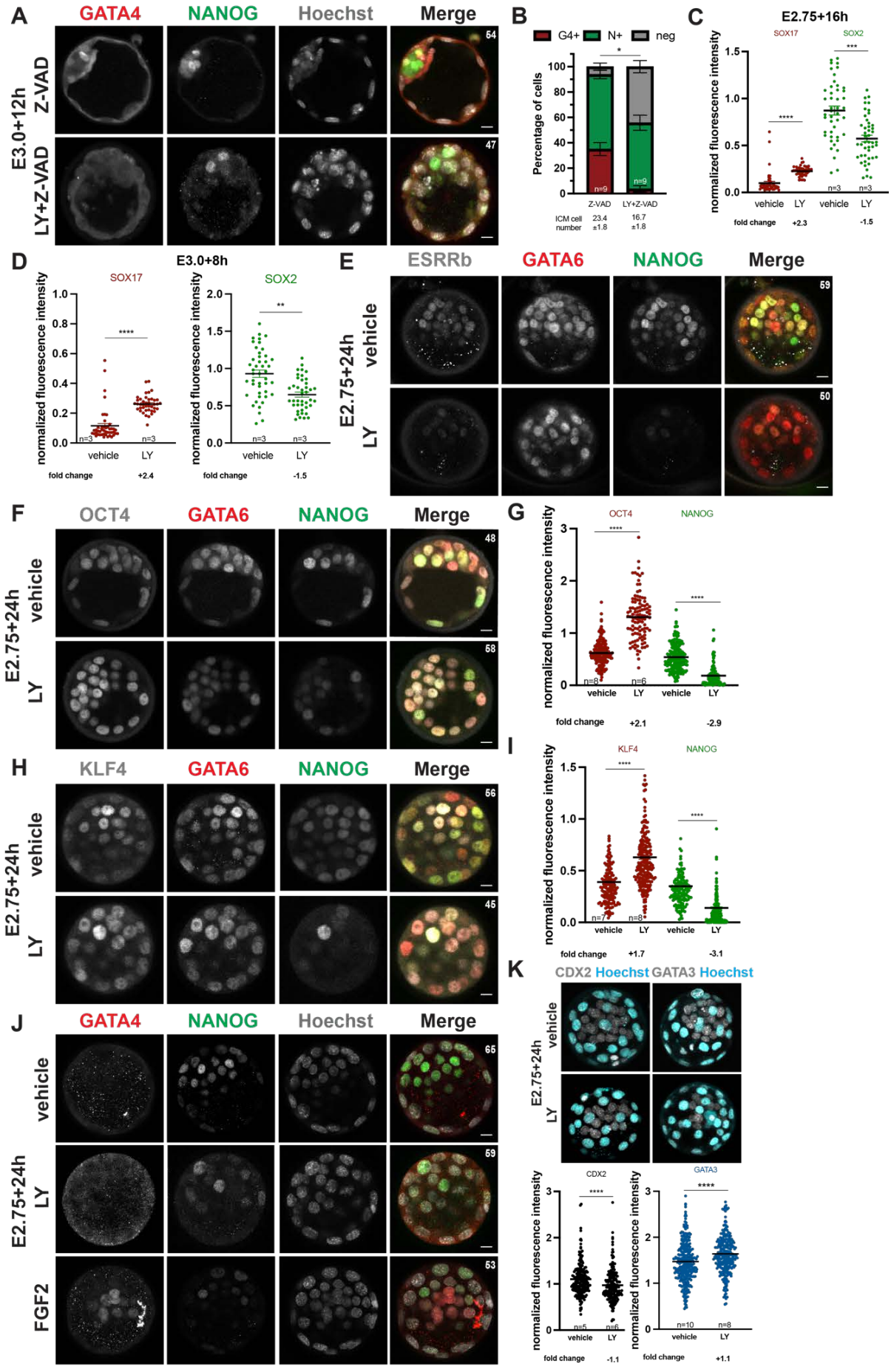
A
GATA4
NANOG
Hoechst
Merge
E3.0+12h Z-VAD
LY+Z-VAD
54
47
B
G4+
N+
neg
Percentage of cells
Z-VAD
LY+Z-VAD
ICM cell number
23.4 ±1.8
16.7 ±1.8
C
E2.75+16h
SOX17
SOX2
normalized fluorescence intensity
vehicle
LY
fold change
+2.3
-1.5
D
E3.0+8h
SOX17
SOX2
normalized fluorescence intensity
vehicle
LY
fold change
+2.4
-1.5
E
ESRRb
GATA6
NANOG
Merge
E2.75+24h vehicle
LY
59
50
F
OCT4
GATA6
NANOG
Merge
E2.75+24h vehicle
LY
48
58
G
OCT4
NANOG
normalized fluorescence intensity
vehicle
LY
fold change
+2.1
-2.9
H
KLF4
GATA6
NANOG
Merge
E2.75+24h vehicle
LY
56
45
I
KLF4
NANOG
normalized fluorescence intensity
vehicle
LY
fold change
+1.7
-3.1
J
GATA4
NANOG
Hoechst
Merge
vehicle
E2.75+24h LY
FGF2
65
59
53
K
CDX2 Hoechst GATA3 Hoechst
E2.75+24h vehicle
LY
CDX2
GATA3
normalized fluorescence intensity
vehicle
LY
fold change
-1.1
+1.1

Figure S3: No reduction of Epi markers OCT4 and KLF4 and the TE markers CDX2 and GATA3 upon PI3K inhibition.
(A) Immunodetection of GATA4 (red), NANOG (green) and Hoechst (grey) and (B) distribution of GATA4 (G4+, red), NANOG (N+, green) or GATA4- and NANOG-negative cells (neg, grey) in embryos cultured for 12h from E3.0. (C-D) Quantification of SOX17 (red) and SOX2 (green) in embryos cultured for (C) 16h from E2.75 and (D) 8h from E3.0. (E) Immunodetection of ESRRB (grey), GATA6 (red) and NANOG (green) in embryos cultured for 24h from E2.75. (F, H) Immunodetection and (G, I) quantification of OCT4/KLF4 (grey), GATA6 (red), NANOG (green) and Hoechst (grey) in embryos cultured for 24h from E2.75. (J) Immunodetection of GATA4 (red), NANOG (green) and Hoechst (grey) in embryos cultured for 24h from E2.75. At E2.75+24h vehicle-treated embryos rarely expressed GATA4, we therefore included in our experiment embryos cultured with FGF2 + Heparin to verify the functionality of the GATA4 staining. (K) Quantification of CDX2 (right) and GATA3 (left) in TE cells of embryos cultured for 24h from E2.75. Data are from one (A, C-J) experiment, representative of two (A-B, F-J) and more than three (C-E, K) independent experiments. Pictures do correspond to the projection of 5 optical slices. Number of cells per embryo indicated on the top right of images. Scale bar = 20µM. Statistical significance (*$p < 0.05$, ***$p < 0.001$, ****$p < 0.0001$) indicated. Error bars show SEM. n, number of embryos.

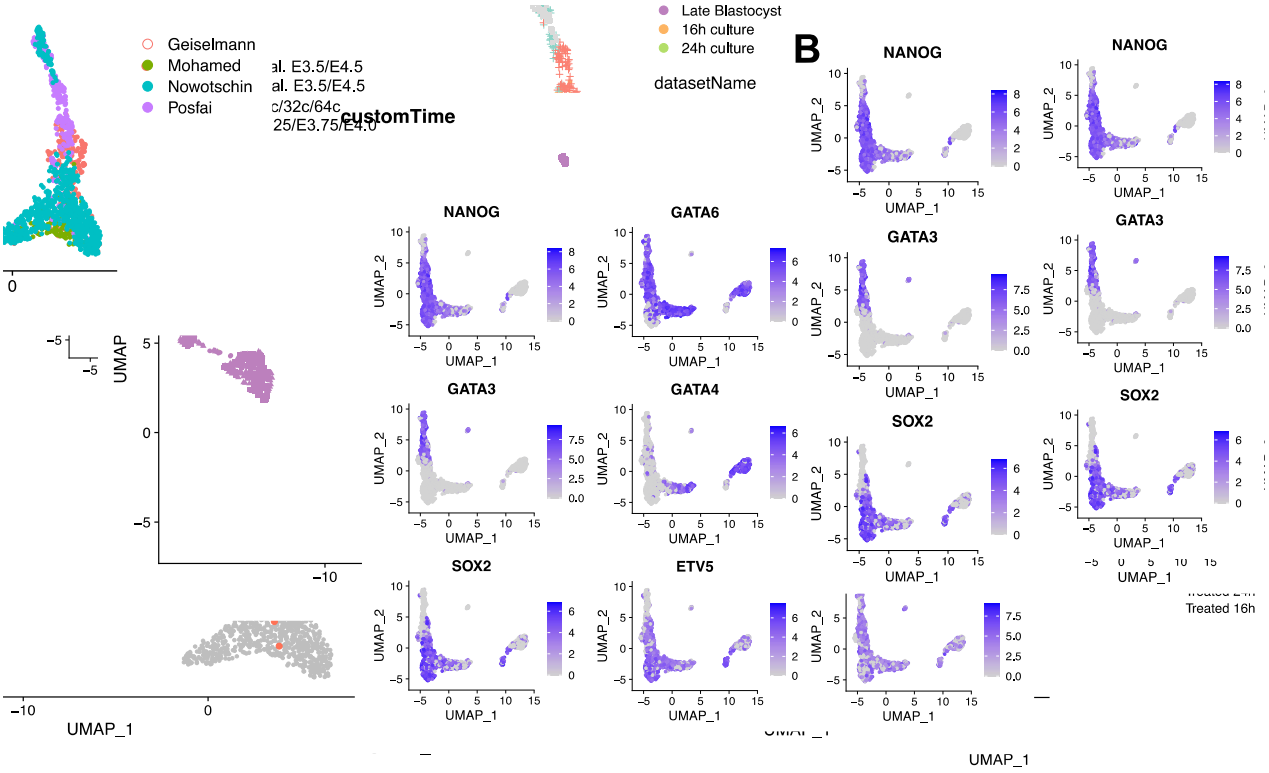
Geiselmann
Mohamed
Nowotschin
Posfai
customTime
datasetName
Late Blastocyst
16h culture
24h culture
B
NANOG
GATA6
GATA3
GATA4
SOX2
ETV5
UMAP_1
UMAP_2
Treated 16h

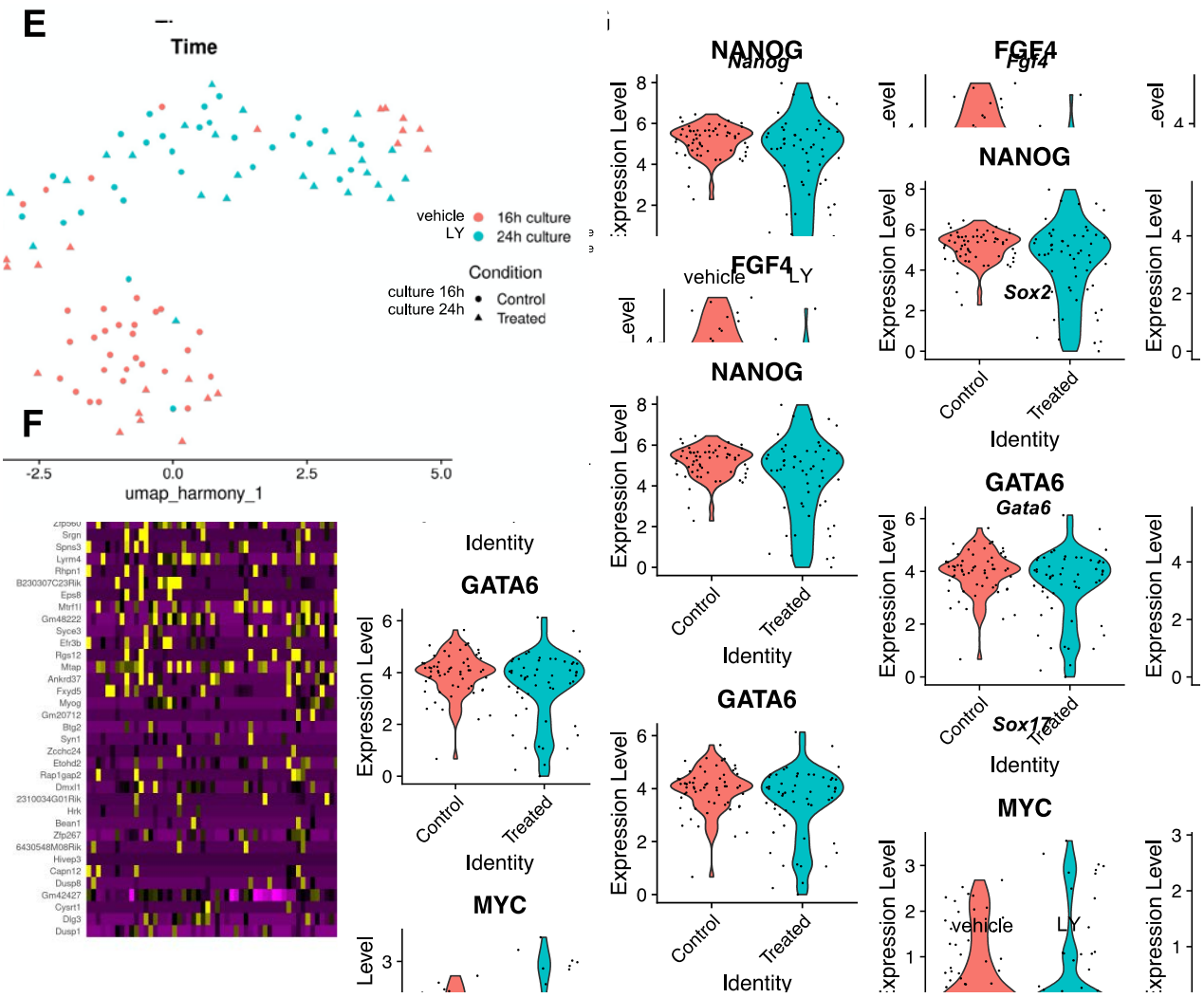
E
Time
vehicle
LY
16h culture
24h culture
Condition
culture 16h
culture 24h
Control
Treated
F
umap_harmony_1
Identity
GATA6
MYC
Expression Level
Control
Treated
NANOG
FGF4
Nanog
Fgf4
Sox2
Gata6
Sox17
vehicle
LY

Figure 4: scRNAseq of non-cultured and cultured embryos.
(A) UMAP of all integrated cells showing lineage progression. Color indicates the source of the dataset (left) or embryonic stage (right). Symbols indicate source of the dataset (right). (B) UMAPs of all cells colored by gene expression level of lineage-specific marker. Grey to purple scale indicates average expression. (C) UMAP showing the 9 identified clusters. (D) UMAP of all integrated single cells. Single cells from external datasets in grey (unselected), vehicle (left) and LY-treated (right) single inner cells from our dataset colored by duration of culture. (E) UMAP of control and treated cells. (F) Heatmap (left) of down- and upregulated genes in cultured vehicle versus treated single cells. Top 20 genes are downregulated in treated cells, bottom 20 genes are upregulated. Boxblots (right) indicate the relative expression (max=1) of the top 20 downregulated (upper panel) and upregulated (lower panel) genes during development according to RNAseq data from Boroviak and colleagues (Boroviak et al., 2015) (G) Violin plots of average expression level of Epi- and PrE-associated genes in vehicle and LY-treated cells.

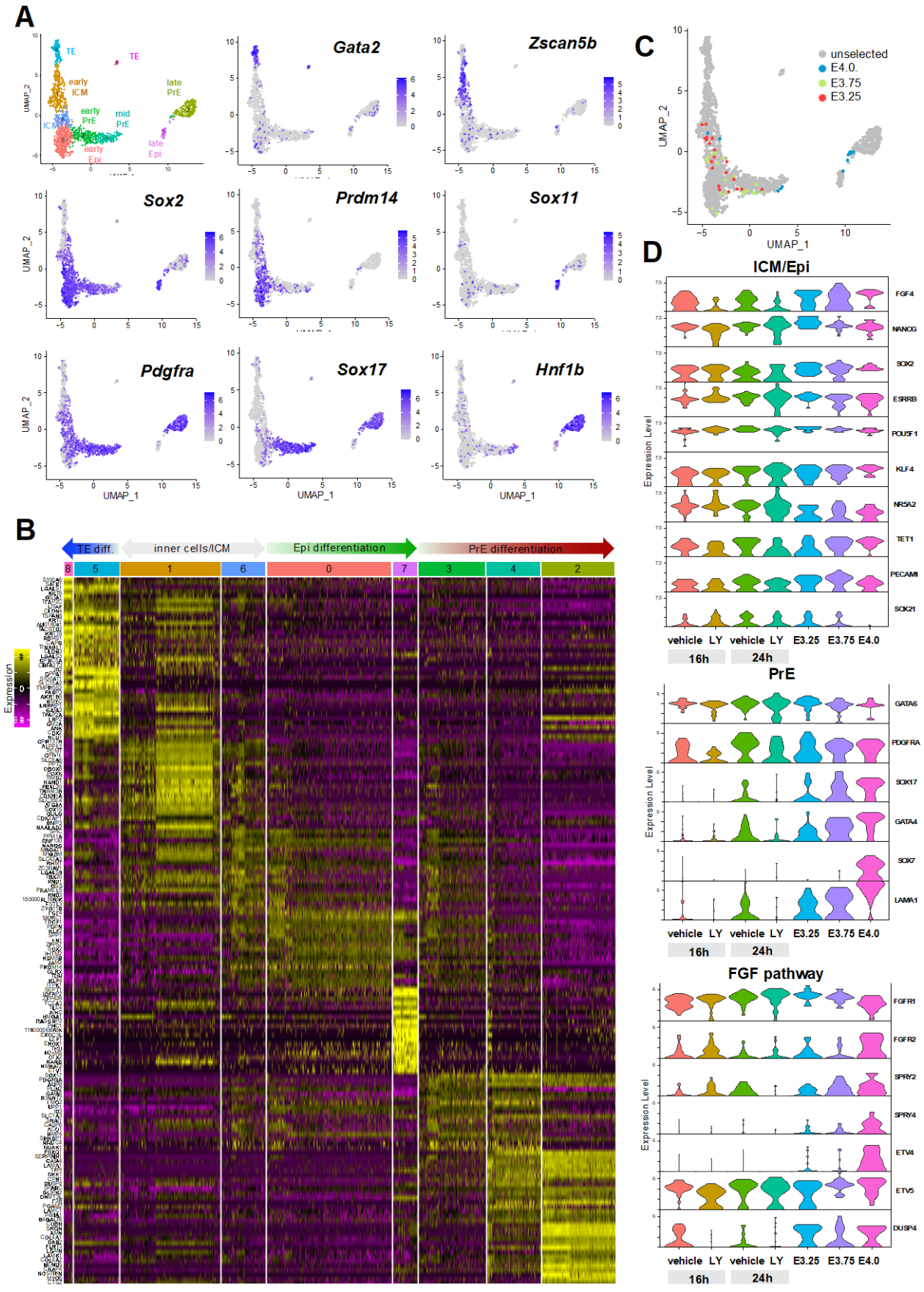
A
TE
TE
early ICM
late PrE
early PrE
mid PrE
ICM
early Epi
late Epi
Gata2
Zscan5b
Sox2
Prdm14
Sox11
Pdgfra
Sox17
Hnf1b
UMAP_1
UMAP_2
B
TE diff.
inner cells/ICM
Epi differentiation
PrE differentiation
8
5
1
6
0
7
3
4
2
Expression
C
unselected
E4.0.
E3.75
E3.25
D
ICM/Epi
FGF4
NANOG
SOX2
ESRRB
POUSF1
KLF4
NR5A2
TET1
PECAM1
SOX21
Expression Level
vehicle
LY
vehicle
LY
E3.25
E3.75
E4.0
16h
24h
PrE
GATA6
PDGFRA
SOX17
GATA4
SOX7
LAMA1
FGF pathway
FGFR1
FGFR2
SPRY2
SPRY4
ETV4
ETV5
DUSP4

Figure S4: ICM progenitor transcriptome is mildly affected by PI3K inhibition.
(A) UMAPs of all cells colored by gene expression level of markers enriched in the different clusters. Grey to purple scale indicates average expression. (B) Heatmap of differentially expressed genes between the 9 identified clusters. Top 20 enriched markers ranked according to the p value are indicated for each cluster. (C) UMAP of all integrated single cells. Single cells from external datasets in grey (unselected), non-cultured E3.25 cells in red, non-cultured E3.75 in green and non-cultured E4.0 cells in blue. (D) Violin plots of average expression level of Epi- and PrE-related genes as well as genes of the FGF pathway in cultured vehicle and LY-treated cells from 16h and 24h treatment and non-cultured E3.25, E3.75 and E4.0 cells.

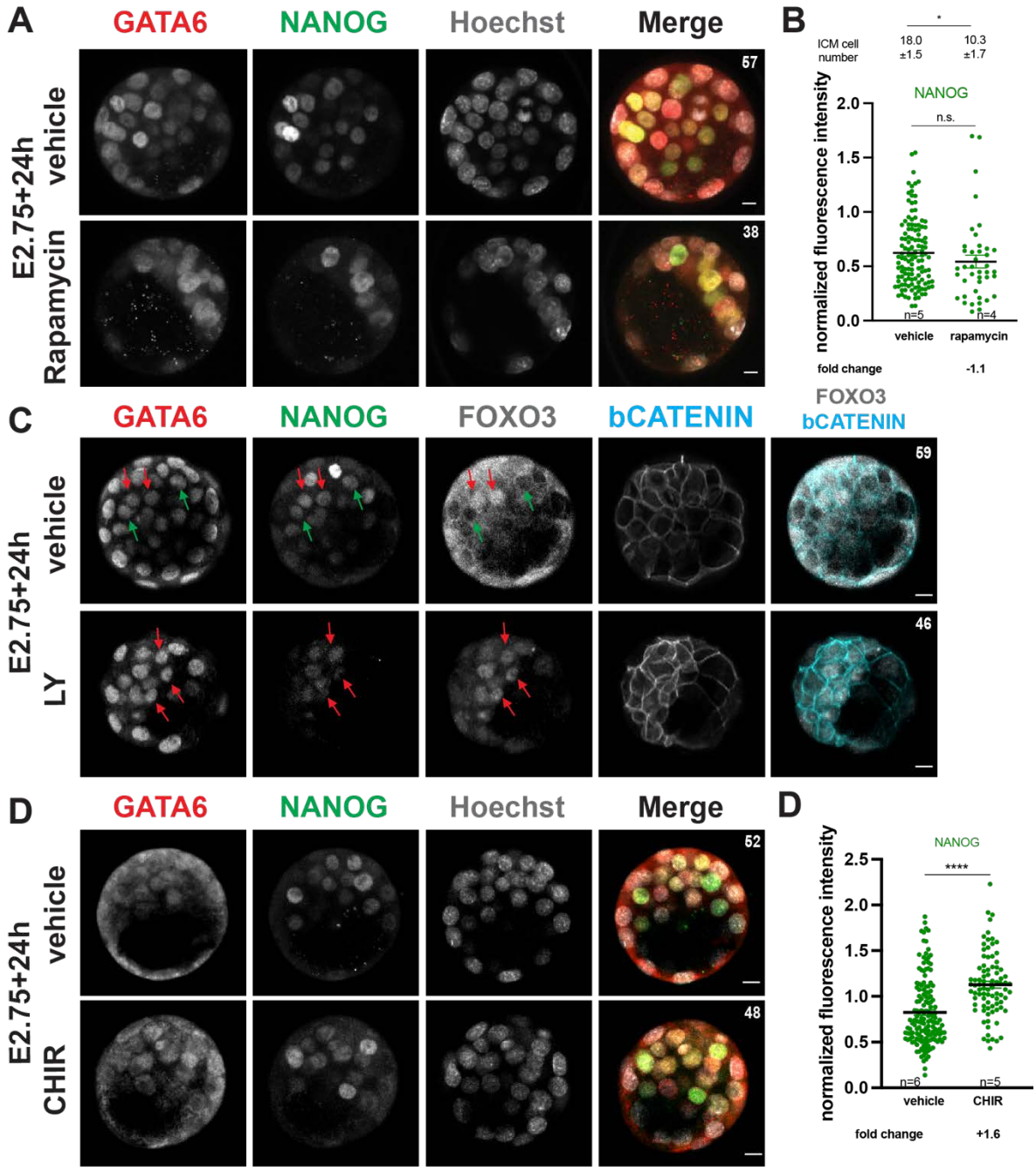

Figure 5: GSK3 but not other downstream target of PI3K/AKT regulates NANOG levels in ICM progenitors.

(A) Immuodetection of GATA6 (red), NANOG (green) and Hoechst (grey) and (B) quantification of NANOG (green) in embryos cultured for 24h from E2.75. (C) Immunodetection of GATA6 (red), NANOG (green), FOXO3 (grey) and b-CATENIN (cyan) in embryos cultured for 24h from E2.75. Green arrows point to examples of inner cells with cytoplasmic FOXO3. Red arrows point to examples of inner cells with nuclear FOXO3. (D) Immuodetection of GATA6 (red), NANOG (green) and Hoechst (grey) and (D) quantification of NANOG (green) in embryos cultured for 24h from E2.75. Data are from one experiment, representative of two (A-B, D-E) and three (C) independent experiments. Pictures do correspond to the projection of 5 optical slices. Number of cells per embryo indicated on the top right of images. Scale bar = 20µM. Statistical significance (****$p < 0.0001$) and insignificance (n.s.) indicated. Error bars show SEM. n, number of embryos.

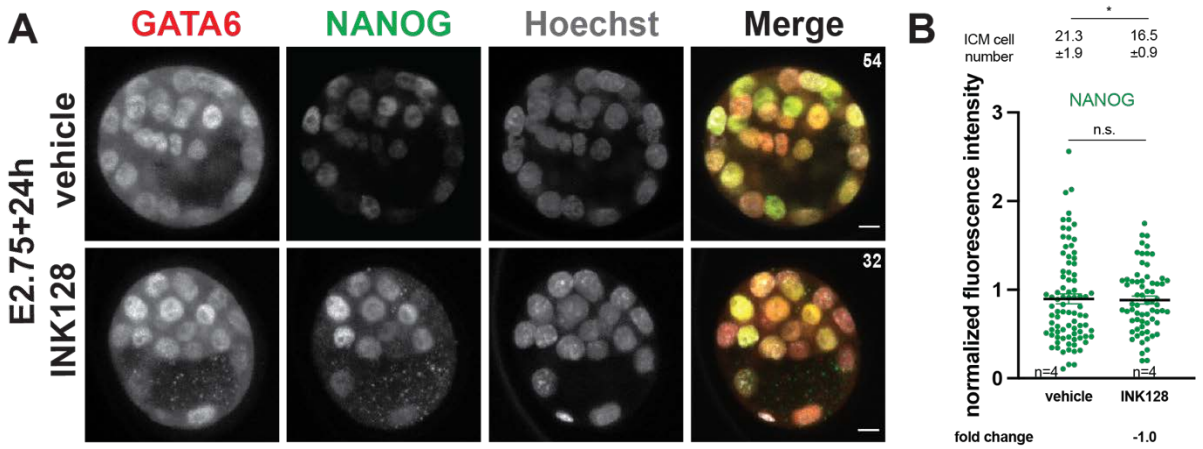

Figure S5: NANOG levels are unaffected by inhibition of mTOR.
(A) Immuodetection of GATA6 (red), NANOG (green) and Hoechst (grey) and (B) quantification of NANOG (green) in embryos cultured for 24h from E2.75. Embryos cultured with INK128 showed reduced cell number with no sign of cell death probably due to its known pausing action on cellular metabolism (Bulut-Karslioglu et al., 2016; Xu et al., 2021). Data are from one experiment, representative of three independent experiments. Pictures do correspond to the projection of 5 optical slices. Number of cells per embryo indicated on the top right of images. Scale bar = 20µM. Statistical insignificance (n.s.) indicated. Error bars show SEM. n, number of embryos.

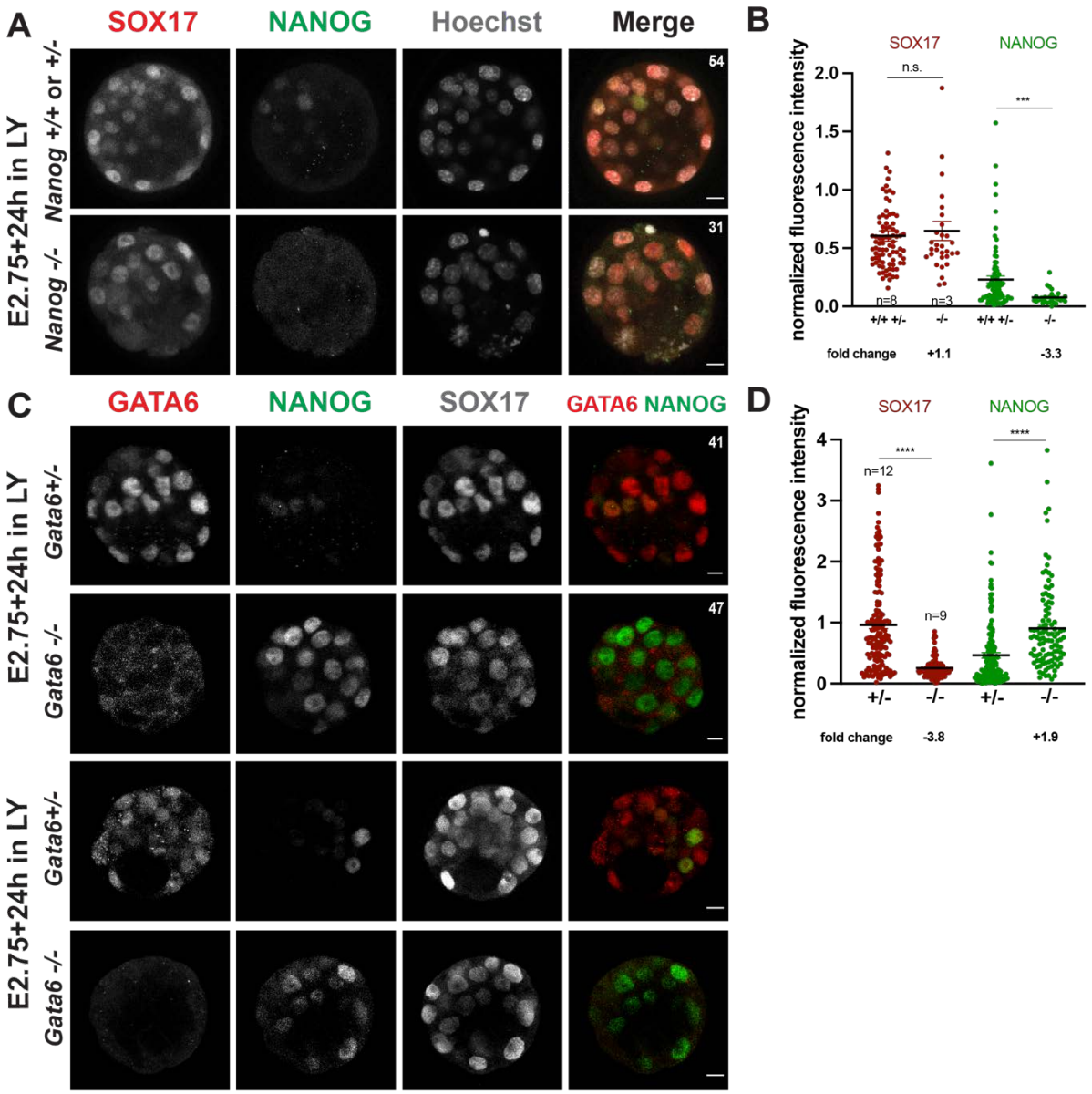

Figure 6: SOX17 upregulation occurs in *Gata6* mutant embryos.
(A) Immunodetection and (B) quantification of SOX17 (red), NANOG (green) and Hoechst (grey) in *Nanog* +/+, +/- *and* -/- embryos cultured for 24h from E2.75. (C) Immunodetection and (D) quantification of GATA6 (red), NANOG (green) and SOX17 (grey) in maternal-zygotic *GATA6* +/- *and* -/- embryos cultured for 24h from E2.75. Graphs shows results from three independent experiments. Pictures do correspond to the projection of 5 optical slices. Number of cells per embryo indicated on the top right of images. Scale bar = 20µM. Statistical significance (***$p < 0.001$, ****$p < 0.0001$) and insignificance (n.s.) indicated. n, number of embryos.

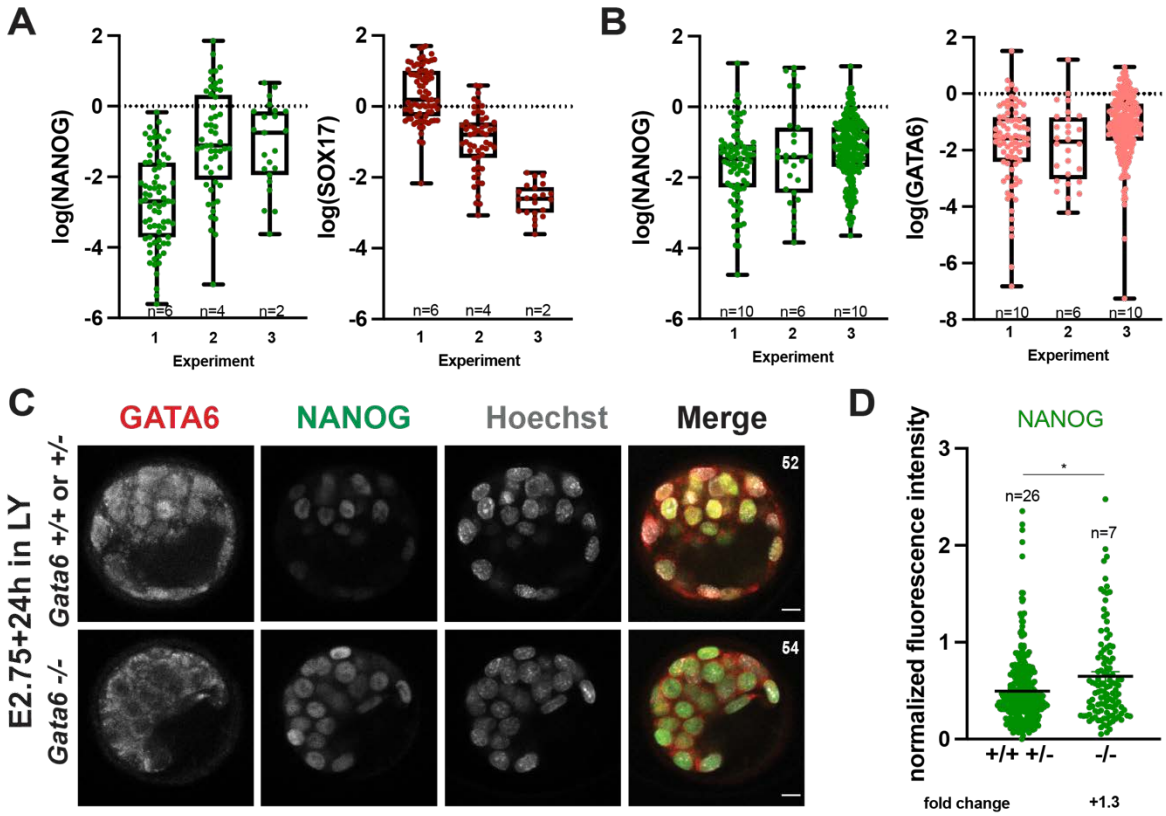

Figure S6: Normalized values of NANOG, SOX17 and GATA6 across independent experiments.

(A) Boxplots showing the normalized values of fluorescence intensities (as logarithm) of maternal-zygotic *Gata6*+/- embryos for three independent experiments of NANOG (right) and SOX17 (left) corresponding to Figure 6D. (B) Boxplots showing the normalized values of fluorescence intensities (as logarithm) zygotic *Gata6*+/+ and *Gata6*+/- embryos for three independent experiments of NANOG (right) and GATA6 (left) corresponding to Figure S6D. (C) Immunodetection of GATA6 (red), NANOG (green) and Hoechst (grey) and (D) quantification of NANOG (green) in zygotic *Gata6* +/+, +/- *and* -/- embryos cultured for 24h from E2.75. Graphs shows results from three independent experiments. Pictures do correspond to the projection of 5 optical slices. Number of cells per embryo indicated on the top right of images. Scale bar = 20µM. Statistical significance (*$p < 0.05$) indicated. n, number of embryos.

Table 5: List of differentially expressed genes (DEG) in vehicle versus LY treated ICM cells.

The upper table displays the list of DEG (FDR<10%). The lower table shows the list of the top 20 genes with highest fold changes between the two conditions. Analyses were performed after pooling 16h and 24h timepoints. Genes upregulated in vehicle and LY treated ICM cells are indicated in green and orange respectively. Pct1 (vehicle) and pct2 (LY) are the fraction of cells in which the gene is detected.

Gene symbol	p_val	avg_log2FC	pct.1	pct.2	p_val_adj
Mrs2	4,53E-06	2,27	0,56	0,14	0,09
Haus8	4,76E-08	2,03	0,93	0,79	0,00
Gm12463	3,82E-06	2,00	0,78	0,38	0,08
Gm13128	3,62E-06	1,54	0,70	0,25	0,07
Lamb1	8,34E-07	1,52	1,00	0,88	0,02
Scd1	1,23E-06	1,27	1,00	0,82	0,02
Scd2	2,32E-06	1,07	1,00	0,91	0,05
Gm5380	2,23E-06	0,67	0,85	0,43	0,05
Plod1	3,96E-06	-1,67	0,92	0,93	0,08
H1f0	7,54E-07	-2,13	0,93	0,89	0,02

Gene Symbol	p_val	avg_log2FC	pct.1	pct.2	p_val_adj
Tuba3b	1,52E-05	3,98	0,42	0,07	0,31
Lama1	4,67E-02	3,89	0,44	0,23	1,00
Zbtb39	5,83E-01	3,73	0,56	0,64	1,00
B9d2	1,33E-02	3,49	0,37	0,29	1,00
Tmem229b	5,82E-03	3,49	0,32	0,11	1,00
Zfp560	4,00E-04	3,45	0,51	0,20	1,00
Srgn	3,16E-02	3,25	0,17	0,04	1,00
Spns3	7,48E-03	3,16	0,27	0,07	1,00
Lyrm4	8,50E-03	3,15	0,51	0,30	1,00
Rhpn1	2,57E-02	3,08	0,22	0,05	1,00
B230307C23Rik	1,30E-02	3,03	0,27	0,09	1,00
Eps8	7,13E-02	2,99	0,12	0,02	1,00
Mtrf1l	5,97E-02	2,78	0,49	0,30	1,00
Gm48222	1,05E-02	2,74	0,54	0,30	1,00
Syce3	3,08E-01	2,70	0,42	0,29	1,00
Efr3b	1,77E-01	2,68	0,31	0,18	1,00
Rgs12	2,25E-04	2,67	0,17	0,00	1,00
Mtap	2,50E-05	2,67	0,51	0,14	0,51
Ankrd37	9,17E-03	2,67	0,32	0,11	1,00
Fxyd5	1,17E-02	2,65	0,32	0,11	1,00
Myog	2,37E-01	-4,56	0,32	0,36	1,00
Gm20712	7,76E-02	-4,28	0,10	0,21	1,00

Btg2	6,30E-04	-3,59	0,20	0,46	1,00
Syn1	1,82E-02	-3,49	0,17	0,38	1,00
Zcchc24	7,40E-02	-3,27	0,07	0,20	1,00
Etohd2	1,12E-01	-3,19	0,32	0,30	1,00
Rap1gap2	5,21E-01	-3,15	0,14	0,11	1,00
Dmxl1	2,50E-01	-3,05	0,46	0,34	1,00
2310034G01Rik	1,29E-01	-3,04	0,12	0,09	1,00
Hrk	2,30E-02	-3,03	0,10	0,21	1,00
Bean1	3,05E-03	-3,00	0,12	0,36	1,00
Zfp267	8,25E-02	-2,94	0,48	0,46	1,00
6430548M08Rik	6,01E-01	-2,87	0,14	0,16	1,00
Hivep3	7,16E-04	-2,86	0,00	0,14	1,00
Capn12	6,61E-01	-2,86	0,12	0,16	1,00
Dusp8	7,94E-02	-2,85	0,20	0,36	1,00
Gm42427	4,22E-02	-2,83	0,93	0,84	1,00
Cysrt1	7,13E-02	-2,81	0,10	0,16	1,00
Dlg3	3,31E-02	-2,76	0,41	0,41	1,00

Table S1: Thresholds used for the different runs from Nowotschin et al, 2019.

Run	Min number of reads	Min number of genes	% of mitochondrial genes
E3.5_Run1	10000	4000	10
E3.5_Run2		2500	11
E4.5_Run1		2500	10
E4.5_Run2	5600		15

Complementary Results

Complementary results

In this second part of the results, I will discuss in greater detail the experiments that were performed to ensure the quality of my scRNAseq data and our strategy to integrate a quantitative and real-time biosensor of PI3K/AKT activity in ES cells and early embryos which will serve as a valuable tool for further studies. Furthermore, I will present the approaches we chose to try to confirm the phenotype induced by LY-mediated PI3K inhibition.

1. Acquisition of a high quality scRNAseq dataset

1.1. Quality control of low-input scRNAseq samples before sequencing

After discovering that PI3K/AKT inhibition dramatically affects NANOG in early embryos during Epi/PrE specification at the beginning of my PhD, we decided early on to perform transcriptomic analysis of the observed phenotype by scRNAseq. One of the platforms of Institut Pasteur provided a pipeline for massively parallel RNA single-cell sequencing (MARS-seq); however, comparative analysis of multiple scRNAseq methods showed that the sequencing depth of MARS-seq is relatively low (<6000 genes per cell) and that the dropout rate is elevated (74%) (Ziegenhain et al., 2017). This was not suitable for us as single cells have to be dissected manually from embryos making high dropout unfavorable and we required high read-depth to capture low expressed genes. Instead, we chose a method related to switching mechanism at 5′ end of RNA template sequencing 2 (SMART-seq2) which provides higher sensitivity (>8000 genes per cell) and significantly lower dropout rates (26%) (Ziegenhain et al., 2017). A unique feature of our model system is that the generation of libraries requires a multi-step protocol including single cell collection by immunosurgery and manual dissociation, cDNA amplification and purification as well as library tagmentation and it consequently took me 1.5 years to complete.

I followed a cDNA amplification protocol (Tang et al., 2009) which was adapted to single oocyte and single blastomere by two laboratories from the Institut Curie in Paris (Borensztein et al., 2018; Pérez-Palacios et al., 2021). The researchers who established these adapted protocols, Maud Borensztein and Raquel Pérez-Palacios, kindly accepted to let me observe how they perform their protocols for one day at their host laboratories and gave me valuable advices for handling the samples. As described in our paper, we decided to sequence

single cells from embryos which were cultured in the presence or absence of the PI3K inhibitor LY for 16h and 24h. Furthermore, we included non-cultured embryos of stage E3.25, E3.75 and E4.0 to establish developmental trajectories and to facilitate the integration with published datasets. E2.75 embryos which are cultured for 16h had on average 30 cells, so they did not correspond to non-cultured E3.25 embryos with approximately 52 cells which were rather comparable to E2.75 embryos cultured for 24h (56 cells). In hindsight, it would have been appropriate to sequence E3.0 embryos (28-32 cells), however in the integrated dataset 32-cell stage embryos were included (Posfai et al., 2017).

Single cells from each condition and stage were obtained from two or three independent experiments (Table 2) and mixed with the same volume of external RNA controls consortium (ERCC) spike-in mix prior to amplification. ERCC provide an external RNA source which are amplified with each single cell to help assessing sample quality and, if needed, normalization. To validate that the LY treatment was effective, to control for the absence of toxicity and ensure correct staging of the embryos which were processed for sequencing, a few embryos of each experiments were fixed, immunostained and imaged. Representative images of non-cultured embryos (Figure 16A upper panel) show expression of NANOG and GATA6 in most of the inner cells at E3.25 which becomes mutually exclusive to Epi and PrE progenitors at E3.75. At E4.0 Epi and PrE progenitors are sorted into two spatially distinct compartments. Representative images of cultured embryos (Figure 16A lower panel) show that NANOG is reduced upon LY treatment as expected.

Table 2. List of amplified single cells.

stage	n(experiments)	mean of embryos/experiment	mean of cells/embryo	% of passed QC
E3.25	3	4.3	10.7	63
E3.75	2	6	5.5	47
E4.0	3	2.7	7	58
E2.75+16h ctrl	3	2.3	4.6	76
E2.75+16h LY	3	2.3	4.3	83
E2.75+24h ctrl	3	4.3	4.7	60
E2.75+24h LY	3	4.7	3.6	54

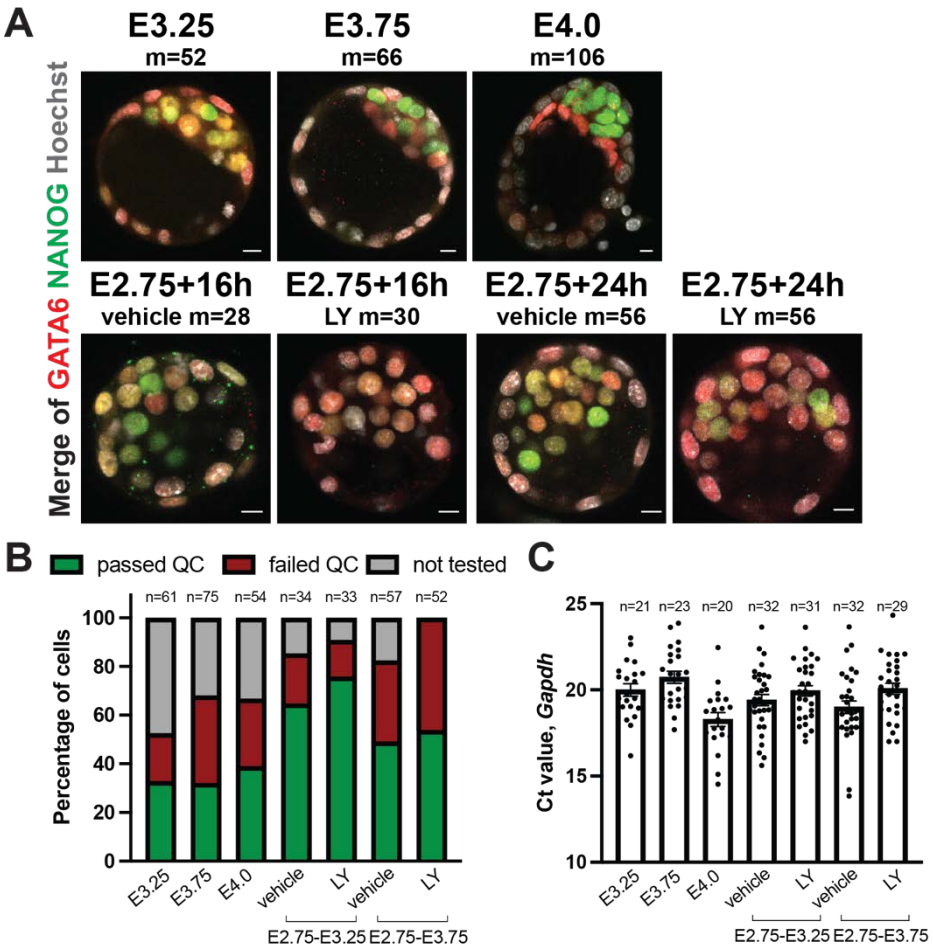

<u>Figure 16:</u> QC of embryos and single cell cDNAs prior to sequencing.
(A) Immunodetection of GATA6 (red), NANOG (green) and Hoechst (grey) in embryos prior to sequencing. (B) Percentage of single cells undergoing QC by RT-qPCR. After enough cells of good quality were collected, QC was stopped (not tested). (C) Distribution of Gapdh Ct values of single cells passing the QC. m, mean of total number of cells. scale bar = 20µm. n, number of embryos.

Quality control (QC) of the preamplified cDNAs was performed by controlling the amplification yield of the housekeeping gene *Gapdh* by RT-qPCR and all cells showing Ct values higher than 25 were excluded. Figure 16B shows the percentage of cells passing the quality check. Once a minimum of 20 for non-cultured and 30 for cultured cells of good quality was reached, the rest of the cells was not further processed (not tested). Figure 16C shows the distribution of *Gapdh* Ct values of cells of good quality. Single cells which were immediately processed after immunosurgery and not frozen at -80°C yielded especially low Ct which was a shared experience with researchers from Institut Curie (Pérez-Palacios et al., 2021). After amplification, I purified the cDNAs by running them on agarose gels and cutting out fragments above 500bp. During library preparation, I used 1ng of each sample to fragment the cDNAs,

tagment them with adapter sequences and amplify them with a unique combination of indexes. After a beads-based clean up step, I verified the profile of three randomly picked cells per condition and stage on TapeStation (Agilent). I produced a total of 185 libraries, pooled 96 and 89 of them at a final concentration of 1nM. I made sure to equally distribute single cells from all stages and conditions between the two runs. After receiving the authorization from the platform, I could autonomously load my library mix and configurate the sequencing program on the NextSeq550 from Illumina. The analysis of the two datasets was performed by the LabEx Revive bioinformatician Vincent Laville with help from Sebastien Mella.

Thus, by selecting a sequencing method which is adapted to our model and biological question and by applying high standards during the cDNA and library preparation, we set all the conditions in the scope of our possibilities to generate a scRNAseq dataset of high quality.

1.2 Quality control of low-input scRNAseq samples after sequencing

As mentioned above, the sequencing was performed in two independent runs. Principal component analysis (PCA) of log-normalized expression values show that sequencing of our cells in two independent sequencing runs (March and May) did not introduce any technical bias (Figure 17A). Prior to transcriptome analysis, different quality control metrics were applied to exclude low-quality cells from the analysis. For each cell, the proportion of reads mapped to spike-in transcripts relative to the total count (nCount_RNA) was calculated and all samples showing >1% of ERCC were eliminated as enrichment of spike-ins often indicates loss of endogenous RNA (Figure 17B). Moreover, cells showing a proportion of reads mapped to mitochondrial genes (mt) greater than 20% were not considered for further analysis, as elevated levels of mitochondrial transcripts are often a result of leakage of endogenous transcripts (Figure 17C). Additionally, the number of features per cells (nFeature), thus the number of endogenous genes with at least one count per million, was assessed as a criteria of quality control. Cells expressing less than 5000 features were not further processed (Figure 17D). As a result, from 185 sequenced cells 15 did not pass the quality control. This low dropout rate was proof that our rigorous standards during cDNA and library generation were a good investment.

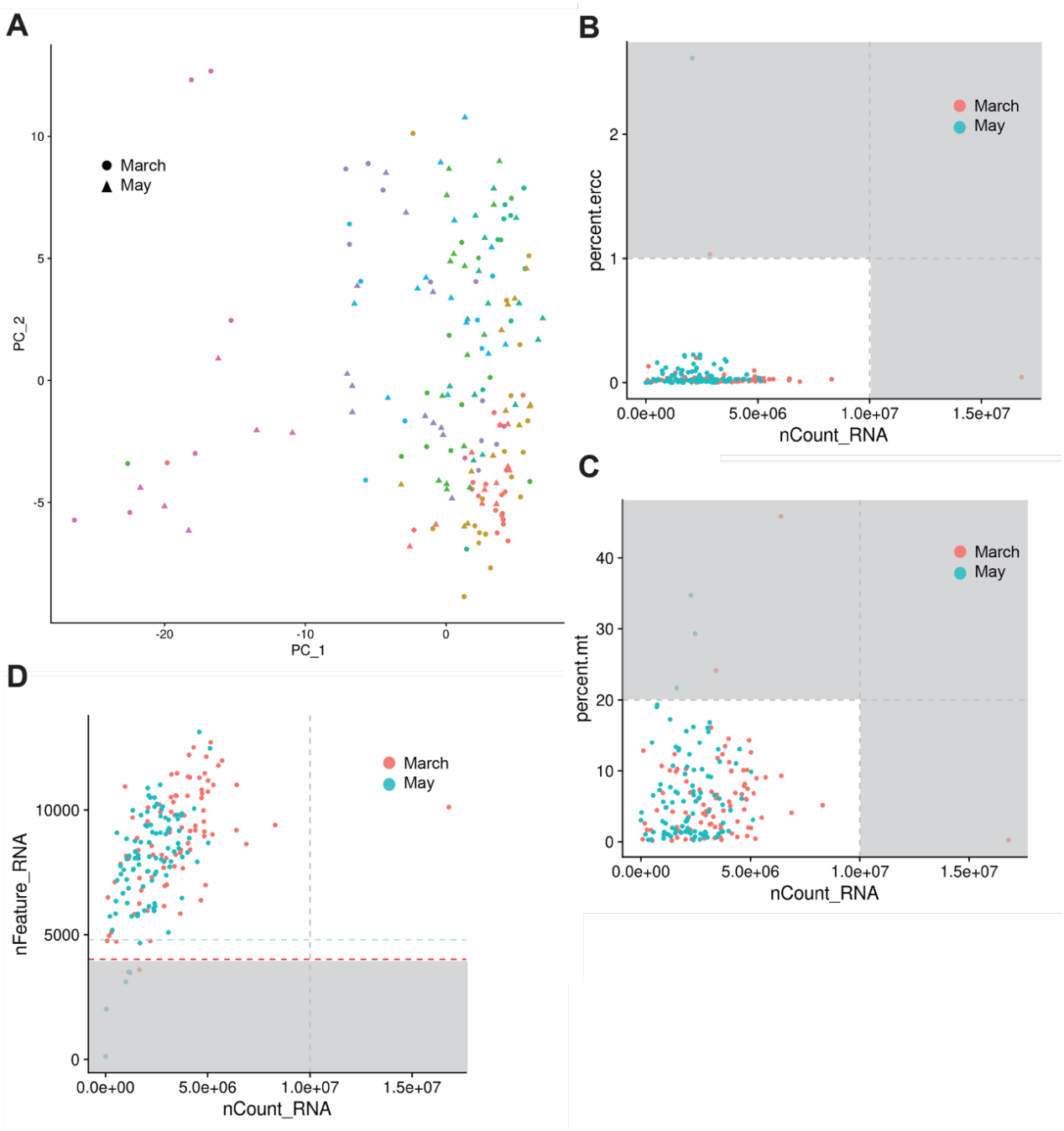

Figure 17: Identification of low-quality single cells after sequencing.

(A) PCA of normalized expression values per single cell sequenced in March (circle) and May (triangle). (B-D) Quality control metrics to filter single cells with an enrichment in ERCC (B), mt (C) or reduction in features (D).

2. Visualization of PI3K/AKT signaling dynamics

pRPS6 has been shown to serve as a faithful readout for PI3K/AKT activity in early embryos and distinct levels of pRPS6 during specification stages of preimplantation development indicated changes in PI3K/AKT activity during cell lineage formation (Paper Figure 1). However, it provides a static snapshot of PI3K/AKT activity. In order to achieve live visualization of PI3K/AKT signaling dynamics, we decided to integrate an Akt-kinase translocation reporter (Akt-KTR) in ES cells and early embryos. This was achieved with great help from Sandrine Vandormael-Pournin who works as an engineer in the lab and has a high technical expertise in working with ES cells and early embryos.

2.1 Establishment of stable Akt-KTR ES cell line

FOXO proteins are direct substrates of AKT and are excluded from the nucleus and blocked from inducing transcription of downstream factors by AKT-mediated phosphorylation (Brunet et al., 1999). In 2016, Maryu and colleagues developed the polycistronic vector pHGEA expressing ERK-KTR, Akt-FoxO3a-KTR, a cell-cycle reporter and a nuclear reporter which allowed to simultaneously follow ERK and AKT activities in live cells (Maryu et al., 2016). By substituting the His residue at the 212 position by Arg, the transcriptional activity of FoxO3a was abolished. Their construct was cloned into the hyPBase donor vector pPBbsr, under the control of the ubiquitous CAG promoter and contains self-cleaving P2A peptides. HyPBase which is a hyperactive form of piggyBac, a moth-derived DNA transposase, is a highly efficient tool for transgenesis in mammalian cells (Yusa et al., 2011). HyPBase binds to two terminal inverted repeats (IRs) flanking the insert in the pPBbsr vector, excises the DNA and integrates the segment into the genome. From the pHGEA plasmid, we removed the ERK-AKT as well as the cell-cycle reporter and replaced the iRFP720 which was fused to H2B with iRFP670 to meet the compatibilities of the integrated laser of our confocal microscope (Figure 18A).

Akt-KTR was integrated in E14Tg2a ES cells by co-transfection of the Akt-KTR construct with an hyPBase expression vector. I then selected multiple clones showing strong iRFP and EGFP signals under a fluorescent microscope and I proceeded to qualitatively characterize one of the generated Akt-KTR cell lines. I could observe that Akt-KTR is predominantly localized in the cytoplasm under serum/LIF conditions (Figure 18B upper panel) and could confirm that this localization is stable during live imaging for 24h (data not shown). Serum contains an abundance of growth factors that potentially could activate PI3K/AKT

signaling and explain the robust cytoplasmic accumulation of the Akt reporter. I therefore prepared 2i/LIF medium using insulin-free B27 to culture Akt-KTR ES cells without PI3K/AKT-stimulating molecules. As seen in the upper panel of Figure 18C, Akt-KTR visibly accumulated in the cytoplasm when cultured under these special 2i/LIF conditions. This indicated that PI3K/AKT is continuously active in mES cells and suggested that PI3K/AKT activity is largely independent of external stimuli. Finally, I tested the sensitivity of the Akt-KTR to PI3K/AKT inhibition. While under control conditions the Akt-KTR remains in the cytoplasm, 4h of LY treatment induced a shuttling of the Akt-KTR to the nucleus in ES cells both in serum/LIF and 2i/LIF culture conditions (Figure 18B-C lower panel). Consequently, the Akt-KTR shows a robust response to modulation of PI3K/AKT signaling.

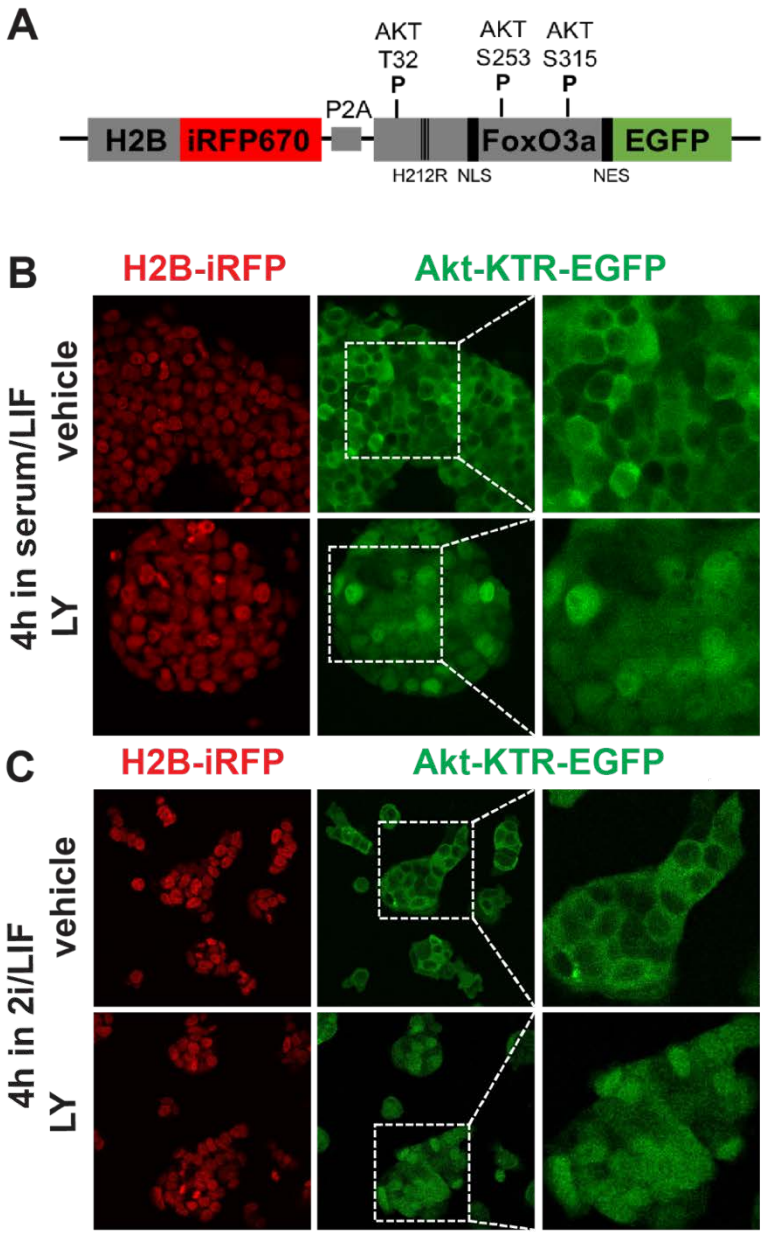

Figure 18: Nuclear accumulation of Akt-KTR upon PI3K inhibition.

(A) Structure of Akt-KTR. AKT phosphorylation sites and H212 mutation are indicated. NLS, nuclear localization signal. NES, nuclear export signal. (B-C) Confocal images of ES cells expressing H2B-iRFP (red) and Akt-KTR-EGFP (green) in serum/LIF (B) and 2i/LIF (C) conditions.

2.2 Expression of Akt-KTR in early mouse embryos

Next, we moved on to induce the expression of Akt-KTR in early embryos by microinjection. Generally, the injection of RNA is less toxic than DNA for the development of early embryos and allows rapid translation. However, the amount of RNA which can be produced with our protocol is limited and RNA is inherently less stable than DNA which can result in RNA degradation before the desired developmental stage is reached. With these constraints in mind, we decided to inject Akt-KTR in the form of DNA but inject the transposase as RNA in zygotes to achieve rapid integration before cell division. Microinjection at the 1-cell stage is technically easier than injection at later stages due to zygote size, it lowers the probability of mosaicism and increases the rate of survival. However, as our focus lied on the observation of PI3K/AKT signaling dynamics during stages of lineage formation, a culture period of several days was required. In this set of experiment, the embryos ranged between 16- and 32 cell stage after 72h of culture. The concentrations used for pronucleus injection during four independent experiments are listed in Table 3. In the first experiment 6/10 GFP+ embryos showed a heterogenous nucleocytoplasmic distribution of EGFP after 48h of culture and in the second experiment 100% of the fluorescent embryos showed blastomeres with various nucleocytoplasmic levels of EGFP after 72h of culture. These preliminary results were encouraging observations which indicated the existence of distinct PI3K/AKT activities in the blastomeres of morula/early blastocyst stages during preimplantation development. The reduction of hyPBase RNA concentration in the third experiment resulted in a reduced number of iRFP/EGFP expressing embryos and the levels of fluorescence were weak. After increasing the hypBase concentration to earlier levels, we observed an increase in the number of fluorescent embryos during the 72h of culture in the fourth experiment. Representative images of embryos are shown in Figure 19A,B, respectively.

The confocal microscope is and was a shared equipment from our department and because microinjection of zygotes required an observation by live imaging over several days, the organization of these experiments was challenging. We therefore decided to transiently express Akt-KTR and injected Akt-KTR RNA into single blastomeres of 4 to 8-cell stage embryos and cultured them for 48h before fixation. Here we chose RNA as our culture period was not extending 2 days and we required rapid translation. From 16 injected embryos, 7 showed EGFP expression after 48h in several blastomeres. The distinct nucleocytoplasmic distribution of EGFP indicated differences in PI3K/AKT activity between neighboring blastomeres (Figure 19C). Within the 48h culture window after injection, every cell underwent

approximately one to two cell division, meaning the number of EGFP expressing inner cells per embryo was limited. Consequently, we would have to considerably increase the number of experiments and embryos to assess a potential correlation of PI3K/AKT activity and Epi/PrE fate. We therefore decided to focus our efforts on to the establishment of a stable Akt-KTR mouse reporter line.

Table 3. Microinjection experiments for Akt-AKT expression in early embryos.

	Akt-KTR DNA (ng/µl)	**hyPBase RNA (ng/µl)**	**n(injected embryos live imaging)**	**% of developping embryos**	***in vitro* culture time**	**% of iRFP/EGFP+ embryos**
1	20	100	15	93	48h	73
2	5	100	13	92	72h	54
3	10	10	43	95	24h	37
				93	48h	51
				90	72h	19
4	10	100	48	98	24h	35
				94	48h	60
				94	72h	73

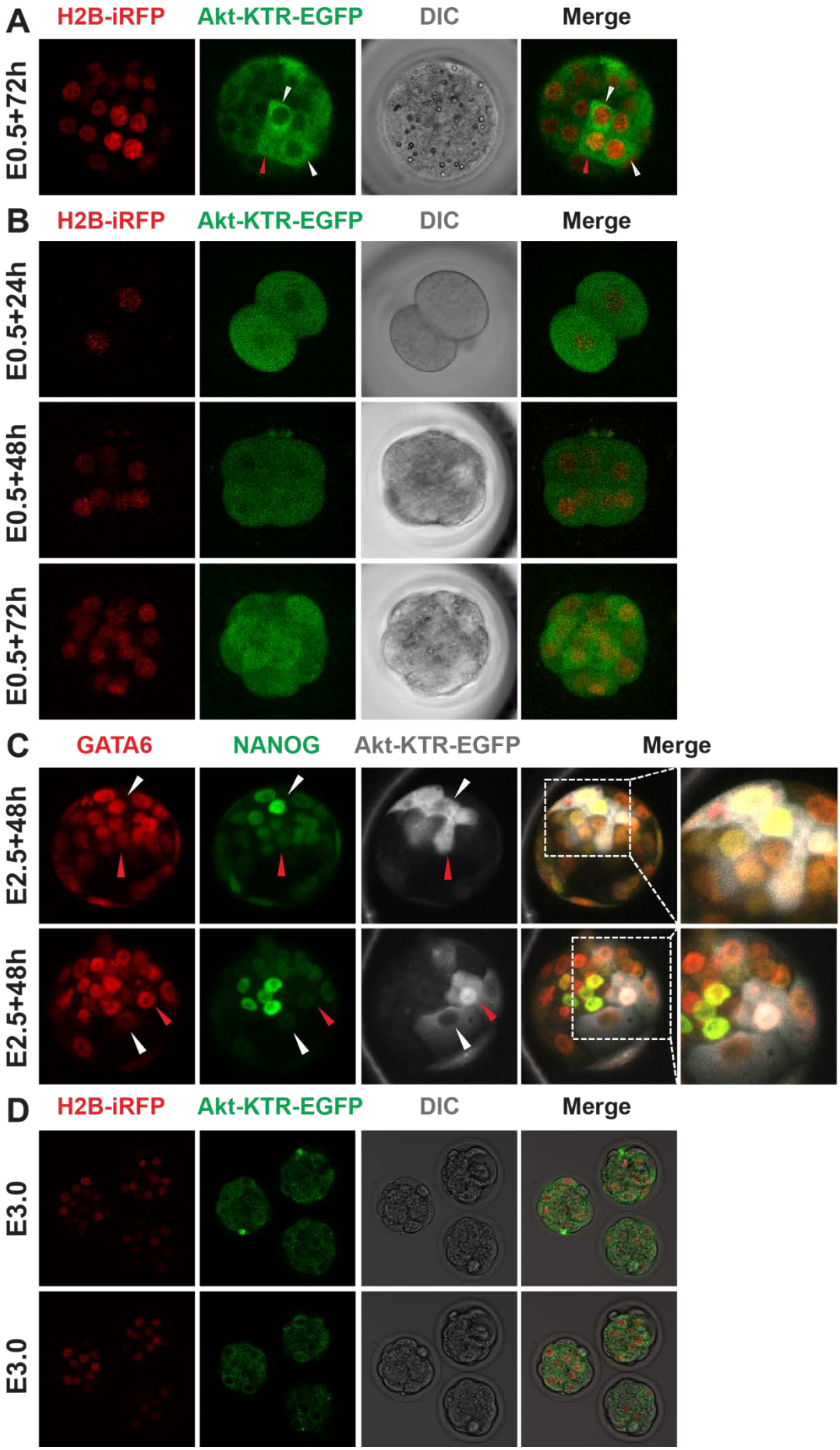
A
H2B-iRFP
Akt-KTR-EGFP
DIC
Merge
E0.5+72h
B
H2B-iRFP
Akt-KTR-EGFP
DIC
Merge
E0.5+24h
E0.5+48h
E0.5+72h
C
GATA6
NANOG
Akt-KTR-EGFP
Merge
E2.5+48h
E2.5+48h
D
H2B-iRFP
Akt-KTR-EGFP
DIC
Merge
E3.0
E3.0

Figure 19: Expression of Akt-KTR in early embryos.
Representative confocal images of embryos expressing H2B-iRFP (red) and Akt-KTR-EGFP (green) after the first (A) and third (B) experiment of microinjection at the zygote stage. (C) Immunodetection of GATA6 (red), NANOG (green) and Akt-KTR-EGFP (grey) in embryos injected at the 4 to 8-cell stage. Note that the indicated cells in the lower panel belong to the TE. (D) Representative images of embryos at E3.0 expressing H2B-iRFP (red) and Akt-KTR-EGFP (green). White arrows point to cells with cytoplasmic Akt-KTR accumulation and red arrows indicate nuclear localization of Akt-KTR.

2.3 Establishment of stable Akt-KTR mouse line

In four independent experiments, zygotes were injected with 10ng/µl of Akt-KTR DNA and 200/100/20/10ng/µl of hyPBase RNA and with the help of the Mouse Genetic Engineering Center (CIGM) at the Institut Pasteur transferred into pseudo pregnant females. In the four experiments, an average of 32% of implanted zygotes gave rise to viable pups and an average of 47% of pups tested positive for iRFP by polymerase chain reaction (PCR). From the 17 iRFP-positive pups, the 8 males were isolated and crossed with CD1 females once they reached reproductive age. 4 out of 8 males produced offspring that showed iRFP expression under our EVOS M5000 microscope (Invitrogen). Interestingly, the transmission rate of iRFP to the offspring was 100% which indicated that the transgene was integrated at multiple sites. The intensity of iRFP varied within the 4 litters but was clearly detectable. In contrast, EGFP was only detectable in the litter of a single male and unfortunately on levels which were insufficient for the quantification of nucleocytoplasmic ratios (Figure 19D). This may be due to the fact that H2B which is fused to iRFP in our construct is a highly represented histone which is stably expressed in cells. We have tested the acquisition of the Akt-KTR embryos using the LSM800 confocal microscope of our department and the light sheet fluorescence microscope of Jean-Leon Maitre's laboratory at the Institut Curie with limited success. Next, we are planning to test live imaging with a LSM900 with Airyscan 2 and simultaneously isolate a Akt-KTR offspring generation carrying only one copy of the transgene.

I was already in my second year when we started this project and decided to randomly integrate Akt-KTR in the mouse genome. This was already done with success to generate a stable Erk-KTR mouse line (Pokrass et al., 2020). However, in hindsight a directed integration of AKkt-KTR into a permissive locus probably would have prevented the problems we encountered.

3. Validation strategies for the LY-induced phenotype

3.1 Inhibition of PI3K/AKT by alternative inhibitors

The effect of PI3K inhibition by LY on NANOG during Epi/PrE specification in early embryos was a striking discovery at the start of my thesis and the characterization of the phenotype revealed a lot of interesting aspects. To validate our observations and strengthen our conclusions, I aimed to recapitulate our results using alternative PI3K/AKT inhibitors. Although many PI3K/AKT pathway inhibitors exist, only a small number has been used in early mouse embryos and it is often challenging to find the appropriate dosage which effectively inhibit signaling activity in the absence of toxicity. In early embryos the genes encoding the three isoforms of class I PI3K p110α/β/δ are expressed, however UMAPs of the integration of our data with published datasets showed low PI3Kδ expression levels (Figure 20A). LY is a highly specific PI3K inhibitor which blocks PI3Kα/β/δ activity with IC50 of 0.5µM/0.97µM/0.57µM, respectively (Chaussade et al., 2007). When used at high concentrations (>10mM), LY can also inhibit other targets like mTOR, DNA-dependent protein kinase (DNA-PK) or casein kinase 2 (CK2) (Brunn et al., 1996; Gharbi et al., 2007). Treating E2.75 embryos for 24h with different concentrations of LY revealed that concentrations below 10µM mildly affected TF patterning of ICM cells (Figure 20B). This suggests that a threshold of 10µM is required to fully induce the phenotypic changes we reported in our paper.

Wortmannin is a potent PI3K inhibitor which prevents the phosphorylation of PI3K targets by binding to the lysine 802 residue of PI3Kα (Wymann et al., 1996) and is, in contrast to LY, irreversible. In mES cells, treatment with 100nM of Wortmannin for 24h significantly reduced *Nanog* (Nur-E-Kamal et al., 2006). However, unlike LY-treated embryos, embryos cultured in the presence of 100nM Wortmannin for 24h expressed NANOG on the same level as control embryos (Figure 20C-D).

PI-103 is a synthetic, ATP-competitive mTORC1/2 inhibitor which has also been shown to inhibit the production of PIP2/3 in adipocytes and myotubes *in vitro* (Knight et al., 2006). In hES cells both LY and PI-103 induce differentiation into cardiomyocytes and 100nM of PI-103 significantly reduced pAKT levels (Y. Yang et al., 2019). In my experimental setup, treatment with 100nM of PI-103 during Epi/PrE specification did not affect NANOG levels in early embryos (Figure 20F-G).

The inhibitory action of LY is directed towards three isoforms of class I PI3Ks (Vlahos et al., 1994). By using selective inhibitors for PI3Kα/β, I aimed to decipher if a specific isoform

of the combination of both are necessary to maintain NANOG during Epi progenitor formation. Synthetic HS-173 (HS) mimics the purine portion of ATP which block the ATP binding pocket of PI3K p110α and therefore inhibit PI3Kα activity (O. Kim et al., 2011). Similar to LY, HS has been shown to inhibit PI3K/AKT-dependent proliferation in hepatic stellate cells which contribute to fibrosis formation in liver disease (Son et al., 2013). I could not find any study using HS in mES/hES cells or early embryos which could give me an indication about appropriate dosage. TGX-221 (TGX) is a potent and selective inhibitor of PI3K p110β (Hennessy et al., 2005) and has been shown to promote differentiation and downregulation of *Nanog* in murine ES cells (Kingham & Welham, 2009). To determine at which concentration HS and TGX effectively inhibit PI3K/AKT signaling, I first tested a range of different concentration in ES cells which were transfected with Akt-KTR and treated with the inhibitors for 4h (Figure 20H). Akt-KTR showed a clear localization to the nucleus at 500nM/1µM of HS and 5µM of TGX. At 100nM of HS and 1µM of TGX the Akt reporter showed a heterogenous response with partial delocalization to the nucleus in a few cells. The reasons for this were unclear. While 1µM of HS had no visible effect on proliferation or cell death in ES cells, embryos treated with 350/500nM of the PI3Kα inhibitor showed a significant reduction in total cell number (Figure 20L). The reduction to 500nM of HS did not cause any significant differences in total cell number and NANOG/GATA6 TF patterning in the ICM and neither did the treatment with 5µM of the PI3Kβ inhibitor TGX (Figure 20I, M). Finally, the combination of both inhibitors did not mimic the effects of LY incubation on NANOG (Figure 20J, N).

In conclusion, I was unable to confirm the LY-induced phenotype by treating embryos with alternative inhibitors using the indicated concentrations. However, it is important to note that some of this data was analyzed at the beginning of my PhD when I subjectively assessed TF patterning by manual cell counting. Only later I became introduced to the image analysis software IMARIS which allowed me to quantitatively measure fluorescent protein levels. Furthermore, I did not stringently verify that the concentrations I used effectively inhibit PI3K/AKT by performing pRPS6 staining. Recently, when I assessed pRPS6 levels in embryos treated with 100nM Wortmannin, I observed no visible difference between vehicle and treated embryos, indicating that PI3K/AKT was insufficiently blocked (Figure 20E). It is therefore possible that the conditions of my experimental setup were not adapted to recapitulate the phenotype resulting from LY treatment.

3.2 Mimicking the inhibition of PI3K/AKT by GSK3 activation

The observation that the inhibition of GSK3 by CHIR during Ep/PrE specification led to a significant increase of NANOG levels indicated that PI3K/AKT might regulate TF expression in the ICM through downstream target GSK3. We therefore asked whether the activation of GSK3 could antagonize PI3K/AKT activity and replicate the effects of LY treatment in early embryos. XAV939 (XAV) is a small molecule which inhibits WNT signaling by preventing the transcription of β-catenin targets. The binding of WNT effector Tankyrase (TNKS) by XAV stabilizes AXIN which is part of the β-catenin destruction complex and in turn enhances β-catenin phosphorylation levels (Huang et al., 2009). In addition, XAV indirectly promotes GSK3 as the stabilization of AXIN increases AXIN-GSK3 complex formation (Huang et al., 2009). In EpiESC, 12h of treatment with 2µM of XAV is sufficient to significantly increase AXIN (S. H. Kim et al., 2014). In early embryos the treatment with 5µM and 10µM XAV for 24h starting at E2.75 did not significantly affect the number of GATA6/NANOG-positive and coexpressing cells (Figure 20K, O). However, in the absence of a reliable readout confirming GSK3 activation with the used concentrations of XAV, I cannot unequivocally conclude that GSK3 activation has no effect on NANOG.

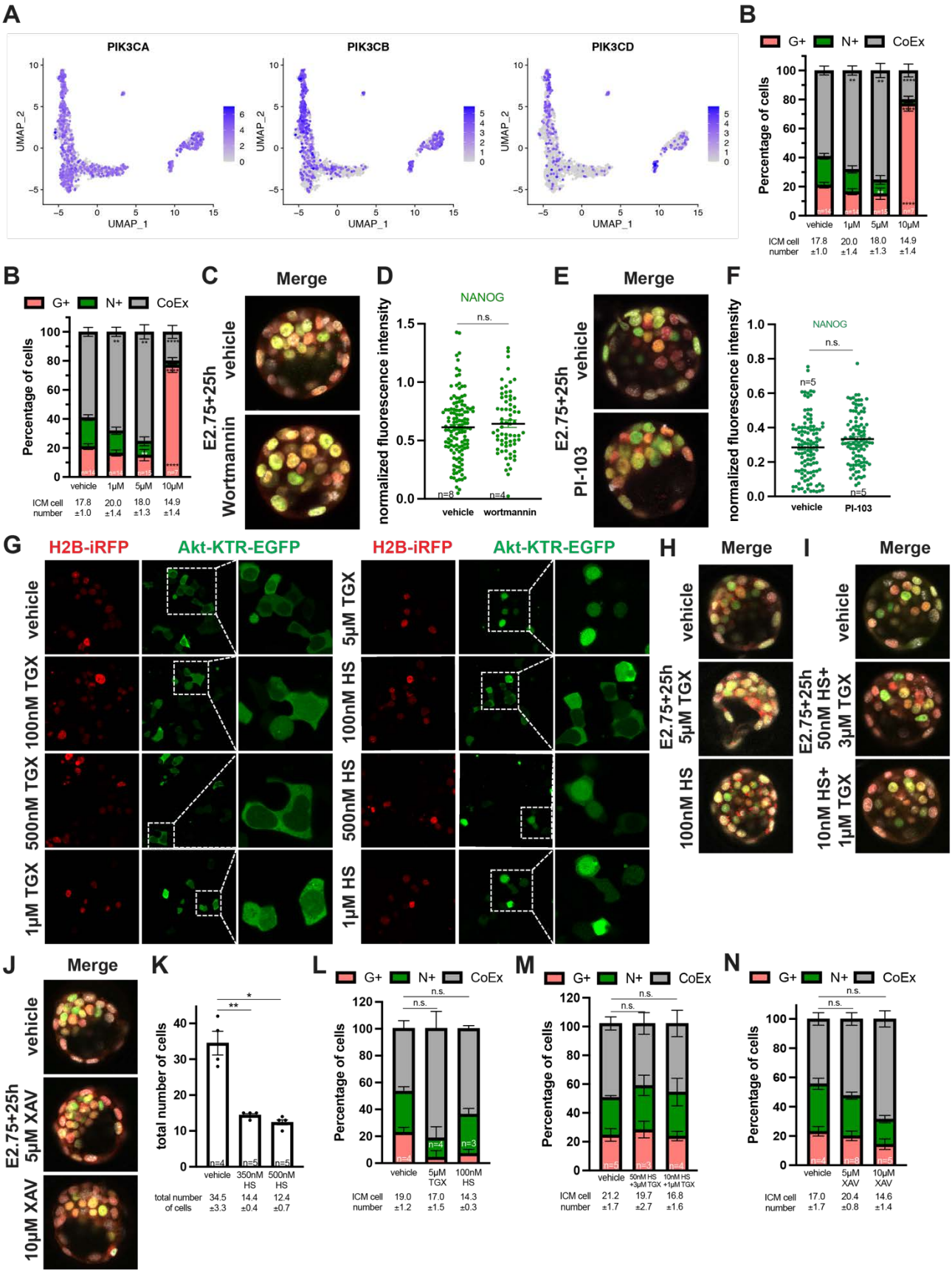
A
PIK3CA
PIK3CB
PIK3CD
UMAP_1
UMAP_2
B
G+
N+
CoEx
Percentage of cells
vehicle
1µM
5µM
10µM
ICM cell number
17.8 ±1.0
20.0 ±1.4
18.0 ±1.3
14.9 ±1.4
C
Merge
E2.75+25h vehicle
E2.75+25h Wortmannin
D
NANOG
n.s.
normalized fluorescence intensity
vehicle
wortmannin
E
Merge
E2.75+25h vehicle
E2.75+25h PI-103
F
NANOG
n.s.
vehicle
PI-103
G
H2B-iRFP
Akt-KTR-EGFP
vehicle
100nM TGX
500nM TGX
1µM TGX
5µM TGX
100nM HS
500nM HS
1µM HS
H
Merge
vehicle
E2.75+25h 5µM TGX
100nM HS
I
Merge
vehicle
E2.75+25h 50nM HS+ 3µM TGX
10nM HS+ 1µM TGX
J
Merge
vehicle
E2.75+25h 5µM XAV
10µM XAV
K
total number of cells
vehicle
350nM HS
500nM HS
total number of cells
34.5 ±3.3
14.4 ±0.4
12.4 ±0.7
L
G+
N+
CoEx
Percentage of cells
vehicle
5µM TGX
100nM HS
ICM cell number
19.0 ±1.2
17.0 ±1.5
14.3 ±0.3
M
G+
N+
CoEx
Percentage of cells
vehicle
50nM HS +3µM TGX
10nM HS +1µM TGX
ICM cell number
21.2 ±1.7
19.7 ±2.7
16.8 ±1.6
N
G+
N+
CoEx
Percentage of cells
vehicle
5µM XAV
10µM XAV
ICM cell number
17.0 ±1.7
20.4 ±0.8
14.6 ±1.4

Figure 20: The treatment with alternative PI3K/AKT inhibitors failed to copy the LY-induced phenotype.
(A) UMAP highlighting the expression levels of indicated genes. Grey (low) to purple (high) scale indicates average expression. (B) Distribution of GATA6 (G+, red), NANOG (N+, green) or both markers (CoEx, grey) in embryos cultured for 24h from E2.75 with or without LY. Immunodetection of merged GATA6 (red), NANOG (green) and Hoechst (grey) (C, F) or (E) pRPS6 (grey) and (D, G) quantification of NANOG (green) in embryos in embryos cultured for 24h from E2.75. (H) Confocal images of ES cells expressing H2B-iRFP (red) and Akt-KTR-EGFP (green) in serum/LIF. (L) Total number of cells in embryos cultured for 24h from E2.75. (I-K) Merge of immunodetection of GATA6 (red), NANOG (green) and Hoechst (grey) and (M-O) distribution of GATA6 (G+, red), NANOG (N+, green) or both markers (CoEx, grey) in embryos in embryos cultured for 24h from E2.75. Statistical significance (*$p < 0.05$, **$p < 0.01$, ****$p < 0.0001$) and insignificance (n.s.) indicated. Error bars show SEM. n, number of embryos.

3.3 Inhibition of PI3K/AKT by expression of dominant negative p85Δ

In addition to testing alternative PI3K/AKT inhibitors, I searched for a genetic tool to inhibit PI3K/AKT signaling in early embryos in order to validate the observations achieved with LY. It has previously been demonstrated that the expression of a dominant negative form of the p85 regulatory subunit of class I PI3K (p85Δ) (Figure 21A) mimics the effects of LY *in vitro* (Kaliman et al., 2007; Storm et al., 2007) and inhibits *Nanog* in ES cells (Storm et al., 2007). To test if I can recapitulate these finding, I transfected Akt-KTR ES cells with p85Δ being expressed under the control of a CAG promotor and a mCherry expressing vector. Indeed, while under control conditions Akt-KTR ES cells exhibit cytoplasmic accumulation of Akt-KTR, p85Δ expression led to a delocalization of Akt-KTR to the nucleus indicating robust inhibition of PI3K/AKT activity (Figure 21C). In addition to p85Δ, I transfected Akt-KTR ES cells with the PTEN-4A and the corresponding control (PTEN-WT) plasmid. PTEN is an antagonist of the PI3K/AKT pathway and the mutation of four serine/threonine phosphorylation sites S380, T382, T383, and S385 (PTEN-4A) (Figure 21B) has been shown to increase PTEN stability and inhibitory function (Vazquez et al., 2000). However, the expression of PTEN-4A had no visible effect on the intracellular distribution of Akt-KTR suggesting that PI3K/AKT remains active in ES cells (Figure 21D). PTEN-4A is expressed under the control of a SV40 promotor which is weaker than CAG, so it is possible that the achieved expression yield was not sufficient to effectively block PI3K/AKT activity.

After confirming that p85Δ is a functional tool to inhibit PI3K/AKT activity in ES cells, we proceeded to express p85Δ in early embryos in an attempt to recapitulate the phenotypic changes caused by LY treatment. In three independent experiments, 4 to 8-cell stage embryos

were injected with mRNA of p85Δ and membrane (mb)GFP at a ratio of 875:800 ng/µl (1, 2) and 875:1250 ng/µl (3) into blastomeres and fixed after 24h of culture (Table 4). We increased the mbGFP concentration because I had difficulties to identify injected cells and their progeny after immunostaining. To assess if p85Δ expression inhibits PI3K/AKT activity in injected cells, I performed immunostaining for pRPS6. Likewise, in order to decipher if p85Δ affects NANOG similarly to LY, embryos were immunostained for NANOG and the nuclear protein levels quantified in non-injected embryos (vehicle) as well as in GFP-negative (GFP-) and GFP-positive (GFP+) of injected embryos. Representative images of embryos from experiment 1 (Figure 22A) and 2 (Figure 22B) as well as the quantification of experiment 2 (Figure 22C) are shown below. Only a small fraction of the injected embryos showed GFP+ ICM cells and due to the reduced visibility of mbGFP it is possible that I overlooked some cells. In the cells I identified as GFP+ I could not detect altered levels of pRPS6 and NANOG. However, as the number of quantitatively analyzed cells was low, we refrain to draw definite conclusions from these experiments.

Table 4. Summary of p85Δ microinjection experiments.

	Number of non-injected embryos (vehicle)	Number injected embryos	Number of embryos with GFP+ ICM cells	Number of quantified GFP+ ICM cells	Qualitative level of pRPS6 (-/+/++)
1	2	22	3	7	+/+/+/-/-/+/-
2	4	37	2	4	+/+/+/-
3	4	34	3	9	+/+/+/+/-/-/-/-/-

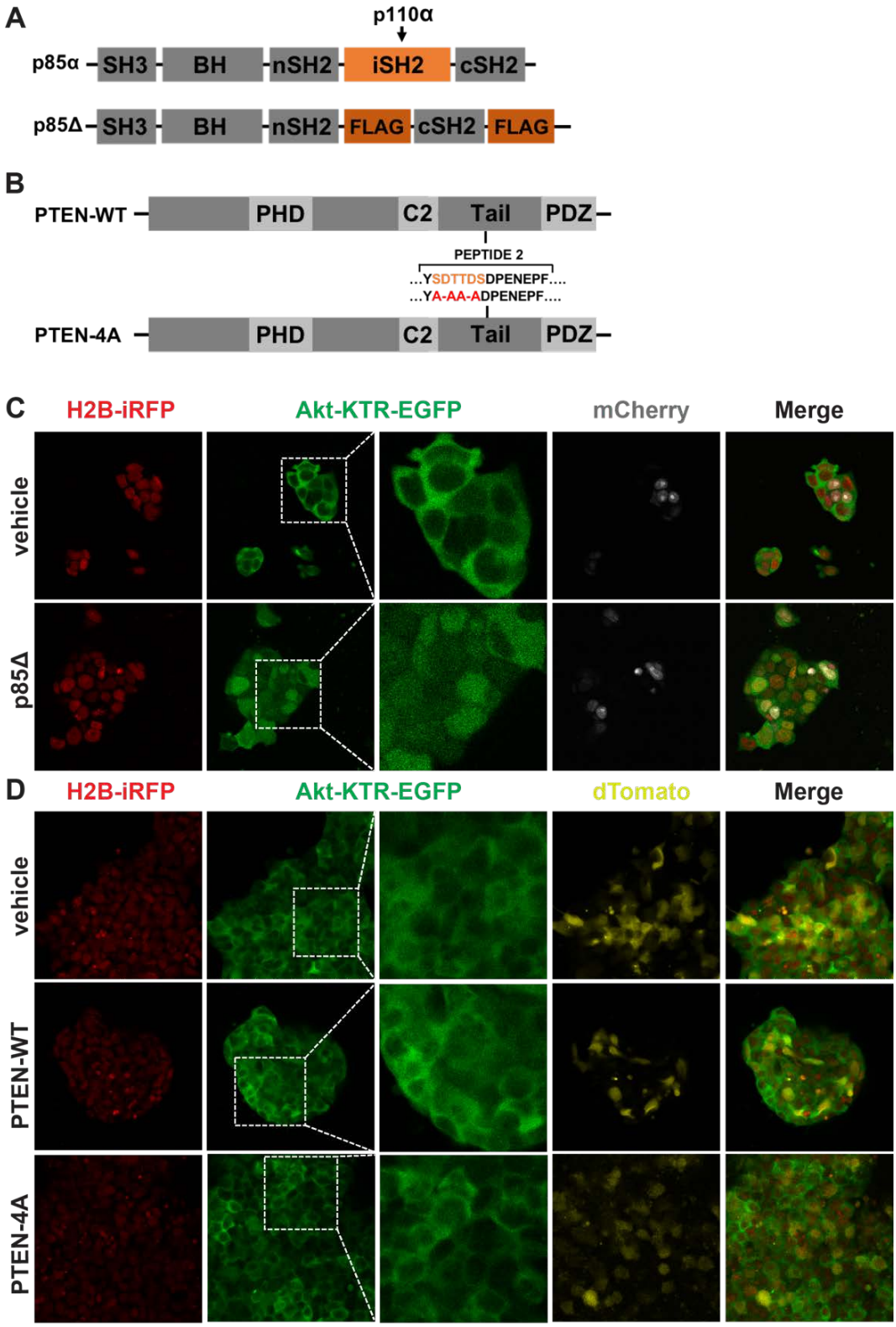

<u>Figure 21:</u> Nuclear accumulation of Akt-KTR upon p85Δ expression.

(A) Structure of p85 α and p85Δ. In p85Δ the p110α biding domain iSH2 is replaced by FLAG-tag. SH3, Src homolog 3. BH, BCR homology. nSH2, N-terminal SH2. iSH2, inter SH2. cSH2, C-terminal SH2. (B) Structure of PTEN-WT and PTEN-4A. In PTEN-4A four amino acids are mutated. PHD, Phosphatase domain. C2, C2 domain. PDZ, PDZ binding domain. (C-D) Confocal images of ES cells expressing H2B-iRFP (red) and Akt-KTR-EGFP (green) upon (C) p85Δ and (D) PTEN-4A and PTEN-WT transfection.

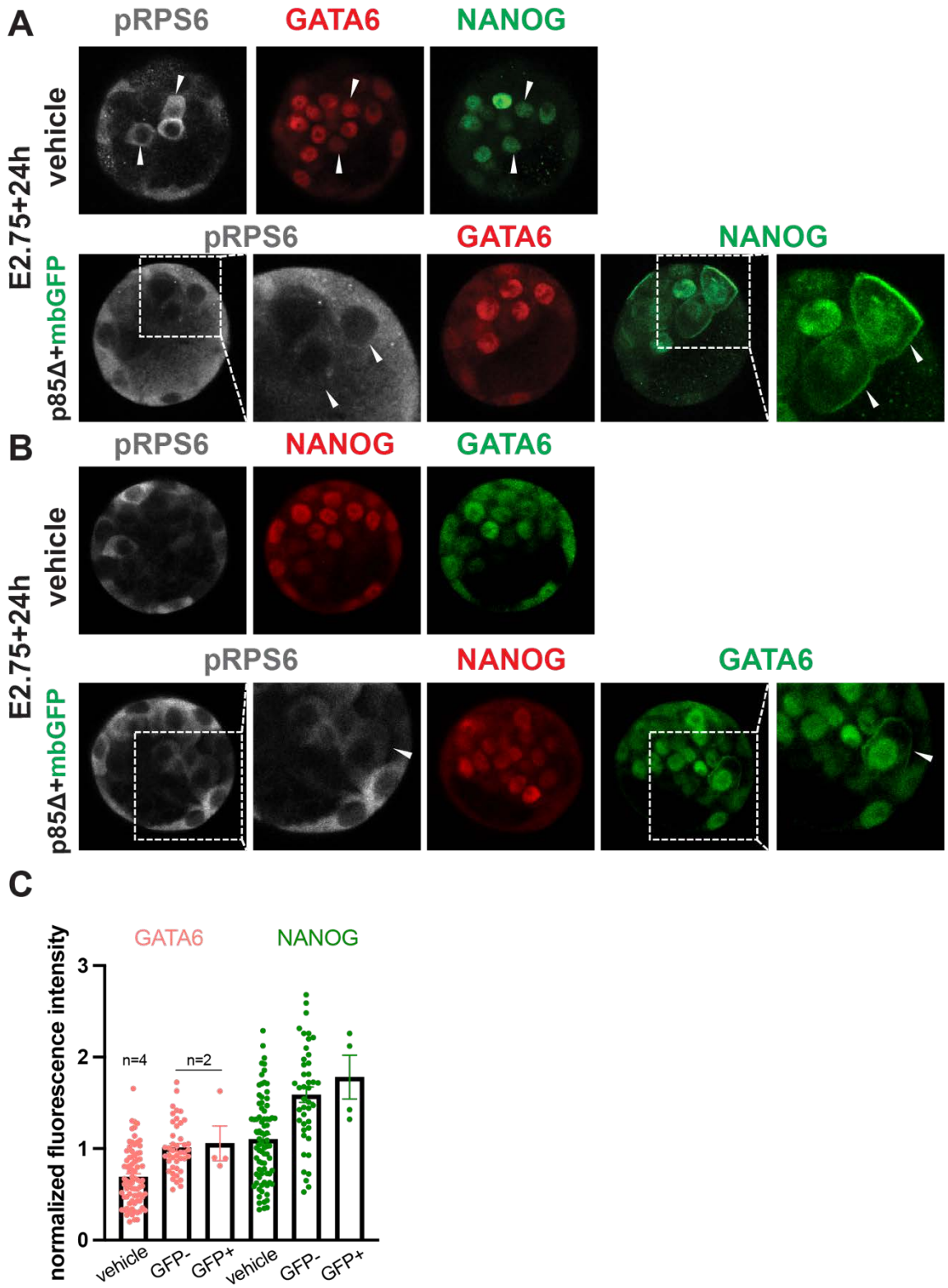

Figure 22: pRPS6 and NANOG unchanged upon p85Δ expression in early embryos.
(A) Immunodetection of pRPS6 (grey), GATA6 (red) and NANOG (green) and in noninjected (vehicle) and injected (p85Δ+mGFP) embryos cultured for 24h from E2.75. Arrows point out pRPS6 in control and injected GFP+ cells. (B) Immunodetection of pRPS6 (grey), NANOG (red) and GATA6 (green) and (C) quantification of GATA6 (red) and NANOG (green) in noninjected (vehicle) and injected (p85Δ+mGFP) embryos cultured for 24h from E2.75. Arrows point out pRPS6 in injected GFP+ cell. n, number of embryos.

Discussion

Discussion

1. Are the effects of PI3K inhibition on the mouse transcriptome really moderate?

The characterization of the PI3K/AKT inhibitory phenotype by immunofluorescence demonstrated that PI3K/AKT activity has a crucial role in the regulation of Epi/PrE-specific TF patterning. To extend the phenotypic analysis to the transcriptomic level, we performed scRNAseq on vehicle and LY-treated embryos as well as non-cultured embryos. The implementation of a new and hand-intensive protocol was a technical and time-intensive challenge for me and due to the sanitary COVID crisis the completion took longer than anticipated. However, the selection of the protocol and the setting of rigorous standards for the different measures of quality control allowed us to achieve a very low dropout rate of 8.1% and a high number of captured genes. We were aware of the fact that having ~60 cells per condition (vehicle versus treated) limits the number of differentially expressed genes, however the work load and financial aspect of library preparation made this compromise necessary. As an example, while we do report a reduction of *Fgf4* in treated single cells, this difference is not statistically significant. Shapiro et al. calculated that in order to achieve a similar coefficient of variation (standard deviation divided by the mean) like in standard bulk RNAseq experiments, a minimum of 50 cells per condition is required (Shapiro et al., 2013). However, the authors emphasize that additional factors like the efficiency of mRNA to cDNA conversion as well as the noise introduced by cDNA amplification are not considered in their calculations. Reverse transcription introduces a 3’ bias and the cDNA fragmentation using the Tn5 transposase causes a loss of sequencing coverage at the 5’-end of transcripts. Thus, it is possible that the number of sequenced cells and/or the preparation of the libraries were not sufficient to account for transcriptional changes induced by PI3K inhibition. We are planning to validate our data by generating cDNA libraries of single ICM of vehicle and LY-treated embryos using an improved protocol called FLASH-seq (Hahaut et al., 2021). This protocol includes modifications which allow to process the transcription and amplification of RNA in one step, add extra nucleotides to improve the generation of extra 5’-sequences and use adapted primers to reduce strand invasion. These changes in addition to an improved reverse transcription enzyme and a single clean-up step reduce library generation to approximately 4.5h. Nicola Festuccia, a permanent CNRS researcher in our unit, already tested the protocol with single 8-cell stage embryos with success. This approach will not only allow us to generate new sequencing data with less time

and effort but also allow us to rapidly assess the expression level of several lineage-specific genes by RT-qPCR. Thus, we will soon be able to conclusively determine if PI3K/AKT inhibition affects key TFs of the ICM on a transcriptional level.

2. What PI3K/AKT downstream mechanisms are at play during specification?

Embryonic stem cells remain a proxy for the Epiblast, however data acquired in stem cells can provide important mechanistic insights that can serve as a working hypothesis for the early embryo. Comparing the existing literature about the regulation of pluripotency in embryonic stem cells and early embryos reveals that while the same genes and signals may be at work, the underlying mechanisms often differ. While *Nanog* is activated in a PI3K/AKT-dependent manner by LIF through TBX3 in mES cells (Niwa et al., 2009), LIF and *Tbx3* are dispensable for early embryonic development (Davenport et al., 2003; Luo et al., 1997; Stewart et al., 1992). In the embryo, *Nanog* is required for ICM maintenance (Mitsui et al., 2003) and Epi initiation (Allègre et al., 2019), however it is not essential for maintaining the self-renewing capacity of mES cells (Chambers et al., 2007). Therefore, our findings showing no reduction in *Nanog* levels in single cells collected from LY-treated embryos, while PI3K inhibition significantly reduces *Nanog* in mES and hES cells after 24h (Storm et al., 2007; Y. Yang et al., 2019), aren't necessary conflicting results. In fact, Epi/PrE specification occurs in a relatively short window of time (24h) and PI3K-mediated regulation of TFs levels by post-transcriptional modifications could be a rapid and straightforward way to promote cell fate choice. Directly affecting protein stability could provide the required reactivity to allow dynamic developmental processes like ICM specification to happen. In mES cells, NANOG has been shown to be stabilized upon phosphorylation to prevent ubiquitin-dependent degradation by currently unknown mechanisms (Moretto-Zita et al., 2010), but has also been shown to be de-stabilized by inhibition of transactivation upon ERK-dependent phosphorylation (S. H. Kim et al., 2014). From our work, two central questions remain: (1) is the reduction of SOX2 and ESRRb independent of NANOG, and (2) through which downstream factor is PI3K/AKT acting? Regarding (1), we know that SOX2 and ESRRb are restricted to Epi progenitors later than NANOG and we show that they are less affected during short durations (16h and 8h) of PI3K inhibition (Paper Figure S3C-D; data not shown). *In vitro*, NANOG is known to directly bind SOX2 (Gagliardi et al., 2013) and ESRRb (Festuccia et al., 2012) and to interact with post-transcriptional modifiers that allow a rapid response to external cues by phosphorylation and ubiquitination (Gagliardi et al., 2013). However, little is known about the interactome of

NANOG in early embryos. Interestingly, SOX17 activation was not limited to ICM but also occurred in TE cells in LY-treated embryos (Paper Figure 3C) and NANOG was ectopically detected in TE cells of *Gata6* null embryos (Schrode et al., 2014; Paper Figure 6B and S6C). This suggests that if post-transcriptional mechanisms are at work to regulate TF patterning during specification, they are happening globally and are not restricted to the ICM.

Concerning (2), the scope of our study did not allow to ultimately determine through which cascade targets PI3K/AKT is regulating TF patterning during Epi/PrE specification. However, the significant upregulation of NANOG upon CHIR treatment identifies GSK3α/β as a potential candidate and makes further investigation necessary. GSK3α/β is antagonizing canonical WNT signaling through phosphorylation of β-catenin (Rubinfeld et al., 1996). The involvement of GSK3α/β in the regulation of pluripotency has been addressed in mES and hES cells and resulted in somewhat contradictory findings which could be due to differing pluripotent states (naïve and primed). In hES cells, GSK3β activity is crucial to maintain self-renewal as inhibition led to downregulation of *Nanog* and activation of mesoendodermal genes by β-catenin (Singh et al., 2012). In contrast, Storm and colleagues postulated that PI3K/AKT maintains NANOG through inhibition of GSK3α/β in mES cells, as blockage of GSK3α/β activity restored NANOG in the absence of PI3K/AKT activity and the expression of constitutively active forms of GSK3β increased NANOG (Storm et al., 2007). It has been shown that blockage of GSK3 leads to enhanced NANOG levels due to *de novo* protein synthesis and increases the proportion of *Nanog* associated to polyribosomes (Sanchez-Ripoll et al., 2013). Furthermore, the AKT-mediated phosphorylation of GSK3β has been shown to maintain pluripotency in mES cells by preventing degradation of GSK3β target c-MYC (Bechard & Dalton, 2009; Cartwright et al., 2005). Thus, it is possible that NANOG is a direct target of GSK3 or is indirectly regulated by GSK3 downstream signaling. In fact, c-MYC, which is a proto-oncogene TF belonging to the superfamily of basic helix-loop-helix (bHLH) DNA-binding proteins, appears to have an important role in preserving the undifferentiated state of mES cells. Knockout of *c-Myc* does not affect blastocyst development and causes embryonic lethality around E10.0 (Baudino et al., 2002), however this can be attributed to the functional redundancy with the Myc family member N-MYC (Malynn et al., 2000). In 2010, Smith et al. demonstrated that the double knockout (DKO) of *c-Myc* and *N-Myc* results in downregulation of *Nanog* while PrE genes like *Gata6* and *Sox17* are induced in mouse pluripotent stem cells (K. N. Smith et al., 2010). They showed that by binding to the *Gata6* promotor c-MYC actively inhibits *Gata6* expression, thereby preventing the activation of the endodermal program (K. N. Smith et al., 2010). We have shown that SOX17 can be activated in the absence of *Gata6*,

suggesting that the activation of the PrE program isn't entirely dependent on *Gata6* in the embryo. In addition to transcriptional mechanisms, c-MYC sustains pluripotency by regulating microRNA (miRNA) clusters. miRNAs belong to the family of non-coding RNAs which can induce degradation and translational repression of target mRNAs. In mES cells, the c-MYC-dependent *mir-17-92* mRNA cluster has been implicated in cell cycle control keeping the majority of cells in S-phase (K. N. Smith et al., 2010). Interestingly, c-MYC has also been shown to control *miR-141* in mES cells (C. H. Lin et al., 2009) which has been shown to bind and inhibit Sox17 in other contexts (Jia et al., 2012). It will be interesting to see if c-MYC regulates transcription and/or the translation and mRNA stability of *Sox17* in embryos as well. Furthermore, it has been demonstrated that c-MYC recruits polycomb repressive complex 2 (PRC2) to epigenetically silence target genes in mES cells, thereby sustaining pluripotency and propagating its own expression (Fagnocchi et al., 2016). In other contexts, *Sox17* has been reported to act as a canonical WNT antagonist that is silenced through promotor methylation (Fu et al., 2010). However, if *Sox17* could be inhibited in a c-MYC/PRC2-dependent manner to prevent differentiation in early embryos is currently unclear.

Interestingly, when *c-Myc* and *N-Myc* DKO mES cells are cultured under 2i/LIF instead of serum/LIF conditions, cells appear to enter a quiescent state (Scognamiglio et al., 2016). The authors of this study claimed that while transcription, translation and proliferation are arrested in the absence of MYC, the pluripotency of mES cells is maintained (Scognamiglio et al., 2016). They further postulated that culturing E3.75 embryos for 18h with the small-molecule MYC inhibitor 10058-F4 (iMYC) induces embryonic diapause as de novo protein synthesis and proliferation are strikingly reduced (Scognamiglio et al., 2016). Indeed, *c-Myc* and *N-Myc* expression is reduced in diapaused embryos upon mTOR inhibition (Boroviak et al., 2015). However, while NANOG is unchanged in mTOR-inhibited blastocyst (Bulut-Karslioglu et al., 2016), immunofluorescence of MYC-inhibited blastocysts showed no nuclear NANOG despite the authors' claims that NANOG is maintained (Scognamiglio et al., 2016). Thus, to address the potential involvement of GSK3/MYC downstream of PI3K/AKT during Epi/PrE specification, we shall first assess c-MYC expression in LY-treated embryos and further investigate the consequences of iMYC treatment on lineage-specific TF expression. In mES cells, c-MYC has been shown to regulate the transcription of *transcription factor 7 like 1* (*Tcf7l1)* and increased binding of c-MYC to the *Tcf7l1* promotor has been observed under 2i/LIF conditions in mES cells (Morrison et al., 2016). Similar to GSK3α/β, TCF7L1 has shown to be implicated in regulating the balance between self-renewal and differentiation in mES cells by antagonizing WNT signaling. In mES cells, TCF7L1 is a transcriptional repressor of core

pluripotency genes including *Nanog* and *Esrrb* (Martello et al., 2012; Pereira et al., 2006), however this repression is relieved by the presence of GSK3α/β inhibitor CHIR under 2i/LIF conditions (Wray et al., 2011). In fact, *Tcf7l1* knockout phenocopies GSK3α/β inhibiton, upregualtes *Nanog* and delays differentiation in mES cells (Pereira et al., 2006; Wray et al., 2011). Thus, it will be a crucial hypothesis to test if c-MYC maintains NANOG by inhibiting *Tcf7l1* in early embryos as well.

3. What is acting upstream of PI3K/AKT during specification?

In this work, we have not addressed the mechanisms regulating TF patterning in early embryos upstream of PI3K/AKT. The PI3K/AKT cascade has been shown to be activated by an abundance of signals like ligand-receptor interactions, by crosstalks with other signaling pathways and by mechanotransduction. It is not only challenging to select candidate inputs and chose an adequate approach to experimentally test these, it is also difficult to draw definite conclusions as PI3K/AKT signaling responses are often unselective. In the introduction of this thesis I discussed the main hypotheses of the field explaining the emergence of heterogeneity in the ICM between the 16- and 32-cell stage which will ultimately trigger the formation of Epi and PrE progenitors. With the identification of PI3K/AKT as an essential requirement for NANOG during the period of Epi specification, new hypotheses arise. I was particularly intrigued by findings published by Boroviak et al. when they demonstrated that single ICM cells isolated from E3.25-E3.5 embryos rarely gave rise to ES cell colonies (Boroviak et al., 2014). They concluded that Epi specification is a premise for ES cell derivation and speculated that cell-to-cell or cell-to-extracellular matrix interactions might be required to acquire Epi identity in the ICM of embryos. By analyzing the RNAseq data of two independent ICM of E3.5 embryos, they discovered that while collagen and integrins are hardly expressed, fibronectin and laminins showed elevated expression levels. They consequently fabricated substrates containing fibronectin and Lam511 which is an isoform of laminin consisting of Lama5, Lamb1 and Lamc1. It was previously reported that Lam511 in combination with serum is sufficient to derive and maintain mES cells (Domogatskaya et al., 2008). Plating single cell of E3.5 embryos on these substrates significantly increased the efficacy of colony formation to 10%. Interestingly, immunofluorescence showed that LAMA5 was specifically enriched between inner cells with high OCT4, which could indicate the formation of an Epi-supporting niche. Both *Lamb1* and *Lamc1* null embryos fail to form basement membranes, show defects in Epi/PrE segregation and die shortly after implantation (Miner et al., 2004; Smyth et al.,

1999). Laminins interact with two sorts of cellular receptors such as dystroglycan and integrins. Homozygous deletion of dystroglycan (*Dag1*) results in embryonic lethality at E6.5 and while Epi/PrE specification and sorting proceeds normally, formation of extra-embryonic basement membranes is defective (Williamson et al., 1997). In turn, embryos deficient for *Rpsa* which encodes the integrin family member Laminin Receptor 1 (LamR1) fail to develop beyond the E3.5 stage (Han, 2008). In other contexts, laminin has been shown to act upstream of PI3K: in mammary gland culture activation of PI3K by laminin is essential for correct patterning of lineage-specific genes (R. Xu et al., 2010) and in rat embryonic stem cells laminin directs PI3K-dependent differentiation into cardiomyocytes (Wang et al., 2019).

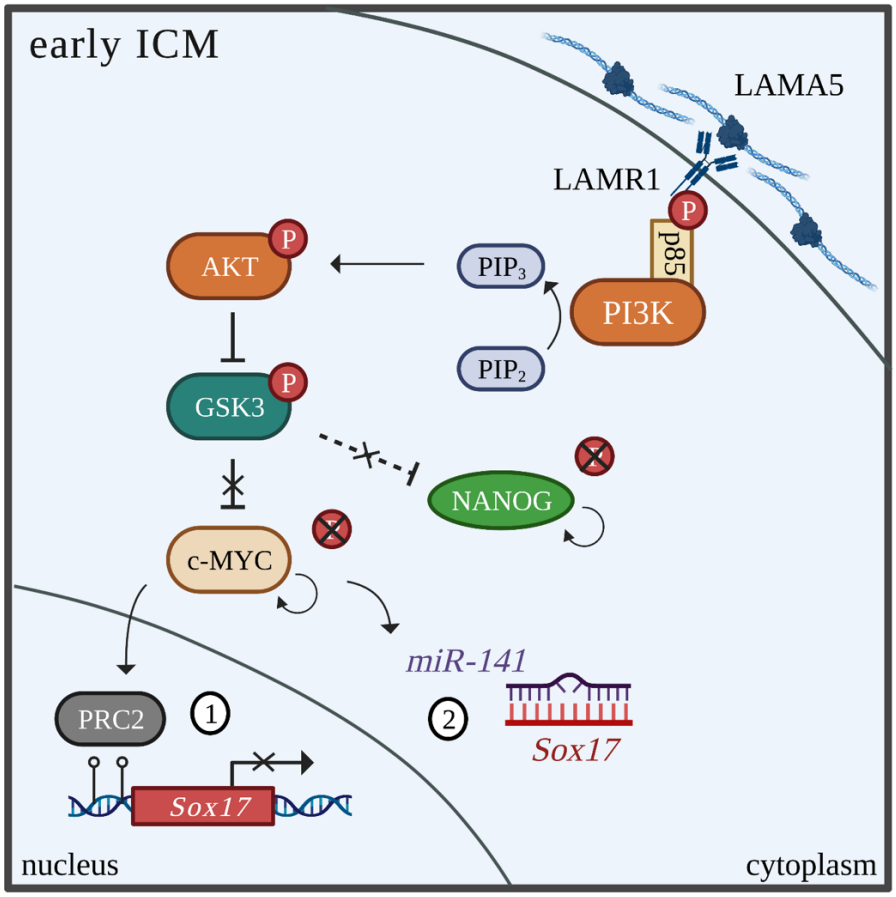

Figure 23: **The laminin/PI3K/AKT/GSK3 axis may control early ICM identity.** Activation of laminin signaling through receptor-ligand interaction of LAMR1 and LAMA5 could stimulate PI3K/AKT activity and facilitate inhibition of GSK3 by AKT-mediated phosphorylation. Blockage of GSK3 activity could prevent NANOG phosphorylation and allow NANOG stabilization and transactivation, however this interaction has not been reported in the literature yet. GSK3 inactivation would release c-MYC from GSK3-dependent inhibition and could prevent SOX17 expression through two mechanisms. (1) c-MYC could recruit PRC2 to transcriptionally silence Sox17 by promoter methylation. (2) Through a post-transcriptional mechanism, c-MYC could indirectly prevent translation or induce degradation of Sox17 mRNA through one or multiple miRNAs.

Several antibodies and small molecule inhibitors that affect laminin-integrin binding have been developed, however it is unclear if these could be effective in a compacted and hardly accessible population of cells like the ICM of the early embryo. Rather, it would be interesting to further characterize the knockout embryos of *Lamb1*, *Lamc1* and *Rpsa* and to assess PI3K/AKT activity by pRPS6 staining as well as measuring NANOG levels. If laminin signaling is indeed acting upstream of PI3K/AKT, we would expect to see a reduction of NANOG and absence of pRPS6 in these mutants and we could try to rescue signaling activity by adding PI3K/AKT-activating molecules like insulin or IGF-1 to the culture. In Figure 23 I illustrated a potential cascade of PI3K/AKT with a selection of discussed up- and downstream mechanisms that could be at work in embryos to secure the state of the early ICM.

4. Capture of signaling dynamics to define role of PI3K/AKT in ICM fate decision

We had several objectives that motivated us to develop an Akt-KTR mouse reporter line which would allow to quantitatively assess PI3K/AKT activity in-real time during preimplantation development. First, we wanted to investigate if PI3K/AKT could be a mediator of early TF heterogeneity which ultimately initiates ICM specification. Allègre and colleagues observed heterogeneous expression of a set of TFs including NANOG which arises between the 16- and 32-cell stage (Allègre et al., 2019) and the underlying mechanisms are currently unclear. Using pRPS6, we detected an increase and variations of PI3K/AKT activities at the mid blastocyst stage, thus after ICM specification is initiated. However, this was a static assessment of PI3K/AKT activity and it is plausible that transient signaling fluctuation occur earlier which are not captured by pRPS6 staining. Thus, it would be interesting to perform live imaging of Akt-KTR embryos starting before early TF heterogeneity is detected (E2.75) until most Epi/PrE progenitors are specified (E3.75) which due to *ex vivo* culture may take up to 2 days. Through cell tracking we could calculate a proxy for PI3K/AKT activity in individual ICM cells over time and by performing immunofluorescence of Epi- and PrE-specific markers after imaging we could retrospectively determine which fate each tracked cell acquired. Ideally, we would combine Akt-KTR with a lineage-specific reporter, however currently available mouse reporter lines for Epi (*Esrrb*$^{Tm(dTomato)}$*;* produced in the lab) or PrE (*Pdgfra*$^{H2B\text{-}GFP}$; Plusa et al., 2008) lineages cannot account for early ICM specification. Regardless, this experiment could provide valuable information and tell us (1) if and when PI3K/AKT signaling variations occur and (2) if a certain activity signature is correlated with the ultimate fate of cells. These results are necessary to further define the role of PI3K/AKT as stable PI3K/AKT levels with

moderate fluctuations would indicate that PI3K/AKT is fine-tuning cell fate choice by balancing TF levels. Instead, if PI3K/AKT displays strong heterogeneities this rather suggests an instructive role and could prove that an on to off mechanism is necessary to allow the activation of PrE program. In HeLa cells, Akt-KTR exhibited significant fluctuations in a cell-cycle dependent manner at baseline levels (Maryu et al., 2016) and similar observations were made in early ERK-KTR embryos (Pokrass et al., 2020). When we qualitatively analyzed the live imaging of our Akt-KTR ES cells and our Akt-KTR embryos which were filmed for 72h after injection at the zygote stage, we did not observe frequent events of reporter shuttling. This served as a first indication that PI3K/AKT activity may not underlie cell-cycle dependent oscillations in pluripotent stem cells and early embryos. Furthermore, analysis of HeLa cells simultaneously expressing Akt-KTR and ERK-KTR showed that AKT and ERK signaling were acting highly coordinated (Maryu et al., 2016). Both Akt-KTR and ERK-KTR were stimulated by epidermal growth factor (EGF) and inhibition of ERK signaling by PD03 treatment led to a temporal increase of AKT activity while Rapamycin treatment slightly enhanced cytoplasmic ERK-KTR accumulation (Maryu et al., 2016). Although our data showed that regulation of TFs by PI3K/AKT occurred independently of ERK activity in early embryos, it would be interesting to express Akt-KTR and ERK-KTR at the same time in embryos to compare the signaling dynamics of both pathways.

5. Temporally limited requirement of PI3K/AKT for cell fate choice

The deficiency of many PI3K/AKT pathway members results in embryonic lethality of mice, highlighting the significance of PI3K/AKT for embryonic development. Meanwhile, the investigation of signaling disruption by genetic approaches is constrained by the abundance of PI3K/AKT isoforms and prevents the assessment of functions which might be restricted in time. We and others therefore often use pharmacological signaling modulators. Previous studies have provided evidence that PI3K/AKT fulfills distinct roles during preimplantation development which are connected to specific periods of development. A study by Chi and colleagues revealed that glucose-dependent activation of mTOR is required for the morula-to-blastocyst transition in early embryos and the initiation of TE specification (Chi et al., 2020). mTOR is a canonical downstream target of PI3K/AKT but has been associated to other inputs as well. Deprivation of glucose or mTOR inhibition blocked embryonic development at the 8-cell stage and prevented the activation of TE-specific TFs like CDX2, nuclear YAP1 and TEAD4, while the ICM markers NANOG and OCT4 were unaffected. They demonstrated that by promoting

the translation of TE-specific TFAP2C, mTOR facilitated the heterodimer formation of TFAP2C, YAP1 and TEAD4 which in turn initiated TE program by activating CDX2 (Chi et al., 2020). Interestingly, we observed high levels of pRPS6 in outer cells of E2.75 to E4.0 embryos, indicating elevated PI3K/AKT activity in TE (Paper Figure 1A and S1A). However, the inhibition of PI3K/AKT by LY during the second cell fate decision did not affect the morphology or number of TE cells and did not reduce TE-specific CDX2 and GATA3 (Figure S3K). We therefore conclude that while mTOR might be an essential driver of TE initiation, it is likely not involved in TE maintenance.

Laying our focus on ICM-specific markers, we determined that while PI3K/AKT is dispensable for NANOG initiation, it displays a unique requirement during the early phase of Epi/PrE specification as LY treatment starting at E3.25 had no effect on NANOG (Paper Figure 2B and S2B). Our observations suggest that by sustaining NANOG and SOX2, PI3K/AKT functions as a guardian of early ICM identity while simultaneously preventing the activation of endodermal SOX17. We and others have previously established that Epi progenitors rapidly lose their plasticity (Sylvain Bessonnard et al., 2017; Grabarek et al., 2012; Saiz et al., 2016; Xenopoulos et al., 2015) and become unresponsive to FGF/ERK signaling modulation (Sylvain Bessonnard et al., 2017). Thus, PI3K/AKT appears to be a premise for Epi formation but not the maintenance of Epi identity until specification is terminated. After a window of insensitivity of TFs to PI3K/AKT inhibition during the late phase of Epi/PrE specification (E3.25 to E3.75), PI3K/AKT activity fulfills a new role by promoting Epi/PrE survival through mTOR (Sylvain Bessonnard et al., 2019). PI3K/AKT/mTOR-dependent PrE maintenance is mediated by PDGF and while *Pgdfra* null embryos form SOX17/GATA4-expressing PrE progenitors, they are significantly reduced in number (Artus et al., 2010, 2013). It is possible that activation of PI3K/AKT by PDGF signaling is limited to the developmental period after Epi/PrE specification when committed Epi and PrE undergo sorting. However, in the case that PDGF is also acting upstream of PI3K/AKT during Epi/PrE specification, the inhibition of SOX17 by PI3K/AKT in early PrE cells might be compensated by GATA6 and/or ERK signaling.

While we see continuous PI3K/AKT activity in all preimplantation stages, PI3K/AKT has distinct functions during defined time windows of development ranging from TE and Epi initiation to PrE lineage survival. Further studies will be required to define which in- and output factors of the PI3K/AKT cascade are at play during different phases of early embryo growth.

6. Future tracks to validate the LY-induced phenotype

The treatment of early embryos with LY during different phases of preimplantation development disclosed the temporally limited requirement of PI3K/AKT activity for NANOG. I was not able to confirm the LY-induced phenotype neither with the selection of alternative PI3K pathway inhibitors nor with the genetic tool I chose to block PI3K signaling. None of the concentrations of inhibitors I used resulted in a significant reduction of NANOG. Considering the absence of a reliable pathway readout after treatment with PI-103, TGX and HS, it is possible that the conditions of my experiments were not adequate to inhibit PI3K/AKT. In the case of Wortmannin, I found that the concentration I applied had no effect on pRPS6 which could explain that no reduction of NANOG was observed. In order to allow a correct interpretation of the existing data, it will be crucial to repeat the experiments including a quantitative assessment of NANOG and pRPS6 levels. It will also be crucial to assess pRPS6 levels when embryos are treated with lower concentrations of LY (<10µM) to verify that the reduction of NANOG is in fact correlated to effective PI3K/AKT blockage. Furthermore, I have to reassess if the doses of XAV I was using effectively activate GSK3 in early embryos. One possibility to do so would be to evaluate the levels of phosphorylated GSK3 and phosphorylated c-MYC upon XAV treatment by immunofluorescence.

The dominant negative isoform p85Δ has been shown to be an effective genetic tool to inhibit PI3K/AKT signaling in mES cells (Kaliman et al., 2007; Storm et al., 2007) which could be confirmed by this work. Despite being a promising candidate for PI3K/AKT inhibition *in vivo,* the injection of p85Δ RNA did not visibly alter pRPS6 levels or induce a reduction of NANOG in early embryos. However, the fact that I had trouble detecting mbGFP after 48h which was co-injected with p85Δ and is known to be a stably expressed protein, indicated that technical issues could have prevented p85Δ function. The quantity of mRNA that can be produced with the applied *in vitro* transcription protocol was limited, thus making it difficult to study the effect of higher p85Δ dosages. Meanwhile, the concentration of RNA also enriches contaminants which are introduced in the sample through *in vitro* transcription and often have toxic effects on embryonic development. Generally, the number of analyzed cells was too low to draw definite conclusions and we are currently trying to improve microinjection at the 8-cell stage into multiple blastomeres. This will shorten the necessary culture time, decrease the probability of protein degradation and increase the number of cells for analysis. In the p85Δ construct, the p110α binding site is replaced by FLAG-tag and does not encode a fluorescent protein. I was not able to detect FLAG-tag expression by immunofluorescence in p85Δ-

transfected ES cells (data not shown) and it was therefore not possible to verify p85Δ expression after embryo injection. In order to verify expression after p85Δ RNA injection in future experiments, it would be important to introduce an alternative fluorescent tag or sequence of a fluorescent protein into the p85Δ plasmid before repeating the *in vitro* transcription of the construct.

In conclusion, with my work I could demonstrate that PI3K/AKT, a conserved pathway frequently associated with cellular processes like proliferation, survival and metabolism, governs a central role in the regulation of early lineage formation in the mouse embryo. The discovery that PI3K/AKT regulates TF levels during a unique time window of early embryogenesis demonstrates that PI3K/AKT is an important mediator of the mammalian regulative development. It has been established that PI3K/AKT signaling is involved in the maintenance of pluripotency in embryonic stem cells, however my results provide evidence that in the embryo different regulatory mechanisms are at work to facilitate dynamic cell fate decisions. Further investigation is required to decipher the mechanistic details of PI3K/AKT function, however this thesis paved the way to a more complete understanding of how different signaling inputs act in synergy with TF networks to constitute a blastocyst competent for implantation and successful postimplantation development.

Annexes

I. Complementary Material and Methods

ES cell culture

ES cell lines were cultured under feeder-free serum/LIF or 2i/LIF conditions at 37°C, 8% CO_2. Serum/LIF medium was constituted using DMEM GlutaMax (Gibco) supplemented with 10% fetal calf serum (Sigma), 2-mercaptoethanol (Gibco) and 10ng/µl LIF (MILTENYI BIOTECH). 2i/LIF medium was constituted using N2B27 base which contains DMEM/F-12 (Life Technologies), Neurobasal (Life Technologies), N2 (Life Technologies), insulin-free B27 (Life technologies), L-Glutamin (Life Technologies), BSA (Sigma) and 2-mercaptoethanol (Gibco). N2B27 was subsequently supplemented with 10ng/µl LIF (MILTENYI BIOTECH), PD03 (Axon) and CHIR (Axon). ES cells were maintained on plastic dishes (TPP) coated with gelatin (Sigma) and transferred to glass lamella coated with Geltrex (Thermo Fisher) to facilitate imaging. Prior to confocal microscopy, ES cells on glass lamella were washed with PBS, fixed with 4% PFA solution for 20 minutes at RT and mounted on microscope slides (Thermo Fisher) using Vectashield (Vector Laboratories).

Akt-KTR ES and mouse line generation

The plasmid pHGEA (pCAG-H2B-iRFP-720_mCherry-hGeminin_Erk-KTR-hmKO_Akt-Foxo3a-KTR-EGFP) (Maryu et al., 2016) as well as the plasmid H2B-iRFP-670 were used as a template to clone the construct H2B-iRFP-670_Akt-Foxo3a-KTR-EGFP. The resulting CAG-H2B-iRFP-670_Akt-Foxo3a-KTR-EGFP plasmid (Akt-KTR) together with hyPBase were then transfected into E14Tg2a using Lipofectamine 2000 (Thermo Fisher Scientific) and positive clones were selected by fluorescent activated cell sorting (FACS) after three days according to their level of EGFP expression. Several clones were expanded and clone 11 was chosen for the experiments displayed in this work due to high expression iRFP/GFP level, low rate of cell death and medium growth rate.

To express Akt-KTR *in vivo*, embryos from crossing super ovulated (C57BL/6xSJL/J) F1 females with CD1 were injected with Akt-KTR and hyPBase at the zygote stage and fixed after 48h or 72h. Superovulation was performed by intra-peritoneal injection of pregnant mare serum

gonadotropin (PMSG, Centravet) and human chorionic gonadotropin (HCG, Centravet). For transient Akt-KTR expression, embryos from crossing super ovulated (C57BL/6xSJL/J) F1 females with CD1 were injected with Akt-KTR RNA (description below) at 4 to 8-cell stage and cultured for 48h before fixation.

To establish a stable mouse Akt-KTR line, zygotes were derived by crossing three-week-old (C57BL/6xSJL/J) F1 female mice (Janvier Laboratories) with CD1 males (Charles River Laboratories). Zygotes were injected with Akt-KTR (10ng/µl) and hyPBase (200/100/20/10ng/µl) and subsequently transferred into pseudo-pregnant females. Transgenic F0 males which tested positive for iRPF by PCR were mated with CD1 females to generate Akt-KTR embryos.

ES plasmid transfection

E14Tg2a and Akt-KTR ES cells were used for transfection experiments. The insert of the p85 Δ plasmid was cloned into the pCAGG plasmid using EcoRI restriction enzyme sites. In line with manufacturer instructions, 2µg of plasmid DNA (Table 5) was used to transfect ES cells with Lipofectamine 2000 (Thermo Fisher Scientific) and cells were fixed after 24h.

Table 5. List of plasmids used in this study.

Plasmid name	Abbreviation	Source	Size (bp)
pHGEA	ERK-AKT-KTR	Gift from Kazuhiro Aoki	12223
pCAGG	pCAGG	in house	4721
pBSSK p85 alpha (delta iSH2)	p85Δ	Addgene #13432	3000
pAdx-CMV-tdTomato	tdTomato	Addgene #73347	3492
977 pSG5L HA PTEN A4	PTEN-A4	Addgene #10753	4100
800 pSG5L HA PTEN WT	PTEN-WT	Addgene #10750	4100
GFPmb	GFPmb	in house	
pCMV-hyPBase	hyPBase	Gift from Jean Livet	
pU6-mCherry	mCherry	Addgene #64324	9276

RNA generation and microinjection

Plasmids (Table 6) were used as a template for *in vitro* transcription using MEGAshortscript T7 Transcription & mMESSAGE mMACHINE T7 Ultra Kits (Thermo Fisher Scientific). The used primers are listed in Table x. mRNAs were purified using LiCl/ethanol precipitation and resuspended in Brinster's Buffer (10 mM Tris-HCl pH 7.5; 0.25 mM EDTA). For injections,

embryos were transferred to a depression slide in EmbryoMax M2 medium (Millipore) covered with embryo-tested mineral oil (Sigma). Microinjections were performed by Sandrine Vandormael-Pournin using an Olympus IMT-2 inverted microscope equipped with a Leitz micromanipulator. For p85Δ expression, mRNA of p85Δ and GFPmb were mixed in a ratio of 875ng/µl+1225ng/µl or 875ng/µl+800ng/µl and injected into single blastomeres of 8-cell stage embryos. Embryos were cultured for 24h in KSOM+AA before fixation.

Table 6. Primers used for *in vitro* transcription.

Gene	Primer sequence
T7-GFPmb-F	5'-GTAATACGACTCACTATAGGGACCATGGTGAGCAAGGGCGAG-3'
T7-GFPmb-R	5'-CGGGGCCACTCTCATCAGGAGAGC-3'
T7-p85Δ-F	5'-GTAATACGACTCACTATAGGGAGAATGAGT-3'
T7-p85Δ-R	5'-AGGTCGACTAACTACTTATCG-3'
T7-Akt-Foxo3-KTR-F	5'-GTAATACGACTCACTATAGGGATGGCAGAGGCACCGGCTTCC-3'
T7-Akt-Foxo3-KTR-R	5'-TTAACAATTGTTACCGCGGCCCGT-3'
T7-hyPBase-F	5'-GTAATACGACTCACTATAGGGATGGGCAGC-3'
T7-hyPBase-R	5'-CAGAAACAGCTCTGGCACATGTCG-3'

References

Aksoy, I., Jauch, R., Chen, J., Dyla, M., Divakar, U., Bogu, G. K., Teo, R., Leng Ng, C. K., Herath, W., Lili, S., Hutchins, A. P., Robson, P., Kolatkar, P. R., & Stanton, L. W. (2013). Oct4 switches partnering from Sox2 to Sox17 to reinterpret the enhancer code and specify endoderm. *EMBO Journal*, *32*(7), 938–953. https://doi.org/10.1038/emboj.2013.31

Alessi, D. R., Andjelkovic, M., Caudwell, B., Cron, P., Morrice, N., Cohen, P., & Hemmings, B. A. (1996). Mechanism of activation of protein kinase B by insulin and IGF-1. *EMBO Journal*, *15*(23), 6541–6551. https://doi.org/10.1002/j.1460-2075.1996.tb01045.x

Allègre, N., Chauveau, S., Dennis, C., Renaud, Y., Estrella, L. V., Pouchin, P., Cohen-Tannoudji, M., & Chazaud, C. (2019). A Nanog-dependent gene cluster initiates the specification of the pluripotent epiblast. *BioRxiv*. https://doi.org/10.1101/707679

Alva, J. A., Lee, G. E., Escobar, E. E., & Pyle, A. D. (2011). Phosphatase and tensin homolog regulates the pluripotent state and lineage fate choice in human embryonic stem cells. *Stem Cells*, *29*(12), 1952–1962. https://doi.org/10.1002/stem.748

Anderson, K. G. V., Hamilton, W. B., Roske, F. V., Azad, A., Knudsen, T. E., Canham, M. A., Forrester, L. M., & Brickman, J. M. (2017). Insulin fine-tunes self-renewal pathways governing naive pluripotency and extra-embryonic endoderm. *Nature Cell Biology*, *19*(10), 1164–1177. https://doi.org/10.1038/ncb3617

Artus, J., Douvaras, P., Piliszek, A., Isern, J., Baron, M. H., & Hadjantonakis, A. K. (2012). BMP4 signaling directs primitive endoderm-derived XEN cells to an extraembryonic visceral endoderm identity. *Developmental Biology*, *361*(2), 245–262. https://doi.org/10.1016/j.ydbio.2011.10.015

Artus, J., Kang, M., Cohen-Tannoudji, M., & Hadjantonakis, A. K. (2013). PDGF signaling is required for primitive endoderm cell survival in the inner cell mass of the mouse blastocyst. *Stem Cells*, *31*(9), 1932–1941. https://doi.org/10.1002/stem.1442

Artus, J., Panthier, J. J., & Hadjantonakis, A. K. (2010). A role for PDGF signaling in expansion of the extra-embryonic endoderm lineage of the mouse blastocyst. *Development*, *137*(20), 3361–3372. https://doi.org/10.1242/dev.050864

Artus, J., Piliszek, A., & Hadjantonakis, A. K. (2011). The primitive endoderm lineage of the mouse blastocyst: Sequential transcription factor activation and regulation of differentiation by Sox17. *Developmental Biology*, *350*(2), 393–404. https://doi.org/10.1016/J.YDBIO.2010.12.007

Azami, T., Cécilia Bassalert, C., Allè Gre, N., Valverde Estrella, L., Pouchin, P., Ema, M., & Chazaud, C. (2019). *Regulation of the ERK signalling pathway in the developing mouse blastocyst*. https://doi.org/10.1242/dev.177139

Baudino, T. A., McKay, C., Pendeville-Samain, H., Nilsson, J. A., Maclean, K. H., White, E. L., Davis, A. C., Ihle, J. N., & Cleveland, J. L. (2002). c-Myc is essential for vasculogenesis and angiogenesis during development and tumor progression. *Genes and Development*, *16*(19), 2530–2543. https://doi.org/10.1101/gad.1024602

Bechard, M., & Dalton, S. (2009). Subcellular Localization of Glycogen Synthase Kinase 3β Controls Embryonic Stem Cell Self-Renewal. *Molecular and Cellular Biology*, *29*(8), 2092–2104. https://doi.org/10.1128/mcb.01405-08

Benchetrit, H., Herman, S., Van Wietmarschen, N., Wu, T., Makedonski, K., Maoz, N., Yom Tov, N., Stave, D., Lasry, R., Zayat, V., Xiao, A., Lansdorp, P. M., Sebban, S., & Buganim, Y. (2015). Extensive Nuclear Reprogramming Underlies Lineage Conversion into Functional Trophoblast Stem-like Cells. *Cell Stem Cell*, *17*(5), 543–556. https://doi.org/10.1016/j.stem.2015.08.006

Bendall, S. C., Stewart, M. H., Menendez, P., George, D., Vijayaragavan, K., Werbowetski-Ogilvie, T., Ramos-Mejia, V., Rouleau, A., Yang, J., Bossé, M., Lajoie, G., & Bhatia, M. (2007). IGF and FGF cooperatively establish the regulatory stem cell niche of pluripotent human cells in vitro. *Nature*, *448*(7157), 1015–1021. https://doi.org/10.1038/nature06027

Bessonnard, S, De Mot, L., Gonze, D., Barriol, M., Dennis, C., Goldbeter, A., Dupont, G., & Chazaud, C. (2014). Gata6, Nanog and Erk signaling control cell fate in the inner cell mass through a tristable regulatory network. *Development*, *141*(19), 3637–3648. https://doi.org/10.1242/dev.109678

Bessonnard, Sylvain, Coqueran, S., Vandormael-pournin, S., Dufour, A., Artus, J., & Cohen-tannoudji, M. (2017). *ICM conversion to epiblast by FGF / ERK inhibition is limited in time and requires transcription and protein degradation*. *September*, 1–12. https://doi.org/10.1038/s41598-017-12120-0

Bessonnard, Sylvain, De Mot, L., Gonze, D., Barriol, M., Dennis, C., Goldbeter, A., Ve Dupont, G., & Chazaud, C. (2014). *Gata6, Nanog and Erk signaling control cell fate in the inner cell mass through a tristable regulatory network*. https://doi.org/10.1242/dev.109678

Bessonnard, Sylvain, Vandormael-Pournin, S., Coqueran, S., Cohen-Tannoudji, M., & Artus, J. (n.d.). *PDGF Signaling in Primitive Endoderm Cell Survival Is Mediated by PI3K-mTOR Through p53-Independent Mechanism*. https://doi.org/10.1002/stem.3008

Bessonnard, Sylvain, Vandormael-Pournin, S., Coqueran, S., Cohen-Tannoudji, M., & Artus, J. (2019). PDGF Signaling in Primitive Endoderm Cell Survival Is Mediated by PI3K-mTOR Through p53-Independent Mechanism. *Stem Cells*, *37*(7), 888–898. https://doi.org/10.1002/stem.3008

Bi, L., Okabe, I., Bernard, D. J., & Nussbaum, R. L. (2002). Early embryonic lethality in mice deficient in the p110β catalytic subunit of PI 3-kinase. *Mammalian Genome*, *13*(3), 169–172. https://doi.org/10.1007/s00335-001-2123-x

Bi, L., Okabe, I., Bernard, D. J., Wynshaw-Boris, A., & Nussbaum, R. L. (1999). Proliferative defect and embryonic lethality in mice homozygous for a deletion in the p110α subunit of phosphoinositide 3-kinase. *Journal of Biological Chemistry*, *274*(16), 10963–10968. https://doi.org/10.1074/jbc.274.16.10963

Borensztein Maudand Syx, L. and S. N. and H. E. (2018). Transcriptome Profiling of Single Mouse Oocytes. In M.-E. Verlhac Marie-Hélèneand Terret (Ed.), *Mouse Oocyte Development: Methods and Protocols* (pp. 51–65). Springer New York. https://doi.org/10.1007/978-1-4939-8603-3_7

Boroviak, T., Loos, R., Bertone, P., Smith, A., & Nichols, J. (2014). The ability of inner-cell-mass cells to self-renew as embryonic stem cells is acquired following epiblast specification. *Nature Cell Biology*, *16*(6), 513–525. https://doi.org/10.1038/ncb2965

Boroviak, T., Loos, R., Lombard, P., Nichols, J., Smith, A., Bertone, P., Boroviak, T., Loos, R., Lombard, P., & Okahara, J. (2015). Lineage-Specific Profiling Delineates the Emergence and Progression of Naive Pluripotency in Mammalian Embryogenesis. *Developmental Cell*, *35*(3), 366–382. https://doi.org/10.1016/j.devcel.2015.10.011

Boroviak, T., Stirparo, G. G., Dietmann, S., Hernando-Herraez, I., Mohammed, H., Reik, W., Smith, A., Sasaki, E., Nichols, J., & Bertone, P. (2018). Single cell transcriptome analysis of human, marmoset and mouse embryos reveals common and divergent features of preimplantation development. *Development (Cambridge)*, *145*(21). https://doi.org/10.1242/dev.167833

Brons, I. G. M., Smithers, L. E., Trotter, M. W. B., Rugg-Gunn, P., Sun, B., Chuva De Sousa Lopes, S. M., Howlett, S. K., Clarkson, A., Ahrlund-Richter, L., Pedersen, R. A., & Vallier, L. (2007). Derivation of pluripotent epiblast stem cells from mammalian embryos. *Nature*, *448*(7150), 191–195. https://doi.org/10.1038/nature05950

Brown, E. J., Albers, M. W., Bum Shin, T., Ichikawa, K., Keith, C. T., Lane, W. S., & Schreiber, S. L. (1994). A mammalian protein targeted by G1-arresting rapamycin-receptor complex. *Nature*, *369*(6483), 756–758. https://doi.org/10.1038/369756a0

Brunet, A., Bonni, A., Zigmond, M. J., Lin, M. Z., Juo, P., Hu, L. S., Anderson, M. J., Arden, K. C., Blenis, J., & Greenberg, M. E. (1999). Akt Promotes Cell Survival by Phosphorylating and Inhibiting a Forkhead Transcription Factor. *Cell*, *96*(6), 857–868. https://doi.org/10.1016/S0092-8674(00)80595-4

Brunn, G. J., Williams, J., Sabers, C., Wiederrecht, G., Lawrence, J. C., & Abraham, R. T. (1996). Direct inhibition of the signaling functions of the mammalian target of rapamycin by the phosphoinositide 3-kinase inhibitors, wortmannin and LY294002. *EMBO Journal*, *15*(19), 5256–5267. https://doi.org/10.1002/j.1460-2075.1996.tb00911.x

Buehr, M., Meek, S., Blair, K., Yang, J., Ure, J., Silva, J., McLay, R., Hall, J., Ying, Q. L., & Smith, A. (2008). Capture of Authentic Embryonic Stem Cells from Rat Blastocysts. *Cell*, *135*(7), 1287–1298. https://doi.org/10.1016/j.cell.2008.12.007

Bulut-Karslioglu, A., Biechele, S., Jin, H., Macrae, T. A., Hejna, M., Gertsenstein, M., Song, J. S., & Ramalho-Santos, M. (2016). Inhibition of mTOR induces a paused pluripotent state. *Nature*, *540*(7631), 119–123. https://doi.org/10.1038/nature20578

Burdon, T., Stracey, C., Chambers, I., Nichols, J., & Smith, A. (1999). Suppression of SHP-2 and ERK Signalling Promotes Self-Renewal of Mouse Embryonic Stem Cells. *Developmental Biology*, *210*(1), 30–43. https://doi.org/10.1006/DBIO.1999.9265

Campbell, J. M., Nottle, M. B., Vassiliev, I., Mitchell, M., & Lane, M. (2012). Insulin increases epiblast cell number of in vitro cultured mouse embryos via the PI3K/GSK3/p53 pathway. *Stem Cells and Development*, *21*(13), 2430–2441. https://doi.org/10.1089/scd.2011.0598

Camus, A., Perea-Gomez, A., Moreau, A., & Collignon, J. (2006). Absence of Nodal signaling promotes precocious neural differentiation in the mouse embryo. *Developmental Biology*,

295(2), 743–755. https://doi.org/10.1016/J.YDBIO.2006.03.047

Carpenter, C. L., Duckworth, B. C., Auger, K. R., Cohen, B., Schaffhausen, B. S., & Cantley, L. C. (1990). Purification and characterization of phosphoinositide 3-kinase from rat liver. *Journal of Biological Chemistry*, *265*(32), 19704–19711. https://doi.org/10.1016/S0021-9258(17)45429-9

Cartwright, P., McLean, C., Sheppard, A., Rivett, D., Jones, K., & Dalton, S. (2005). LIF/STAT3 controls ES cell self-renewal and pluripotency by a Myc-dependent mechanism. *Development*, *132*(5), 885–896. https://doi.org/10.1242/dev.01670

Chambers, I., Silva, J., Colby, D., Nichols, J., Nijmeijer, B., Robertson, M., Vrana, J., Jones, K., Grotewold, L., & Smith, A. (2007). Nanog safeguards pluripotency and mediates germline development. *Nature*, *450*(7173), 1230–1234. https://doi.org/10.1038/nature06403

Chaussade, C., Rewcastle, G. W., Kendall, J. D., Denny, W. A., Cho, K., Grønning, L. M., Chong, M. L., Anagnostou, S. H., Jackson, S. P., Daniele, N., & Shepherd, P. R. (2007). Evidence for functional redundancy of class IA PI3K isoforms in insulin signalling. *Biochemical Journal*, *404*(3), 449–458. https://doi.org/10.1042/BJ20070003

Chazaud, C., Yamanaka, Y., Pawson, T., & Rossant, J. (2006). Early Lineage Segregation between Epiblast and Primitive Endoderm in Mouse Blastocysts through the Grb2-MAPK Pathway. *Developmental Cell*, *10*(5), 615–624. https://doi.org/10.1016/j.devcel.2006.02.020

Chi, F., Sharpley, M. S., Nagaraj, R., Roy, S. Sen, & Banerjee, U. (2020). Glycolysis-Independent Glucose Metabolism Distinguishes TE from ICM Fate during Mammalian Embryogenesis. *Developmental Cell*, *53*(1), 9-26.e4. https://doi.org/10.1016/j.devcel.2020.02.015

Chisholm, J. C., & Houliston, E. (1987). Cytokeratin filament assembly in the preimplantation mouse embryo. In *Development* (Vol. 101).

Cho, L. T. Y., Wamaitha, S. E., Tsai, I. J., Artus, J., Sherwood, R. I., Pedersen, R. A., Hadjantonakis, A. K., & Niakan, K. K. (2012). Conversion from mouse embryonic to extra-embryonic endoderm stem cells reveals distinct differentiation capacities of pluripotent stem cell states. *Development (Cambridge)*, *139*(16), 2866–2877. https://doi.org/10.1242/dev.078519

Cliff, T. S., Wu, T., Boward, B. R., Yin, A., Yin, H., Glushka, J. N., Prestegaard, J. H., & Dalton, S. (2017). MYC Controls Human Pluripotent Stem Cell Fate Decisions through Regulation of Metabolic Flux. *Cell Stem Cell*, *21*(4), 502-516.e9. https://doi.org/10.1016/J.STEM.2017.08.018

Cross, D. A. E., Alessi, D. R., Cohen, P., Andjelkovic, M., & Hemmings, B. A. (1995). Inhibition of glycogen synthase kinase-3 by insulin mediated by protein kinase B. *Nature*, *378*, 785–789. https://doi.org/10.1038/378785a0

Davenport, T. G., Jerome-Majewska, L. A., & Papaioannou, V. E. (2003). Mammary gland, limb and yolk sac defects in mice lacking Tbx3, the gene mutated in human ulnar mammary syndrome. In *Development* (Vol. 130, Issue 10, pp. 2263–2273).

https://doi.org/10.1242/dev.00431

De la Cova, C., Townley, R., Regot, S., & Greenwald, I. (2017). Technology A Real-Time Biosensor for ERK Activity Reveals Technology A Real-Time Biosensor for ERK Activity Reveals Signaling Dynamics during C . elegans Cell Fate Specification. *Developmental Cell*, 1–12. https://doi.org/10.1016/j.devcel.2017.07.014

De Mot, L., Gonze, D., Bessonnard, S., Chazaud, C., Goldbeter, A., & Dupont, G. (2016). Cell Fate Specification Based on Tristability in the Inner Cell Mass of Mouse Blastocysts. *Biophysical Journal*, *110*(3), 710–722. https://doi.org/10.1016/J.BPJ.2015.12.020

Dietrich, J. E., & Hiiragi, T. (2007). Stochastic patterning in the mouse pre-implantation embryo. *Development*, *134*(23), 4219–4231. https://doi.org/10.1242/dev.003798

Ding, Q., Xia, W., Liu, J. C., Yang, J. Y., Lee, D. F., Xia, J., Bartholomeusz, G., Li, Y., Pan, Y., Li, Z., Bargou, R. C., Qin, J., Lai, C. C., Tsai, F. J., Tsai, C. H., & Hung, M. C. (2005). Erk associates with and primes GSK-3β for its inactivation resulting in upregulation of β-catenin. *Molecular Cell*, *19*(2), 159–170. https://doi.org/10.1016/j.molcel.2005.06.009

Do, D. V., Ueda, J., Messerschmidt, D. M., Lorthongpanich, C., Zhou, Y., Feng, B., Guo, G., Lin, P. J., Hossain, M. Z., Zhang, W., Moh, A., Wu, Q., Robson, P., Ng, H. H., Poellinger, L., Knowles, B. B., Solter, D., & Fu, X. Y. (2013). A genetic and developmental pathway from STAT3 to the OCT4-NANOG circuit is essential for maintenance of ICM lineages in vivo. *Genes and Development*, *27*(12), 1378–1390. https://doi.org/10.1101/gad.221176.113

Doble, B. W., Patel, S., Wood, G. A., Kockeritz, L. K., & Woodgett, J. R. (2007). Functional Redundancy of GSK-3α and GSK-3β in Wnt/β-Catenin Signaling Shown by Using an Allelic Series of Embryonic Stem Cell Lines. *Developmental Cell*, *12*(6), 957–971. https://doi.org/10.1016/J.DEVCEL.2007.04.001

Domogatskaya, A., Rodin, S., Boutaud, A., & Tryggvason, K. (2008). Laminin-511 but Not -332, -111, or -411 Enables Mouse Embryonic Stem Cell Self-Renewal In Vitro. *Stem Cells*, *26*(11), 2800–2809. https://doi.org/10.1634/stemcells.2007-0389

Dougherty, M. K., Ritt, D. A., Zhou, M., Specht, S. I., Monson, D. M., Veenstra, T. D., & Morrison, D. K. (2009). KSR2 Is a Calcineurin Substrate that Promotes ERK Cascade Activation in Response to Calcium Signals. *Molecular Cell*, *34*(6), 652–662. https://doi.org/10.1016/j.molcel.2009.06.001

Dumortier, J. G., Le Verge-Serandour, M., Tortorelli, A. F., Mielke, A., De Plater, L., Turlier, H., & Maître, J.-L. (2019). Hydraulic fracturing and active coarsening position the lumen of the mouse blastocyst. *Science*, 465–468. https://doi.org/10.1126/science.aaw7709

Düvel, K., Yecies, J. L., Menon, S., Raman, P., Lipovsky, A. I., Souza, A. L., Triantafellow, E., Ma, Q., Gorski, R., Cleaver, S., Vander Heiden, M. G., MacKeigan, J. P., Finan, P. M., Clish, C. B., Murphy, L. O., & Manning, B. D. (2010). Activation of a metabolic gene regulatory network downstream of mTOR complex 1. *Molecular Cell*, *39*(2), 171–183. https://doi.org/10.1016/j.molcel.2010.06.022

Erlebacher, A., Price, K. A., & Glimcher, L. H. (2004). Maintenance of mouse trophoblast stem cell proliferation by TGF-β/activin. *Developmental Biology*, *275*(1), 158–169.

https://doi.org/10.1016/j.ydbio.2004.07.032

Evans, M. J., & Kaufman, M. H. (1981). Establishment in culture of pluripotential cells from mouse embryos. *Nature*, *292*, 154–156.

Fagnocchi, L., Cherubini, A., Hatsuda, H., Fasciani, A., Mazzoleni, S., Poli, V., Berno, V., Rossi, R. L., Reinbold, R., Endele, M., Schroeder, T., Rocchigiani, M., Szkarł At, Z., Oliviero, S., Dalton, S., & Zippo, A. (2016). A Myc-driven self-reinforcing regulatory network maintains mouse embryonic stem cell identity. *Nature Communications*, *7*(May). https://doi.org/10.1038/ncomms11903

Fang, L., Zhang, L., Wei, W., Jin, X., Wang, P., Tong, Y., Li, J., Du, J. X., & Wong, J. (2014). A Methylation-Phosphorylation Switch Determines Sox2 Stability and Function in ESC Maintenance or Differentiation. *Molecular Cell*, *55*(4), 537–551. https://doi.org/10.1016/J.MOLCEL.2014.06.018

Festuccia, N., Osorno, R., Halbritter, F., Karwacki-Neisius, V., Navarro, P., Colby, D., Wong, F., Yates, A., Tomlinson, S. R., & Chambers, I. (2012). Esrrb is a direct Nanog target gene that can substitute for Nanog function in pluripotent cells. *Cell Stem Cell*, *11*(4), 477–490. https://doi.org/10.1016/j.stem.2012.08.002

Foster, K. G., Acosta-Jaquez, H. A., Romeo, Y., Ekim, B., Soliman, G. A., Carriere, A., Roux, P. P., Ballif, B. A., & Fingar, D. C. (2010). Regulation of mTOR complex 1 (mTORC1) by raptor Ser863 and multisite phosphorylation. *Journal of Biological Chemistry*, *285*(1), 80–94. https://doi.org/10.1074/jbc.M109.029637

Frankenberg, S., Gerbe, F., Bessonnard, S., Belville, C., Pouchin, P., Bardot, O., & Chazaud, C. (2011). Primitive Endoderm Differentiates via a Three-Step Mechanism Involving Nanog and RTK Signaling. *Developmental Cell*, *21*(6), 1005–1013. https://doi.org/10.1016/j.devcel.2011.10.019

Frum, T., Halbisen, M. A., Wang, C., Amiri, H., Robson, P., & Ralston, A. (2013). Oct4 Cell-autonomously promotes primitive endoderm development in the mouse blastocyst. *Developmental Cell*, *25*(6), 610–622. https://doi.org/10.1016/j.devcel.2013.05.004

Fu, D. Y., Wang, Z. M., Li-Chen, Wang, B. L., Shen, Z. Z., Huang, W., & Shao, Z. M. (2010). Sox17, the canonical Wnt antagonist, is epigenetically inactivated by promoter methylation in human breast cancer. *Breast Cancer Research and Treatment*, *119*(3), 601–612. https://doi.org/10.1007/s10549-009-0339-8

Fujikura, J., Yamato, E., Yonemura, S., Hosoda, K., Masui, S., Nakao, K., Miyazaki, J. I., & Niwa, H. (2002). Differentiation of embryonic stem cells is induced by GATA factors. *Genes and Development*, *16*(7), 784–789. https://doi.org/10.1101/gad.968802

Gagliardi, A., Mullin, N. P., Tan, Z. Y., Colby, D., Kousa, A. I., Halbritter, F., Weiss, J. T., Felker, A., Bezstarosti, K., Favaro, R., Demmers, J., Nicolis, S. K., Tomlinson, S. R., & Poot, R. A. (2013). A direct physical interaction between Nanog and Sox2 regulates embryonic stem cell self-renewal. *The EMBO Journal*, *32*(16), 2231–2247. https://doi.org/10.1038/emboj.2013.161

Gerbe, F., Cox, B., Rossant, J., & Chazaud, C. (2008). Dynamic expression of Lrp2 pathway members reveals progressive epithelial differentiation of primitive endoderm in mouse

blastocyst. *Developmental Biology*, *313*(2), 594–602. https://doi.org/10.1016/J.YDBIO.2007.10.048

Gharbi, S. I., Zvelebil, M. J., Shuhleworth, S. J., Hancox, T., Saghir, N., Timms, J. F., & Waterfield, M. D. (2007). Exploring the specificity of the PI3K family inhibitor LY294002. *Biochemical Journal*, *404*(1), 15–21. https://doi.org/10.1042/BJ20061489

Goldfarb, M. (2001). Signaling by Fibroblast Growth Factors: The Inside Story. *Science Signaling* , *2001*(106), 37–42.

Grabarek, J. B., Zyzyńska, K., Saiz, N., Piliszek, A., Frankenberg, S., Nichols, J., Hadjantonakis, A.-K., & Plusa, B. (2012). Differential plasticity of epiblast and primitive endoderm precursors within the ICM of the early mouse embryo. *Development*, *139*(1), 129–139. https://doi.org/10.1242/dev.067702

Gressner, A. M., & Wool, I. G. (1974). The phosphorylation of liver ribosomal proteins in vivo. Evidence that only a single small subunit protein (S6) is phosphorylated. *Journal of Biological Chemistry*, *249*(21), 6917–6925. https://doi.org/10.1016/S0021-9258(19)42145-5

Guo, Ge, Yang, J., Nichols, J., Hall, J. S., Eyres, I., Mansfield, W., & Smith, A. (2009). Klf4 reverts developmentally programmed restriction of ground state pluripotency. *Development*, *136*(7), 1063–1069. https://doi.org/10.1242/dev.030957

Guo, Guoji, Huss, M., Tong, G. Q., Wang, C., Li Sun, L., Clarke, N. D., & Robson, P. (2010). Resolution of Cell Fate Decisions Revealed by Single-Cell Gene Expression Analysis from Zygote to Blastocyst. *Developmental Cell*, *18*(4), 675–685. https://doi.org/10.1016/j.devcel.2010.02.012

Guzman-Ayala, M., Ben-Haim, N., Beck, S., & Constam, D. B. (2004). Nodal protein processing and fibroblast growth factor 4 synergize to maintain a trophoblast stem cell microenvironment. *Proceedings of the National Academy of Sciences of the United States of America*, *101*(44), 15656–15660. https://doi.org/10.1073/pnas.0405429101

Hahaut, V., Pavlinic, D., Cowan, C., & Picelli, S. (2021). Lightning Fast and Highly Sensitive Full-Length Single-cell sequencing using FLASH-Seq. *BioRxiv*. https://doi.org/10.1101/2021.07.14.452217

Halet, G., Viard, P., & Carroll, J. (2008). Constitutive Ptdlns(3,4,5)P3 synthesis promotes the development and survival of early mammalian embryos. *Development*, *135*(3), 425–429. https://doi.org/10.1242/dev.014894

Hallmann, D., Trümper, K., Trusheim, H., Ueki, K., Kahn, C. R., Cantley, L. C., Fruman, D. A., & Hörsch, D. (2003). Altered Signaling and Cell Cycle Regulation in Embryonal Stem Cells with a Disruption of the Gene for Phosphoinositide 3-Kinase Regulatory Subunit p85α. *Journal of Biological Chemistry*, *278*(7), 5099–5108. https://doi.org/10.1074/JBC.M208451200

Han, J. (2008). LAMR1 +/- mice as a model for Diamond-Blackfan anemia. *The Jackson Laboratory*.

Harvey, M. B., & Kaye, P. L. (1992). Insulin-Like Growth Factor-1 Stimulates Growth of

Mouse Preimplantation Embryos In Vitro. In *MOLECULAR REPRODUCTION AND DEVELOPMENT* (Vol. 31).

Hashimoto, M., & Sasaki, H. (2019). Epiblast Formation by TEAD-YAP-Dependent Expression of Pluripotency Factors and Competitive Elimination of Unspecified Cells. *Developmental Cell*, *50*(2), 139-154.e5. https://doi.org/10.1016/j.devcel.2019.05.024

Hatano, S. Y., Tada, M., Kimura, H., Yamaguchi, S., Kono, T., Nakano, T., Suemori, H., Nakatsuji, N., & Tada, T. (2005). Pluripotential competence of cells associated with Nanog activity. *Mechanisms of Development*, *122*(1), 67–79. https://doi.org/10.1016/J.MOD.2004.08.008

Hennessy, B. T., Smith, D. L., Ram, P. T., Lu, Y., & Mills, G. B. (2005). Exploiting the PI3K/AKT pathway for cancer drug discovery. In *Nature Reviews Drug Discovery* (Vol. 4, Issue 12, pp. 988–1004). https://doi.org/10.1038/nrd1902

Hesse, M., Franz, T., Tamai, Y., Taketo, M. M., & Magin, T. M. (2000). Targeted deletion of keratins 18 and 19 leads to trophoblast fragility and early embryonic lethality. *EMBO Journal*, *19*(19), 5060–5070.

Ho, L., Tan, S. Y. X., Wee, S., Wu, Y., Tan, S. J. C., Ramakrishna, N. B., Chng, S. C., Nama, S., Szczerbinska, I., Chan, Y. S., Avery, S., Tsuneyoshi, N., Ng, H. H., Gunaratne, J., Dunn, N. R., & Reversade, B. (2015). ELABELA Is an Endogenous Growth Factor that Sustains hESC Self-Renewal via the PI3K/AKT Pathway. *Cell Stem Cell*, *17*(4), 435–447. https://doi.org/10.1016/J.STEM.2015.08.010

Holz, M. K., Ballif, B. A., Gygi, S. P., & Blenis, J. (2005). mTOR and S6K1 Mediate Assembly of the Translation Preinitiation Complex through Dynamic Protein Interchange and Ordered Phosphorylation Events. *Cell*, *123*(4), 569–580. https://doi.org/10.1016/J.CELL.2005.10.024

Hosaka, T., Biggs III, W. H., Tieu, D., Boyer, A. D., Varki, N. M., Cavenee, W. K., & Arden, K. C. (2004). Disruption of forkhead transcription factor (FOXO) family members in mice reveals their functional diversification. *PNAS*, *101*(9), 2975–2980. https://doi.org/10.1073

Huang, S. M. A., Mishina, Y. M., Liu, S., Cheung, A., Stegmeier, F., Michaud, G. A., Charlat, O., Wiellette, E., Zhang, Y., Wiessner, S., Hild, M., Shi, X., Wilson, C. J., Mickanin, C., Myer, V., Fazal, A., Tomlinson, R., Serluca, F., Shao, W., … Cong, F. (2009). Tankyrase inhibition stabilizes axin and antagonizes Wnt signalling. *Nature*, *461*(7264), 614–620. https://doi.org/10.1038/nature08356

Ivanova, N., Dobrin, R., Lu, R., Kotenko, I., Levorse, J., DeCoste, C., Schafer, X., Lun, Y., & Lemischka, I. R. (2006). Dissecting self-renewal in stem cells with RNA interference. *Nature*, *442*(7102), 533–538. https://doi.org/10.1038/nature04915

Jia, Y., Yang, Y., Zhan, Q., Brock, M. V., Zheng, X., Yu, Y., Herman, J. G., & Guo, M. (2012). Inhibition of SOX17 by MicroRNA 141 and methylation activates the WNT signaling pathway in esophageal cancer. *Journal of Molecular Diagnostics*, *14*(6), 577–585. https://doi.org/10.1016/j.jmoldx.2012.06.004

Jirmanova, L., Afanassieff, M., Gobert-Gosse, S., Markossian, S., & Savatier, P. (2002). Differential contributions of ERK and PI3-kinase to the regulation of cyclin D1 expression

and to the control of the G1/S transition in mouse embryonic stem cells. *Oncogene*, *21*(36), 5515–5528. https://doi.org/10.1038/sj.onc.1205728

Johnson, M. H., & Ziomek, C. A. (1981). The foundation of two distinct cell lineages within the mouse morula. *Cell*, *24*(1), 71–80. https://doi.org/10.1016/0092-8674(81)90502-X

Johnson, M., & McConnell JML. (2004). Lineage allocation and cell polarity during mouse embryogenesis. *Seminars in Cell & Developmental Biology*, *15*(5), 583–597.

Kang, M., Garg, V., & Hadjantonakis, A. K. (2017). Lineage Establishment and Progression within the Inner Cell Mass of the Mouse Blastocyst Requires FGFR1 and FGFR2. *Developmental Cell*, *41*(5), 496-510.e5. https://doi.org/10.1016/J.DEVCEL.2017.05.003

Kang, M., Piliszek, A., Artus, J., & Hadjantonakis, A.-K. (2013). FGF4 is required for lineage restriction and salt-and-pepper distribution of primitive endoderm factors but not their initial expression in the mouse. *Development (Cambridge, England)*, *140*(2), 267–279. https://doi.org/10.1242/dev.084996

Kim, J., Kundu, M., Viollet, B., & Guan, K. L. (2011). AMPK and mTOR regulate autophagy through direct phosphorylation of Ulk1. *Nature Cell Biology*, *13*(2), 132–141. https://doi.org/10.1038/ncb2152

Kim, O., Jeong, Y., Lee, H., Hong, S. S., & Hong, S. (2011). Design and synthesis of imidazopyridine analogues as inhibitors of phosphoinositide 3-kinase signaling and angiogenesis. *Journal of Medicinal Chemistry*, *54*(7), 2455–2466. https://doi.org/10.1021/jm101582z

Kim, S. H., Kim, M. O., Cho, Y. Y., Yao, K., Kim, D. J., Jeong, C. H., Yu, D. H., Bae, K. B., Cho, E. J., Jung, S. K., Lee, M. H., Chen, H., Kim, J. Y., Bode, A. M., & Dong, Z. (2014). ERK1 phosphorylates Nanog to regulate protein stability and stem cell self-renewal. *Stem Cell Research*, *13*(1), 1–11. https://doi.org/10.1016/j.scr.2014.04.001

Kingham, E., & Welham, M. (2009). Distinct roles for isoforms of the catalytic subunit of class-IA PI3K in the regulation of behaviour of murine embryonic stem cells. *Journal of Cell Science*, *122*(13), 2311–2321. https://doi.org/10.1242/jcs.046557

Kinoshita, M., Shimosato, D., Yamane, M., & Niwa, H. (2015). Sox7 is dispensable for primitive endoderm differentiation from mouse ES cells Early development. *BMC Developmental Biology*, *15*(1), 1–11. https://doi.org/10.1186/s12861-015-0079-4

Knight, Z. A., Gonzalez, B., Feldman, M. E., Zunder, E. R., Goldenberg, D. D., Williams, O., Loewith, R., Stokoe, D., Balla, A., Toth, B., Balla, T., Weiss, W. A., Williams, R. L., & Shokat, K. M. (2006). A Pharmacological Map of the PI3-K Family Defines a Role for p110α in Insulin Signaling. *Cell*, *125*(4), 733–747. https://doi.org/10.1016/j.cell.2006.03.035

Kojima, Y., Kaufman-Francis, K., Studdert, J. B., Steiner, K. A., Power, M. D., Loebel, D. A. F., Jones, V., Hor, A., De Alencastro, G., Logan, G. J., Teber, E. T., Tam, O. H., Stutz, M. D., Alexander, I. E., Pickett, H. A., & Tam, P. P. L. (2014). The Transcriptional and Functional Properties of Mouse Epiblast Stem Cells Resemble the Anterior Primitive Streak. *Cell Stem Cell*, *14*(1), 107–120. https://doi.org/10.1016/J.STEM.2013.09.014

Korotkevich, E., Niwayama, R., Courtois, A., Friese, S., Berger, N., Buchholz, F., & Hiiragi, T. (2017). The Apical Domain Is Required and Sufficient for the First Lineage Segregation in the Mouse Embryo. *Developmental Cell*, *40*(3), 235-247.e7. https://doi.org/10.1016/J.DEVCEL.2017.01.006

Kouhara, H., Hadari, Y. R., Spivak-Kroizman, T., Schilling, J., Bar-Sagi, D., Lax, I., & Schlessinger, J. (1997). A Lipid-Anchored Grb2-Binding Protein That Links FGF-Receptor Activation to the Ras/MAPK Signaling Pathway. *Cell*, *89*(5), 693–702. https://doi.org/10.1016/S0092-8674(00)80252-4

Krawchuk, D., Honma-Yamanaka, N., Anani, S., & Yamanaka, Y. (2013). FGF4 is a limiting factor controlling the proportions of primitive endoderm and epiblast in the ICM of the mouse blastocyst. *Developmental Biology*, *384*(1), 65–71. https://doi.org/10.1016/j.ydbio.2013.09.023

Krupa, M., Mazur, E., Szczepańska, K., Filimonow, K., Maleszewski, M., & Suwińska, A. (2014). Allocation of inner cells to epiblast vs primitive endoderm in the mouse embryo is biased but not determined by the round of asymmetric divisions (8→16- and 16→32-cells). *Developmental Biology*, *385*(1), 136–148. https://doi.org/10.1016/J.YDBIO.2013.09.008

Kuijk, E. W., van Tol, L. T. A., van de Velde, H., Wubbolts, R., Welling, M., Geijsen, N., & Roelen, B. A. J. (2012). The roles of FGF and MAP kinase signaling in the segregation of the epiblast and hypoblast cell lineages in bovine and human embryos. *Development*, *139*(5), 871–882. https://doi.org/10.1242/dev.071688

Kunath, T., Arnaud, D., Uy, G. D., Okamoto, I., Chureau, C., Yamanaka, Y., Heard, E., Gardner, R. L., Avner, P., & Rossant, J. (2005). Imprinted X-inactivation in extra-embryonic endoderm cell lines from mouse blastocysts. *Development*, *132*(7), 1649–1661. https://doi.org/10.1242/dev.01715

Kurimoto, K., Yabuta, Y., Ohinata, Y., Ono, Y., Uno, K. D., Yamada, R. G., Ueda, H. R., & Saitou, M. (2006). An improved single-cell cDNA amplification method for efficient high-density oligonucleotide microarray analysis. *Nucleic Acids Research*, *34*(5). https://doi.org/10.1093/nar/gkl050

Lee, J. V., Carrer, A., Shah, S., Snyder, N. W., Wei, S., Venneti, S., Worth, A. J., Yuan, Z. F., Lim, H. W., Liu, S., Jackson, E., Aiello, N. M., Haas, N. B., Rebbeck, T. R., Judkins, A., Won, K. J., Chodosh, L. A., Garcia, B. A., Stanger, B. Z., … Wellen, K. E. (2014). Akt-dependent metabolic reprogramming regulates tumor cell Histone acetylation. *Cell Metabolism*, *20*(2), 306–319. https://doi.org/10.1016/j.cmet.2014.06.004

Lehr, S., Kotzka, J., Avci, H., Sickmann, A., Meyer, H. E., Herkner, A., & Muller-Wieland, D. (2004). Identification of major ERK-related phosphorylation sites in Gab1. *Biochemistry*, *43*(38), 12133–12140. https://doi.org/10.1021/bi049753e

Levental, K. R., Yu, H., Kass, L., Lakins, J. N., Egeblad, M., Erler, J. T., Fong, S. F. T., Csiszar, K., Giaccia, A., Weninger, W., Yamauchi, M., Gasser, D. L., & Weaver, V. M. (2009). Matrix Crosslinking Forces Tumor Progression by Enhancing Integrin Signaling. *Cell*, *139*(5), 891–906. https://doi.org/10.1016/j.cell.2009.10.027

Li, Z., Fei, T., Zhang, J., Zhu, G., Wang, L., Lu, D., Chi, X., Teng, Y., Hou, N., Yang, X.,

Zhang, H., Han, J. D. J., & Chen, Y. G. (2012). BMP4 signaling acts via dual-specificity phosphatase 9 to control ERK activity in mouse embryonic stem cells. *Cell Stem Cell*, *10*(2), 171–182. https://doi.org/10.1016/j.stem.2011.12.016

Lim, H. Y. G., Alvarez, Y. D., Gasnier, M., Wang, Y., Tetlak, P., Bissiere, S., Wang, H., Biro, M., & Plachta, N. (2020). Keratins are asymmetrically inherited fate determinants in the mammalian embryo. *Nature*, *585*(7825), 404–409. https://doi.org/10.1038/s41586-020-2647-4

Lin, C. H., Jackson, A. L., Guo, J., Linsley, P. S., & Eisenman, R. N. (2009). Myc-regulated microRNAs attenuate embryonic stem cell differentiation. *EMBO Journal*, *28*(20), 3157–3170. https://doi.org/10.1038/emboj.2009.254

Lin, H.-Y., Kaplow, J., Jaye, M., & Hayman, M. J. (1997). Ligand-binding specificity of human fibroblast growth factor receptor-3 IIIc. *FEBS*, *18887*(411), 389–392.

Lin, T.-C., Yen, J.-M., Gong, K.-B., Hsu, T.-T., & Chen, L.-R. (2003). IGF-1/IGFBP-1 increases blastocyst formation and total blastocyst cell number in mouse embryo culture and facilitates the establishment of a stem-cell line. *BMC Developmental Biology*, *4*(14). https://doi.org/10.1186/1471-2121-4-14

Lin, T., Chao, C., Saito, S., Mazur, S. J., Murphy, M. E., Appella, E., & Xu, Y. (2005). p53 induces differentiation of mouse embryonic stem cells by suppressing Nanog expression. *Nature Cell Biology*, *7*(2), 165–171. https://doi.org/10.1038/ncb1211

Lin, Y., Yang, Y., Li, W., Chen, Q., Li, J., Pan, X., Zhou, L., Liu, C., Chen, C., He, J., Cao, H., Yao, H., Zheng, L., Xu, X., Xia, Z., Ren, J., Xiao, L., Li, L., Shen, B., … Wang, Y. J. (2012). Reciprocal Regulation of Akt and Oct4 Promotes the Self-Renewal and Survival of Embryonal Carcinoma Cells. *Molecular Cell*, *48*(4), 627–640. https://doi.org/10.1016/j.molcel.2012.08.030

Lindgren, A. G., Natsuhara, K., Tian, E., Vincent, J. J., Li, X., Jiao, J., Wu, H., Banerjee, U., & Clark, A. T. (2011). Loss of Pten causes tumor initiation following differentiation of murine pluripotent stem cells due to failed repression of sanog. *PLoS ONE*, *6*(1). https://doi.org/10.1371/journal.pone.0016478

Loh, Y., Wu, Q., Chew, J., Vega, V. B., Zhang, W., Chen, X., Bourque, G., George, J., Leong, B., Liu, J., Wong, K., Sung, K. W., Lee, C. W. H., Zhao, X., Chiu, K., Lipovich, L., Kuznetsov, V. A., Robson, P., Stanton, L. W., … Ng, H. (2006). The Oct4 and Nanog transcription network regulates pluripotency in mouse embryonic stem cells. *Nature Genetics*, *38*(4), 431–440. https://doi.org/10.1038/ng1760

Lorthongpanich, C., Doris, T. P. Y., Limviphuvadh, V., Knowles, B. B., & Solter, D. (2012). Developmental fate and lineage commitment of singled mouse blastomeres. *Development (Cambridge)*, *139*(20), 3722–3731. https://doi.org/10.1242/dev.086454

Luo, J., Sladek, R., Bader, J.-A., Matthyssen, A., Rossant, J., & Giguè re, V. (1997). Placental abnormalities in mouse embryos lacking the orphan nuclear receptor ERR. In *NATURE* (Vol. 388).

Ma, G. T., Soloveva, V., Tzeng, S. J., Lowe, L. A., Pfendler, K. C., Iannaccone, P. M., Kuehn, M. R., & Linzer, D. I. H. (2001). Nodal regulates trophoblast differentiation and placental

development. *Developmental Biology*, *236*(1), 124–135. https://doi.org/10.1006/dbio.2001.0334

Ma, L., Chen, Z., Erdjument-Bromage, H., Tempst, P., & Pandolfi, P. P. (2005). Phosphorylation and functional inactivation of TSC2 by Erk: Implications for tuberous sclerosis and cancer pathogenesis. *Cell*, *121*(2), 179–193. https://doi.org/10.1016/j.cell.2005.02.031

Madsen, R. R., Knox, R. G., Pearce, W., Lopez, S., Mahler-Araujo, B., Mcgranahan, N., Vanhaesebroeck, B., & Semple, R. K. (2019). Oncogenic PIK3CA promotes cellular stemness in an allele dose-dependent manner. *PNAS*, *116*(17), 8380–8389. https://doi.org/10.1073/pnas.1821093116

Maehama, T., & Dixon, J. E. (1998). The Tumor Suppressor, PTEN/MMAC1, Dephosphorylates the Lipid Second Messenger, Phosphatidylinositol 3,4,5-Trisphosphate. *Journal of Biological Chemistry*, *273*(22), 13375–13378. https://doi.org/10.1074/JBC.273.22.13375

Maître, J. L., Turlier, H., Illukkumbura, R., Eismann, B., Niwayama, R., Nédélec, F., & Hiiragi, T. (2016). Asymmetric division of contractile domains couples cell positioning and fate specification. *Nature*, *536*(7616), 344–348. https://doi.org/10.1038/nature18958

Malynn, B. A., Moreno De Alboran, I., Ná, R., O'hagan, C., Bronson, R., Davidson, L., Depinho, R. A., & Alt, F. W. (2000). *N-myc can functionally replace c-myc in murine development, cellular growth, and differentiation*. www.genesdev.org

Martello, G., Sugimoto, T., Diamanti, E., Joshi, A., Hannah, R., Ohtsuka, S., Göttgens, B., Niwa, H., & Smith, A. (2012). Esrrb is a pivotal target of the Gsk3/Tcf3 axis regulating embryonic stem cell self-renewal. *Cell Stem Cell*, *11*(4), 491–504. https://doi.org/10.1016/j.stem.2012.06.008

Martin, G. R. (1981). Isolation of a pluripotent cell line from early mouse embryos cultured in medium conditioned by teratocarcinoma stem cells. *Proceedings of the National Academy of Sciences of the United States of America*, *78*(12 II), 7634–7638. https://doi.org/10.1073/pnas.78.12.7634

Maryu, G., Matsuda, M., & Aoki, K. (2016). *Multiplexed Fluorescence Imaging of ERK and Akt Activities and Cell-cycle Progression*. *92*, 81–92.

Meilhac, S. M., Adams, R. J., Morris, S. A., Danckaert, A., Le Garrec, J. F., & Zernicka-Goetz, M. (2009). Active cell movements coupled to positional induction are involved in lineage segregation in the mouse blastocyst. *Developmental Biology*, *331*(2), 210–221. https://doi.org/10.1016/j.ydbio.2009.04.036

Meng, Y., Moore, R., Tao, W., Smith, E. R., Tse, J. D., Caslini, C., & Xu, X. X. (2018). GATA6 phosphorylation by Erk1/2 propels exit from pluripotency and commitment to primitive endoderm. *Developmental Biology*, *436*(1), 55–65. https://doi.org/10.1016/j.ydbio.2018.02.007

Mesnard, D., Guzman-Ayala, M., & Constam, D. B. (2006). Nodal specifies embryonic visceral endoderm and sustains pluripotent cells in the epiblast before overt axial patterning. *Development*, *133*(13), 2497–2505. https://doi.org/10.1242/dev.02413

Mihajlovic, A. I., Thamodaran, V., & Bruce, A. W. (2015). The first two cell-fate decisions of preimplantation mouse embryo development are not functionally independent. *Scientific Reports*, *5*. https://doi.org/10.1038/srep15034

Miner, J. H., Li, C., Mudd, J. L., Go, G., & Sutherland, A. E. (2004). Compositional and structural requirements for laminin and basement membranes during mouse embryo implantation and gastrulation. *Development*, *131*(10), 2247–2256. https://doi.org/10.1242/dev.01112

Mitsui, K., Tokuzawa, Y., Itoh, H., Segawa, K., Murakami, M., Takahashi, K., Maruyama, M., Maeda, M., & Yamanaka, S. (2003). The Homeoprotein Nanog Is Required for Maintenance of Pluripotency in Mouse Epiblast and ES Cells. *Cell*, *113*(5), 631–642. https://doi.org/10.1016/S0092-8674(03)00393-3

Miyanari, Y., & Torres-Padilla, M.-E. (2012). Control of ground-state pluripotency by allelic regulation of Nanog. *Nature*, *483*, 470–473. https://doi.org/10.1038/nature10807

Molkentin, J. D., Lin, Q., Duncan, S. A., & Olson, E. N. (1997). Requirement of the transcription factor GATA4 for heart tube formation and ventral morphogenesis. *Genes and Development*, *11*, 1061–1072.

Molotkov, A., Mazot, P., Brewer, J. R., Cinalli, R. M., & Soriano, P. (2017). Distinct Requirements for FGFR1 and FGFR2 in Primitive Endoderm Development and Exit from Pluripotency. *Developmental Cell*, *41*(5), 511-526.e4. https://doi.org/10.1016/J.DEVCEL.2017.05.004

Moretto-Zita, M., Jin, H., Shen, Z., Zhao, T., Briggs, S. P., & Xu, Y. (2010). Phosphorylation stabilizes Nanog by promoting its interaction with Pin1. *Proceedings of the National Academy of Sciences of the United States of America*, *107*(30), 13312–13317. https://doi.org/10.1073/pnas.1005847107

Morris, S. A., Graham, S. J. L., Jedrusik, A., & Zernicka-Goetz, M. (2013). The differential response to Fgf signalling in cells internalized at different times influences lineage segregation in preimplantation mouse embryos. *Open Biology*, *3*(NOV). https://doi.org/10.1098/rsob.130104

Morris, S. A., Teo, R. T. Y., Li, H., Robson, P., Glover, D. M., Zernicka-Goetz, M., & Gurdon, J. B. (2010). Origin and formation of the first two distinct cell types of the inner cell mass in the mouse embryo. *PNAS*, *107*(14), 6364–6369. https://doi.org/10.1073/pnas.0915063107

Morrisey, E. E., Tang, Z., Sigrist, K., Lu, M. M., Jiang, F., Ip, H. S., & Parmacek, M. S. (1998). GATA6 regulates HNF4 and is required for differentiation of visceral endoderm in the mouse embryo. *Genes and Development*, *12*, 3579–3590. https://doi.org/10.1101/gad.12.22.3579

Morrison, G., Scognamiglio, R., Trumpp, A., & Smith, A. (2016). Convergence of cMyc and β-catenin on Tcf7l1 enables endoderm specification. *The EMBO Journal*, *35*(3), 356–368. https://doi.org/10.15252/embj.201592116

Murakami, M., Ichisaka, T., Maeda, M., Oshiro, N., Hara, K., Edenhofer, F., Kiyama, H., Yonezawa, K., & Yamanaka, S. (2004). mTOR Is Essential for Growth and Proliferation

in Early Mouse Embryos and Embryonic Stem Cells. *Molecular and Cellular Biology*, *24*(15), 6710–6718. https://doi.org/10.1128/mcb.24.15.6710-6718.2004

Ngondo, R. P., Cirera-Salinas, D., Yu, J., Wischnewski, H., Bodak, M., Vandormael-Pournin, S., Geiselmann, A., Wettstein, R., Luitz, J., Cohen-Tannoudji, M., & Ciaudo, C. (2018). Argonaute 2 Is Required for Extra-embryonic Endoderm Differentiation of Mouse Embryonic Stem Cells. *Stem Cell Reports*, *10*(2), 461–476. https://doi.org/10.1016/j.stemcr.2017.12.023

Niakan, K. K., Ji, H., Maehr, R., Vokes, S. A., Rodolfa, K. T., Sherwood, R. I., Yamaki, M., Dimos, J. T., Chen, A. E., Melton, D. A., McMahon, A. P., & Eggan, K. (2010). Sox17 promotes differentiation in mouse embryonic stem cells by directly regulating extraembryonic gene expression and indirectly antagonizing self-renewal. *Genes and Development*, *24*(3), 312–326. https://doi.org/10.1101/gad.1833510

Nichols, J., Silva, J., Roode, M., & Smith, A. (2009). Suppression of Erk signalling promotes ground state pluripotency in the mouse embryo. *Development (Cambridge, England)*, *136*(19), 3215–3222. https://doi.org/10.1242/dev.038893

Nichols, J., Zevnik, B., Anastassiadis, K., Niwa, H., Klewe-Nebenius, D., Chambers, I., Schö, H., & Smith, A. (1998). Formation of Pluripotent Stem Cells in the Mammalian Embryo Depends on the POU Transcription Factor Oct4. In *Cell* (Vol. 95). https://doi.org/10.1016/s0092

Nishioka, N., Inoue, K. ichi, Adachi, K., Kiyonari, H., Ota, M., Ralston, A., Yabuta, N., Hirahara, S., Stephenson, R. O., Ogonuki, N., Makita, R., Kurihara, H., Morin-Kensicki, E. M., Nojima, H., Rossant, J., Nakao, K., Niwa, H., & Sasaki, H. (2009). The Hippo Signaling Pathway Components Lats and Yap Pattern Tead4 Activity to Distinguish Mouse Trophectoderm from Inner Cell Mass. *Developmental Cell*, *16*(3), 398–410. https://doi.org/10.1016/J.DEVCEL.2009.02.003

Niwa, H., Ogawa, K., Shimosato, D., & Adachi, K. (2009). A parallel circuit of LIF signalling pathways maintains pluripotency of mouse ES cells. *Nature*. https://doi.org/10.1038/nature08113

Nur-E-Kamal, A., Ahmed, I., Kamal, J., Schindler, M., & Meiners, S. (2006). Three-Dimensional Nanofibrillar Surfaces Promote Self-Renewal in Mouse Embryonic Stem Cells. *Stem Cells*, *24*(2), 426–433. https://doi.org/10.1634/stemcells.2005-0170

Ohinata, Y., Endo, T. A., Sugishita, H., Watanabe, T., Iizuka, Y., Kawamoto, Y., Saraya, A., Kumon, M., Koseki, Y., Kondo, T., Ohara, O., & Koseki, H. (2022). Establishment of mouse stem cells that can recapitulate the developmental potential of primitive endoderm. *Science*, *375*(6580), 574–578. https://doi.org/10.1126/science.aay3325

Ohnishi, Y., Huber, W., Tsumura, A., Kang, M., Xenopoulos, P., Kurimoto, K., Oleå, A. K., Araúzo-Bravo, M. J., Saitou, M., Hadjantonakis, A. K., & Hiiragi, T. (2014). Cell-to-cell expression variability followed by signal reinforcement progressively segregates early mouse lineages. *Nature Cell Biology*, *16*(1), 27–37. https://doi.org/10.1038/ncb2881

Ohnishi, Y., Huber, W., Tsumura, A., Kang, M., Xenopoulos, P., Kurimoto, K., Oleś, A. K., Araúzo-Bravo, M. J., Saitou, M., Hadjantonakis, A.-K., & Hiiragi, T. (2014). Cell-to-cell expression variability followed by signal reinforcement progressively segregates early

mouse lineages. *Nature Cell Biology*, *16*(1), 27–37. https://doi.org/10.1038/ncb2881

Okumura-Nakanishi, S., Saito, M., Niwa, H., & Ishikawa, F. (2005). Oct-3/4 and Sox2 Regulate Oct-3/4 Gene in Embryonic Stem Cells. *Journal of Biological Chemistry*, *280*(7), 5307–5317. https://doi.org/10.1074/JBC.M410015200

Paling, N. R. D., Wheadon, H., Bone, H. K., & Welham, M. J. (2004). Regulation of embryonic stem cell self-renewal by phosphoinositide 3-kinase-dependent signaling. *Journal of Biological Chemistry*, *279*(46), 48063–48070. https://doi.org/10.1074/jbc.M406467200

Peng, X. ding, Xu, P. Z., Chen, M. L., Hahn-Windgassen, A., Skeen, J., Jacobs, J., Sundararajan, D., Chen, W. S., Crawford, S. E., Coleman, K. G., & Hay, N. (2003). Dwarfism, impaired skin development, skeletal muscle atrophy, delayed bone development, and impeded adipogenesis in mice lacking Akt1 and Akt2. *Genes and Development*, *17*(11), 1352–1365. https://doi.org/10.1101/gad.1089403

Pereira, L., Yi, F., & Merrill, B. J. (2006). Repression of Nanog Gene Transcription by Tcf3 Limits Embryonic Stem Cell Self-Renewal. *Molecular and Cellular Biology*, *26*(20), 7479–7491. https://doi.org/10.1128/mcb.00368-06

Pérez-Palacios, R., Fauque, P., Teissandier, A., & Bourc'his, D. (2021). Deciphering the early mouse embryo transcriptome by low-input RNA-Seq. In *Methods in Molecular Biology* (Vol. 2214, pp. 189–205). Humana Press Inc. https://doi.org/10.1007/978-1-0716-0958-3_13

Piliszek, A., Madeja, Z. E., & Plusa, B. (2017). Suppression of ERK signalling abolishes primitive endoderm formation but does not promote pluripotency in rabbit embryo. *Development (Cambridge)*, *144*(20), 3719–3730. https://doi.org/10.1242/dev.156406

Piotrowska-Nitsche, K., Perea-Gomez, A., Haraguchi, S., & Zernicka-Goetz, M. (2005). Four-cell stage mouse blastomeres have different developmental properties. *Development*, *132*(3), 479–490. https://doi.org/10.1242/dev.01602

Plachta, N., Bollenbach, T., Pease, S., Fraser, S. E., & Pantazis, P. (2011). Oct4 kinetics predict cell lineage patterning in the early mammalian embryo. *Nat Cell Biol*, *13*(2), 117–123. https://doi.org/10.1038/ncb2154

Plusa, B., Piliszek, A., Frankenberg, S., Artus, J., & Hadjantonakis, A.-K. (2008). Distinct sequential cell behaviours direct primitive endoderm formation in the mouse blastocyst. *Development*, *135*(18), 3081–3091. https://doi.org/10.1242/dev.021519

Pokrass, M. J., Ryan, K. A., Xin, T., Pielstick, B., Timp, W., Greco, V., & Regot, S. (2020). Cell-Cycle-Dependent ERK Signaling Dynamics Direct Fate Specification in the Mammalian Preimplantation Embryo. *Developmental Cell*, *55*(3), 328-340.e5. https://doi.org/10.1016/j.devcel.2020.09.013

Posfai, E., Petropoulos, S., Oliveira De Barros, F. R., Schell, J. P., Jurisica, I., Sandberg, R., Lanner, F., & Rossant, J. (2017). *Position-and Hippo signaling-dependent plasticity during lineage segregation in the early mouse embryo*. https://doi.org/10.7554/eLife.22906.001

Pritsker, M., Ford, N. R., Jenq, H. T., & Lemischka, I. R. (2006). *Genomewide gain-of-function*

genetic screen identifies functionally active genes in mouse embryonic stem cells. https://doi.org/10.1073

Raina, D., Bahadori, A., Stanoev, A., Protzek, M., Koseska, A., & Schroter, C. (2021). Cell-cell communication through FGF4 generates and maintains robust proportions of differentiated cell types in embryonic stem cells. *Development (Cambridge)*, *148*(21). https://doi.org/10.1242/dev.199926

Ralston, A., Cox, B. J., Nishioka, N., Sasaki, H., Chea, E., Rugg-Gunn, P., Guo, G., Robson, P., Draper, J. S., & Rossant, J. (2010). Gata3 regulates trophoblast development downstream of Tead4 and in parallel to Cdx2. *Development*, *137*(3), 395–403. https://doi.org/10.1242/dev.038828

Rennebeck, G., Kleymenova, E. V, Anderson, R., Yeung, R. S., Artzt, K., & Walker, C. L. (1998). Loss of function of the tuberous sclerosis 2 tumor suppressor gene results in embryonic lethality characterized by disrupted neuroepithelial growth and development. In *Medical Sciences* (Vol. 95). www.pnas.org.

Riley, J. K., Carayannopoulos, M. O., H. Wyman, A., Chi, M., Ratajczak, C. K., & Moley, K. H. (2005). The PI3K/Akt pathway is present and functional in the preimplantation mouse embryo. *Developmental Biology*, *284*(2), 377–386. https://doi.org/10.1016/J.YDBIO.2005.05.033

Rodda, D. J., Chew, J. L., Lim, L. H., Loh, Y. H., Wang, B., Ng, H. H., & Robson, P. (2005). Transcriptional Regulation of Nanog by OCT4 and SOX2. *Journal of Biological Chemistry*, *280*(26), 24731–24737. https://doi.org/10.1074/JBC.M502573200

Rodriguez-Viciana, P., Warne, P. H., Dhandt, R., Vanhaesebroeck, B., Gout, I., Fry, M. J., Waterfieldtt, M. D., & Downward, J. (1986). Tsukuba, 1992). 71. Hemley. In *65. Giggenbach, W. F. Econ. Geol* (Vol. 88). Miner. Soc. Am.

Rodríguez, A., Allegrucci, C., & Alberio, R. (2012). Modulation of Pluripotency in the Porcine Embryo and iPS Cells. *PLoS ONE*, *7*(11). https://doi.org/10.1371/journal.pone.0049079

Rommel, C., Clarke, B. A., Zimmermann, S., Nunez, L., Rossman, R., Reid, K., Moelling, K., Yancopoulos, G. D., & Glass, D. J. (1999). Differentiation Stage–SpecificInhibition of the Raf-MEK-ERKPathway by Akt. *Science*, *286*, 1738–1741.

Roode, M., Blair, K., Snell, P., Elder, K., Marchant, S., Smith, A., & Nichols, J. (2012). Human hypoblast formation is not dependent on FGF signalling. *Developmental Biology*, *361*(2), 358–363. https://doi.org/10.1016/J.YDBIO.2011.10.030

Rossant, J. (1975). Investigation of the determinative state of the mouse inner cell mass II. The fate of isolated inner cell masses transferred to the oviduct. In *Embryol. exp. Morph* (Vol. 33).

Rubashkin, M. G., Cassereau, L., Bainer, R., DuFort, C. C., Yui, Y., Ou, G., Paszek, M. J., Davidson, M. W., Chen, Y. Y., & Weaver, V. M. (2014). Force engages vinculin and promotes tumor progression by enhancing PI3K activation of phosphatidylinositol (3,4,5)-triphosphate. *Cancer Research*, *74*(17), 4597–4611. https://doi.org/10.1158/0008-5472.CAN-13-3698

Rubinfeld, B., Albert, I., Pofiri, E., Fiol, C., Munemitsu, S., & Polakis, P. (1996). Binding of GSK3β to the APC-β-Catenin Complex and Regulation of Complex Assembly. *Science*, *272*(5264), 1023–1026.

Sacco, A., Morcavallo, A., Pandini, G., Vigneri, R., & Belfiore, A. (2009). Differential signaling activation by insulin and insulin-like growth factors I and II upon binding to insulin receptor isoform A. *Endocrinology*, *150*(8), 3594–3602. https://doi.org/10.1210/en.2009-0377

Saiz, N., & Hadjantonakis, A.-K. (2020). Coordination between patterning and morphogenesis ensures robustness during mouse development. *Philosophical Transactions of the Royal Society B: Biological Sciences*, *375*(1809), 20190562. https://doi.org/10.1098/rstb.2019.0562

Saiz, N., Williams, K. M., Seshan, V. E., & Hadjantonakis, A.-K. (2016). Asynchronous fate decisions by single cells collectively ensure consistent lineage composition in the mouse blastocyst. *Nature Communications*, *7*, 13463. https://doi.org/10.1038/ncomms13463

Sanchez-Ripoll, Y., Bone, H. K., Owen, T., Guedes, A. M. V., Abranches, E., Kumpfmueller, B., Spriggs, R. V., Henrique, D., & Welham, M. J. (2013). Glycogen Synthase Kinase-3 Inhibition Enhances Translation of Pluripotency-Associated Transcription Factors to Contribute to Maintenance of Mouse Embryonic Stem Cell Self-Renewal. *PLoS ONE*, *8*(4), 1–14. https://doi.org/10.1371/journal.pone.0060148

Schrode, N., Saiz, N., Di Talia, S., & Hadjantonakis, A. K. (2014). GATA6 levels modulate primitive endoderm cell fate choice and timing in the mouse blastocyst. *Developmental Cell*, *29*(4), 454–467. https://doi.org/10.1016/j.devcel.2014.04.011

Schröter, C., Rué, P., Mackenzie, J. P., & Arias, A. M. (2015). FGF/MAPK signaling sets the switching threshold of a bistable circuit controlling cell fate decisions in embryonic stem cells. *Development (Cambridge)*, *142*(24), 4205–4216. https://doi.org/10.1242/DEV.127530/-/DC1

Scognamiglio, R., Cabezas-Wallscheid, N., Thier, M. C., Altamura, S., Reyes, A., Prendergast, Á. M., Baumgärtner, D., Carnevalli, L. S., Atzberger, A., Haas, S., Von Paleske, L., Boroviak, T., Wörsdörfer, P., Essers, M. A. G., Kloz, U., Eisenman, R. N., Edenhofer, F., Bertone, P., Huber, W., … Trumpp, A. (2016). Myc Depletion Induces a Pluripotent Dormant State Mimicking Diapause. *Cell*, *164*(4), 668–680. https://doi.org/10.1016/j.cell.2015.12.033

Shapiro, E., Biezuner, T., & Linnarsson, S. (2013). Single-cell sequencing-based technologies will revolutionize whole-organism science. In *Nature Reviews Genetics* (Vol. 14, Issue 9, pp. 618–630). https://doi.org/10.1038/nrg3542

Shi, J., Chen, Q., Li, X., Zheng, X., Zhang, Y., Qiao, J., Tang, F., Tao, Y., Zhou, Q., & Duan, E. (2015). Dynamic transcriptional symmetry-breaking in pre-implantation mammalian embryo development revealed by single-cell rna-seq. *Development (Cambridge)*, *142*(20), 3468–3477. https://doi.org/10.1242/dev.123950

Shimosato, D., Shiki, M., & Niwa, H. (2007). Extra-embryonic endoderm cells derived from ES cells induced by GATA Factors acquire the character of XEN cells. *BMC Developmental Biology*, *7*. https://doi.org/10.1186/1471-213X-7-80

Simon, C. S., Rahman, S., Raina, D., Schröter, C., & Hadjantonakis, A. K. (2020). Live Visualization of ERK Activity in the Mouse Blastocyst Reveals Lineage-Specific Signaling Dynamics. *Developmental Cell*, *55*(3), 341-353.e5. https://doi.org/10.1016/J.DEVCEL.2020.09.030

Singh, A. M., Reynolds, D., Cliff, T., Ohtsuka, S., Mattheyses, A. L., Sun, Y., Menendez, L., Kulik, M., & Dalton, S. (2012). Signaling Network Crosstalk in Human Pluripotent Cells: A Smad2/3-Regulated Switch that Controls the Balance between Self-Renewal and Differentiation. *Cell Stem Cell*, *10*(3), 312–326. https://doi.org/10.1016/J.STEM.2012.01.014

Smith, A. G., Heath, J. K., Donaldson, D. D., Wong, G. G., Moreau, J., Stahl, M., & Rogers, D. (1988). Inhibition of pluripotential embryonic stem cell differentiation by. *Nature*, *336*, 688–690. https://www.nature.com/articles/336688a0.pdf

Smith, K. N., Singh, A. M., & Dalton, S. (2010). Myc represses primitive endoderm differentiation in pluripotent stem cells. *Cell Stem Cell*, *7*(3), 343–354. https://doi.org/10.1016/j.stem.2010.06.023

Smyth, N., Seda Vatansever, H., Murray, P., Meyer, M., Frie, C., Paulsson, M., & Edgar, D. (1999). Absence of Basement Membranes after Targeting the LAMC1 Gene Results in Embryonic Lethality Due to Failure of Endoderm Differentiation. In *The Journal of Cell Biology* (Vol. 144, Issue 1). http://www.jcb.org

Son, M. K., Ryu, Y. L., Jung, K. H., Lee, H., Lee, H. S., Yan, H. H., Park, H. J., Ryu, J. K., Suh, J. K., Hong, S., & Hong, S. S. (2013). HS-173, a novel pi3k inhibitor, attenuates the activation of hepatic stellate cells in liver fibrosis. *Scientific Reports*, *3*. https://doi.org/10.1038/srep03470

Spanos, S., Becker, D. L., Winston, R. M. L., & Hardy, K. (2000). Anti-Apoptotic Action of Insulin-Like Growth Factor-I During Human Preimplantation Embryo Development. In *BIOLOGY OF REPRODUCTION* (Vol. 63). http://www.biolreprod.org

Stewart, C. L., Kaspar, P., Brunet, L. J., Bhatt, H., Gadi, I., Koentgen, F., & Abbondanzo, S. J. (1992). Blastocyst implantation depends on maternal ex- pression of leukaemia inhibitory factor. *Natu*, *359*, 76–79. https://doi.org/10.1038/359076a0

Storm, M. P., Bone, H. K., Beck, C. G., Bourillot, P. Y., Schreiber, V., Damiano, T., Nelson, A., Savatier, P., & Welham, M. J. (2007). Regulation of Nanog Expression by Phosphoinositide 3-Kinase-dependent Signaling in Murine Embryonic Stem Cells. *Journal of Biological Chemistry*, *282*(9), 6265–6273. https://doi.org/10.1074/JBC.M610906200

Strumpf, D., Mao, C. A., Yamanaka, Y., Ralston, A., Chawengsaksophak, K., Beck, F., & Rossant, J. (2005). Cdx2 is required for correct cell fate specification and differentiation of trophectoderm in the mouse blastocyst. *Development*, *132*(9), 2093–2102. https://doi.org/10.1242/dev.01801

Suwinska, A., Czolowska, R., & Tarkowski, A. K. (2008). Blastomeres of the mouse embryo lose totipotency after the fifth cleavage division : Expression of Cdx2 and Oct4 and developmental potential of inner and outer blastomeres of 16- and 32-cell embryos. *Developmental Biology*, *322*, 133–144. https://doi.org/10.1016/j.ydbio.2008.07.019

Takahashi, K., Mitsui, K., & Yamanaka, S. (2003). Role of ERas in promoting tumour-like properties in mouse embryonic stem cells. *Nature*, *423*(6939), 537–541. https://doi.org/10.1038/nature01633

Tanaka, S., Kunath, T., Hadjantonakis, A. K., Nagy, A., & Rossant, J. (1998). Promotion to trophoblast stem cell proliferation by FGF4. *Science*, *282*(5396), 2072–2075. https://doi.org/10.1126/science.282.5396.2072

Tang, F., Barbacioru, C., Wang, Y., Nordman, E., Lee, C., Xu, N., Wang, X., Bodeau, J., Tuch, B. B., Siddiqui, A., Lao, K., & Surani, M. A. (2009). mRNA-Seq whole-transcriptome analysis of a single cell. *Nature Methods*, *6*(5), 377–382. https://doi.org/10.1038/nmeth.1315

Tarkowski, A., & Wróblewska, J. (1967). Development of blastomeres of mouse eggs isolated at the 4- and 8-cell stage. *J Embryol Exp Morphol*, *1*, 155–180.

Tesar, P. J., Chenoweth, J. G., Brook, F. A., Davies, T. J., Evans, E. P., Mack, D. L., Gardner, R. L., & McKay, R. D. G. (2007). New cell lines from mouse epiblast share defining features with human embryonic stem cells. *Nature*, *448*(7150), 196–199. https://doi.org/10.1038/nature05972

Thorpe, L. M., Yuzugullu, H., & Zhao, J. J. (2015). PI3K in cancer: Divergent roles of isoforms, modes of activation and therapeutic targeting. In *Nature Reviews Cancer* (Vol. 15, Issue 1, pp. 7–24). Nature Publishing Group. https://doi.org/10.1038/nrc3860

Tomioka, M., Nishimoto, M., Miyagi, S., Katayanagi, T., Fukui, N., Niwa, H., Muramatsu, M., & Okuda, A. (2002). Identifcation of Sox-2 regulatory region which is under the control of Oct-3/4±Sox-2 complex. *Nucleic Acids Research*, *30*(14), 3202–3213. https://doi.org/10.1093/nar/gkf435

Torres-Padilla, M. E., Parfitt, D. E., Kouzarides, T., & Zernicka-Goetz, M. (2007). Histone arginine methylation regulates pluripotency in the early mouse embryo. *Nature*, *445*(7124), 214–218. https://doi.org/10.1038/nature05458

Tosenberger, A., Gonze, D., Bessonnard, S., Cohen-Tannoudji, M., Chazaud, C., & Dupont, G. (2017). A multiscale model of early cell lineage specification including cell division. *Npj Systems Biology and Applications*, *3*(1). https://doi.org/10.1038/s41540-017-0017-0

Vallier, L., Mendjan, S., Brown, S., Ching, Z., Teo, A., Smithers, L. E., Trotter, M. W. B., Cho, C. H. H., Martinez, A., Rugg-Gunn, P., Brons, G., & Pedersen, R. A. (2009). Activin/Nodal signalling maintains pluripotency by controlling Nanog expression. *Development*, *136*(8), 1339–1349. https://doi.org/10.1242/dev.033951

Vazquez, F., Ramaswamy, S., Nakamura, N., & Sellers, W. R. (2000). Phosphorylation of the PTEN Tail Regulates Protein Stability and Function. In *MOLECULAR AND CELLULAR BIOLOGY* (Vol. 20, Issue 14). https://journals.asm.org/journal/mcb

Vlahos, C. J., Matter, W. F., Hui, K. Y., & Brown, R. F. (1994). A specific inhibitor of phosphatidylinositol 3-kinase, 2-(4-morpholinyl)-8-phenyl-4H-1-benzopyran-4-one (LY294002). *Journal of Biological Chemistry*, *269*(7), 5241–5248. https://doi.org/10.1016/S0021-9258(17)37680-9

Wamaitha, S. E., Del Valle, I., Cho, L. T. Y., Wei, Y., Fogarty, N. M. E., Blakeley, P., Sherwood, R. I., Ji, H., & Niakan, K. K. (2015). Gata6 potently initiates reprograming of pluripotent and differentiated cells to extraembryonic endoderm stem cells. *Genes Dev*, *29*(12), 129–1255. https://doi.org/10.1101/gad.257071

Wamaitha, S. E., Grybel, K. J., Alanis-Lobato, G., Gerri, C., Ogushi, S., McCarthy, A., Mahadevaiah, S. K., Healy, L., Lea, R. A., Molina-Arcas, M., Devito, L. G., Elder, K., Snell, P., Christie, L., Downward, J., Turner, J. M. A., & Niakan, K. K. (2020). IGF1-mediated human embryonic stem cell self-renewal recapitulates the embryonic niche. *Nature Communications*, *11*(1). https://doi.org/10.1038/s41467-020-14629-x

Wang, D., Wang, Y., Liu, H., Tong, C., Ying, Q., Sachinidis, A., Li, L., & Peng, L. (2019). Laminin promotes differentiation of rat embryonic stem cells into cardiomyocytes by activating the integrin/FAK/PI3K p85 pathway. *Journal of Cellular and Molecular Medicine*, *23*(5), 3629–3640. https://doi.org/10.1111/jcmm.14264

Wat, M. J., Beck, T. F., Herněndez-García, A., Yu, Z., Veenma, D., Garcia, M., Holder, A. M., Wat, J. J., Chen, Y., Mohila, C. A., Lally, K. P., Dickinson, M., Tibboel, D., De klein, A., Lee, B., & Scott, D. A. (2012). Mouse model reveals the role of SOX7 in the development of congenital diaphragmatic hernia associated with recurrent deletions of 8p23.1. *Human Molecular Genetics*, *21*(18), 4115–4125. https://doi.org/10.1093/hmg/dds241

Watanabe, S., Umehara, H., Murayama, K., Okabe, M., Kimura, T., & Nakano, T. (2006). Activation of Akt signaling is sufficient to maintain pluripotency in mouse and primate embryonic stem cells. *Oncogene*, *25*(19), 2697–2707. https://doi.org/10.1038/sj.onc.1209307

White, M. D., Angiolini, J. F., Alvarez, Y. D., Kaur, G., Zhao, Z. W., Mocskos, E., Bruno, L., Bissiere, S., Levi, V., & Plachta, N. (2016). Long-Lived Binding of Sox2 to DNA Predicts Cell Fate in the Four-Cell Mouse Embryo. *Cell*, *165*(1), 75–87. https://doi.org/10.1016/J.CELL.2016.02.032

White, M. D., & Plachta, N. (2020). Specification of the first mammalian cell lineages in vivo and in vitro. *Cold Spring Harbor Perspectives in Biology*, *12*(4). https://doi.org/10.1101/cshperspect.a035634

Wicklow, E., Blij, S., Frum, T., Hirate, Y., Lang, R. A., Sasaki, H., Ralston, A., & Downs, K. M. (2014). *HIPPO Pathway Members Restrict SOX2 to the Inner Cell Mass Where It Promotes ICM Fates in the Mouse Blastocyst*. https://doi.org/10.1371/journal.pgen.1004618

Williamson, R. A., Henry, M. D., Daniels, K. J., Hrstka, R. F., Lee, J. C., Sunada, Y., Ibraghimov-Beskrovnaya, O., & Campbell, K. P. (1997). Dystroglycan is essential for early embryonic development: Disruption of Reichert's membrane in Dag1-null mice. *Human Molecular Genetics*, *6*(6), 831–841. https://doi.org/10.1093/hmg/6.6.831

Wray, J., Kalkan, T., Gomez-Lopez, S., Eckardt, D., Cook, A., Kemler, R., & Smith, A. (2011). Inhibition of glycogen synthase kinase-3 alleviates Tcf3 repression of the pluripotency network and increases embryonic stem cell resistance to differentiation. *Nature Cell Biology*, *13*(7), 838–845. https://doi.org/10.1038/ncb2267

Wymann, M. P., Bulgarelli-Leva, G., Zvelebil, M. J., Pirola, L., Vanhaesebroeck, B.,

Waterfield, M. D., & Panayotou, G. (1996). Wortmannin Inactivates Phosphoinositide 3-Kinase by Covalent Modification of Lys-802, a Residue Involved in the Phosphate Transfer Reaction. In *MOLECULAR AND CELLULAR BIOLOGY* (Vol. 16, Issue 4). https://journals.asm.org/journal/mcb

Xenopoulos, P., Kang, M., Talia, S. Di, Xenopoulos, P., Kang, M., Puliafito, A., Talia, S. Di, & Hadjantonakis, A. (2015). Heterogeneities in Nanog Expression Drive Stable Commitment to Pluripotency in the Mouse Article Heterogeneities in Nanog Expression Drive Stable Commitment to Pluripotency in the Mouse Blastocyst. *CellReports*, *10*(9), 1508–1520. https://doi.org/10.1016/j.celrep.2015.02.010

Xie, Y., Jin, Y., Merenick, B. L., Ding, M., Fetalvero, K. M., Wagner, R. J., Mai, A., Gleim, S., Tucker, D. F., Morris, †, Birnbaum, J., Ballif, B. A., Luciano, A. K., Sessa, W. C., Rzucidlo, E. M., Powell, R. J., Hou, L., Zhao, H., Hwa, J., … Martin, K. A. (2015). *Phosphorylation of GATA-6 is required for vascular smooth muscle cell differentiation after mTORC1 inhibition*. https://doi.org/10.1126/scisignal.2005482

Xu, B. E., Wilsbacher, J. L., Collisson, T., & Cobb, M. H. (1999). The N-terminal ERK-binding Site of MEK1 Is Required for Efficient Feedback Phosphorylation by ERK2 in Vitro and ERK Activation in Vivo. *Journal of Biological Chemistry*, *274*(48), 34029–34035. https://doi.org/10.1074/JBC.274.48.34029

Xu, R., Spencer, V. A., Groesser, D. L., & Bissell, M. J. (2010). Laminin regulates PI3K basal localization and activation to sustain STAT5 activation. *Cell Cycle*, *9*(21), 4315–4322. https://doi.org/10.4161/cc.9.21.13578

Yagi, R., Kohn, M. J., Karavanova, I., Kaneko, K. J., Vullhorst, D., DePamphilis, M. L., & Buonanno, A. (2007). Transcription factor TEAD4 specifies the trophectoderm lineage at the beginning of mammalian development. *Development*, *134*(21), 3827–3836. https://doi.org/10.1242/dev.010223

Yamanaka, Y, Lanner, F., & Rossant, J. (2010). FGF signal-dependent segregation of primitive endoderm and epiblast in the mouse blastocyst. *Development*, *137*(5), 715–724. https://doi.org/10.1242/dev.043471

Yamanaka, Yojiro, Lanner, F., & Rossant, J. (2010). FGF signal-dependent segregation of primitive endoderm and epiblast in the mouse blastocyst. *Development*, *137*(5), 715–724. https://doi.org/10.1242/dev.043471

Yang, J. Y., Zong, C. S., Xia, W., Yamaguchi, H., Ding, Q., Xie, X., Lang, J. Y., Lai, C. C., Chang, C. J., Huang, W. C., Huang, H., Kuo, H. P., Lee, D. F., Li, L. Y., Lien, H. C., Cheng, X., Chang, K. J., Hsiao, C. D., Tsai, F. J., … Hung, M. C. (2008). ERK promotes tumorigenesis by inhibiting FOXO3a via MDM2-mediated degradation. *Nature Cell Biology*, *10*(2), 138–148. https://doi.org/10.1038/ncb1676

Yang, Y., Ren, Z., Xu, F., Meng, Y., Zhang, Y., Ai, N., Long, Y., Fok, H. I., Deng, C., Zhao, X., Huang, L., Zhao, Q., Wang, J., Liu, W., Ge, W., & Chen, G. (2019). Endogenous IGF Signaling Directs Heterogeneous Mesoderm Differentiation in Human Embryonic Stem Cells. *Cell Reports*, *29*(11), 3374-3384.e5. https://doi.org/10.1016/j.celrep.2019.11.047

Ying, Q. L., Wray, J., Nichols, J., Batlle-Morera, L., Doble, B., Woodgett, J., Cohen, P., & Smith, A. (2008). The ground state of embryonic stem cell self-renewal. *Nature*,

453(7194), 519–523. https://doi.org/10.1038/nature06968

Yu, C. F., Liu, Z. X., & Cantley, L. G. (2002). ERK negatively regulates the epidermal growth factor-mediated interaction of Gab1 and the phosphatidylinositol 3-kinase. *Journal of Biological Chemistry*, *277*(22), 19382–19388. https://doi.org/10.1074/jbc.M200732200

Yu, J. S. L., & Cui, W. (2016). Proliferation, survival and metabolism: The role of PI3K/AKT/mTOR signalling in pluripotency and cell fate determination. In *Development (Cambridge)* (Vol. 143, Issue 17, pp. 3050–3060). Company of Biologists Ltd. https://doi.org/10.1242/dev.137075

Yusa, K., Zhou, L., Li, M. A., Bradley, A., & Craig, N. L. (2011). A hyperactive piggyBac transposase for mammalian applications. *Proceedings of the National Academy of Sciences of the United States of America*, *108*(4), 1531–1536. https://doi.org/10.1073/pnas.1008322108

Zhang, X., Yalcin, S., Lee, D., Yeh, T. J., Lee, S., Su, J., Mungamuri, S. K., Rimmelé, P., Kennedy, M., Sellers, R., Tuschl, T., Chi, N., Lemischka, I., & Keller, G. (2011). FOXO1 is an essential regulator of pluripotency in human embryonic stem cells. *Nat Cell Biol.*, *13*(9), 1092–1099. https://doi.org/10.1038/ncb2293.FOXO1

Zhao, J., Zhai, B., Gygi, S. P., & Goldberg, A. L. (2015). MTOR inhibition activates overall protein degradation by the ubiquitin proteasome system as well as by autophagy. *Proceedings of the National Academy of Sciences of the United States of America*, *112*(52), 15790–15797. https://doi.org/10.1073/pnas.1521919112

Zhou, J., Su, P., Wang, L., Chen, J., Zimmermann, M., Genbacev, O., Afonja, O., Horne, M. C., Tanaka, T., Duan, E., Fisher, S. J., Liao, J., Chen, J., & Wang, F. (2009). *mTOR supports long-term self-renewal and suppresses mesoderm and endoderm activities of human embryonic stem cells*. https://doi.org/10.1073/pnas.0901854106

Zhu, M., Cornwall-Scoones, J., Wang, P., Handford, C. E., Na, J., Thomson, M., & Zernicka-Goetz, M. (2020). Developmental clock and mechanism of de novo polarization of the mouse embryo. *Science*, *370*(6522). https://doi.org/10.1126/science.abd2703

Ziegenhain, C., Vieth, B., Parekh, S., Reinius, B., Guillaumet-Adkins, A., Smets, M., Leonhardt, H., Heyn, H., Hellmann, I., & Enard, W. (2017). Comparative Analysis of Single-Cell RNA Sequencing Methods. *Molecular Cell*, *65*(4), 631-643.e4. https://doi.org/10.1016/j.molcel.2017.01.023